SURFACES FUNCTIONALITY OF PRECISION MACHINED COMPONENTS: MODELLING, SIMULATION, OPTIMIZATION AND CONTROL

A thesis submitted for the degree of Doctor of Philosophy

by

Najmil Faiz Mohamed Aris

School of Engineering and Design Brunel University

June 2008

Abstract

This research develops an analytical scientific approach for investigating the high precision surface generation and the quantitative analysis of the effects of direct factors in precision machining. The research focuses on 3D surface characterization with particular reference to the turning process and associated surface generation. The most important issue for this research is surface functionality which is becoming important in the current engineering industry. The surface functionality should match with the characterization parameters of the machined surface, which can be expressed in formula form as proposed in chapter 4. Modelling and simulation are extensively used in the research. The modelling approach integrates the cutting forces model, thermal model, vibration model, tool wear model, machining system response model and surface topography model. All of those models are integrated as a whole model. The physical model with such as direct inputs is formed. The major inputs to the model are tooling geometry and the process variables. The outputs from the modelling approach are cutting force, surface texture parameters, dimensional errors, residual stress and material removal rate. MATLAB and Simulink are used as tools to implement the modelling and simulation. According to the simulation results, it is found that the feed rate has the most profound effect on in surface generation. The influence of the vibrations between the cutting tool and the workpiece on the surface roughness may be minimised by the small feed rate and large tool nose radius. Surface functionality simulation has been developed to model and simulate the surface generation in precision turning. The surface functionality simulation model covers the material and tool wear as well. It shows that chip formation is resulted from cutting forces. Cutting trials are conducted to validate the modelling and simulation developed. There are positive results that show the agreement between the simulation and experimental results. The analysis of the results of turning trials and simulations are conducted in order to find out the effects of process variables and tooling characteristics on surface texture and topography and machining instability. From the research, it can be concluded that the investigation on modelling and

simulation of precision surfaces generation in precision turning is performed well against the research objectives as proposed. Recommendations for future work are to improve the model parameters identification, including comprehensive tool wear, chip formation and using Neural Networks modelling in the engineering surface construction system.

Table of Contents

Acknowledgements

Foremost I would like to thank my supervisor, Professor Kai Cheng for his invaluable support and guidance throughout the course of this research. He has definitely influenced my approach to many things not just in engineering research. Professor Kai Cheng also deserves particular gratitude, as he has been a first class supervisor throughout this research except that he also gives precious advice and encouragement. I am sure without that, the completion of the project would not have been possible.

I would like to thank Brunel University and the School of Engineering and Design for their support such as research facilities which made this research possible. Special thanks also go to my colleagues, Mr. Khalifa Blau, Dr. Xi Chun Luo, Dr. De Hong Huo for their assistance in the machining trials and valuable discussions in the project.

For my employer Universiti Teknologi Tun Hussien Onn (UTHM) for their financial support, without them I would not be able to do my Doctoral study. Thank you very much.

I am deeply indebted to my parents and parents in-law Mr. Mohamed Aris Yahya and Mrs Haminah Hasan, Mr Jusoh Mohd and Mrs Nilam Mohd Noor for their wonderful encouragement. Their love, and support during the entire project have greatly enhanced and eased the way I conducted this research.

Finally, as always, my love and gratitude go to my beloved wife Norul Asmak Jusoh for her never-ending love, encouragement and support. Lastly lot of love goes to my beloved daughter Nur Khaleeda for her patience and understanding to inspire my research work from the beginning till the end of my studies and always makes me happy.

List of Figures

List of Tables

Nomenclature

A	empirical constant
A_{ce}	cohesion energy of the repulsive pair potential function (kgm^2s^{-2})
A_e	the amplitude of the error (mm)
A_{ij}	the interfacial area of the smallest sampling quadrilateral (mm^2)
A_p	nominal surface area (mm^2)
A_s	fundamental scale of interaction
A_t	cross-sectional area of the cutting tool (mm^2)
A_{ts}	apparent area of the surface at the fundamental scale of interaction
A_w	cross-sectional area of the workpiece (mm^2)
$\overline{AT}$	differential chip thickness (mm)
B	empirical constant
B_{ce}	cohesion energy of the attractive pair potential function (kgm^2s^{-2})
B_i	bulk modulus
B_{sf}	a functional stands for the basic function of the component;
Cw	the workpiece cross sectional area (mm^2)
C_1, C_2, C_3	empirical coefficients
C_{ex}	thermal expansion coefficient
C_{ij}	the interfacial area of the smallest sampling quadrilateral. (mm^2)
Cl_f	side clearance angle of the cutting tool (degree or rad)
Cl_p	end clearance angle of the cutting tool (degree or rad)
$C_p(g)$	heat capacities under standard atmospheric pressure of the gas state (K)
$C_p(s)$	heat capacities at constant pressure of the solid state (K)
Ct	the cutting tool cross sectional area (mm^2)
D	workpiece diameter (mm)
D_1	cut-off length (mm)
E	environment pressure (Pa)
E	process activation energy (Pa)

E_{sub}	sublimation energy (J)
E_t	modulus elasticity of the cutting tool material
E_w	modulus elasticity of the workpiece material
F	ratio of the frictional force (N)
F_c	force component in the cutting direction (N)
F_{max}	the maximum normal force acted on the tip of the diamond grit (N)
F_{mn}	the mean normal cutting force (N)
F_{sf}	a functional which stands for the basic function of the component
F_R	resultant cutting force (N)
F_T	force component normal to the cutting direction (N)
G_{abt}	corresponding response of the tooling structure in a-th direction due to the force acting in the b-th direction when the other two force components are zero
G_{abw}	corresponding response of the workpiece structure in a-th direction due to the force acting in the b-th direction when the other two force components are zero (a and b stand for the X/Y/Z direction respectively)
Hf	the length out tool holder (mm)
Hw	the length of the workpiece outside the chuck (mm)
H	height vector of the intersections points of the sequence tool path (mm)
H_t	hardness of the cutting tool material (Pa)
H_w	material hardness of the workpiece (Pa)
I_w	cross-sectional moment of inertia of the workpiece (kgm^2)
I_x	cross-sectional moments of inertia with respect to X axis (kgm^2)
I_y	cross-sectional moments of inertia with respect to Y axis (kgm^2)
K_1, K_2, K_3	empirical constants
K_{aach}	stiffness of the chuck in the "a" direction (N/mm)
K_{aafs}	stiffness of the feed screw in the "a" direction (N/mm)
K_{aans}	stiffness of the nut-slide in the "a" direction (N/mm)
K_{aasp}	stiffness of the spindle in the "a" direction (N/mm) (Here a stands for

	the X, Y,and Z directions respectively.)
K_{ab}	structural stiffness of the workpiece and tooling system in a-th direction due to a force acting in the b-th direction when the other two force components are zero (N/mm)
K_{fa}	cutting constant at rake face in feed direction
K_{fc}	cutting constant at flank face in feed direction
K_{fe}	cutting constant at cutting edge in feed direction
K_l	straightness errors of the X axis and Z axis
K_{ra}	cutting constant at rake face in radial direction
K_{rc}	cutting constant at flank face in radial direction
K_{re}	cutting constant at cutting edge in radial direction
K_{ta}	cutting constant at rake face in tangential direction
K_{te}	cutting constant at cutting edge in tangential direction
K_{tc}	cutting constant at clearance face in tangential direction
K_{yyth}	stiffness of the tool holder in the "a" direction. (N/mm) (Here a stands for theX, Y, and Z directions respectively.)
L	surface form parameters
L_t	tool length out of the tool holder (mm)
L_w	length of the workpiece outside the chuck (mm)
Mcw	cutting distance (mm)
M, N	sampling numbers in the X and Y directions within the sampling area
M, N	sampling numbers in the X and Y directions within the s sampling and area respectively
M_w	cross sectional moment of inertia of the workpiece (kgm^2)
N_z	number of sample points in the Z direction
P	Normal Force (N)
P	environmental pressure (Pa)
P_{el}	Peclet number of the workpiece material
P_{ij}	Critical damping coefficient $(N/\mu m/s)$
Pul	Pulse function which generates square wave with equal interval
Qy	cross sectional moments of inertia with respect to Y (kgm^2)

Qx	cross sectional moments of inertia with respect to X (kgm^2)
Qw	cross sectional moment of inertia of the workpiece (kgm^2)
R	universal gas constant
R_0	tool nose radius (mm)
Rse	a function to generate an arbitrarily shaped period signal
Rw	total mass of the tooling workpiece system (kg)
R_t	surface roughness expressed maximum peak to valley measurement
R_w	radius of the workpiece (mm)
R_i^0	equilibrium nearest-neighbor distance (mm)
SP	surface form parameter(s). $(3D)$
S	the area of interface plane (mm^2)
S_e	shape function for elliptical heat source
S_F	surface functionality $(3D)$
S_s	strength of an individual bond
S_t	adhesive strength
T	Torque
Tt	workpiece material modulus elasticity
T	working temperature (K)
T_{amb}	room temperature (K)
T_{melt}	melting temperature (K)
Tw	the workpiece material modulus elasticity
T_2	cutting temperature in the tool flank zone (K)
U_{work}	relative speed between the workpiece and cutting tool $(m/\min)$
U_{chip}	the tool is oriented in a different relative mode
V	working lateral velocity of the component $(m/\min)$
V_c	chip velocity in the direction parallel to the rake face $(m/\min)$
$V_{\perp c}$	chip velocity in the direction vertical to the rake face $(m/\min)$
V_s	sliding speed $(m/\min)$
W	working load (N)

W	the product working distance (mm)
Y_l	linear motion error of the slideway (m / min)
Y_s	spindle synchronous error (Hz)
Z_i	the number of the nearest neighbors of the i-th atom
a	elastic modulus
a_i	flank-workpiece contact length (mm)
a_{ij}, b_{ij}	bond order functions
b	cutting width (mm)
c_{aat}	damping coefficient of the tool system in the X, Y and Z directions ($N / \mu m / s$)
c_{aaw}	damping coefficient of the workpiece system in the X, Y and Z directions ($N / \mu m / s$)
c_{crij}	critical damping coefficient ($N / \mu m / s$)
c_e	elastic constant
c_t	coefficient of thermal linear expansion of the workpiece material
d_e	elastic constant
dA	area of differential chip (mm^2)
dS	profile length of differential chip (mm)
$d\theta$	angle of differential chip (degree or rad)
d_m	humidity index of the working environment
dp	variations of the cutting forces (N)
dr	variations of penetration rate (mm / r)
ds	variations of the chip thickness (mm)
$d\Omega$	variations of the spindle speed (m / min)
f	feed rate per revolution of the spindle (mm / r)
f_A	an attractive pair potential associated with bonding
f_R	a repulsive potential
$f_c(r_{ij})$	a smooth cut-off function (mm)
fdV	material is removed in the form of chips, at the feed rate (mm / r)
f_{ev}	frequency of the environmental vibration (Hz)

h	cutting thickness (mm)
h_c	indentation depth (mm)
h_{cl}	hysteric damping constant of workpiece and cutting tool $(N/mm/s)$
h_s	integral time step
h_l	elastic constant
h_m	humidity index of the working environment;
i	equivalent inclination angle
i, j	corresponding index of the sampling points
i_o	inclination angle or oblique angle
k_{aat}	stiffness of the tooling system in the X, Y and Z directions (N/mm)
k_{aaw}	stiffness of the workpiece system in the X, Y and Z directions. (Here, a stands for X, Y and Z directions respectively) (N/mm)
k_{ec}	empirical constant
k_y	yield stress of the workpiece material
k_l	thermal conductivity of the workpiece material (K)
k_2	spring back constant
l	moving distance of the slideway (mm)
l	working load (N)
l_{cw}	cutting distance (mm)
l_w	wear land length (mm)
m_{aat}	mass of the tooling system in the X, Y and Z directions (kg)
m_{aaw}	mass of the workpiece system in the X, Y and Z directions (kg)
m_f	the fraction of the possible bonding sites that are active
m_i	mass of i-atom (kg)
m_n	3D motifs number
m_t	the total mass of the tooling structural system (kg)
m_{ti}	mass of the tooling atom (kg)
m_w	the total mass of the workpiece system (kg)
m_{wi}	mass of the workpiece atom (kg)
p	mean pressure of elastic contact (Pa)

q	rate of heat supply per unit area (mm/r)
q_1	shear plane work rate per unit area (mm/r)
r_1	total mass of the tooling structural system (kg)
r_c	cut off distance beyond which the potential energy is approaching zero (mm)
r_x, r_y	the vectors in the X and Y directions
$r(t)$	step function
s_b	spring back of the machined surface
t	revolution time of the spindle (mm/r)
ti	index for the tool tip position in the tangential force direction (mm)
tj	index for the tool tip position along the feed direction (mm)
u	a two body potential
μ_f	coefficient between the tool flank face and the workpiece
w_t	workpiece length in face turning (mm)
$x_i, y_i,$	Cartesian coordinates of the i-th motif
x_{in}, y_{in}	Cartesian coordinates of the closest motif neighbour of the i-th motif
α	high order constant
α_A	amplitude of the variation of real rake angle due to BUE
α_f	side rake angle(degree or rad)
α_n	normal rake angle(degree or rad)
α_n^*	equivalent normal rake angle(degree or rad)
α_p	back rake angle of the cutting tool(degree or rad)
α_r	tool rake angle(degree or rad)
β	bond order parameter
β_a	friction angle(degree or rad)
β_n	normal friction angle(degree or rad)
δ	modification function
$\overline{\sigma}$	flow stress
$\overline{\varepsilon}$	plastic strain
$\dot{\overline{\varepsilon}}$	strain rate

ε	small side length of the little cubes (mm)
ε_e	strain due to the elastic recovery of the machined surfaces
ε_{en}	energy at the minimum potential energy (J)
ε_m	strain due to the mechanical deformation
ε_t	strain due to the thermal deformation
η	chip flow angle(degree or rad)
η'_s	shear flow angle(degree or rad)
η_0	chip flow due to the effect of tool nose radius (mm/r)
η'_0	projected angle of η_0 on the tool rake face plane(degree or rad)
$\eta_{0.05}$	surface height at 5% bearing area (mm)
η^*_c	equivalent chip flow angle(degree or rad)
η_{pl} , η_{vl}	five highest surface summits and lowest surface valleys respectively ($3D$)
η_{pl} , η_{vl}	the five highest surface summits and lowest surface valleys respectively ($3D$)
η_r	residual surface
θ_{ijk}	bond angle between bonds ij and ik (degree or rad)
θ_0	initial approach angle(degree or rad)
θ_l	end approach angle(degree or rad)
κ	thermal diffusivity of the workpiece material (K)
λ	modification function;
λ_s	slope of the stiffness function at origin(degree or rad)
λ_1	slope parameter of the repulsive pair potential curve(degree or rad)
λ_2	slope parameter of the attractive pair potential curve(degree or rad)
λ_3	slope parameter of the cut-off potential function(degree or rad)
ζ_{ab}	damping ratio of the workpiece and tooling system in a-th direction due to a force acting in the b-th direction when the other two force components are zero ($N/mm/s$)
ξ_{ij}	damping ratio ($N/mm/s$)

ρ_i	electron density of the real lattice
$\bar{\rho}_i$	electron density of the reference lattice
τ_A	amplitude of the increment of the shear stress due to the hard grain (mm)
τ_s	shear yield stress
$\tau_s(t)$	real shear stress in cutting processes
φ_c	shear angle(degree or rad)
ϕ_n	normal shear angle in oblique cutting(degree or rad)
ϕ_0	initial shear angle(degree or rad)
ψ_t	side cutting edge angle of the cutting tool(degree or rad)
ψ_{ij}	angular potential function(degree or rad)
ω	spindle angular speed $(m/\min)$
ω_c	chatter frequency (Hz)
ω_{nab}	structural natural frequency of the workpiece and tooling system in a-th direction due to a force acting in the b-th direction when the other two force components are zero (Hz)
ω_α	frequency of the generation and removal of BUE (Hz)
$\Delta\alpha$	variation of rake angle due to BUE
ΔT_f	temperature rise in the tool flank – workpiece zone
ΔV	wear volume (K)
Δs	average distance between the shear-localized chips (mm)
Δx, Δy	deviation length (mm)
$\Delta\tau_l$	increment of the shear stress due to the hard grain
Δx, Δy	deviation length. (mm)

Abbreviations

AACF	Area Autocorrelation Function
APSD	Area Power Spectrum Density
ANOVA	Analysis Variance
BP	Back propagation
BR	Free forward-forward back regression
BUE	Build-up edge
CNN	Computer Neural Networks
CNMA	Tool inserts type
CNC	Computer Numerical Control
Coef	Coefficient
DCFCs	Dynamic Cutting Force Coefficients
FFT	Fast Fourier Transform
MLE	Maximum Likelihood Equation
MCT	Minimum Undeformed Chip Thickness
MRR	Material Removal Rate
NN	Neural Network
OLS	Ordinary Least Square
PLS	Partial Least Square
RA	Regression Analysis
RMS	Root-Mean-Square
RSM	Response Surface Method
SE coef	Standard Error coefficient
SCMT	Tool inserts type
VBMT	Tool inserts type
VIF	Variance inflation factor

Chapter 1 Introduction

1.1 Background

The area of surface functionality is becoming important for precision manufacturing industry because there is an increasingly high demand of components with precision surfaces and micro featured surfaces in the industry such as, braking disc, gear tooth profiling, bearings and medical devices as well [1]. High precision manufacturing potentially offers good quality control, reliability and desired functionality for these products. The product performance heavily depends on their surface quality such as lubrication capacity and wear and tear resistance, etc. Precision manufacturing development rapidly increases the need for high precision products and components in advanced science and technology, for instance, those in medical, computer and mechanical industry.

1.2 Machine tool technology

To meet the requirement for manufacturing high precision products, many ultra-precision machining mechanical tools have been developed since 1970, which include the Large Optics Diamond Turning Machine (LODTM) [2] and the Cranfield nanocenter [3]. Fig 1.1 shows that in the early 1970 are a number of surveys were carried out on the productivity of machine shops in the UK, Europe and the USA [4].

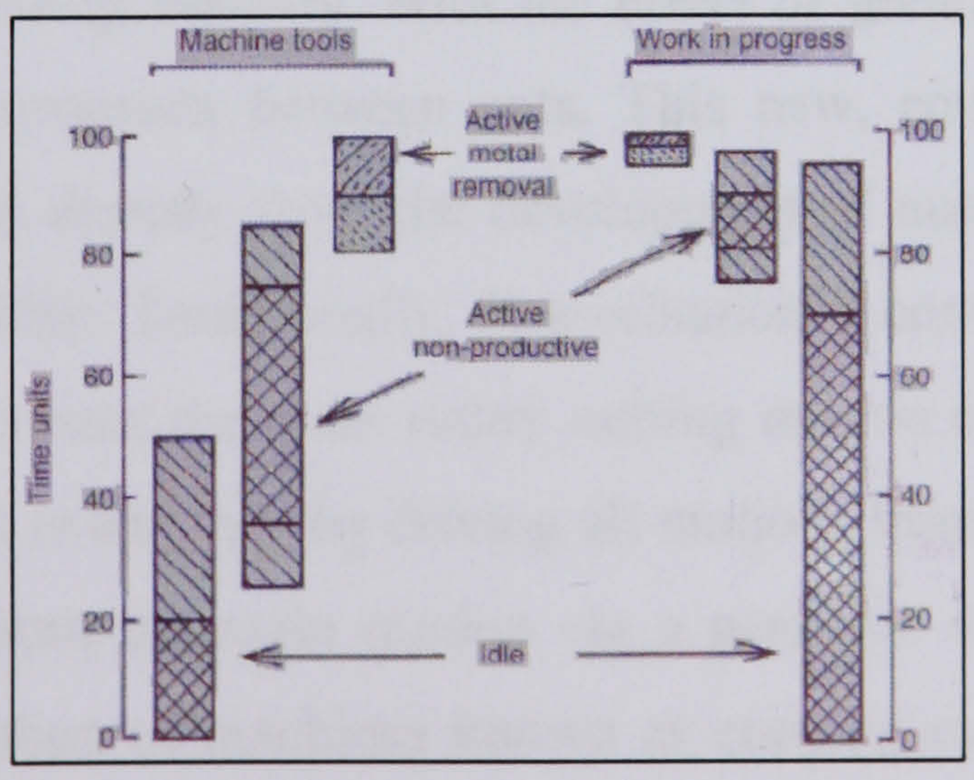

Fig. 1.1 Unused and active times in batch manufacturing, from surveys circa 1970s

It was found that they were actually productive in removing metal, for only 10% to 20% of the time. For 40% to 60% of the time the machine tools were in use but not productively, i.e. they were being set up for manufacturing or being loaded and unloaded, or during manufacturing, tools were being moved and positioned for cutting but they were not removing metal. For 20% to 50% of the time they were totally unused. As far as work in progress was concerned the batches of components typically spent 70% to 95% of their time being inactive on the shop floor. So overwhelming was the clutter of partly finished work that a component required several different operations for its completion. On different machine tools, it might find these carried out at the rate of only one a week. For 10% to 20% of their time components were being positioned for machining and for only from 1% to 5% of the time metal was actually being removed. From the late 1960s to the early 1970s both forms of waste - the active, non-productive end the idle times - began significantly to be attacked, the former mainly by developing machine tool technology and the latter by new forms of manufacturing organization.

In late 1980s it was even proved that nanometric chip removal is feasible by some researchers at Lawrence Livermore National Laboratory (LLNL) in the USA [5].

1.3 Turning machines technology

From 1970s onwards, machine tools of new design started to be introduced in significant numbers into manufacturing industry, with the effect of greatly reducing the times for tool positioning and movement between cuts. This new, computer numerical control (CNC), design stemmed directly from the development of numerically controlled (NC) machine tools in the 1960s. Traditionally, in mechanically controlled machine tools, the coordination needed between the main rotary cutting motion of the work piece and the feed motions of the tool is obtained by driving all motions from a single motor. The feed motions are obtained from the main motion via a gear box and lead screw for thread cutting. With the exception of machines known as copying machines which derive the feed motion by following a copy of a shape to be made, only simple feed motions are

obtainable on a lathe. For example, these are in the axial and radial directions; to machine a radius on a lathe requires the use of a form tool. In addition, the large amount of backlash in the mechanical chain requires time and a skilled operator to set the tool at the right starting point for a particular cut.

In a CNC machine tool, all the motions are mechanically separate, each driven by its own motor and each coordinated by the computer with the others. Not only is a much more complicated feed motion are possible, for example a combined radial and axial feed to create a radius or to take the shortest path between two points at different axial and radial positions, but also the requirement of coordination has led to the development of much more precise, backlash-free ball-screw feed drives. This precise numerical control of feed motions, with the ability also to drive the tools quickly between cuts, together with other reductions in set-up times has approximately halved machine tool non-productive cycle time, relative to its pre-1970s levels.

A further halving of non-productive cycle time has been possible since about 1980s onwards, with the spread throughout all manufacturing industry of new types of machine tools that have become called turning centres and machining centres. These new machines, first developed for mass production, individually can carry out operations that previously would have required several machine tools. For example, it is possible on a traditional lathe to present a variety of tools to the workpiece by mounting the tools on a turret. In a new turning centre, some of the tools may be power driven and the main power drive, usually used to rotate the workpiece in turning operations, may be used as a feed drive to enable milling and drilling as well as turning to be carried out on the one machine.

Precision manufacturing concerns the creation of components with high form and dimensional accuracy and surface quality, which will affect the components specified functionality and performance. The surface accuracy may be at micrometer and even nanometric level, so both the machine design and process behaviour must be well

understood as well as the interaction between the process and machine, i.e. the interaction between the tool and workpiece surface and associated tool-workpiece loop [6]. The increased versatility of machine tools has been briefly considered: the freedom given by CNC to create more complicated feed motions, both by path and speed control; and the evolution of multi-function machine tools. The cost penalty has just been mentioned. As part of the continuing scene setting for the conditions in which metal cutting is carried out, this will be combined with systems and materials technology considerations.

1.4 Surface functionality

Surface functionality in precision manufacturing takes an interest in the construction of surface texture or topography of components in addition to dimensional accuracy and surface quality, which will affect the component's function and performance. The surface precision could be at micrometer or nanometer level.

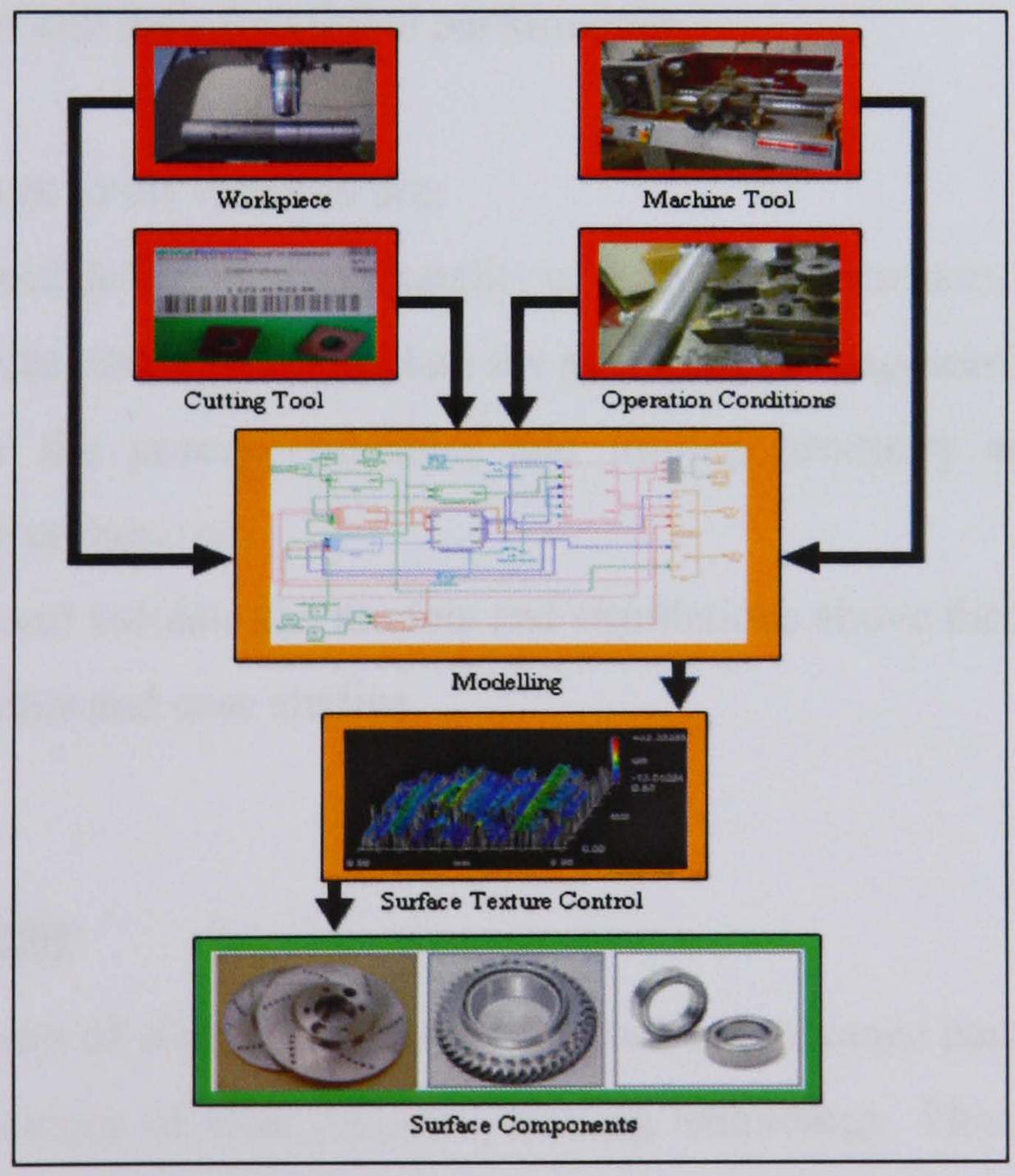

Fig. 1.2 Four categories of factors influencing the surface functionality generation

The surface functionality control of precision machined surface is dependent on four categories of factors as shown in Fig. 1.2. They are compromise of the machined workpiece, machine tool, operation condition and cutting tool. A scientific research is really required to develop a theoretical basis to link the machined surface and the main factor from the four categories of factor and also to investigate the foundation to achieve the desired surface functionality. Hence it is important to look into the principles of surface functionalities generation from the precision machining.

1.5 Aim and objectives of the research

The overall aim of this research project is to develop a modelling and simulation approach for investigating the generation of surface functionality in relation with machining process and tooling geometry. The optimal control of surface generation and the associated functionality formation would significantly benefit the achievement of high quality surfaces and their functional performance.

The distinct objectives of the research are:

(1) To identify and define the functionality of engineering surfaces.

(2) To characterize, model and simulate the generation of engineering surfaces.

(3) To optimize the process variables and tooling geometry against the surface functionality as required.

(4) To evaluate and validate the models and simulations above through well designed machining trials and case studies.

1.6 Research scope

The rapid development of sophisticated machine tool and advance control system has led to an increased efficiency of ultra precision turning technology. The selection of set up parameters for the turning process is done with aid of trial cutting test, which are both time consuming and costly. The modelling technique used in the present study could be extended to other machining process as well tool and workpiece combination. The three-

dimensional modelling techniques used in the present study could be extended the turning operation provided that a workpiece could be cut perpendicularly.

The simulation model was evaluated through a series of the cutting experiments. All the experiments were carried out on Harisson M250 turning machine. The workpiece material is a steel and alloy. The three dimensional surface topography and surface roughness parameters of the machined surface were measured by Zygo 3D surface profiler. In order to ensure the compatibility and consistency between the predicted and measured result, all simulations and measurements were made athe centre of the workpiece.

As we known, turning process is expensive process. The simulation model help to determine the optimal cutting conditions without need for costly trial and error cutting test. It also helps to identify the best surface quality that can be achieved under a particular vibration condition.

From this research, it contribute to improve the environment and satisfying consumer's need for better and lower cost components. By improving the useful life of components, surface technology avoids society more frequent need to exhaust natural resources or consume energy. A painted garden seat look smarter and last much longer than unpainted one.

In automotive engineering, motor vehicles are critically dependent on surface engineered components for their extended warranties and emission controls. A hardened engine valve will last a minimum of five years without replacement

1.6 Chapter plan of the thesis

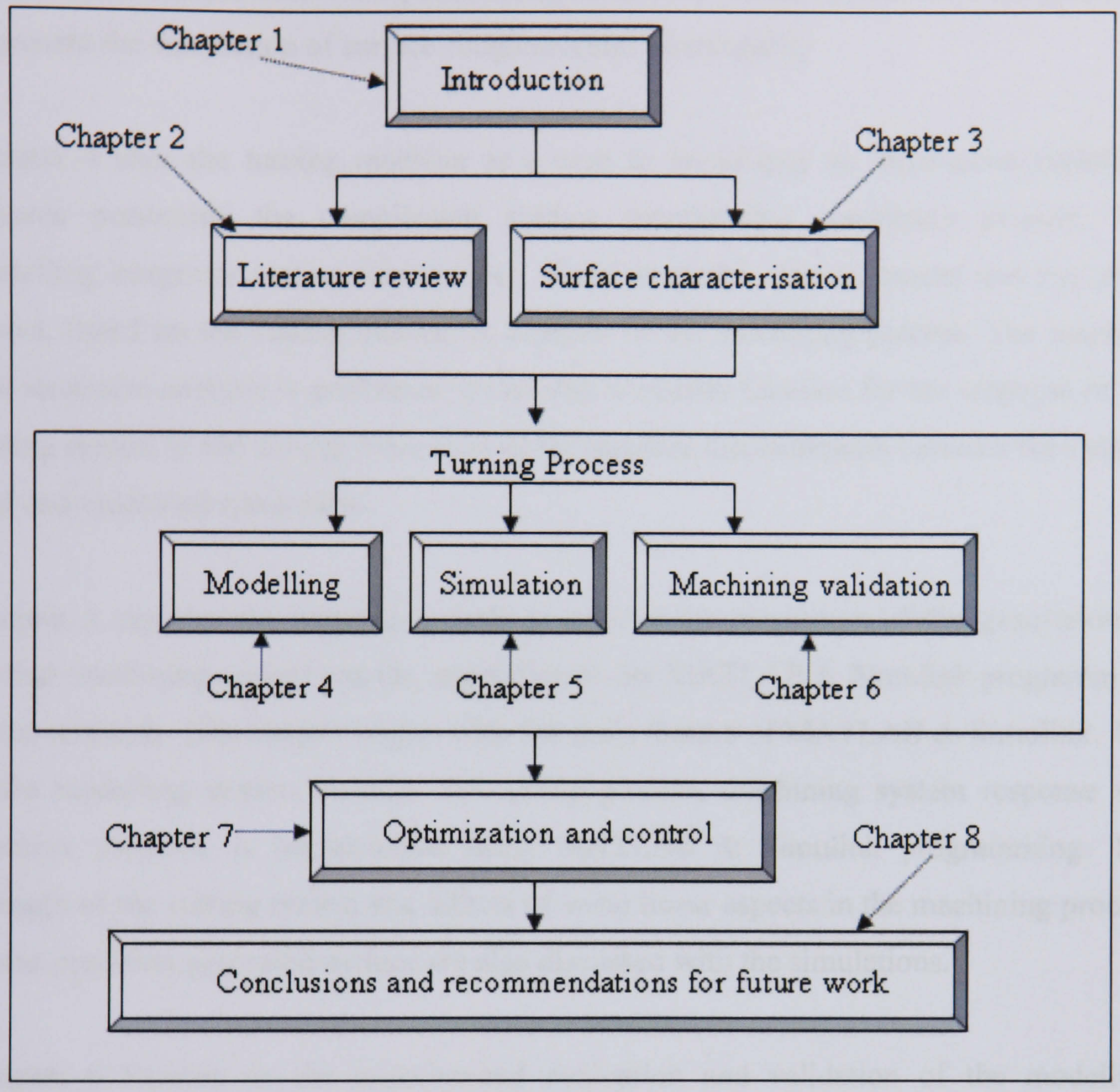

Fig. 1.3 Structure of the thesis based on research flow and findings

As illustrated in Fig. 1.3 the thesis is presented in eight chapters. Chapter 1 describes the determination and objectives of the work. Chapter 2 reviews the surface metrology, tribology for machining process including the machined surface generation, the surface generation modelling, simulation, optimisation and control. The literature review reveals the investigation of a new approach which is important to present useful and easy techniques in addition to acquiring technical knowledge of the surface functionality generation correlation to the surface machining processes.

Chapter 3 presents the characterization parameters for 2D and 3D surface functionalities on machined components. New parameters, such as 3D surface parameters are proposed to present the correlation of surface roughness and functionality.

Chapter 4 uses the turning machine as a case to investigate an innovative modelling towards presenting the complicated surface functionality generation process. The modelling integrates cutting force model, vibration model, thermal model and tool wear model, based on the cutting mechanics analysis of the machining process. The machine tool structural analysis is performed to develop a transfer function for the response of the cutting system to the cutting force such as the positive displacements between the cutting tool and machined component.

Chapter 5 explains the simulation tools to achieve the simulation of the generation of surface machining system and the motivation to use MATLAB & Simulink programming in the research. This chapter begins with the main feature of MATLAB & Simulink. The entire modelling system includes the cutting process, machining system response and machine surfaces, is implemented using MATLAB & Simulink programming. The strength of the cutting system and effects of some linear aspects in the machining process on the precision generated surface are also discussed with the simulations.

Chapter 6 focuses on the experimental evaluation and validation of the modelling approach proposed. This includes the method and understanding of turning trials. The cutting forces and machined surface are used to evaluate and validate the modelling approach and simulations. The effect of operation variables and tooling characteristics on the machined surface texture and topography generation is further investigated with the results from both machining trials and simulations.

Chapter 7 concerns the optimization and control of surface functionalities in machining generation processes. The MATLAB Neural Networks and Minitab 1.5 ANOVA technique are proposed to control and optimizes the machining process. The influences of

the process on machined surface roughness are further investigated with the results from both machining trials and simulations.

Chapter 8 draws up the conclusions and outcomes from this research and the recommendations are created for future work.

Chapter 2 Literature review

2.1 Introduction

Chapter 2 will focus on the overview of the state-of-art relevant to the work as presented in all the chapters. There are six sub topics to be discussed. Fig. 2.1 shows these topics including turning process, Zygo 3D surface profiler, simulation, optimization, control and modelling approach.

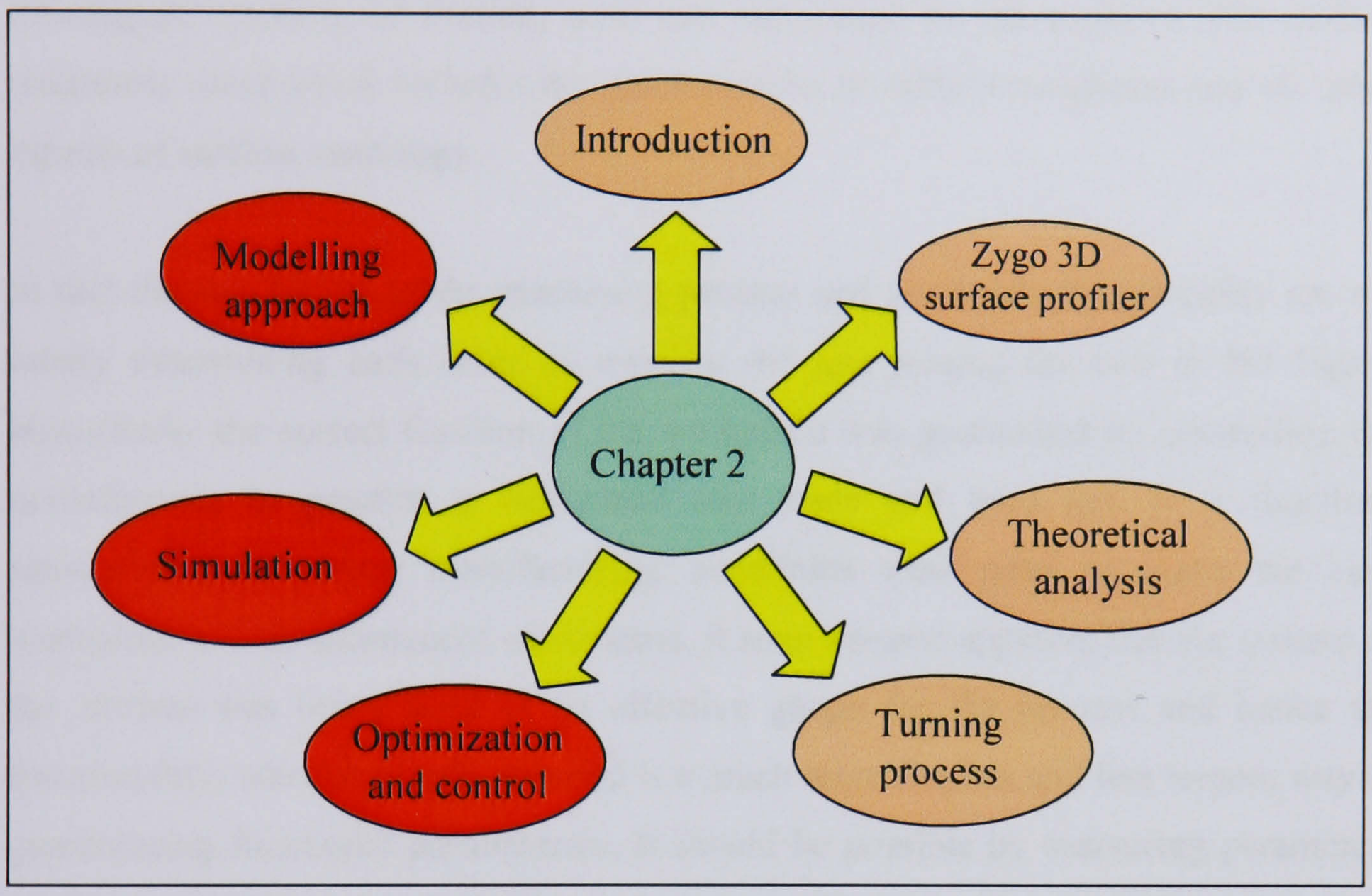

Fig. 2.1 The flow of Chapter 2

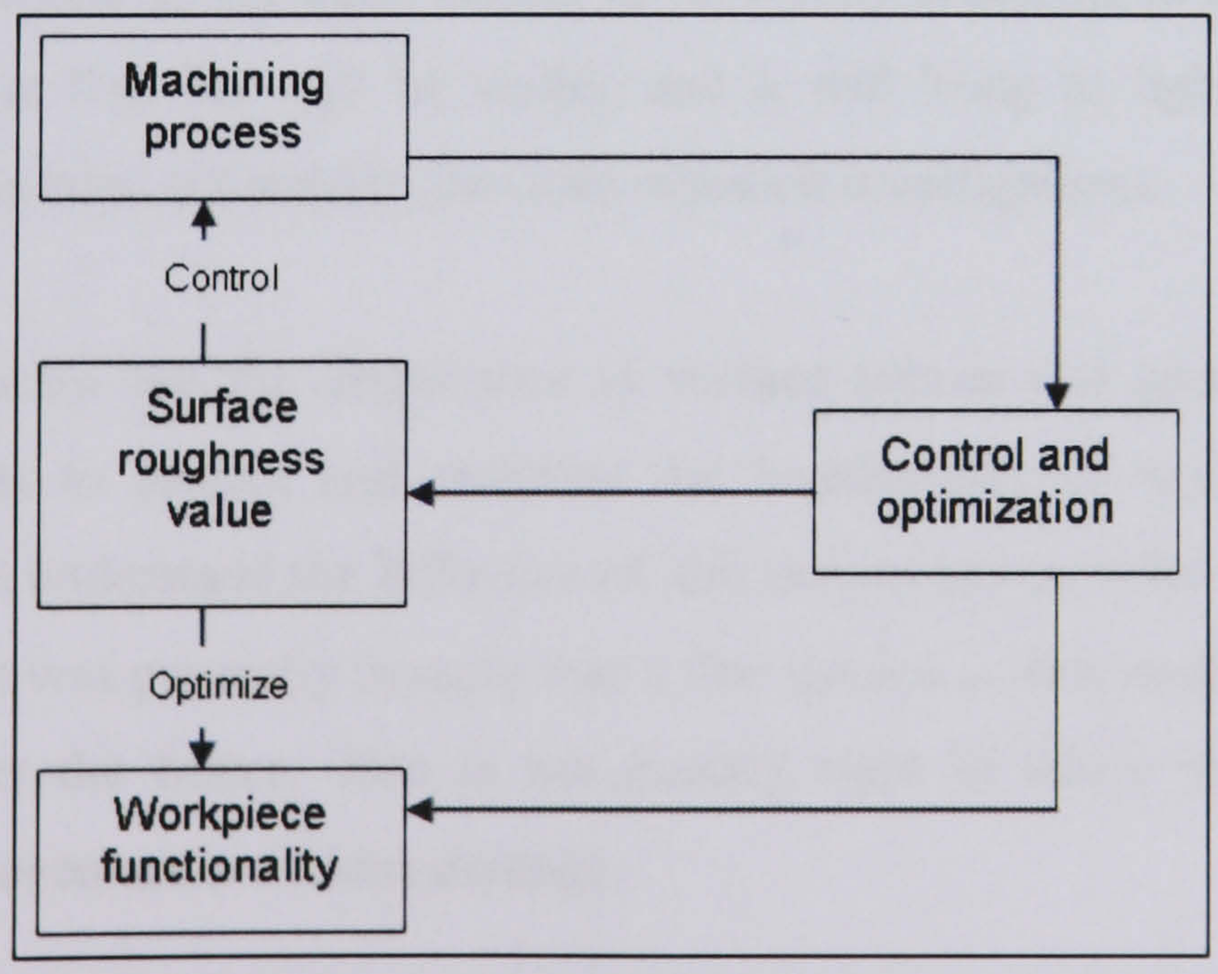

Fig. 2.2 Manufacturing of surface functionality

As a general rule measurement must take place in order to ensure that the workpiece will function as required for the time specified to guarantee its quality. Fig. 2.2 shows the block diagram representing surface characterisation can be set fairly to bridge the gap between the machining process, surface generation and workpiece function. In the machining process block it includes all aspects of the machining system such as machine performance, tool wear and chatter; whereas in the workpiece functionality block it includes all functional properties of the component surfaces such as the tribological attention of friction, wear and lubrication on the surfaces. The surface roughness value block includes the measurement of surface roughness and all other aspects of surface metrology.

In fact the two blocks of the machining process and workpiece functionality are not totally determining each other as seen by the line joining the two in the figure. Historically the correct function of the workpiece was guaranteed by controlling the manufacture. In practice a workpiece was made and tried out. If it functions satisfactorily the same manufacturing conditions were used to make the next workpiece and all subsequent workpieces. It soon became apparent that the control of the surface was being used as an effective gauge for the process and hence the functionality; what obviously required is a much more flexible and less remote way of guaranteeing functional performance. It should be possible by measuring parameters of the surface texture to predict the functionality. This may seem an obvious statement but within it lies one of the main causes for everyday problems in engineering. The block diagram in Fig. 2.2 will be visible and it will bring to light by taking into account what has been revealed in previous research investigations.

Fig. 2.2 also shows that the importance of surface texture and geometry should be recognized so as to control and optimize the functionality of workpiece surfaces. Researcher must understand the influence of the surface has on behaviour and specify it accordingly. It was generally thought that a fine surface is necessarily a smooth one, i.e the smoother the better. This is not exactly right in many application cases, however, it can even cause serious damage.

The research and practice has set out that there is fundamental influence between the surface and the machining process. Firstly the influence is attentive to the nature of the geometric characteristics created on the surface by the machining process. It is shown that the Fourier kernel and its derivatives such as the Wigner function can be used to great effect. In what follows the way in which most conventional machining processes and some less conventional processes affect the surface will be examined. In order to do this it is often necessary to describe the basic mechanisms of the process and sometimes to attempt to determine how these mechanisms are reflected in the surface characteristics. Consequently, although the process will be described, the investigation will only be carried out as far as necessary to explore the surface implications.

2.2 Surface metrology and surface characterization

Surface metrology is the evaluation of the variation of a workpiece from its planned form that is specified on the functionality. It includes the measurement of surface texture. It could be the method to design the role of surface metrology measured in order to enable a component to function according to the surface functionality.

The dimensional metrology is a first aim because it ensures that the texture of the workpiece surface complies with the functionality as designed. This by itself is not sufficient to ensure that the workpiece will satisfy its function; it may not be able to turn or move, for example. This is where surface metrology becomes important. Surface metrology verifies that all aspects of the surface geometry are noted and ideally controlled. If the shape and surface texture of the workpiece are correct then it will be able to function as required and the dynamic characteristics therefore satisfied.

The classification of measurements will deal with the physical and chemical condition of the workpiece. This will be called here physical metrology. It includes the hardness of the materials, both in the surface layers, and the residual stress of the surface, both in compression or left in the material by the machining process or the heat treatment. It also includes measurement of the metallurgical structure of the material, and its chemical construction. All these and more contribute to the durability of the

component, for example, its resistance to corrosion or fatigue. Physical metrology is therefore an important part of engineering metrology. As a general rule this must take place with other types of measurement in order to ensure that the workpiece will function as required for the time specified to guarantee its quality.

2.3 Surface tribology in machining

Tribology is defined as the science of interacting surfaces in relative motion. The word tribology comes from the Greek tribos, meaning rubbing. In any machine there are lots of machined components and parts that operate by interacting with each other and involving friction, wear and lubrication and other tribological issue. Some examples are bearings, gears, cams and tappets, tyres, brakes, and piston rings. All of these components and parts have machined surfaces which come into contact, supporting a load, or moving with respect to each other. Sometimes the surfaces machined have their own functionality requirement such as low friction, saving energy, or high friction, as in the case of brake surfaces. If the component needs to reduce the friction or wear they are lubricated. The knowledge of friction, wear, lubrication and contact mechanics are all parts of tribology. It is one of the important aspects of surface engineering because a machined component surface has to improve its function, for example by applying a surface coating, surface roughness, and rolling contact fatigue where repeated contacts cause fatigue to occur.

Surface tribolgy is used to describe a number of industrial processes that can be applied to improve the surface of a machined component. The major reason to apply these processes is to improve surface interaction such as corrosion protection, wear resistance and friction control which are areas where performance can be enhanced by these processes. The machining operation is influenced by the dynamics of the machine tool structure and the cutting process. The dynamics of the machine tool structure is customarily analyzed using the general well-developed methods and theories of structural dynamics, and is at present better understood than the cutting process. The dynamics of the cutting process is much less tractable since theoretical and experimental methods for its study are still under development and many outstanding issues remain [10].

One of the first analytical formulations of the dynamic cutting force variation due to chip thickness variation, the rate of penetration and the cutting velocity was established by Tobias and Fishwick [11]. They present the following important relationship:

$$dp_t = K_1 \cdot ds + K_2 \cdot dr + K_3 \cdot d\Omega \tag{2-1}$$

dp_t – variations of the cutting forces;

ds – variations of the chip thickness;

dr – variations of penetration rate;

$d\Omega$ – variations of the spindle speed;

K_1, K_2, K_3 – constants.

Tlusty and Polacek [12] also developed dynamic cutting force model to model the dynamic cutting forces by using a proportional relation:

$$dF = k_{ec} ds \tag{2-2}$$

k_{ec} – constant.

Equation (2-2) is the foundation of the of dynamic cutting force theory. Some dynamic cutting force models [13-15] developed later just follow the approach, even though the focus is on the prediction of the dynamic cutting force coefficients or the calculation of chip area.

Experimental evidences clearly show that the dynamic cutting process is nonlinear [16]. Hanna and Tobias developed the theory of nonlinear regenerative chatter where the machining system structure was presented by an equivalent single degree of freedom system with nonlinear stiffness characteristics and the cutting force was approximated by a third order polynomial of the chip thickness [17]:

$$dF = C_1 ds + C_2 ds^2 + C_3 ds^3 \tag{2-3}$$

C_1, C_2, C_3 – coefficients.

Recently the simulation and measurement of tool displacement show that chatter may even happen in diamond turning of aluminium because of the nonlinear regenerative vibration [18]. The loss of contact between tool and workpiece with increased vibrations was analyzed by Tlusty and Ismail [19]. With the wide application of high speed machining, the nonlinearities caused by the chip formation are attracting considerable interest - Hou and Komanduri. They have studied the shear instability in machining using a thermo-mechanical model [20].

Davies, Burn and Evans have explained the chip segmentation phenomenon in high speed machining by using a simplified one dimensional thermo-mechanical model [21] and carried out numerical simulation and machining trials to study the rule of the segmented chip formation [22]. Other nonlinearities, such as ploughing process [23] and tool chip interface [24] have also been studied by some researchers.

The nonlinear effects will become evident because of the rise of specific cutting energy at small depth of cut [25]. The rotating of the resultant cutting force vector in light cutting depth may further increase the potential for chatter feedback to cutting tool [26]. Therefore, more attention should be paid to model the nonlinearities and their effects on machined surface quality in precision machining. The design of rolling bearings and gears is such that the load is supported on a small area. This leads to high stresses over small areas of the components. This can cause high friction, wear, and contact fatigue. Contact mechanics is therefore an important part of tribology. In the early study of nonlinearities of metal cutting, empirical approach has been used to predict the nonlinear cutting force by some researchers [17, 27, 28].

2.3.1 Surface contact and pressure on machined surface

The machined surfaces may look smooth, but at the microscopic scale they are rough. When two surfaces are pressed together, contact is made at the peaks of the roughness or asperities. The real area of contact can be much less than the apparent or nominal area as shown in Fig. 2.3. At the points of intimate contact, adhesion, or even local welding, can take place. If we want to slide one surface over the other then we have to apply a force to break those junctions.

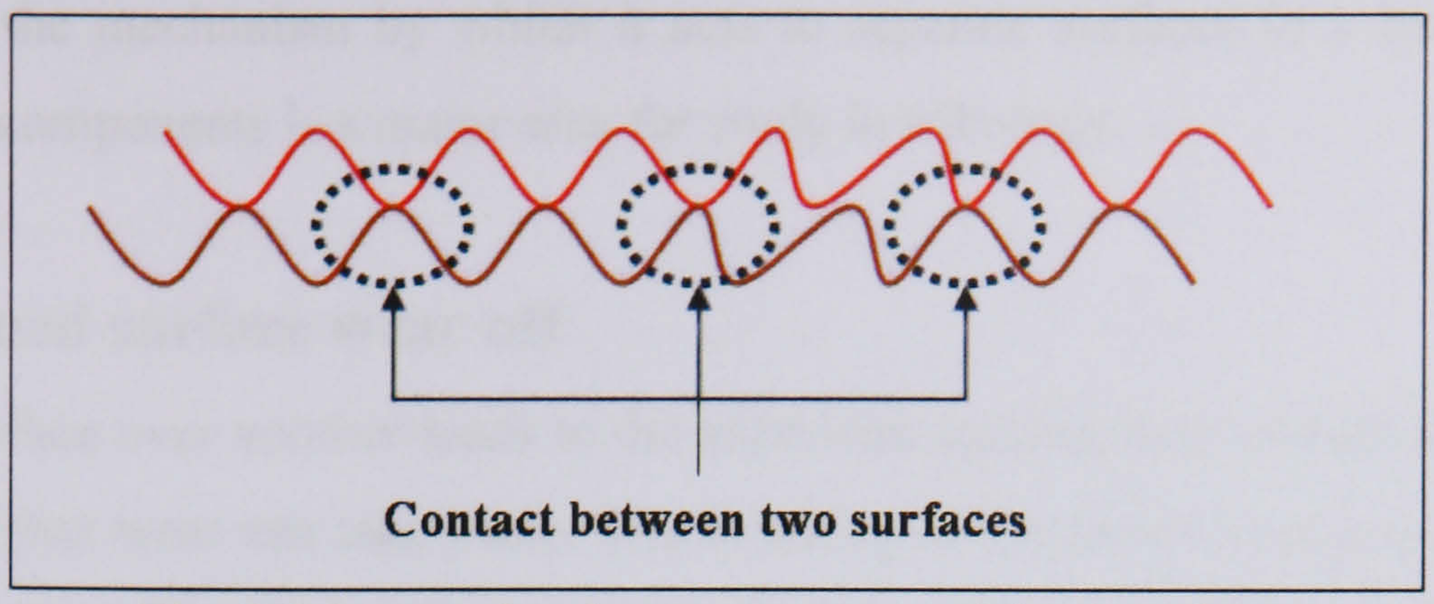

Fig. 2.3 Interaction between two machined surfaces

2.3.2 Friction and force on machined surfaces

As illustrated in Fig. 2.4. the friction force is the resistance encountered when one body moves relative to another body with which it is in contact. The static friction force is how hard you have to push something to make it move, whilst the dynamic friction force is how hard you push to keep it moving. The ratio of the frictional force F to the normal force P is called the coefficient of friction.

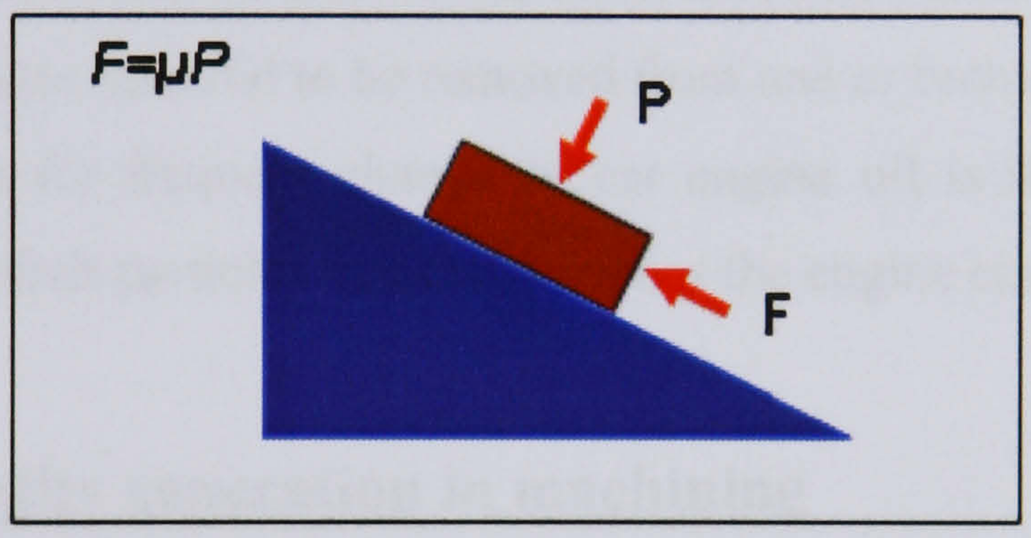

Fig. 2.4 Friction and force diagram

In a sample case low friction such as that in the car engine, for example, does not require excessive energy to it moving. However, in another case high friction is needed such as in brakes, for instance. Friction is also important for car tyres to grip the road and between shoes and the ground for walking.

2.3.3 Lubrication for partition of two machined surface

The layer of oil between the surfaces can separate them and easily slide one over the other with reduced friction and wear. Mineral oils are the most common lubricants, but other low shear strength materials are also used; for example graphite, PTFE, and soft metals like lead or gold. The selection of different type of lubricant viscosity and

understanding the mechanism by which it acts to separate surfaces in a bearing or other machine components is a major area for study in tribology.

2.3.4 Machined surface wear off

The sliding surface over another leads to the asperities coming into contact and there is a possibility that wear can take place. The breaking of the entire little junction can cause material removal called adhesive wear. Or the asperities of a hard surface can plough grooves in a soft surface called abrasive wear. Wear is usually unwelcome because it leads to increased clearances between moving components and increases mechanical loading and maybe even fatigue. But in grinding and polishing process the generation of high wear rates is desirable.

As well as adhesive and abrasive wear, there are other mechanisms whereby material can be removed from a surface. Erosive wear occurs when particles or even water droplet strike a surface and break off a bit of the material. Hard particles can become trapped in contacts and cause material to be removed from one or both of the surfaces. One of the main reasons for frequent change of car engine oil is that it becomes contaminated with hard debris particles that can wear out the engine components.

2.4 Surface functionality generation in machining

In order to reshape raw material into a workpiece having the desired shape, size and surface quality, it has to be processed by some means. There are many different ways in which this reshape can be achieved. Every way has its own certain advantages and disadvantages. Some machined components are produced by one process and others by many. The shape and roughness implication will be focused on. The method of surface roughness produced will be one consideration but the importance is what the functionality can discover through the surface roughness.

The machining processes can be subcategorized into the following:

(1) Cutting with single or multiple tool tips-this includes turning, milling, broaching and planning.

(2) Abrasive machining-this includes grinding, polishing, honing.

(3) Physical and chemical machining-this includes electrochemical machining, electrodischarge machining, etc.

(4) Forming, casting, extrusion.

(5) Other macroscopic machining includes laser machining, high-power water jet.

(6) Ultra-fine machining (nanomachining) include ion beam milling and energy beam machining.

2.5 Theoretical analysis

2.5.1 Machining mechanics for cutting processes

Machining mechanics for cutting process involves friction, plastic flow and fracture of materials under conditions more extreme than those normally found in materials testing or in other production processes. Investigators in the metal cutting field have attempted to develop an analysis of the cutting process which gives a clear understanding of the mechanism involved and enables the prediction of the important cutting parameters, without the need for empirical testing [8].

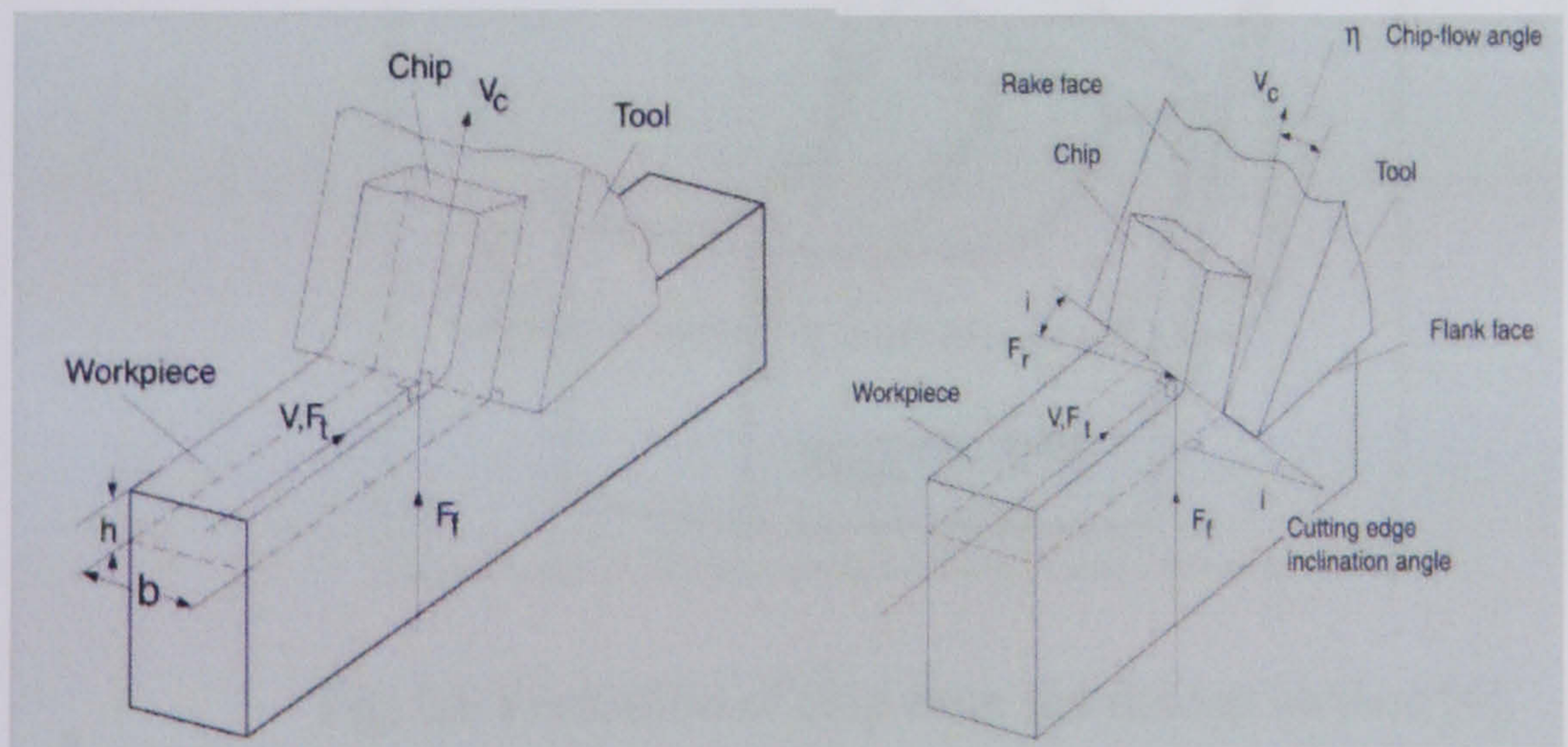

(a) Orthogonal cutting (b) Oblique cutting

Fig. 2.5 The illustration of orthogonal and oblique cutting processes [9].

Fig. 2.5 (a) shows an orthogonal cutting model; the cutting edge is perpendicular to the relative cutting velocity between the tool and workpiece. The orthogonal cutting resembles a shaping process with a straight tool whose cutting edge is perpendicular to the cutting velocity (V). A metal chip with a width of cut (b) and uncut chip thickness (h) is sheared away from the workpiece. The cutting is assumed to be uniform along the cutting edge where it is a two-dimensional plane strain deformation process without side flow of the material. Instead, cutting forces are exerted only in the direction of velocity and uncut chip thickness, which are called tangential (F_t) and feed forces (F_f). Fig. 2.5 (b) shows a single cutting edge inclined to the cutting velocity in oblique cutting. The cutting edge is oriented with an inclination angle (i) and the additional third force acts in the radial direction (F_r).

For this research, 3D or non – orthogonal cutting process has been chosen. Fig. 2.6 shows a formation of the chip from the flat top surface of workpiece by cutting tool to reduce the height of the plate. It also shows that the tool is stationary and the plate is moving. The relative speed between the workpiece and cutting tool is expressed by U_{work} •

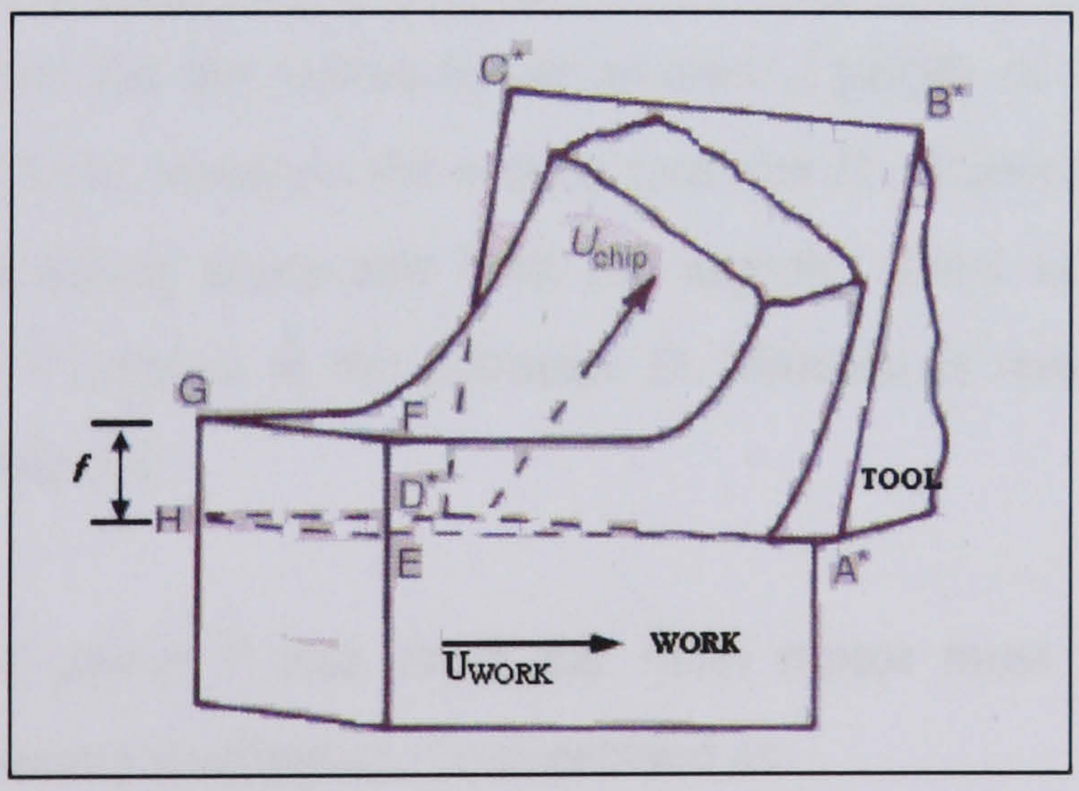

Fig. 2.6 Formation of chip from the flat top surface [4].

It also shows U_{chip} is the same but the tool is oriented in a different relative mode as the plate and a different geometrical aspect of the chip formation is introduced.

According to the Fig. 2.6 above the rotation of cutting edges is along with the axis of (AD)*. The section of removed material EFGH stays rectangular but U chip becomes inclined to the cutting edge.

Neither U_{work} nor U_{chip} is perpendicular to the cutting edge. Chip formation is then known as non–orthogonal. The rotation angle (AD)* is called the cutting edge inclination angle, λ_s. The mechanics of non orthogonal chip formation is more complicated than those of orthogonal chip formation, because the direction of chip flow is not fixed by λ_s.

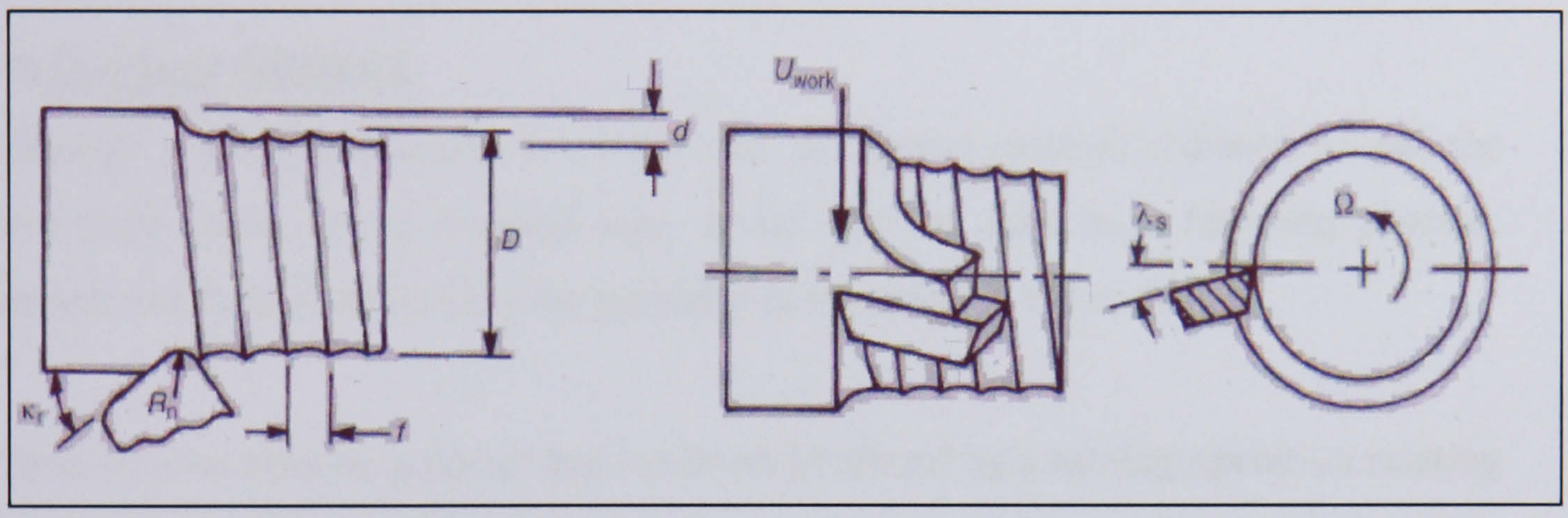

Fig. 2.7 A turning operation [4]

Figure 2.7 shows a turning operation where the cutting tool moves an axial distance *f* (feed rate) to reduce the bar radius by an amount *d* (depth of cut). The figure also shows the cutting force acting on the cutting tool, the *D* (diameter) at which point the cutting process is taking place and both the angular speed Ω at rotation and the consequent linear *V* (speed) at the diameter *D*. Material is removed in the form of chips, at the feed rate *fdV*.

The torque T and power P that drive the main motor must support this turning operation by elementary mechanics, i.e expressed as:

$$T = F_c(D/2) \equiv (F_c^* fd)(D/2) \quad (2\text{-}4)$$

$$P = F_c V \equiv (F_c^* fd)V \text{ or } F_c^*(fdV) \quad (2\text{-}5)$$

A new quantity *Fc* has been introduced. It is the cutting force per unit area of removed material. Called the specific cutting force, it depends on a first approximation mainly

on the material being cut. Equation (2-4) indicates that, for a constant area of cut *fd,* a turning machine should be fitted with a motor with a torque capacity proportional to the largest diameter being cut. It is shown later that for any combination of the work and tool there is a preferred linear cutting speed *V*. Equation (2.5) suggests that for a constant area of cut the required motor power should be independent of the diameter being cut. Observing what motors, with their torque and power capacities, are fitted to production machine tools can give insight into what duties the machine tools are expected to perform; and what forces the cutting tools are expected to withstand. This is going to be further explored below.

2.6 Surface finished

Although a turning machine is often used to remove enough material to get the workpiece down to the required size, it can also be used as a finishing process. Surface roughness values (R_a) are typically in the range of 0.5 to 1.0 μm.

There are two discrete types of surface finish produced by a turning operation relating to a single cutting tool. Firstly the surface roughness is due to the primary cutting edge and secondly the surface roughness due to the secondary cutting edge. The first usually refers to surface broaching and form turning. The second is conventional turning with a round-nosed tool. Fig. 2.8 shows the position of the cutting edges on a typical tool.

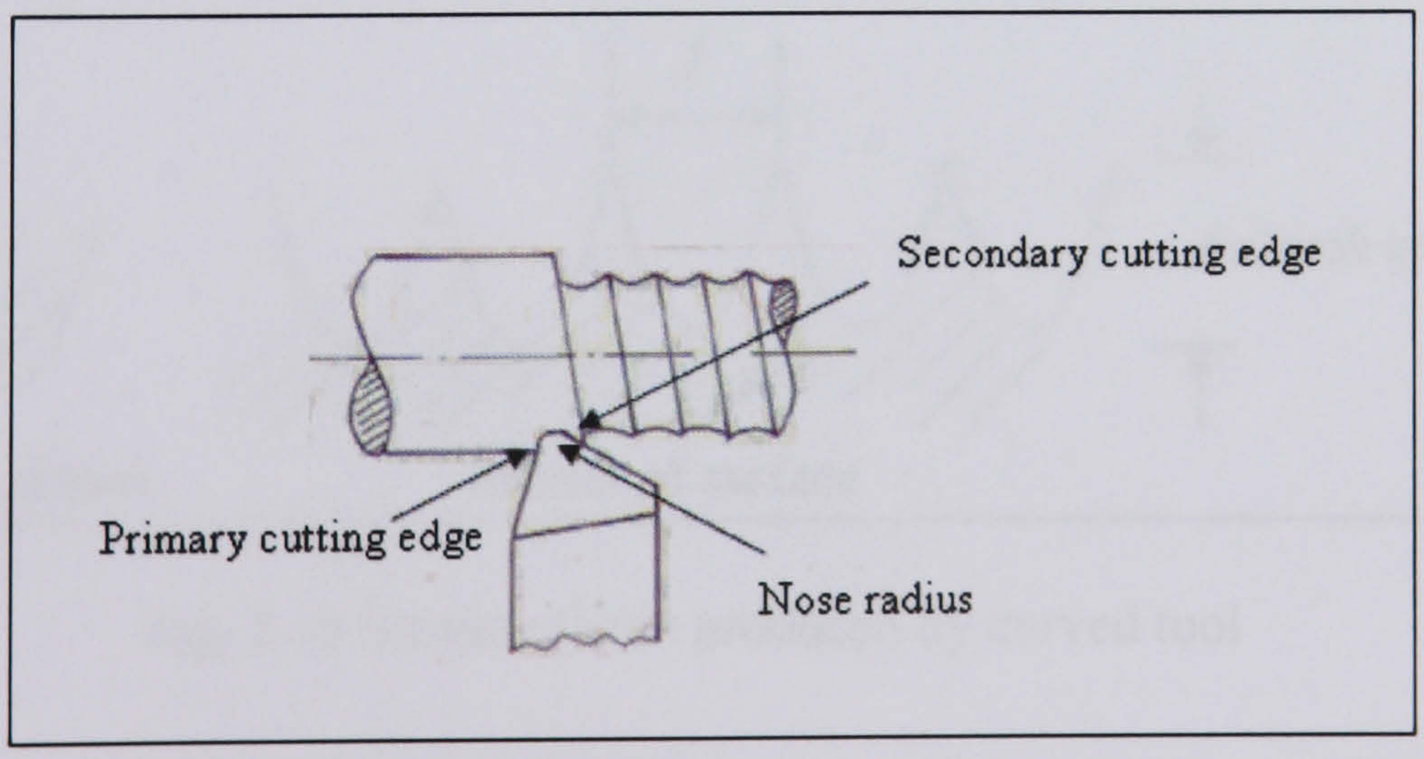

Fig. 2.8 Cutting tool with respect to the two cutting edges [4]

2.7 Effect of tool geometry

The tool could be thought of as a triangle. If f is the feed and d is the depth of cut, then there is

$$R_a = d/4 \qquad R_t = d \tag{2-6}$$

The surface texture is independent of the tool feed if the tool tip is perfectly triangular. Equation (2-6) does not involve f, the feed. However the triangular tip is hardly practical. It is more often used with a curved tip of radius R is as shown in Fig. 2.10. In this case the roughness, at least in principle, is a function of the feed.

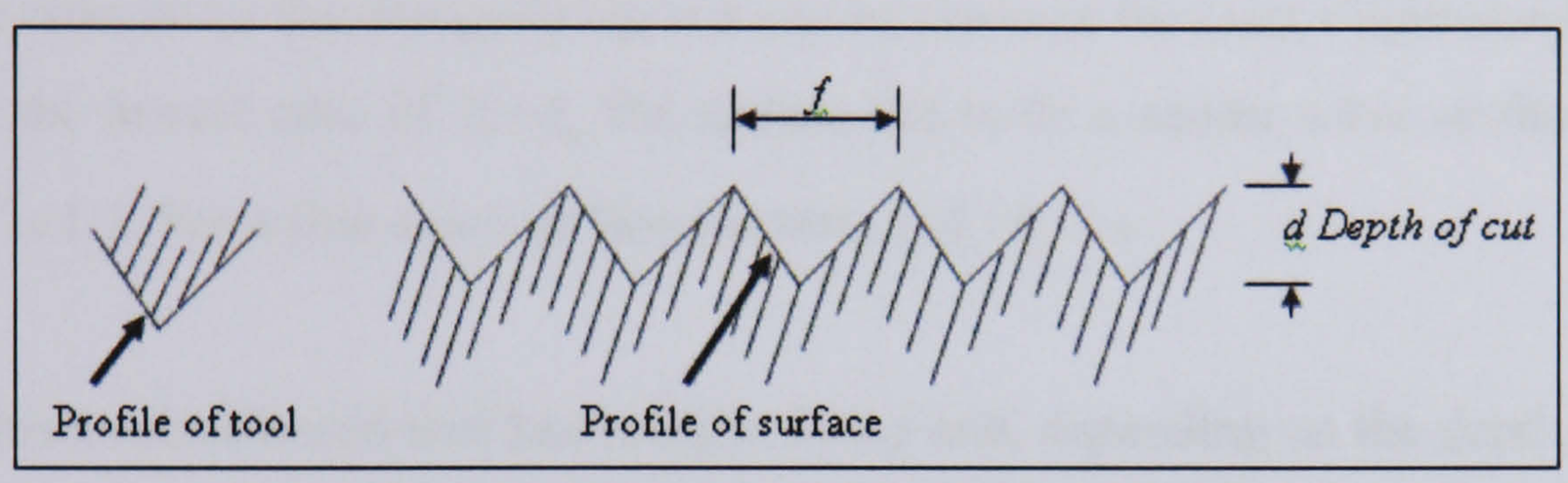

Fig. 2.9 Surface finish produce by a triangular tool

Assume that all the cutting takes place on the radius part of the tool as shown in the figure. The roughness can be given by

$$R_t = R - \sqrt{R^2 - f^2/4} = R(1 - \sqrt{1 - f^2/4R^2}) \tag{2-7}$$

for

$$f \le R \qquad R_t \approx f^2/8R \tag{2-8}$$

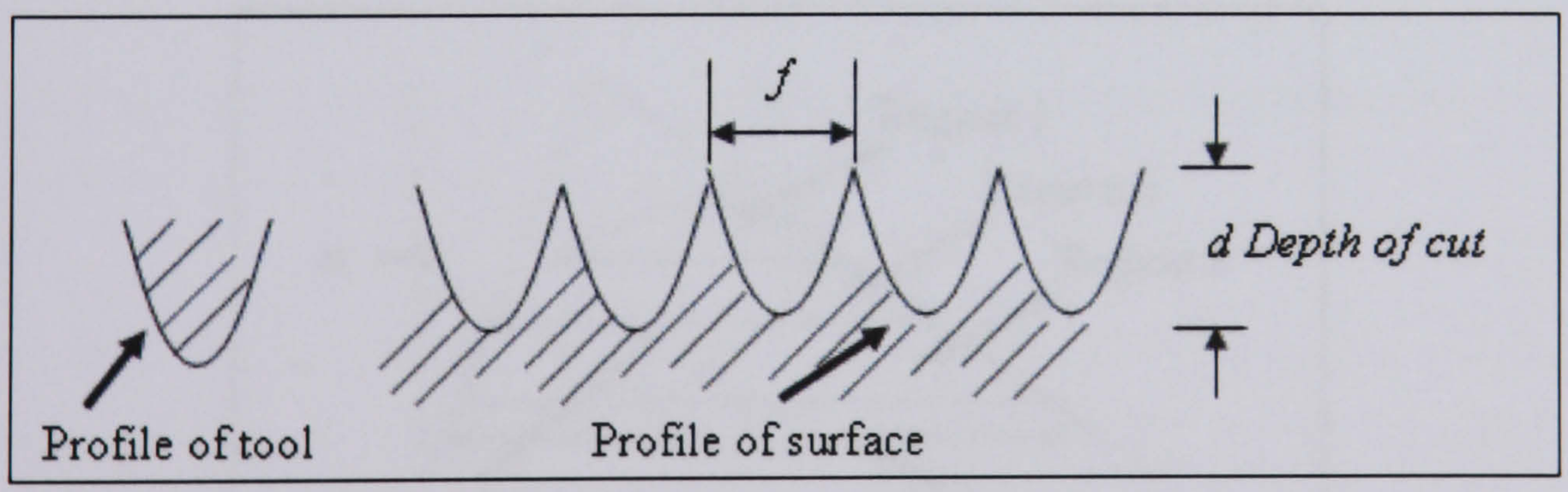

Fig. 2.10 Surface finish produced by curved tool

From (2-8) it can be found that for a given tool tip radius the surface roughness can be improved quite dramatically, simply by reducing the feed. In fact the roughness is

very much more sensitive to feed than it is to the tip radius. Before the R_a can be found, the mean line has to be established. This is obviously trivial in the case of the triangular tip; it is half way down the depth of cut. In the case of the curved tip it is $R_t/8$ from the bottom of the trough.

Using the mean line the R_a value is approximately

$$0.032f^2/R \qquad (2\text{-}9)$$

which is about one-quarter of the R_t value as can be seen from Equation (2.8). This is the same ratio as for the triangular tip and can be assumed for most single-shaped tool tips. For the lowest ratio of R_t/R_a the surface has to be a square wave surface; then the ratio is 1:1. For a sine wave surface the ratio is $R_t/R_a = \pi$.

Most often a round-nosed tool has straight flanks and, depending on the depth of cut, these flanks enter into the calculation of the theoretical surface roughness. Three conditions apply (Fig. 2.11):

(1) round nose only producing the surface (case I);

(2) round nose and straight edge in primary cutting position (case II);

(3) round noise and straight edge in primary cutting position and straight edge in secondary cutting position (case III).

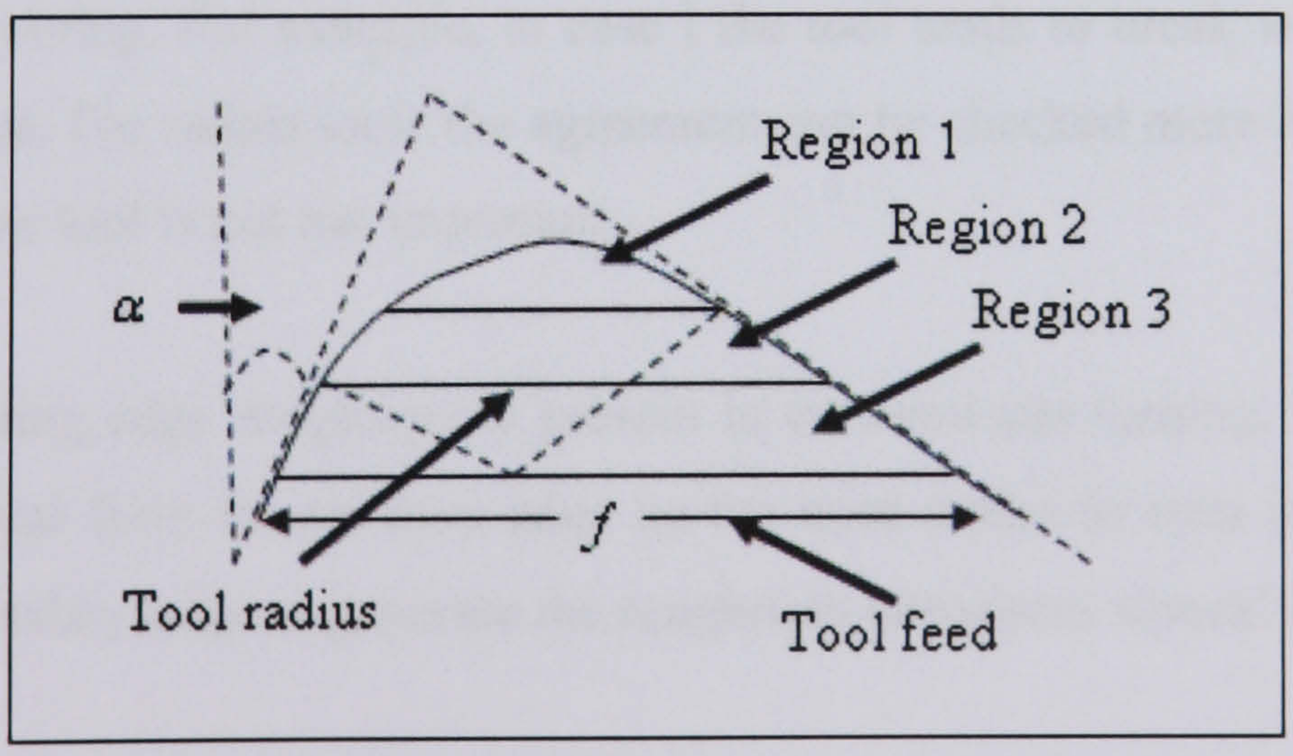

Fig. 2.11 Varied surface roughness produced by different regions

Thus in terms of the R and case I, there is [9]:

$$\frac{R_t}{R} = \frac{1}{8}\left(\frac{f}{R}\right)^2 \tag{2-10}$$

Equation (2-10) is the same as Equation (2.8). As more of the flank is included, the roughness ratio R_t / R becomes more involved [2], as seen in Equation (2-6) below. Thus for case II, there is [43]:

$$\frac{f}{R} = \left[2\frac{R_t}{R} - \left(\frac{R_t}{T}\right)^2\right]^{1/2} + \sin\beta + \left(\frac{R_t}{R} - 1 + \cos\beta\right)\cot\beta \tag{2-11}$$

which can be extended to the more general case as [43]:

$$\frac{R_t}{R} = \frac{f/R}{\tan\alpha + \cot\beta} - \frac{\cos(\frac{\pi}{4} - \frac{\alpha}{2} - \frac{\beta}{2})}{\sin(\frac{\pi}{4} + \frac{\alpha}{2} + \frac{\beta}{2})} \tag{2-12}$$

Equation (2-12) can be simplified to [43]:

$$\frac{R_t}{R} = \frac{f/R}{(\tan\alpha + \cot\beta)} \tag{2-13}$$

Obviously in this treatment R is a theoretical value of roughness determined by the geometrical aspects of the tool tip. In practice the texture will not be equal to this for a number of reasons including built-up edge. A definition of efficiency of cutting has been used in the past.

Checking the Equations against practical tests is very difficult if not impossible for conventional turning. For example, in case I the tool tends to break when it engages with the surface. For radius tools the agreement can be checked more readily because alignment of the tool is not too important.

Secondary cutting edge roughness is present in conventional turning. The secondary edge is separated from the primary edge by the nose radius as seen in Fig. 2.8. The use of the secondary edge to generate the roughness introduces several complications.

The most important ones are:

(1) The geometry of the tool at its nose is replicated in the surface at feed mark intervals.

(2) There is some uncertainty of the geometry of the cut at the trailing edge because the chip thickness goes gradually to a small value.

(3) The metal at the trailing edge of the tool is subjected to unusually high normal stress and tends to flow to the side in order to relieve this stress. This can produce a furrow which can contribute to the roughness, especially in the case of a soft ductile metal. In this case the tool profile is not properly replicated in the surface.

Surfaces generated by the secondary cutting edge are in general more complicated than those produced by a primary cutting edge. The surface roughness quoted is always taken as the maximum value. For the secondary edge, roughness is in the axial direction.

2.8 Turning processes

The turning process is simple for generating the main dimension of the part and, as the name implies, involves an axis of rotation somewhere in the generation. Figure 2.12 shows the turning modes.

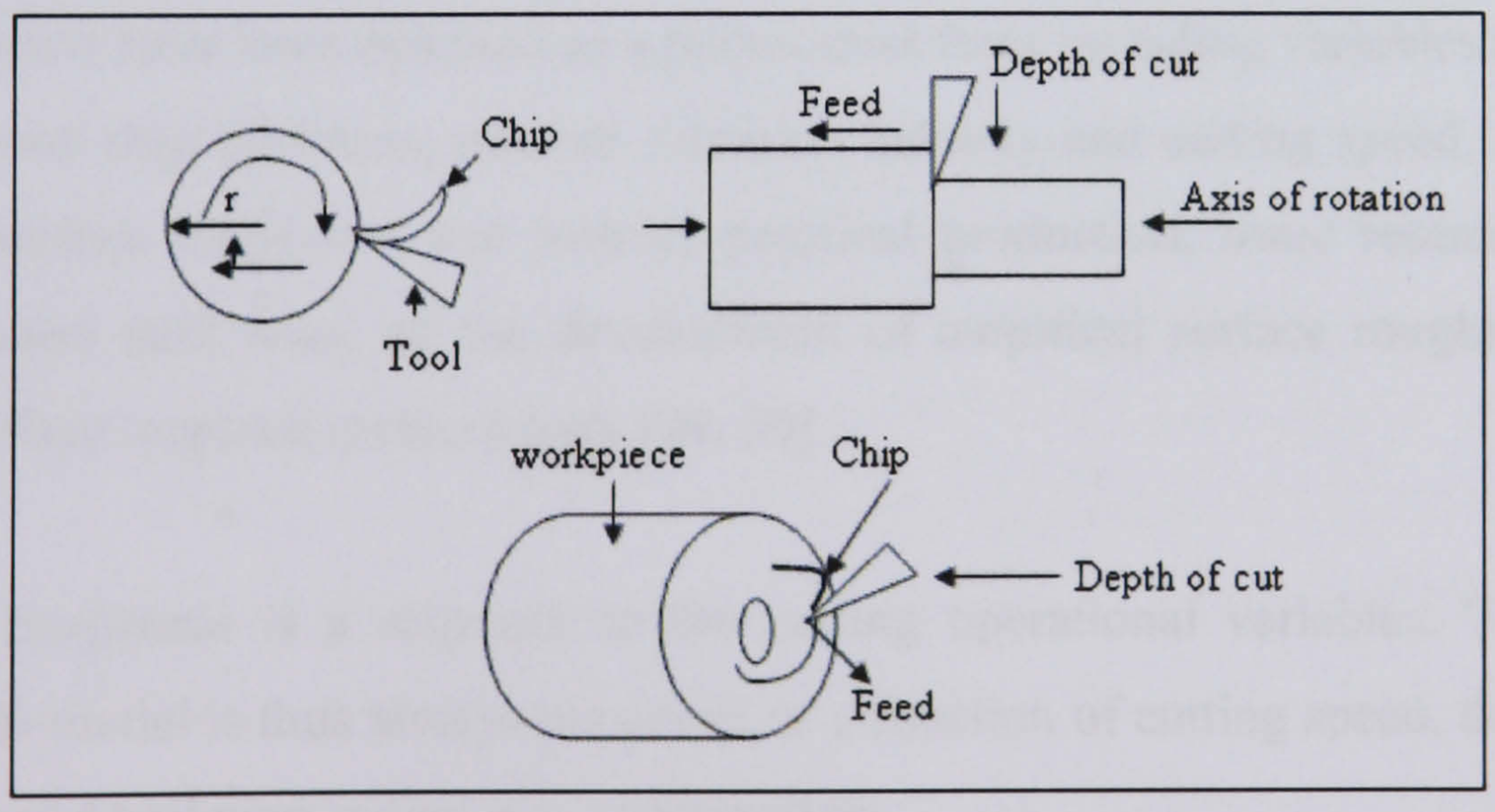

Fig. 2.12 Illustration of the turning modes

Typical variables are cutting speed, i.e. workpiece peripheral speed relative to the tool, axial feed-the advancement of the tool per revolution of the workpiece, the shape of the tool and the depth of cut of the tool into the workpiece material.

There are some features which are not shown on the diagrams but contribute a considerable difference to the form and surface roughness. These include the non existence of coolant and the effect of the machine tool itself. In general, the actual value of the roughness can be estimated at least roughly in terms of height and form from knowledge of the basic process parameters.

Normally as the turning process concerned, it is not often used for very fine finishing except in the case of diamond turning. It is a very practical process for removing material in order to manufacture the essential size and shape. As a common rule, the surface roughness has tendency to be too rough to be used in very critical applications in which high stresses could be damaging. But even so there are many applications where single-point machining is used because of the efficiency and flexibility of the process.

2.9 Modelling approach

In the early study of nonlinearities in metal cutting, the empirical approach has been used to predict the nonlinear cutting force by some researchers [17, 27, 28]. Cutting force models have been assumed as a polynomial form including variables such as the undeformed chip thickness, relative vibration velocity and cutting speed. In order to predict surface roughness and instruct practical production, some researchers have also focused their work on the development of empirical surface roughness model using surface response methodology [29, 30].

Surface roughness is a response to the cutting operational variables. The surface roughness model is thus always presented as a function of cutting speed, depth of cut, feed rate and tool nose radius, e.g. expressed as:

$$R_a = k_a V^{k_b} f^{k_c} d_c^{k_d} R_0^{k_e} \tag{2-13}$$

where k_a, k_b, k_c, k_d, k_e – constants.

To build up the empirical surface roughness model, a set of designed machining trials need to be carried out for acquiring the surface roughness data under different machining conditions. By some algorithms, such as the least squares method, first order regression or second order regression, the constants in the roughness model will be acquired. The surface response method can also be used to predict tool life and cutting force [31].

Another kind of empirical surface roughness model was built by Grzesik, based on the theoretical surface roughness model and tribological analysis of the strong adhesion at the tool rake face-chip interface [32].This simple empirical function would facilitate rapid data processing. However, the cost of machining experiments and the applicability of the model to the variation of machining conditions have limited the development of the approach. Although there is an effort to improve the applicability of the method by a reference-based model, the cost for obtaining the reference model is still very high, especially for precision machining [33].

A neural network is a kind of Artificial Intelligence method. It has been used in optimizing machining parameters [34-36]. Because the experimental data will be used to train the designed Neural Networks, it can be classified in the empirical approach category. The Neural Networks model has somewhat intelligence, so it is robust to some extent to the variation of machining conditions. The accuracy of this notifies that the term computer simulation is broader than computer modelling, which implies that all aspects are being modelled in the computer representation. However, computer simulation also includes generating inputs from simulated users to run actual computer software or equipment, with only part of the system being modelled an example would be flight simulators which can run machines as well as actual flight software.

2.10 Machining validation

Zygo Corporation is a special equipment manufacturer that specializes in optical systems and equipment for areas such as optical metrology. Zygo's metrology systems are based on optical interferometry measuring displacement, surface figure, and optical wave front. Metrology and optical markets for end-user and OEM applications include semiconductor capital equipment, aerospace, automotive, and research. Now in its fourth decade, Zygo Corporation leverages its core competencies in metrology and optics to serve a worldwide customer base. Recognized as a valued partner by its customers for its innovation, technology, and responsiveness, the Company assists these customers in becoming leaders in their respective markets.

In this research, a Zygo 3D surface profiler is substantially used for evaluation and validation of the models, simulation and the cutting trials.

2.11 Simulations

Traditionally, the formal modelling of systems has been via a mathematical model, which attempts to find analytical solutions to problems which enables the prediction of the behaviour of the system from a set of parameters and initial conditions.

While computer simulations might use some algorithms from purely mathematical models, computers can combine simulations with reality of actual events, such as generating input responses, to simulate test subjects who are no longer present. Whereas the missing test subjects are being modeled, the system they use could be the actual equipment, revealing performance limits or defects in long-term use by the simulated users.

2.12 Optimization and control

2.12.1 Introduction of neural network

An artificial neural network (ANN) is a mathematical model or computational model based on biological neural networks. It consists of an interconnected group of artificial neurons and processes information using a connectionist approach to

computation as shown in Fig. 2.13. In most cases an ANN is an adaptive system that changes its structure based on external or internal information that flows through the network during the learning phase. In more practical terms neural networks are non-linear statistical data modelling tools. They can be used to model complex relationships between inputs and outputs.

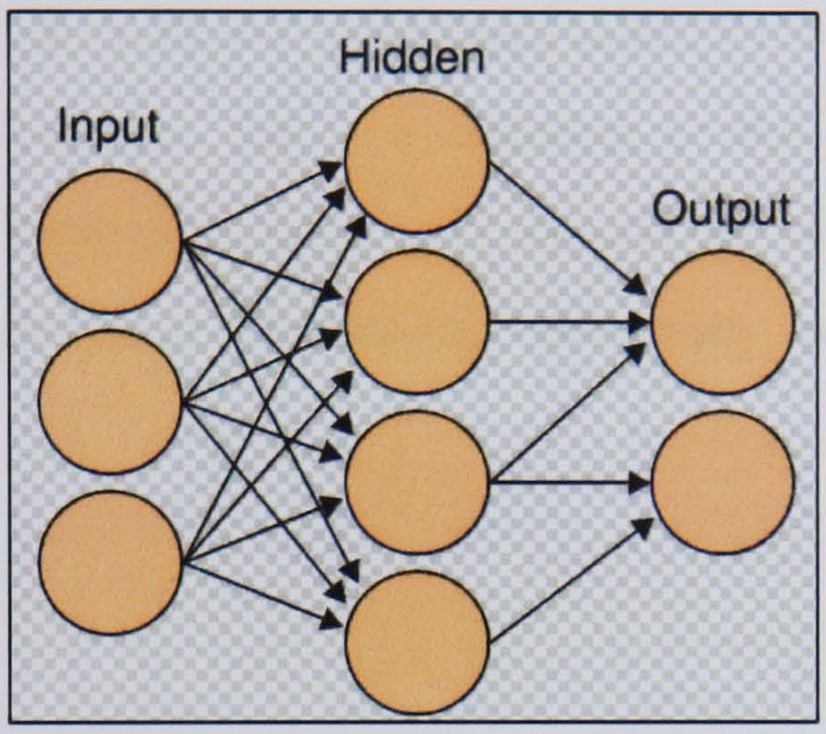

Fig. 2.13 Neural network structure

There is no precise agreed definition among researchers as to what a neural network is, but most would agree that it involves a network of simple processing elements (neurons), which can exhibit complex global behaviour, determined by the connections between the processing elements and element parameters. The original inspiration for the technique was from examination of the central nervous system and the neurons (and their axons, dendrites and synapses) which constitute one of its most significant information processing elements. In a neural network model, simple nodes (called variously "neurons", "neurodes", "processing elements" or "units") are connected together to form a network of nodes — hence the term "neural network." While a neural network does not have to be adaptive per sé, its practical use comes with algorithms designed to alter the strength (weights) of the connections in the network to produce a desired signal flow.

These networks are also similar to the biological neural networks in the sense that functions are performed collectively and in parallel by the units, rather than there being a clear delineation of subtasks to which various units are assigned. Currently, the term Artificial Neural Network (ANN) tends to refer mostly to neural network models employed in statistics, cognitive psychology and artificial intelligence.

In modern software implementations of artificial neural networks the approach inspired by biology has more or less been abandoned for a more practical approach based on statistics and signal processing. In some of these systems neural networks, or parts of neural networks (such as artificial neurons) are used as components in larger systems that combine both adaptive and non-adaptive elements. While the more general approach of such adaptive systems is more suitable for real-world problem solving, it has far less to do with the traditional artificial intelligence connectionist models. What they do, however, have in common is the principle of non-linear, distributed, parallel and local processing and adaptation, which is suit well to the complex scenario of precision machining processes and associated surface generations.

2.12.2 ANOVA

As first suggested by Conover and Iman in 1981 [37], in many cases when the data does not meet the assumptions of ANOVA (analysis of variance), one can replace each original data value by its rank from 1 for the smallest to N for the largest, then run a standard ANOVA calculation on the rank-transformed data. Where no equivalent nonparametric methods have yet been developed such as for the two-way design, rank transformation results in tests are more robust to non-normality, and resistant to outliers and non-constant variance, than ANOVA without the transformation. A variant of rank-transformation is 'quantile normalization' in which a further transformation is applied to the ranks such that the resulting values have some defined distribution (often a normal distribution with a specified mean and variance). Further analyses of quantile-normalized data may then assume the distribution to compute significance values [37- 40].

2.13 Conclusion

This chapter has presented a review of research on surface functionality, modelling, simulation, control and optimisation. From this review, it was found that each method has its own advantages and disadvantages in investigation area. The analysis has

shown the main features of metal cutting in millimetre and micrometre scales. However, it cannot predict the details of some local stress and strain. But, it suffers from less computational power. Empirical approach in precision machining shows that it is simple but involves high cost. It may be helpful to model some intermediate phenomenon, such as wear. Surface functionality simulation is used to study the turning mechanism. However, it also suffers from the limitation of computational power.

It is important to investigate theoretical analysis, empirical approach and simulation in a comprehensive and analytical way so as to utilize their individual advantages. The scope of the investigation will include the cutting actions between the workpiece and cutting tool at three aspects including, the turning process, machine tool structure and the nonlinear effects and to acquire quick simulations with acceptable accuracy.

Chapter 3 Characterizations of high precision machined surfaces

3.1 Introduction

The properties and performance of engineering products such as friction, sealing, lubricant retention, load bearing capacity are related to their component surfaces. Therefore, the assessment of the product performance of the product is essential to check the dimensional accuracy and surface quality of the comprised component.

During the machining process, the surface is only generated at the end stage of the machining. The surface consists of roughness, waviness and topography resulted from the effect of the cutting tool, the deflection of the machine tool or workpiece, vibrations, chatters, the flexibility of the machine or workpiece, the error in the slideway, etc. all will leave their signature marks on the machined surface. For the process control of the machined surface generation, all the information can be used as control parameters in order to get the achieved surface target. From the discussion and exploration presented in this chapter, it is clearly evident that the surface characterization can be used to control the machining process and thus ensure the desired component performance.

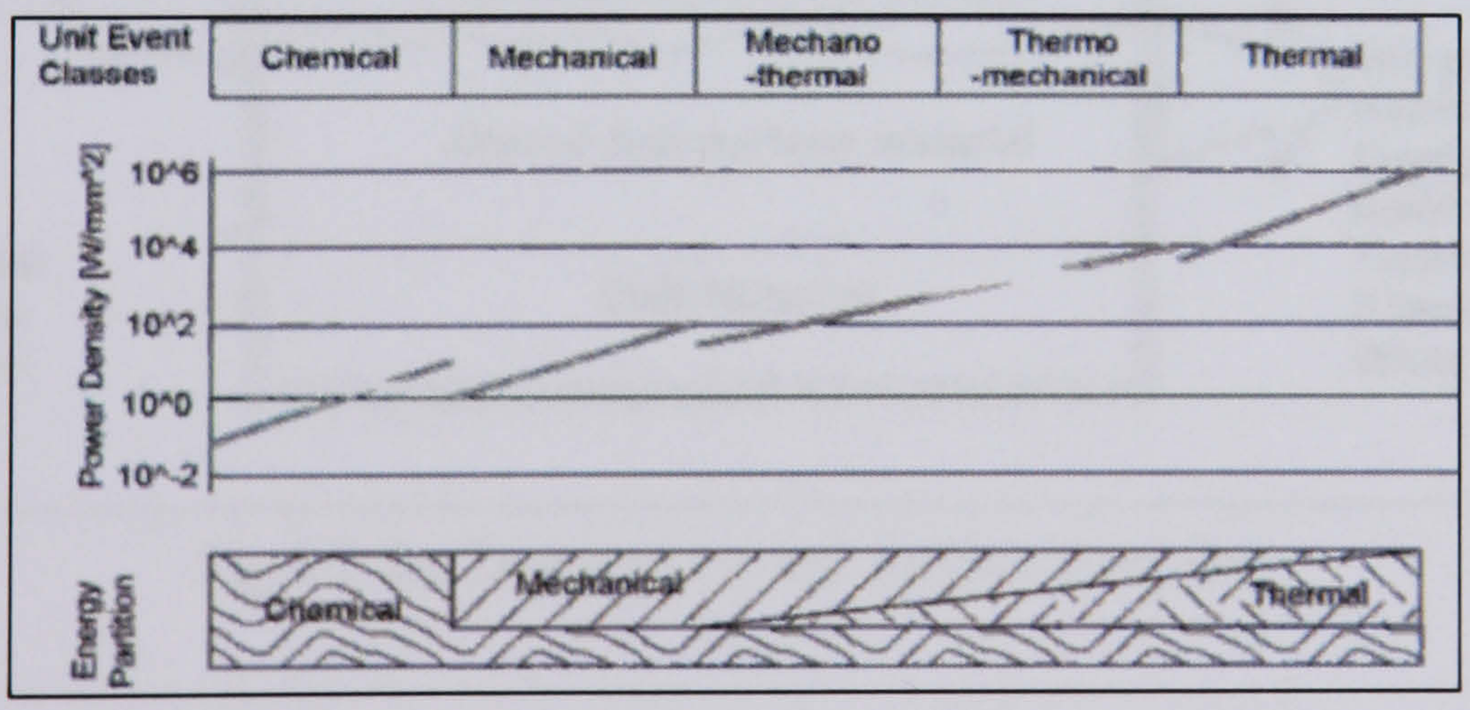

Fig. 3.1 Manufacturing stage process [68]

It is also found that all the effective factors are in need of each other for the required functional behaviour of the machined surface and the surface characterization. Furthermore, of factors such as topography, metallographic, chemical composition, and residual stress interact, and all together accomplish the surface behaviour as illustrated in Fig. 3.1 [41, 42].

In this chapter, the characterizations of surfaces are formulated. This formulation aims to bridge the gaps among the surface characterization, surface functionality and machining process. This chapter also presents the surface functionality in a generic form, with some characterization parameters proposed particularly for the surface functionality.

3.2 Characterization of machined surfaces

In the engineering surface, it can be categorized into two types which are surface integrity and surface texture as shown in Fig. 3.2. Generally, the surface integrity has much focus on the physical condition of the surface, whereas the surface texture represents the geometric properties of the surface.

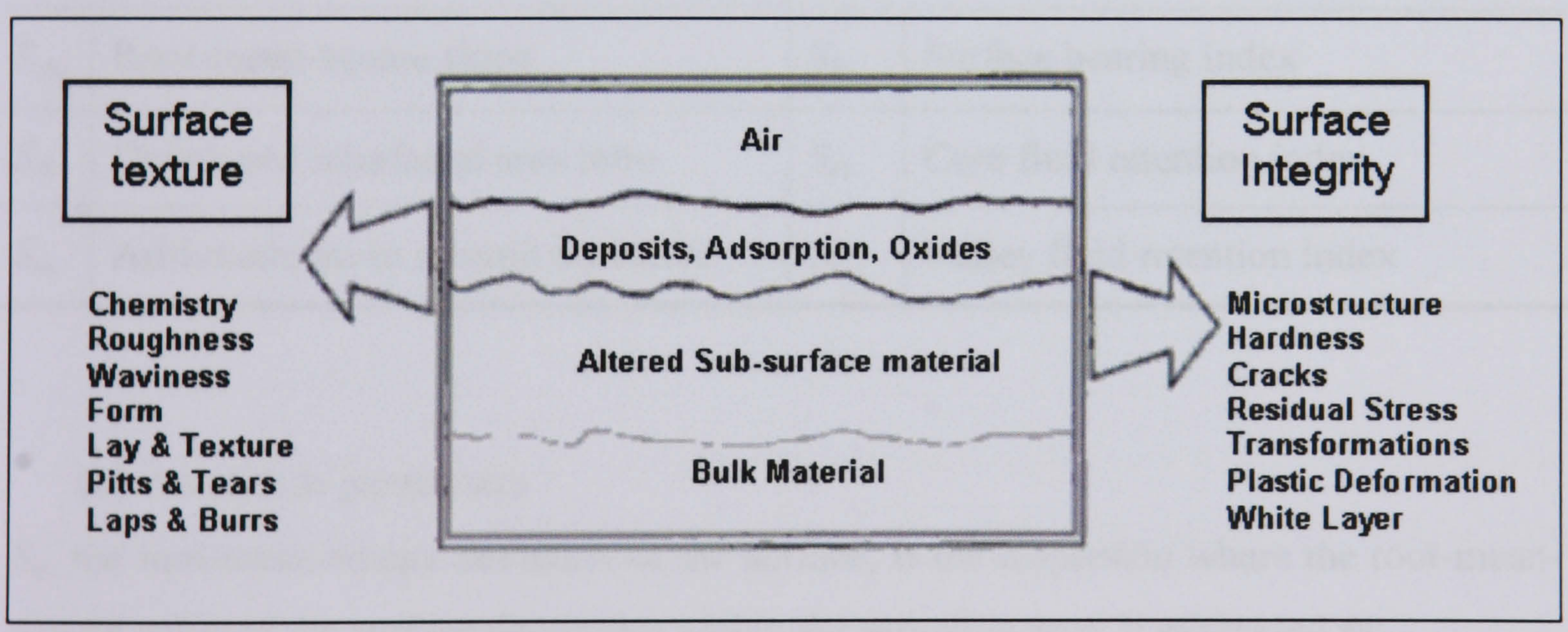

Fig.3.2 Surface texture and surface integrity.

3.2.1 3D characterization parameters for surface texture

Nowadays, so many instruments with the powerful support from hardware and software of data acquisition, manipulation and visualization functions have been developed.

However the international standard for 3D surface texture measurement is still not covered yet.

Professor Stout et al. have proposed fourteen 3D parameters in the research carried out within an European program [43]. These parameters are indicated by "*S*" instead of "*R*" calculated over a surface. They have been classified into the four categories and list in Table 3.1

Table 3.1 Parameters for characterizing 3D surface topography [43]

Amplitude Parameters		**Spatial Parameters**	
S_q	Root-mean-square deviation	S_{ds}	Density of summits
S_z	Ten point height	S_{tr}	Surface texture aspect ratio
S_{sk}	Skewness of height distribution	S_{al}	Fastest decay autocorrelation length
S_{ku}	Kurtosis of height distribution	S_{td}	Texture direction
Hybrid Parameters		**Functional Parameters**	
$S_{\Delta q}$	Root-mean-square slope	S_{bi}	Surface bearing index
S_{dr}	Developed interfacial area ratio	S_{ci}	Core fluid retention index
S_{sc}	Arithmetic mean summit curvature	S_{vi}	Valley fluid retention index

(1) Amplitude parameters

S_q, the root-mean-square deviation of the surface, is the dispersion where the root-mean-square value of the surface departures within the sampling area. It expressed as:

$$S_q = \sqrt{\frac{1}{MN}\sum_{j=1}^{N}\sum_{i=1}^{M}\eta_r{}^2(x_i, y_j)} \tag{3-1}$$

M, *N* – sampling numbers in the X and Y directions within the sampling, area, respectively;

i, j – corresponding index of the sampling points;

η_r – residual surface.

Ten point height of the surface is an extreme parameter defined as the average value of the absolute height of the five highest peaks and the depths of the five deepest pits or valleys within the sampling area. It can be expressed as:

$$S_z = \frac{\sum_{l=1}^{5}\left|\eta_{pl}\right| + \sum_{l=1}^{5}\left|\eta_{vl}\right|}{5} \qquad (l = 1, 2, \ldots, 5) \tag{3-2}$$

η_{pl} , η_{vl} - the five highest surface summits and lowest surface valleys respectively.

Skewness of the topography height distribution is the measure of asymmetry of surface deviations about the mean plane. It is given by:

$$S_{sk} = \frac{1}{MNS_q^3}\sum_{j=1}^{N}\sum_{i=1}^{M}\eta^3(x_i, y_j) \quad (i = 1, 2, \ldots, M)\ (j=1, 2, \ldots, N) \tag{3-3}$$

Kurtosis of the topography height distribution is a measure of the peakness or sharpness of the surface height distribution. It is described as:

$$S_{ku} = \frac{1}{MNS_q^4}\sum_{j=1}^{N}\sum_{i=1}^{M}\eta^4(x_i, y_j) \quad (i = 1, 2, \ldots, M)\ (j=1, 2, \ldots, N) \tag{3-4}$$

(2) Spatial parameters

The spatial parameters are used to describe the spatial property of the surfaces. Density of summits of the surface is the number of summits of a unit sampling area. It is described as:

$$S_{ds} = \frac{\text{Number of summits}}{(M-1)(N-1)\cdot\Delta x\cdot\Delta y} \tag{3-5}$$

Δx, Δy - deviation length.

Three spatial parameters are devised for surface characterisation. These are based on the normalised area autocorrelation function (AACF) and the area power spectrum density (APSD).

S_{tr}, texture aspect ratio of the surface, is the ratio between the distance where the fastest AACF decay is 0.2 in any direction and the same function has the slowest distance decay 0.2 in any direction. It is used to identify the texture pattern such as the uniform texture aspect. S_{al}, fastest autocorrelation length decay is the distance AACF has the fastest decay to 0.2 in any direction. S_{td}, is texture direction for angle measuring of direction for surface texture with respect to the y axis. S_{td}, is used to determine the surface lay direction.

(3) Hybrid Parameters

The hybrid property is a combination of amplitude and spacing. Any changes which occur in either amplitude or spacing may have an effect on the hybrid property. $S_{\Delta q}$ Root-mean-square slope of the surface, is the root-mean-square value of the surface slope within the sampling area.

$$S_{\Delta q} = \sqrt{\frac{1}{(M-1)(N-1)} \sum_{j=2}^{N} \sum_{i=2}^{M} [(\frac{\eta(x_i, y_j) - \eta(x_{i-1}, y_j)}{\Delta x})^2 + (\frac{\eta(x_i, y_j) - \eta(x_i, y_{j-1})}{\Delta y})^2]} \quad (3\text{-}6)$$

S_{sc}, is defined as the average of the principle curvature of the summits within the sampling area. It is expressed as:

$$S_{sc} = -\frac{1}{2} \cdot \frac{1}{n} \sum_{k=1}^{n} (\frac{\eta(x_{p+1}, y_q) + \eta(x_{p-1}, y_q) - 2\eta(x_p, y_q)}{\Delta x^2} + \frac{\eta(x_p, y_{q+1}) + \eta(x_p . y_{q-1}) - 2\eta(x_p, y_q)}{\Delta y^2}) \quad (3\text{-}7)$$

Hybrid parameter is the developed interfacial area ratio, i.e. the ratio of the increment of the interfacial area of a surface over the sampling area. It is given as:

$$S_{dr} = \frac{\sum_{j=1}^{N-1}\sum_{i=1}^{M-1} C_{ij} - (M-1)(N-1)\Delta x \cdot \Delta y}{(M-1)(N-1)\Delta x \cdot \Delta y} \cdot 100\% \tag{3-8}$$

C_{ij} – the interfacial area of the smallest sampling quadrilateral.

(4) Functional parameters

A large surface bearing index indicates a good bearing property. Surface bearing index is the ratio of the RMS deviation over the surface height at 5% bearing area, which is:

$$S_{bi} = \frac{S_q}{\eta_{0.05}} \tag{3-9}$$

$\eta_{0.05}$ – surface height at 5% bearing area.

Core fluid retention index is the ratio of the void volume of the unit sampling area at the core zone over the RMS deviation, i.e. it is:

$$S_{ci} = \frac{(\frac{V_v(h_{0.05)} - V_v(h_{0.8})}{(M-1)(N-1)\cdot\Delta x \cdot \Delta y})}{S_q} \tag{3-10}$$

A bigger S_{ci} indicates a good fluid retention in the core zone.

Valley fluid retention index is the ratio of the void volume of the unit sampling area at the valley zone over the RMS deviation, which can be expressed as:

$$S_{vi} = \frac{(\frac{V_v(h_{0.8})}{(M-1)(N-1)\cdot\Delta x \cdot \Delta y})}{S_q} \tag{3-11}$$

A larger S_{vi} indicates a good fluid retention in the valley zone.

Generally speaking, there is a lack of the exhaustive experimental documentation for these parameters, which however represent the state-of-the-art in 3D parameters standardisation and most of the parameters are derived from the 2D parameters [44]. Some researchers have used some novel numerical analysis methods, such as Fourier

transform [45], fractal [46], wavelet [47] and hybrid fractal-wavelet [48] to characterize the 3D surface topography. Hybrid fractal-wavelet is the best suitable method to characterize tribological surfaces because it can address the multi-scale and non-stationary nature of tribological surfaces [49]. The characterization of surface functionality becomes difficult because of the failure of classification strategy with regard to the product performance term. Unfortunately there is no international standard that can be used as a guide to determine what the surface integrity is although there have been so many research that has been done.

3.3 Machining system analysis

Modern experimental analysis techniques have been reviewed by Schwarz and Richardson [76], in which the three main topics pertaining to modal testing was covered, i.e. on Frequency Response Function (FRF) measurement techniques, excitation techniques, parameter estimation (curve fining) methods. Modal testing is used as a simple and efficient means, for characterizing resonant vibrations. The majority of structures can be made to resonate under the proper conditions. A structure can be made to vibrate with excessive, sustained or oscillatory motion. Modes or resonances are inherent properties of a structure where resonances are determined by the mass, stiffness, and damping properties, and boundary conditions of the structure. Each mode is defined by a natural frequency, modal damping, and a mode shape.

Schwarz and Richardson explained [76], if either the material properties or the boundary conditions of a structure change, its modes will change. The forces, which can be considered as the sum of steady, harmonic and random forces, act on the cutting tool and contribute to the modification of the dynamic response of the tool, by affecting its stiffness and damping. The focuses are on the collection and analysis of the data of cutting-force, tool-vibration and tool-modal parameter, generated by dry turning of mild carbon steel samples at different speeds, feeds, depths of cut, tool nose radii, tool lengths and workpiece lengths. Furthermore, this investigates the effect of each cutting parameter

on tool stiffness and damping, and yields an empirical model for predicting the behaviour of the tool stiffness variation.

Thomas and Beauchamp [77] have also mentioned that surface roughness does not depend solely on the feed rate, the tool nose radius and cutting speed; but can be deteriorated by excessive tool vibrations, the built-up edge, the friction of the cut surface against the tool point, and the embedding particles of the materials being machined.

Tool vibrations have been described to affect surface profiles in microscopic level and in the form of flutes number, orientation, and spacing, as determined by the integer and fraction of the frequency ratio of the tool vibration to the spindle speed by Kim et al. [80]. They have also proposed a metrological scheme to identify any existence of tool vibrations with a minimum effort of surface measurement and analysis. As a systematic approach to identify the tool frequency from measured surface profiles, they have proposed two methods of spiral and radial-circumferential analysis using microscopic surface profile data obtained by phase measuring interferometry [80]. Concluded from [81], the computer simulation and experimental results have proved that their approach is capable of identifying any existence of tool vibration with a minimum effort of surface measurement and analysis.

Cho and Eman [79] have proposed a work study in solving the main problems associated with the in-process identification of the instantaneous dynamics of a machining system. The main problems of that are related to the time variant nature of the process and the three dimensionality of the system, which leads to complex analytical procedures and both are closely associated with the experimental difficulties. During the cutting experiments, the parameters of the machining process changes due to factors.

This in turn imposes the requirement for the identification of the instantaneous dynamics, relatively short data records must be used during which the system may be considered time invariant concluded that the three dimensional closed loop dynamics was formulated

in the form of a multi-variate time series model whose parameters can be estimated from relative displacements and force components measured under actual cutting conditions.

3.4 Surface integrity

Rao and Shunmugam [60] have elaborated that any metal-cutting process, the material is subject to plastic deformation, work hardening and heating of the surface layer so that the resulting geometrical form has certain physical properties. They also added that a definite relationship exists between the machining process employed and the functional characteristics of the component probably in terms of friction, wear, and load-carrying capacity, etc. Griffiths [61] has presented a description of surface integrity with its two divisions of topography and metallurgy. The functional and performance factors are affected by surface integrity. However, a large proportion of the industry still only specifies surface finish on drawings and it is on such surface parameters as Rr and Rq, that quality assurance is based.

Surface integrity, also defined by Chevrier et al. [62] as a measure of the quality of a machined surface and is interpreted as an element that describes the actual structure of both surface and subsurface. The main objective is to obtain the best quality of machined surface, which depends on roughness, microhardness, residual stresses and material microstructure, but without neglecting productivity and workpiece cost. These characteristic parameters cover the crucial features that determine surface functionality. For instance, microhardness is responsible for the durability of the surface and its resistant to wear, and plastic and elastic deformation.

Cheng, et al. take account of surface integrity as the surface properties affecting the functional performance of the product. They include surface roughness, microhardness, microstructure, residual stress and fatigue. These characteristics will determine the product performance. For instance, the residual stress has the effect on enhancing the wear and fatigue properties of the surface and improving the resistance to stress

corrosion. On the other hand, Tönshoff and Brinksmeier measured microhardness and residual stress to further quantity their effects [50, 51].

Lonardo et al. addressed characterization of the surface microtopography [52] and Vorburger et al. presented the uses of STM and AFM [55]. Lucca summarized a variety of techniques employed for the characterization of surface and subsurface integrity. A review paper in 1998 [54]. Field and Kahles firstly coined "surface integrity" in 1964 when they analysed the principal causes of the defects of critical components and the surface integrity is defined as "the inherent or enhanced condition of a surface produced in a machining or other surface generating operation". Surface integrity includes the changes of surface alterations including mechanical, metallurgical and chemical aspect, etc. These changes may limit component quality or render the component useless [49].

3.5 Surface functionality

The surface functionality definition is different from the surface's operational performance. If translational surfaces are used, the tribological functionality will become dominant. Whitehouse [57] proposed a novel function map to express the function classification. It is classified according to the normal gap between two surfaces and their lateral movement. The function map lays its foundation for the classification of surface function. The joint stiffness, contact and adhesion functionality will behave significantly for static contact surfaces; finishing, reflective or hygiene functionalities are important for some non-contact surfaces, such as optical mirrors and precision lenses. Nevertheless, for some MEMS products, some special functional surfaces, such as anti-reflection, light distribution or self-cleaning will be required [56]. Therefore, the definition of the surface functionality should be acquired from the real working condition in which the product is in use. Based on the tribological mechanism, the generic term of surface functionality an express as:

$$S_F = B_{sf}(W, Vc) + \lambda(l, E, T, h_m, SP) \tag{3-12}$$

S_F – surface functionality;

B_{sf} – a functional stands for the basic function of the component;

W– the product working distance;

Vc – working lateral velocity of the component;

λ– modification function;

l– working load;

E – environment pressure;

h_m – humidity index of the working environment;

SP – surface form parameter(s).

The modification functional λ is used to express the modification for the basic function because the surface functionalities are related to the system working environment. The surface form parameter(s) SP represents the form features of the product, such as cylindricity. The working distance W can vary from minus value or positive value, to infinity, which will stand for the plastic contact, elastic contact and light scatter respectively.

The environment pressure, working temperature and air dampness will change the product function. The formulation indicates the potential of such an approach. The correct functionality of a product can therefore be determined easily by this approach and formulation.

Surface functionality – the surface functionality should be acquired from the real working condition in which the product is in use

Surface function – the application of a workpiece surface.

Surface texture – the geometry imparted

Surface integrity – properties taken sometimes to mean ohysical and geometrical properties.

Surface roughness – Irregularities in the surface texture which are inherent in manufacturing process but excluding waviness and errors of form

Surface topography – the study of surface feature

Surface parameter - surface feature to be quatified

3.6 Residual stress

Griffiths [68] has stated that as a result of the unit event generating mechanisms, a surface can often be left in a stressed state after machining. Residual stresses in a structural material or component exist without the application of external load or other source of stress, such as thermal gradients. The causes of residual stress can be found in Park et al. article [69] where it has mentioned that manufacturing and fabrication processes such as casting, welding, machining, moulding, heat treatment are having the most common causes for residual stress. Futhermore, in-service repair or modification is also a common cause of the residual stress, albeit residual stress may also be induced later in the life of the structure. Compressive residual stresses are to be preferred since they will reduce externally applied tensile stresses and tend to close surface cracks. The formation of tensile residual stress may result in initiation of fatigue cracks, stress corrosion cracking, or other types of fracture [68]. According to Park et al. [69], residual stress state consists of two types which are the macro and microstresses. Macrostresses are those residual stresses which are in equilibrium within macro domains, covering volumes comparable in size to the part; and they concur with the concept of isotropic material. Macrostresses are the most commonly studied as they can affect the service performance of a component. Microstresses on the other hand, are crystal stresses within single metal grains or groups of grains in equilibrium within volumes comparable with dimensions of the grains. These include submicroscopic stresses which are related to distortions in atomic lattices of crystals. They tend to occur in multiphase alloys and composites due to differences in thermal expansion on coefficients between phases.

The measurement techniques of residual stress have been reviewed by Withers and Bhadeshia [70] where some of the measurement techniques are destructive, while others can be used without significantly altering the component. Some have excellent spatial

resolution, whereas others are restricted to near-surface stresses or to specific classes of material. More work in this can be found in [71, 72, 73, 74].

3.7 Conclusions

This chapter focuses more on characterisations of 3D surface texture, surface integrity and critical review of the characterisation techniques. Surface functionality is important topic for the characterisation of high precision machined surfaces. The surface functionality can be expressed in the generic form of a versatile formulation. The characterisation parameters for high machined surfaces are categorized to match the surface functionality, which will be further discussed in Chapter 4 and 5.

Chapter 4 Modelling on the surfaces generation in precision turning processes

4.1 Introduction

The equation of turning processes is not taking into account any machining errors. In fact the factors from the dynamic cutting process, machine tool motions errors and environmental disturbances, will result in structural deformation and motion errors of the machine tool and cutting tool, and lead the tool path to deviate from the ideal tool path. For example, deformation of the machine tool structure under the action of dynamic cutting forces will deflect the cutting tool; the linear alignment error of the slideway will make the motion of the cutting tool away from the designed tool path. Environmental vibrations, even a fluctuation in temperature, can contribute to the deviation of the tool path as well. The calculation of the real tool path becomes the critical part in the modelling approach since the accuracy of the generated surface is largely determined by the relative motions between the cutting tool edge and the workpiece surface on a machine tool as proved by Lee and Cheung's studies [58, 59]. Nevertheless, the tool edge quality is another important factor.

A systematic modelling needs to identify the affecting factors and to model those factors which will contribute to the surface generation. Those factors will be the inputs to the process model. The cutting mechanics and cutting dynamics model, machine tool dynamics model will be integrated into the process model. The outputs will include 3D surface topography, characterization parameters and surface integrity parameters as shown in Fig. 4.1. Surface function according the application function scenario.

To generate the surface, the complex material removal process will take place. The material removal processes have four factors which affect the result. They are the machine tool, cutting tool, workpiece material properties and operation conditions. This chapter will cover all the modelling that can be used to analytically predict the

surface generation, instead of investigation on the four main factors above. This chapter also discusses how the modelling approach is systematically developed.

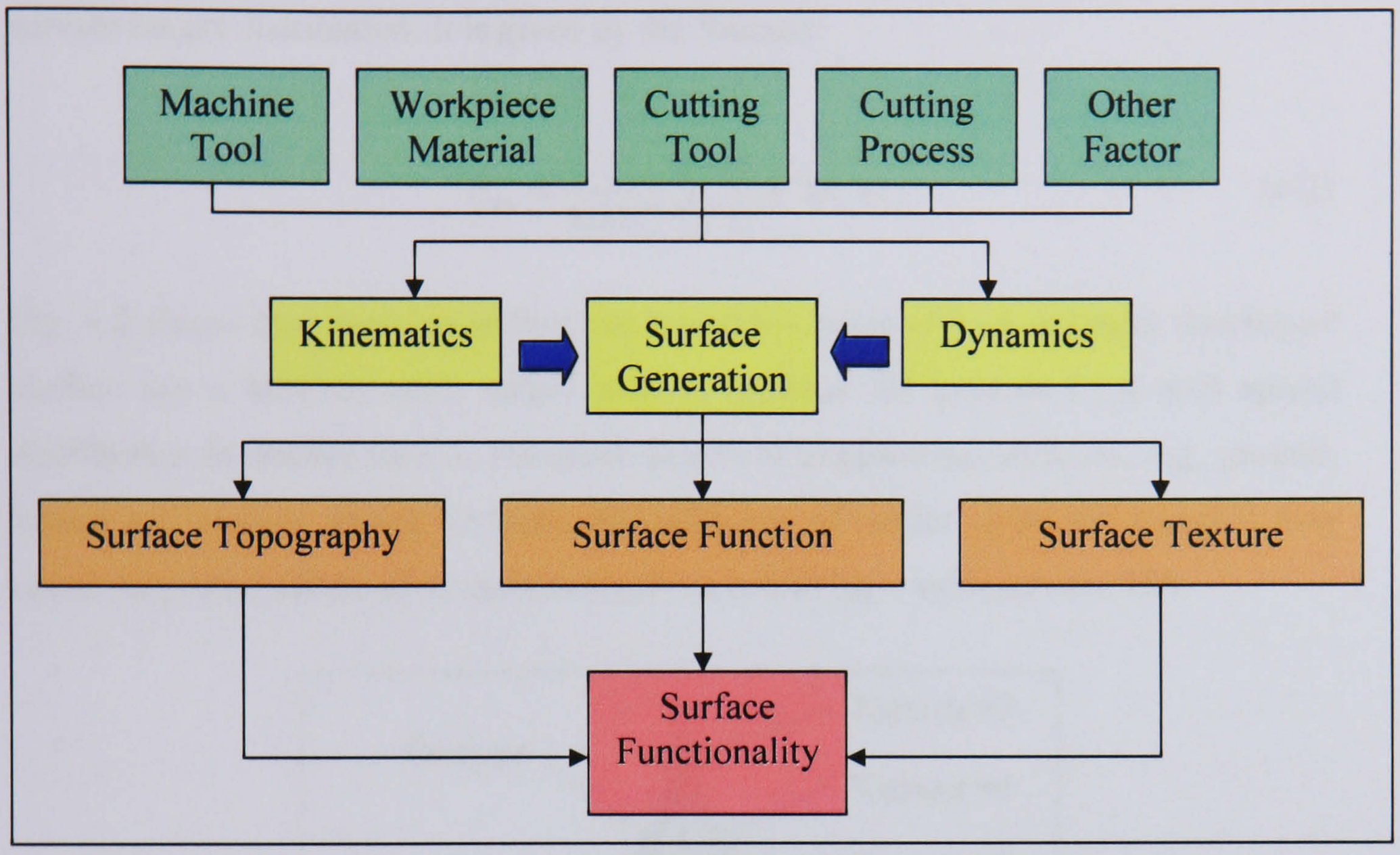

Fig. 4.1 Flow chart of the modelling approach

4.2 A proposed modelling approach

This research focuses on 3D surface functionality where five modelling elements are needed to form the modelling approach and they are tooling geometry, 3D kurtosis (*Sku*) modelling, machine parameter modelling, operation condition modelling and surface functionality modelling. The equation below shows the modelling approach representing the surface functionality:

$$Sfc \approx Function\ (Ct + Mc) \tag{4-1}$$

Sfc - *Sku* parameters;

Ct - Cutting tool;

Mc - Machine condition.

Sfc is a straight forward *Sku* parameter used to describe and evaluate the machined surfaces in terms of the surface contact functionality. *Sku* is the mean for Kurtosis of Topography Height Distribution. This is a measure of the peakness or sharpness of the surface height distribution. It is given by the formula:

$$S_{ku} = \frac{1}{MNS_q^4} \sum_{j=1}^{N} \sum_{i=1}^{M} \eta^4(x_i, y_j) \qquad (4\text{-}2)$$

Fig. 4.2 shows the Gaussian surface has a kurtosis value of 3. A centrally distributed surface has a kurtosis value larger than 3, whereas the kurtosis of a well spread distribution is smaller than 3. For some practical engineering surfaces, e.g. ground, honed and plateau honed surfaces, the existence of outliers (pits and troughs) may cause very large values of kurtosis, sometimes achieving a value of over 100.

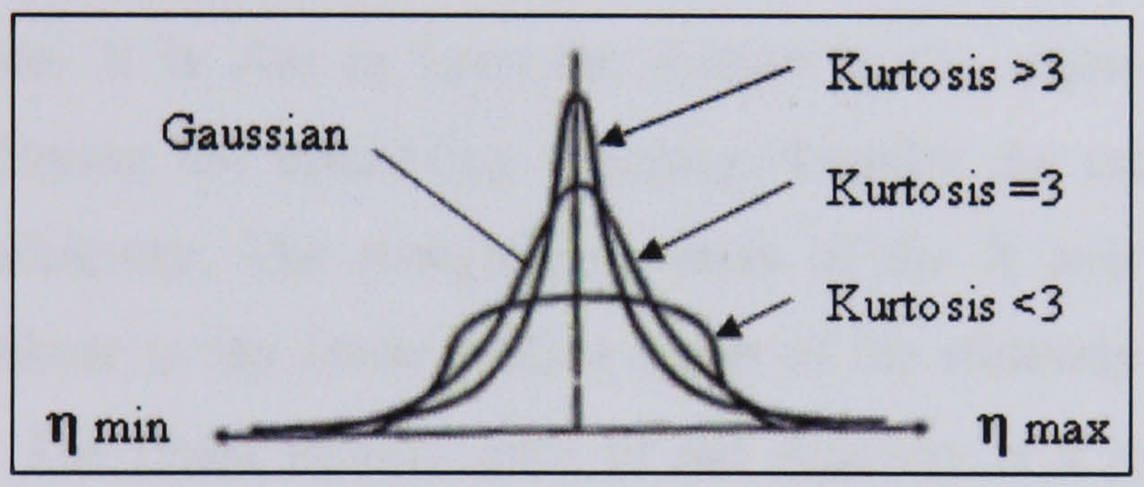

Fig. 4.2 Kurtosis of surfaces

Ct represents the cutting tool details including nose radius, initial side rake angle, side clearance angle, back rake angle and back clearance angle. *Mc* or machine condition is related with the machine operation during the process.

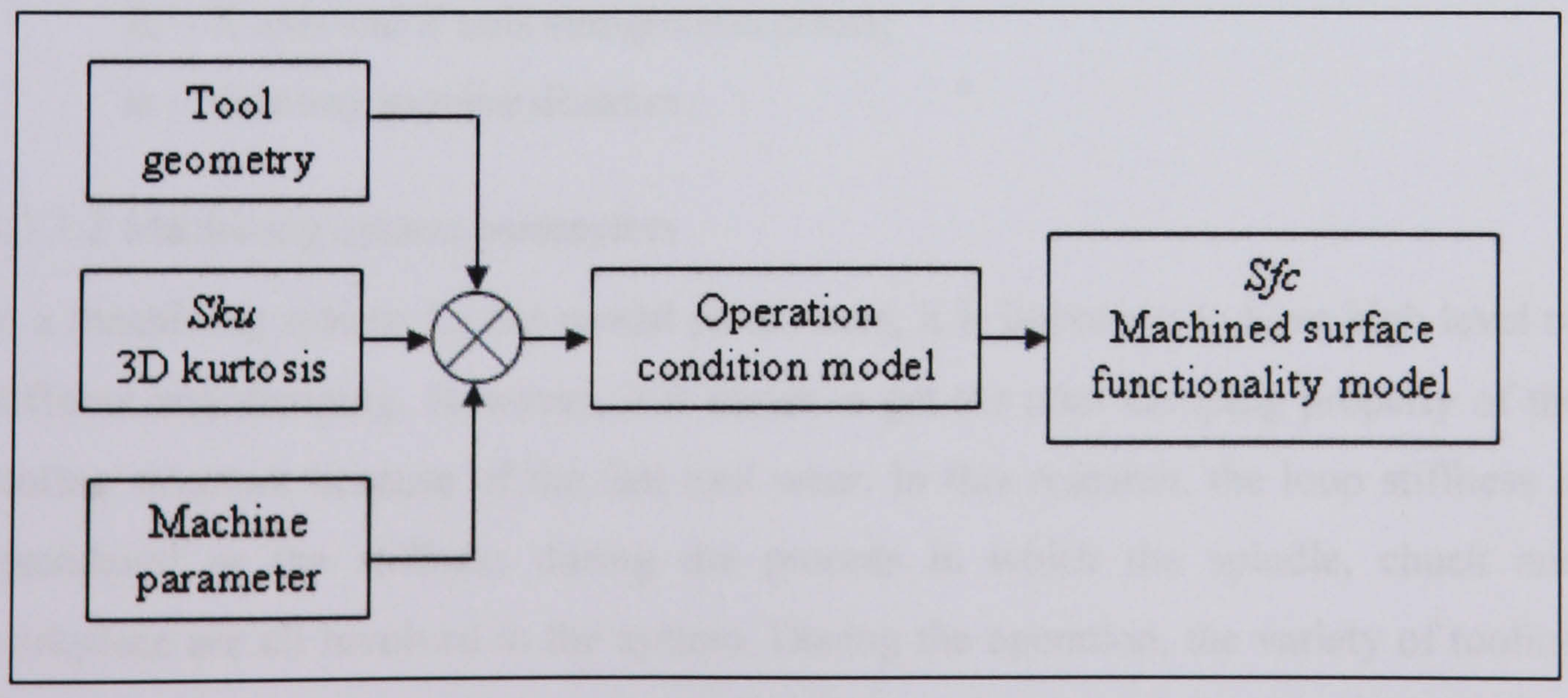

Fig. 4.3 Modelling surface generation to control surface functionality

The flow of the modelling approach can also be illustrated in the diagram Fig. 4.3. It shows the surface functionality modelling consists of three combinations factors. Those factors will be inputs to the investigation of the relationship between three element models. It is important to illustrate the model because from the illustration, the effecting factors can be identified. The outputs will include 3D surface topography, characterization parameters and surface functionality parameters.

4.3 The inputs to the modelling surface generation

4.3.1 Direct inputs

4.3.1.1 Machine tool

The main function of a machine tool in the turning process is to maintain the tool and workspiece position. It is also to keep the motion in the required path and thus important for rendering the machining accuracy. Usually the major motion error comes from the slideway. The straightness errors of the X axis and Z axis will significantly contribute to the linear motion errors of the slideway and result in the machining errors. The linear motion error of the slideway is a length based error. Formula below shows the linear motion error modelling based on the length based error.

$$P_l = R_l m \tag{4-3}$$

P_l – slideway linear motion error;

R_l – X axis and Z axis straightness errors;

m – slideway moving distance.

4.3.1.2 Machining system parameters

In a machining system for the modal parameters, it is important to have high level of stiffness and damping. However, it is easier to get the poor damping property of the tooling structure because of the fast tool wear. In this research, the loop stiffness is considered as the stiffness during the process in which the spindle, chuck and workpiece are all involved in the system. During the operation, the variety of tooling structure can cause movement. The static stiffness is adopted for this research and

known as stiffness coefficient S_{ij} (where *i* and *j* indicates X, Y or Z directions). However the stiffness coupling can only be found in two directions and not in three dimensions. The formula below show the stiffness of a workpiece structure in X, Y and Z directions.

$$S_{xxwp} = \frac{3E_w I_w (3L_w{}^2 - l_{cw}^2)}{2l_{cw}(2L_w{}^2 - l_{cw}^2)(4L_w{}^2 - l_{cw}^2)} \quad (4\text{-}4)$$

$$S_{yywp} = \frac{3E_w I_w (3L_w{}^2 - l_{cw}^2)}{2l_{cw}(2L_w{}^2 - l_{cw}^2)(4L_w{}^2 - l_{cw}^2)} \quad (4\text{-}5)$$

$$S_{zzwp} = \frac{E_w A_w}{L_w} \quad (4\text{-}6)$$

E_w– the workpiece material modulus elasticity;

Aw – the workpiece cross-sectional area;

L_w – length of the workpiece outside the chuck;

l_{cw} – cutting distance;

I_w – cross-sectional moment of inertia of the workpiece.

In turning process the stiffness workpiece structure formula can be modelled as a cantilever beam with one fixed and one at the end acted on by three dimensional cutting forces. Therefore the three dimensional cutting forces can be described as:

$$S_{xxwp} = \frac{3E_w I_w}{L_w^3} \quad (4\text{-}7)$$

$$S_{yywp} = \frac{3E_w I_w}{L_w^3} \quad (4\text{-}8)$$

$$S_{zzwp} = \frac{E_w A_w}{L_w} \quad (4\text{-}9)$$

The stiffness matrix of the workpiece system, which is the equivalent stiffness of the workpiece, spindle and chuck arranged in series, can be described as:

$$[S_w]=\begin{bmatrix} S_{xxw} & S_{xyw} & S_{xzw} \\ S_{yxw} & S_{yyw} & S_{yzw} \\ S_{zxw} & S_{zyw} & S_{zzw} \end{bmatrix}=$$

$$\begin{bmatrix} \dfrac{S_{xxsp}S_{xxch}+S_{xxwp}S_{xxch}+S_{xxwp}S_{xxsp}}{S_{xxwp}S_{xxsp}S_{xxch}} & 0 & 0 \\ 0 & \dfrac{S_{yysp}S_{yych}+S_{yywp}S_{yych}+S_{yywp}S_{yysp}}{S_{yywp}S_{yysp}S_{yych}} & 0 \\ 0 & 0 & \dfrac{S_{zzsp}S_{zzch}+S_{zzwp}S_{zzch}+S_{zzwp}S_{zzsp}}{S_{zzwp}S_{zzsp}S_{zzch}} \end{bmatrix} \quad (4\text{-}10)$$

S_{aasp} – stiffness of the spindle in the "*a*" direction;

S_{aach} – stiffness of the chuck in the "*a*" direction.

(Here *a* stands for the X, Y and Z directions respectively.)

Instead of cutting forces, the tooling structure includes the feed screw and nut-slide. The tool holder and cutting tool are also part of turning process inputs. The cutting tool can also be simplified as a cantilever beam with one end fixed at the tool holder. So there are:

$$S_{xxct}=\frac{3T_tQ_y}{H_t^3} \quad (4\text{-}11)$$

$$S_{yyct}=\frac{3T_tQ_x}{H_t^3} \quad (4\text{-}12)$$

$$S_{zzct}=\frac{T_tC_t}{H_t} \quad (4\text{-}13)$$

T_t – workpiece material modulus elasticity;

Q_y – cross-sectional moments of inertia with respect to Y axis;

Q_x – cross-sectional moments of inertia with respect to X axis;

H_t – the length out tool holder;

C_t – the cutting tool cross-sectional area.

The static stiffness matrix of the tooling structure, which is the equivalent stiffness of feed screw, nut-slides, tool holder and cutting tool arranged in series, can be calculated as:

$$[S_t]=\begin{bmatrix} S_{xxt} & S_{xyt} & S_{xzt} \\ S_{yxt} & S_{yyt} & S_{yzt} \\ S_{zxt} & S_{zyt} & S_{zzt} \end{bmatrix}=$$

$$\begin{bmatrix} \dfrac{1}{\dfrac{1}{S_{xxfs}}+\dfrac{1}{S_{xxns}}+\dfrac{1}{S_{xxth}}+\dfrac{1}{S_{xxcu}}} & 0 & 0 \\ 0 & \dfrac{1}{\dfrac{1}{S_{yyfs}}+\dfrac{1}{S_{yyns}}+\dfrac{1}{S_{yyth}}+\dfrac{1}{S_{yycu}}} & 0 \\ 0 & 0 & \dfrac{1}{\dfrac{1}{S_{zzfs}}+\dfrac{1}{S_{zzns}}+\dfrac{1}{S_{zzth}}+\dfrac{1}{S_{zzcu}}} \end{bmatrix} \quad (4\text{-}14)$$

where S_{aafs} – stiffness of the feed crew in the "*a*" direction;

S_{aans} – stiffness of the nut-slide in the "*a*" direction;

S_{yyth} – stiffness of the tool holder in the "*a*" direction.

(Here *a* stands for the X, Y nd Z directions respectively.)

The mass coefficient R_{ij} is the force developed at coordinate *i* due to unit acceleration at X, Y or Z directions. It can be assumed that there is no mass coupling in the workpiece and tooling structural system. By using the consistent mass method, the mass coefficient of the workpiece and tooling structure in the three directions are nearly same, i.e. it is one third of the total mass of the system respectively. The mass matrixes of the workpiece system and tooling structure could be:

$$[R_w]=\begin{bmatrix} r_{xxw} & r_{xyw} & r_{xzw} \\ r_{yxw} & r_{yyw} & r_{yzw} \\ r_{zxw} & r_{zyw} & r_{zzw} \end{bmatrix}=\begin{bmatrix} \dfrac{r_w}{3} & 0 & 0 \\ 0 & \dfrac{r_w}{3} & 0 \\ 0 & 0 & \dfrac{r_w}{3} \end{bmatrix} \quad (4\text{-}14)$$

$$[R_t] = \begin{bmatrix} r_{xxt} & r_{xyt} & r_{xzt} \\ r_{yxt} & r_{yyt} & r_{yzt} \\ r_{zxt} & r_{zyt} & r_{zzt} \end{bmatrix} = \begin{bmatrix} \frac{r_t}{3} & 0 & 0 \\ 0 & \frac{r_t}{3} & 0 \\ 0 & 0 & \frac{r_t}{3} \end{bmatrix} \quad (4\text{-}15)$$

R_w is the total mass of the workpiece system. While R_t is the total mass of the tooling structural system.

The damping coefficients of the cutting system are defined in a manner entirely parallel to the definition of the stiffness coefficient or the mass coefficient. Specifically, the damping coefficient P_{ij} is defined as the force developed at coordinate i due to a unit velocity at direction j (here, i and j stands for X, Y or Z directions). It can be calculated by the following formulation:

$$P_{ij} = \xi p_{prij} = 2\lambda_{ij}\sqrt{s_{ij} r_{ij}} \quad (4\text{-}16)$$

p_{ij} – critical damping coefficient;

λ_{ij} – damping ratio.

The damping ratio is usually obtained experimentally. The damping matrix of the workpiece and tooling structural system can be calculated by formulation (4-15).

4.3.1.3 Workpiece and tooling material properties

Shear stress, thermal conductivity, heat specific and thermal expansion coefficients are mechanical and thermal properties of the workpiece material and cutting material. All these will becomes the inputs to modelling approach.

4.3.1.4 Tooling geometric parameters

The tooling geometric parameters include rake angle, clearance angle, cutting edge radius and tool nose radius. They are essential inputs to the modelling modelling approach in relation with tooling geometry.

4.3.1.5 Operation conditions

The operational conditions play as the inputs to the modelling approach. They are spindle speed, feed rate, depth of cut and coolant type, etc.

4.4 Indirect inputs

4.4.1 Spindle motion error

To get the accuracy of the machine, understanding the spindle synchronous error motion is very important. The errors forming the spindle error motions include the axial and radial synchronous with sinusoidal feature, depending on the spindle speed. They can be modelled in the form of sinusoidal function.

$$S_s = T_s \sin(\beta t + F) \tag{4-17}$$

S_s – spindle synchronous error;

T_s – the amplitude of the error;

β – spindle angular speed;

t – revolution time of the spindle;

F – phase shift.

4.4.2 Coolant in turning process

The coolant is the main source which can change the friction coefficient or friction angle between the tool rake face and chip. The impact of coolant for the machining process is drastic particularly on the tool wear, tool life, surface quality and machining productivity, etc. It can be emulated in the modelling with a step function, such as:

$$\Delta u(t) = p(t) \tag{4-18}$$

$\Delta u(t)$ - impact of coolant for the machining

$p(t)$ - step function.

This numerical modelling is used to emulate the switch on or off of the coolant in the machining process but in a quantitative manner.

4.5 Cutting mechanics

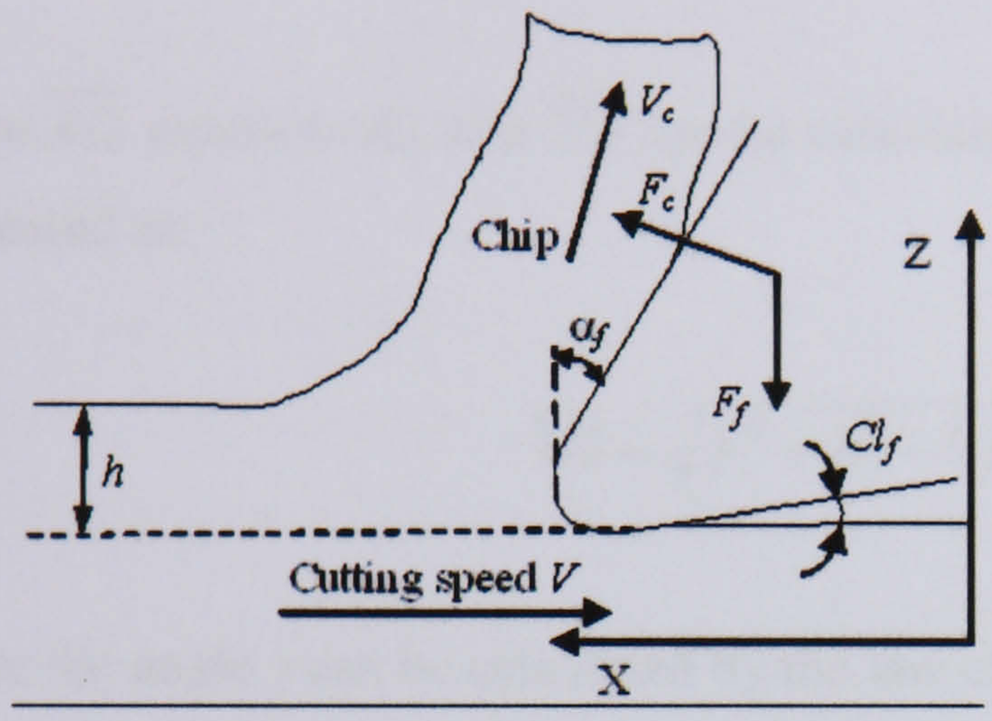

(a) Side view

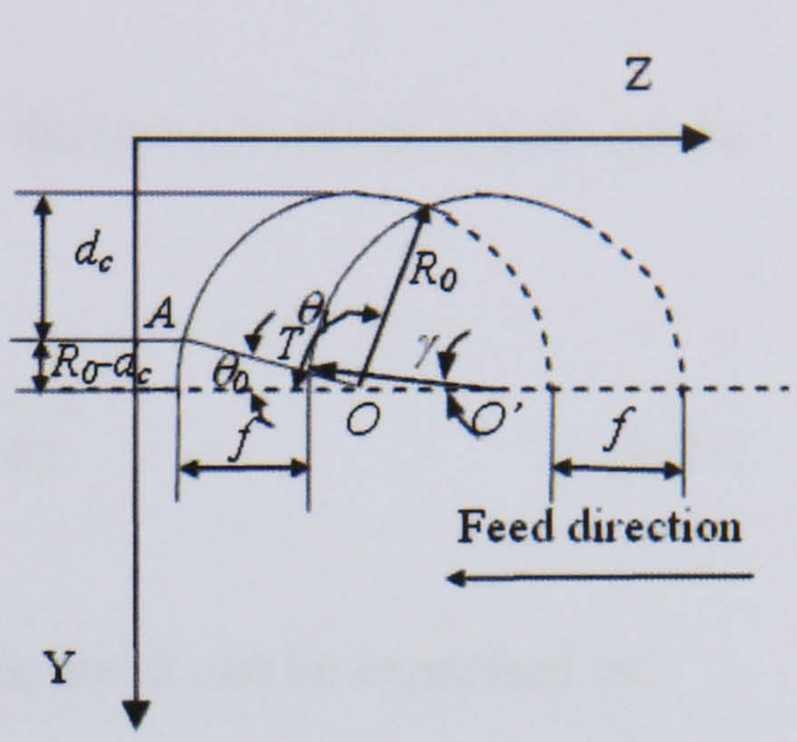

(b) Top view

Fig. 4.4 The side view and top view of the tool/workpiece contact area.

The main function of cutting model in turning process is to calculate the cutting constant and the contact area. The contact area will act on the tool rake face, cutting edge and flank face. To detect the contact profile, it can be found that the thickness reduces continuously and meanwhile the cutting oblique can change the directions and the curved chip thickness segment. Fig. 4.4 shows the side view and top view of the tool/workpiece contact area. The side view of the contact area clearly shows that the cutting forces will act on the tool rake face, cutting edge and flank face. The top view of the contact area shows the contact profile, in which it can be seen that the chip thickness reduces continuously and the oblique cutting forces change their directions around the curved chip segment. The chip thickness can be calculated by integration along the chip area [9]:

$$dA = \overline{AT}dS = \overline{AT}R_0 d\theta \tag{4-19}$$

dA – area of differential chip;

$\overline{AT}$ – differential chip thickness;

dS – profile length of differential chip;

$d\theta$ – angle of differential chip.

The differential chip thickness $\overline{AT}$ can be expressed as:

$$\overline{AT} = \overline{AO} - \overline{TO} \tag{4-20}$$

where $\overline{AO}$ equals to R_0, and $\overline{TO}$ can be calculated by the law of cosines, which can be expressed as:

$$\overline{TO} = \sqrt{f^2 + R_0^2 - 2fR_0 \cos\gamma} \tag{4-21}$$

where the angle γ can be calculated by the law of sines, and it can be expressed as:

$$\gamma = \theta - \sin^{-1}[\frac{f}{R_0}\sin(\pi - \theta)] = \theta - \sin^{-1}(\frac{f}{R_0}\sin\theta) \tag{4-22}$$

Substituting R_0 and (4-21) into (4-20), the differential chip thickness can be further expressed as:

$$\overline{AT} = h(\theta) = R_0 - \sqrt{f^2 + R_0^2 - 2fR_0 \cos\gamma} \tag{4-22}$$

The tangential, radial and feed forces acting on the differential chip element can be expressed as:

$$\begin{cases} dF_t = K_{ta}dA + K_{te}dS + K_{tc}dS = [K_{ta}h(\theta) + K_{te} + K_{tc}]rd\theta \\ dF_r = K_{ra}dA + K_{re}dS + K_{rc}dS = [K_{ra}h(\theta) + K_{re} + K_{rc}]rd\theta \\ dF_f = K_{fa}dA + K_{fe}dS + K_{fc}dS = [K_{fa}h(\theta) + K_{fe} + K_{fc}]rd\theta \end{cases} \tag{4-24}$$

K_{ta} – cutting constant at rake face in tangential direction;

K_{te} – cutting constant at cutting edge in tangential direction;

K_{tc} – cutting constant at flank face in tangential direction;

K_{ra} – cutting constant at rake face in radial direction;

K_{re} – cutting constant at cutting edge in radial direction;

K_{rc} – cutting constant at flank face in radial direction;

K_{fa} – cutting constant at rake face in feed direction;

K_{fe} – cutting constant at cutting edge in feed direction;

K_{fc} – cutting constant at flank face in feed direction.

4.5.1 Cutting constants

4.5.1.1 Rake face

The cutting constants at the rake face can be deduced by coordinate transform from the shear plane force. Here the oblique cutting force model proposed by Armarego is adopted [8]. Fig. 4.5 shows the force components in oblique cutting. The shear force is inclined at angle η to the normal to the cutting edge in the shear plane. To analyze the forces in oblique cutting it is helpful to resolve the resultant force into two components, R' in a plane perpendicular to the cutting edge, and F'_R along the cutting edge. From Fig. 4.3, it can be found that R' can be further resolved, the resultant force is therefore given by:

$$R = \sqrt{(R')^2 + (F_R')^2} = \sqrt{(F_t')^2 + (F_f')^2 + (F_r')^2} = \sqrt{F_t^2 + F_f^2 + F_r^2} \quad (4\text{-}25)$$

The direction of the shear force are found from the forces in Fig. 4.3, thus

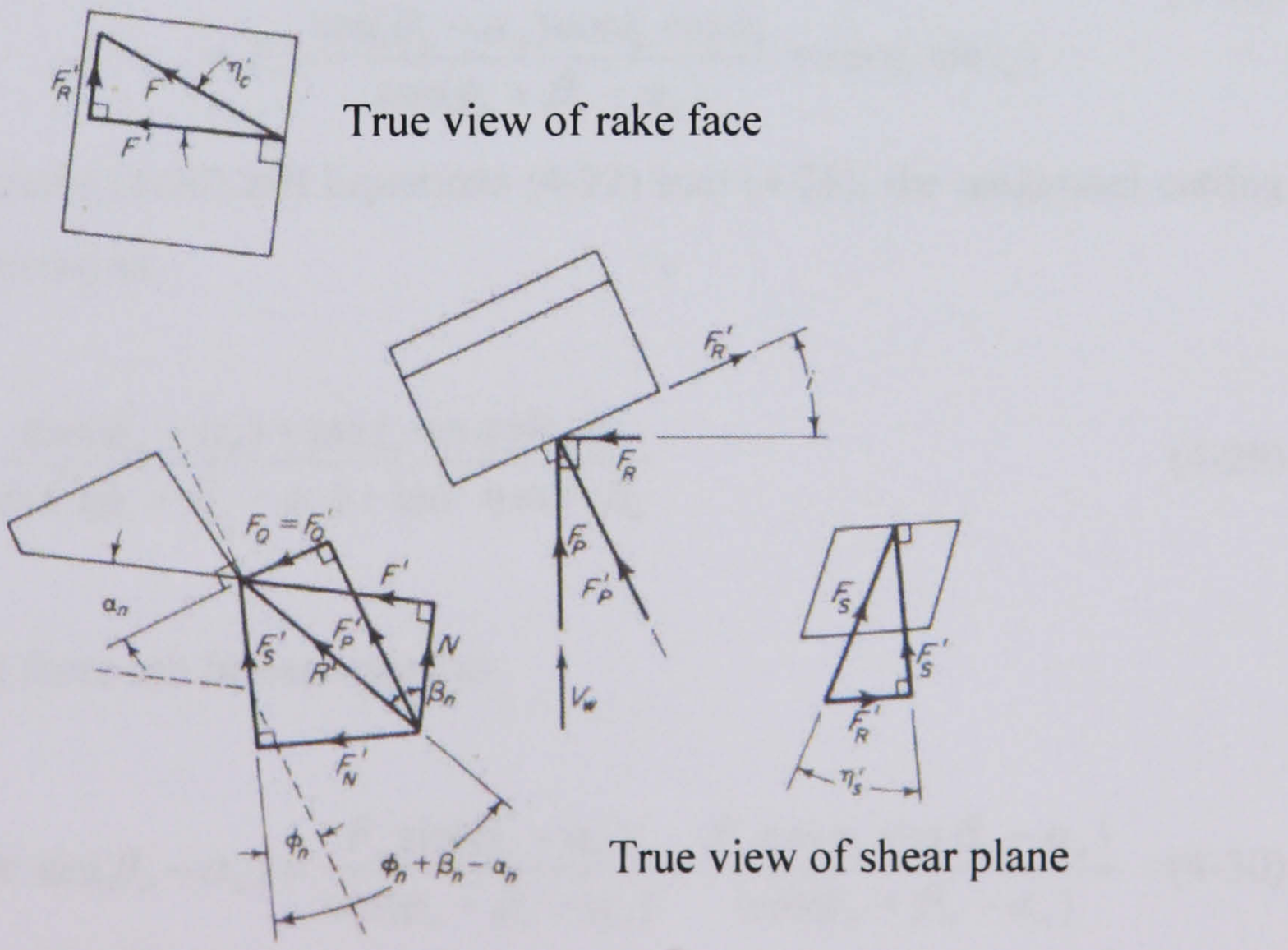

Fig.4.5 The force components in oblique cutting

$$\tan\eta_s' = \frac{F_R'}{F_S'} = \frac{F'\tan\eta}{R'\cos(\phi_n+\beta_n-\alpha_n)} = \frac{\tan\eta\sin\beta_n}{\cos(\phi_n+\beta_n-\alpha_n)} \tag{4-26}$$

η - chip flow angle;

η'_s – shear flow angle;

β_n – normal friction angle;

ϕ_n – normal shear angle in oblique cutting.

The shear force in the shear plane is given by

$$F_S = \tau_s A_S = \tau_s \frac{bh}{\sin\phi_n\cos i_o} \tag{4-27}$$

τ_s – shear yield stress;

A_s – the shear-plane area;

b – cutting width;

h – cutting thickness;

i_o – oblique angle or inclination angle.

The force component F_t in Fig. 4.5 can be expressed as:

$$\begin{aligned} F_t &= F_t'\cos i_o + F_r'\sin i_o = F_s'\frac{\cos(\beta_n-\alpha_n)\cos i_o}{\cos(\phi_n+\beta_n-\alpha_n)} + F_s\sin\eta_s'\sin i_o \\ &= F_s[\frac{\cos(\beta_n-\alpha_n)\cos i_o\cos\eta_s'}{\cos(\phi_n+\beta_n-\alpha_n)} + \sin\eta_s'\sin i_o] \end{aligned} \tag{4-28}$$

substituting Equations (4-26) and Equations (4-27) into (4-28), the tangential cutting force can be expressed as:

$$F_t = \frac{\tau_s bh}{\sin\phi_n}\frac{\cos(\beta_n-\alpha_n)+\tan i_o\tan\eta\sin\beta_n}{\cos^2(\phi_n+\beta_n-\alpha_n)+\tan^2\eta\sin^2\beta_n} \tag{4-29}$$

Similarly the feed force can be expressed as:

$$F_f = F_f' = R'\sin(\beta_n-\alpha_n) = \frac{F_s'\sin(\beta_n-\alpha_n)}{\cos(\phi_n+\beta_n-\alpha_n)} = \frac{F_s\cos\eta_s'\sin(\beta_n-\alpha_n)}{\cos(\phi_n+\beta_n-\alpha_n)} \tag{4-30}$$

Substituting Equations (4-26) and (4-27) into (4-30) gives:

$$F_f = \frac{\tau_s bh}{\sin\phi_n \cos i_o} \cdot \frac{\sin(\beta_n - \alpha_n)}{\sqrt{\cos^2(\phi_n + \beta_n - \alpha_n) + \tan^2\eta \sin^2\beta_n}} \tag{4-31}$$

The radial cutting force can be written as:

$$F_r = F_t' \sin i_o - F_M' \cos i_o = F_s[\frac{\cos(\omega_n - \alpha_n)\cos\mu_s' \sin i_o}{\cos(\phi_n + \omega_n - \alpha_n)} - \sin\mu_s' \cos i_o] \tag{4-32}$$

Substituting Equations (4-26) and (4-27) into Equation (4-32), the radial cutting force can further be expressed as:

$$F_r = \frac{\tau_s bh}{\sin\phi_n} \frac{\cos(\beta_n - \alpha_n)\tan i_o - \tan\eta \sin\beta_n}{\sqrt{\cos^2(\phi_n + \beta_n - \alpha_n) + \tan^2\eta \sin^2\beta_n}} \tag{4-33}$$

Equations (4-29), (4-31) and (4-33) are the oblique cutting force proposed by Armarego [8].

For some practical cutting tools, which have the side rake angle and back rake angle, the Equivalent oblique angle and normal rake angle can be evaluated by the following Equation [37]:

$$\begin{cases} \tan\alpha_0 = \tan\alpha_f \cos\psi_r + \tan\alpha_f \sin\psi_f \\ \tan i_o = \tan\alpha_p \cos\psi_r + \tan\alpha_f \sin\psi_r \\ \tan\alpha_n = \tan\alpha_0 \cos i_o \end{cases} \tag{4-34}$$

where α_p – back rake angle of the cutting tool;

ψ_t – side cutting edge angle of the cutting tool.

For simplicity, the chip flow angle can be assumed to be equal to the oblique angle as suggested by Stabler [26].

In the cutting process, some parameters, such as normal friction angle, normal rake angle, normal shear angle and shear stress, are all variant as functions of time. Bearing this in mind, the corresponding cutting constants at rake face can be expressed as:

$$\begin{cases} K_{ta} = \dfrac{\tau_s(t)}{\sin\phi_n(t)} \dfrac{\cos(\beta_n(t)-\alpha_n(t)) + \tan i \tan\eta \sin\beta_n(t)}{\sqrt{\cos^2(\phi_n(t)+\beta_n(t)-\alpha_n(t) + \tan^2\eta \sin^2\beta_n(t)}} \\ K_{ra} = \dfrac{\tau_s(t)}{\sin\phi_n(t)} \dfrac{\cos(\beta_n(t)-\alpha_n(t))\tan i - \tan\eta \sin\beta_n(t)}{\sqrt{\cos^2(\phi_n(t)+\beta_n(t)-\alpha_n(t)) + \tan^2\eta \sin^2\beta_n(t)}} \\ K_{fa} = \dfrac{\tau_s(t)}{\sin\phi_n(t)\cos i} \dfrac{\sin(\beta_n(t)-\alpha_n(t))}{\sqrt{\cos^2(\phi_n(t)+\beta_n(t)-\alpha_n(t)) + \tan^2\eta \sin^2\beta_n(t)}} \end{cases} \quad (4\text{-}35)$$

The expressions for those time dependent parameters will be deduced in the following part of this chapter.

4.5.1.2 Cutting edge

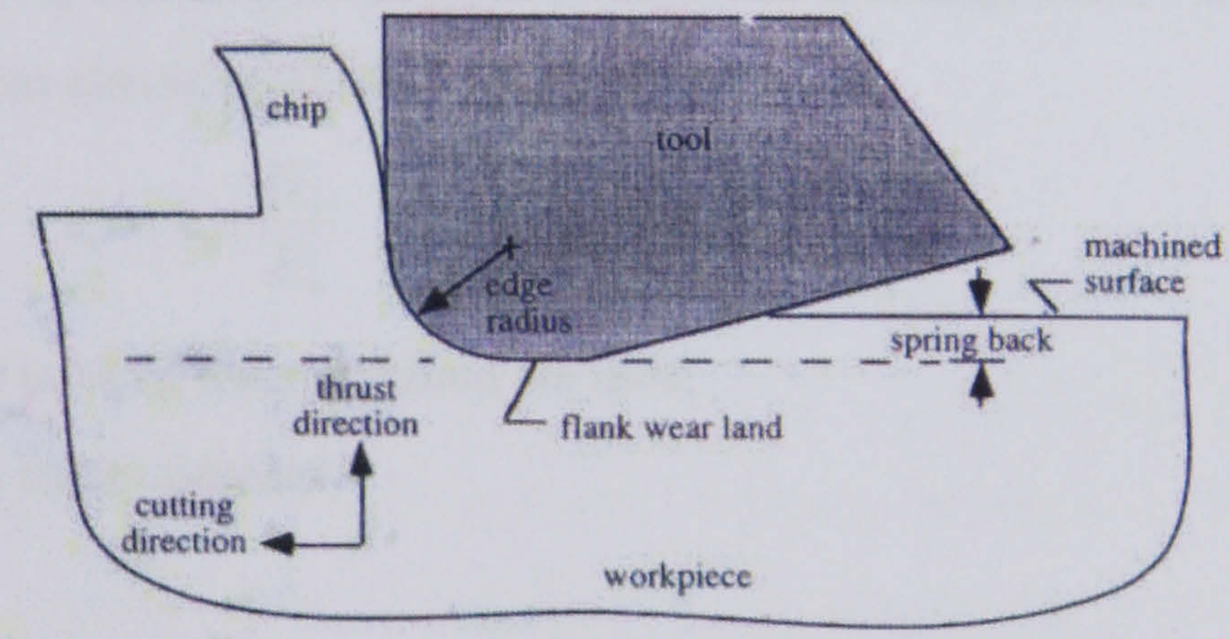

Fig. 4.6 Interface stress acting on the cutting edge

Fig. 4.6 shows the interface stress acting on the cutting edge. Here an empirical formula is adopted to express the tool/workpiece interface stress σ_f, which is:

$$\sigma_f = k_1 H_w \sqrt{\frac{H_w}{E_w}} \quad (4\text{-}36)$$

where k_1 – constant;

H_w – material hardness of the workpiece.

Arcona and Dow have proved that $k_l = 4.1$ is the best agreement with measured data [38].

The cutting constants in the tangential direction, radial and feed directions are derived using σ_f consistent; i.e;

$$\begin{cases} K_{te} = \sigma_f (\frac{\pi}{2} + \alpha_f) r[\sin(\frac{\pi}{4} + \frac{\alpha_f}{2}) + \mu_f \cos(\frac{\pi}{4} + \frac{\alpha_f}{2})] \\ K_{re} = \sigma_f (\frac{\pi}{2} + \alpha_p) r[\cos(\frac{\pi}{4} + \frac{\alpha_p}{2} - \mu_f \cos(\frac{\pi}{4} + \frac{\alpha_p}{2})] \\ K_{fe} = \sigma_f (\frac{\pi}{2} + \alpha_f) r[\cos(\frac{\pi}{4} + \frac{\alpha_f}{2}) - \mu_f \sin(\frac{\pi}{4} + \frac{\alpha_f}{2})] \end{cases} \quad (4\text{-}37)$$

μ_f – coefficient between the tool flank and workpiece;

r – cutting edge radius.

4.5.1.3 Flank face

There is compression interaction between the tool flank face and workpiece material in the contact area. Arcona and Dow's work demonstrate that spring back in metal machining can be represented as a linear function of tool edge radius and the ratio of material hardness to elastic modulus [38].

$$s_b = k_2 r \frac{H_w}{E_w} \quad (4\text{-}38)$$

s_b – spring back of the machined surface;

k_2 – spring back constant.

The forces act on the clearance wear land and the straight flank area. The cutting constants in tangential, radial and feed directions can be expressed as:

$$\begin{cases} K_{tc} = \sigma_f (l_w + \frac{2s_b}{3\tan Cl_f})(\sin Cl_f - \mu_f \cos Cl_f) \\ K_{rc} = \sigma_f (l_w + \frac{2s_b}{3\tan Cl_p})(\cos Cl_p + \mu_f \cos Cl_p) \\ K_{fc} = \sigma_f (l_w + \frac{2s_b}{3\tan Cl_f})(\cos Cl_f + \mu_f \cos Cl_f) \end{cases} \quad (4\text{-}39)$$

l_w – wear land length;

Cl_f – side clearance angle of the cutting tool;

Cl_p – end clearance angle of the cutting tool.

On the Cartesian coordinate, the cutting forces in the X, Y and Z directions are:

$$\begin{cases} F_x = \int_{\theta_0}^{\theta_1} F_t \\ F_y = \int_{\theta_0}^{\theta_1} F_f \cos\theta - \int_{\theta_0}^{\theta_1} F_r \cos\theta \\ F_z = \int_{\theta_0}^{\theta_1} F_f \cos\theta + \int_{\theta_0}^{\theta_1} F_r \sin\theta \end{cases} \quad (4\text{-}40)$$

θ_0 – initial approach angle;

$$\theta_0 = \sin^{-1}(\frac{R_0 - d_c}{R_0}) \quad (4\text{-}41)$$

θ_1 – end approach angle.

$$\theta_1 = \pi - \cos^{-1}(\frac{f}{2R_0}) \quad (4\text{-}41)$$

4.6 Vibration model

A stable machining process is desired for producing a good surface finish. But the disturbance from environment and some mechanisms inherent in the machining process may lead the innately stable machining system to work at a dynamic unstable status. This results in unsatisfactory workpiece surface quality. The unstable sources can be classified into two categories: chatter vibrations and random/free vibrations [176]. The vibration models are focused on some random and free vibrations in this part. The chatter vibrations will be discussed in the next section.

Precision/ultra-precision machining is very sensitive to the environmental disturbances. This is the reason why more and more vibration isolation systems or measures are applied in the state-of-the-art ultra-precision machine tools. The environmental vibrations exist in the whole machining process. They can be modelled

as a sinusoidal function with the amplitude of 0.2 μm for the Harisson M250 turning machine, which can be described as:

$$E_v = 0.2\sin(2\pi f_{ev} t) \tag{4-42}$$

f_{ev} – frequency of the environmental vibration.

For face turning, the environmental disturbance in Z direction is significant to contribute to the surface finish and form errors. For cylindrical turning, the environmental disturbance in the X direction will become important. Therefore, in the modelling approach the environmental vibration will be applied in the X and Z direction respectively, which depends on the turning operations.

A typical random vibration is the cutting tool vibration when the cutting tool strikes at a hard grain in the workpiece during the machining process. When it happens, the cutting tool will bounce or vibrate relative to the workpiece. The existence of this phenomenon depends on the workpiece material properties. The source of this kind of vibration comes from sudden increases in the shear stress, which can be expressed as:

$$\Delta\tau_1 = \tau_A Pul(t) \tag{4-44}$$

$\Delta\tau_1$ – increment of the shear stress due to the hard grain;

τ_A – amplitude of the increment of the shear stress due to the hard grain;

Pul – Pulse function generating square wave with equal interval.

Equation (4-44) will be an additional item in the shear stress calculation in Equation (4-35).

Under some machining conditions, such as low cutting speed, a built-up edge (BUE) will be generated and it may be removed under changing machining conditions. The generation and removal of the BUE will change the effective rake angle and the variation of the cutting force, and result in the cutting tool vibration. The variation of effective rake angle can be modelled as:

$$\Delta\alpha = \alpha_A Rse(\omega_\alpha t) \tag{4-45}$$

$\Delta\alpha$ – variation of the rake angle due to the BUE;

α_A – amplitude of the variation of the rake angle due to the BUE;

ω_α – frequency of the generation and removal of the BUE;

Rse – a function to generate an arbitrarily shaped period signal.

The variation of the effective rake angle will be used to modify the rake angle in Equations (4-34).

4.7 Chatter model

Regenerative vibration is a typical chatter vibration. It is excited by the cutting forces, as a wavy surface finish left at the previous revolution, is removed during the successive revolution which also leaves a wavy surface owing to machine structural vibration. Regenerative vibration will result in the variation of the chip thickness and width and excite variations in cutting forces and vice versa. So the regenerative vibration is generated in cycles. It can be modelled as the variation of cutting thickness and width:

$$\Delta c_t = x(t) - x(t-T) \tag{4-46}$$

$$\Delta c_w = y(t) - y(t-T) \tag{4-47}$$

Equations (4-46) and (4-47) will be used to update the real feed rate and depth of cut in the machining model to emulate the regenerative vibration.

In the cutting process, the tangential cutting force and radial cutting force may be coupled and will result in shear angle oscillation. The shear angle oscillation will also cause the variance of cutting force and tool vibration thereafter. The variation of the shear angle can be expressed as:

$$\phi_n(t) = \phi_0 Chirp(t) \tag{4-48}$$

ϕ_0 – initial shear angle;

Chirp – chirp function to generate a sine wave with increasing frequency.

Chip formation is a highly dynamic and nonlinear process involving a very complex thermoplastic flow of workpiece material. Experiments show that, for most ductile metals, as the cutting speed increases monotonically in orthogonal cutting, a transition takes place from continuous to shear-localized chip formation in the flow field of the material being cut. The research carried out in NIST indicates that the formation of shear-localized chips is periodic at high cutting speed [39]. The shear stress of the material under the tool tip will vary from 0 to a maximum value because of the period thermal softening and straining harden of the workpiece with the formation of a series of segmented chips. Basically, the change of shear stress is caused by the variation of dislocation density in the work. The real shear stress in the cutting process can be expressed as:

$$\tau_s(t) = (\frac{V_c t}{\Delta s})k_y \tag{4-49}$$

$\tau_s(t)$ – real shear stress in the cutting process;

k_y – yield stress of the workpiece material;

Δs – average distance between the shear-localized chips;

Vc – chip velocity in the direction parallel to the rake face.

4.8 Thermal model

The heat sources in the cutting zones include the work of shear deformation in the shear zone, friction work at interfaces between tool rake face and chip, between tool flank face and machined surface, and elastic contact work between tool nose, cutting edge and workpiece material. Because the heat piled up at the interface of the tool flank face and the machined surface may have significant effects on tool wear and surface integrity, the thermal model is focused on the calculation of temperature rise in the tool flank face zone.

The heating resulted from flank-workpiece friction can be regarded as an elliptical shape heat source with uniform heat flux distribution. The temperature rise is given by:

$$\Delta T_f = \frac{2qa_i}{k_1\sqrt{\pi(1.3S_e + P_{e1})}} \tag{4-50}$$

ΔT_f – temperature rise in the tool flank – workpiece zone;

q – rate of heat supply per unit area;

a_i – flank-workpiece contact length;

k_1 – thermal conductivity of the workpiece material;

P_{e1} – Peclet number of the workpiece material;

4.9 Tool wear model

Flank wear is a major form of tool wear in precision turning process. It may result in the rubbing of the tool nose on the workpiece surface and bring forth the so called stick-slip oscillations. Generally speaking, tool flank wear is caused by the friction between the flank face of the tool and the machined surface. Its wear mechanism is very complex. At the tool flank-workpiece surface contact area, tool particles adhere to the workpiece surface and are periodically sheared off. Adhesion of the tool and workpiece increases at higher temperatures. Abrasive wear occurs when hard inclusions of work material or escaped tool particles scratch the flank and workpiece as they move across the contact area as well. Although adhesive and abrasive wear mechanisms are predominant in flank wear, some diffusion wear also exists [8]. Due to the complex mechanism of the tool flank wear, an empirical model is used to calculate the tool flank wear width, which is expressed as:

$$l_w(t) = \frac{A}{H_t}\frac{F_r}{Vf}V_s + B\exp(\frac{-E}{RT_f}) \tag{4-51}$$

H_t – hardness of the cutting tool material;

V – cutting speed;

V_s – sliding speed;

E – process activation energy;

R – universal gas constant;

T_f – cutting temperature in the tool flank zone;

A, B – constants.

The first item in Equation (4-51) stands for the adhesive and abrasive wear [4], the last item stands for the diffusion wear [109].

4.10. Machining system

Fig. 4.7 shows the machining dynamics model. The workpiece and cutting tool are simplified as a second-order spring-damper vibratory system in the X, Y and Z directions.

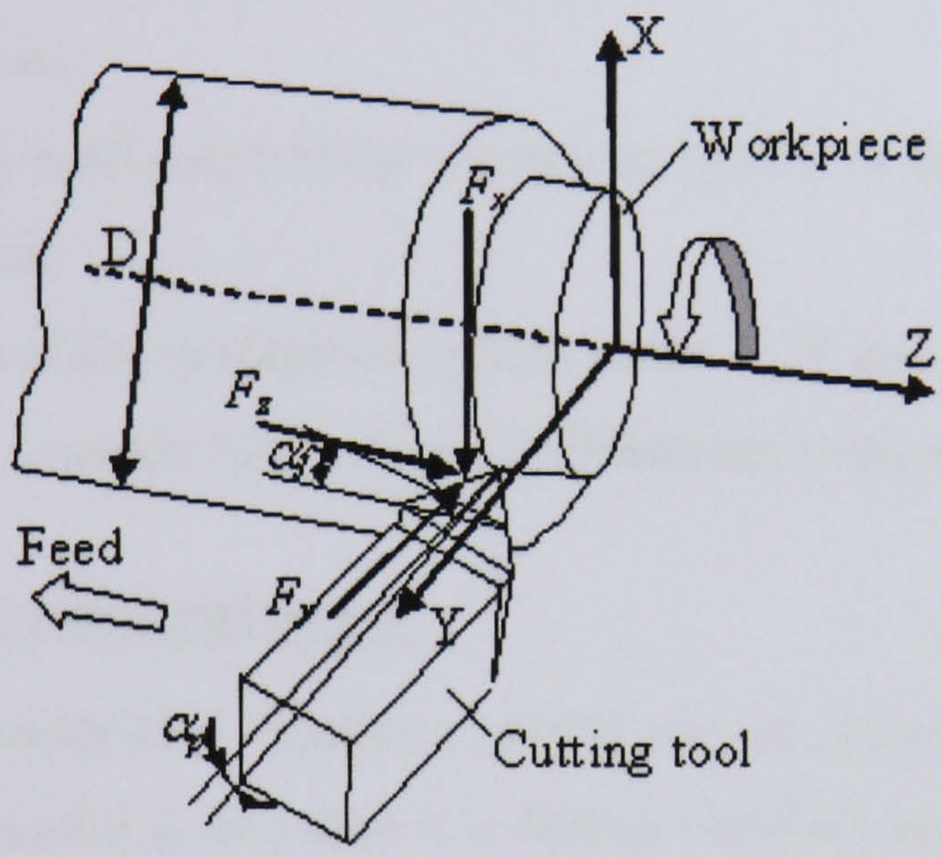

Fig. 4.7 Machining system diagram

The cutting forces excite the dynamic displacements of the cutting tool and the workpiece in the X, Y and Z directions respectively. According to the stiffness matrix, damping matrix and mass matrix of the tooling system and workpiece system, there is no axial coupling in the machining system. Therefore, the whole cutting system can be described as:

$$\begin{cases} m_{xxt}\ddot{xt}(t)+c_{xxt}\dot{xt}(t)+k_{xxt}xt(t)=F_x(t) \\ m_{yyt}\ddot{yt}(t)+c_{yyt}\dot{yt}(t)+k_{yyt}yt(t)=F_y(t) \\ m_{zzt}\ddot{zt}(t)+c_{zzt}\dot{zt}(t)+k_{zzt}zt(t)=F_z(t) \\ m_{xxw}\ddot{xw}(t)+c_{xxw}\dot{xw}(t)+k_{xxw}xw(t)=-F_x(t) \\ m_{yyw}\ddot{yw}(t)+c_{yyw}\dot{yw}(t)+k_{yyw}yw(t)=-F_y(t) \\ m_{zzw}\ddot{zw}(t)+c_{zzw}\dot{zw}(t)+k_{zzw}zw(t)=-F_z(t) \end{cases} \quad (4\text{-}52)$$

m_{aat} - the mass equivalent of the tooling system in the X, Y and Z directions;

c_{aat} - damping coefficient of the tool system in the X, Y and Z directions;

k_{aat} - stiffness of the tooling system in the X, Y and Z directions;

m_{aaw} - the mass equivalent of the workpiece system in the X, Y and Z directions;

c_{aaw} - damping coefficient of the workpiece system in the X, Y and Z directions;

k_{aaw} - stiffness of the workpiece system in the X, Y and Z directions.

(Here, *a* stands for X, Y and Z directions respectively.)

4.11 Machining system response

The cutting system modelling Equation (4-52) can be transformed into frequency domain by Laplace transform, and then it is further rewritten as:

$$\begin{bmatrix} xt(s) \\ yt(s) \\ zt(s) \\ xw(s) \\ yw(s) \\ zw(s) \end{bmatrix} = (1-e^{-sT}) \begin{bmatrix} G_{xxt} & G_{xyt} & G_{xzt} & 0 & 0 & 0 \\ G_{yxt} & G_{yyt} & G_{yzt} & 0 & 0 & 0 \\ G_{zxt} & G_{zyt} & G_{zzt} & 0 & 0 & 0 \\ 0 & 0 & 0 & G_{xxw} & G_{xyw} & G_{xzw} \\ 0 & 0 & 0 & G_{yxw} & G_{yyw} & G_{yzw} \\ 0 & 0 & 0 & G_{zxw} & G_{zyw} & G_{zzw} \end{bmatrix} \begin{bmatrix} F_x(s) \\ F_y(s) \\ F_z(s) \\ -F_x(s) \\ -F_y(s) \\ -F_z(s) \end{bmatrix} \quad (4\text{-}53)$$

In Equation (4-53), the machining system response model is just the matrix below:

$$\begin{bmatrix} G_{xxt} & G_{xyt} & G_{xzt} & 0 & 0 & 0 \\ G_{yxt} & G_{yyt} & G_{yzt} & 0 & 0 & 0 \\ G_{zxt} & G_{zyt} & G_{zzt} & 0 & 0 & 0 \\ 0 & 0 & 0 & G_{xxw} & G_{xyw} & G_{xzw} \\ 0 & 0 & 0 & G_{yxw} & G_{yyw} & G_{yzw} \\ 0 & 0 & 0 & G_{zxw} & G_{zyw} & G_{zzw} \end{bmatrix} \quad (4\text{-}54)$$

The tooling response model and the workpiece response model are the sub-matrix in Equation (4-54):

$$\begin{bmatrix} G_{xxt} & G_{xyt} & G_{xzt} \\ G_{yxt} & G_{yyt} & G_{yzt} \\ G_{zxt} & G_{zyt} & G_{zzt} \end{bmatrix} \quad (4\text{-}55)$$

$$\begin{bmatrix} G_{xxw} & G_{xyw} & G_{xzw} \\ G_{yxw} & G_{yyw} & G_{yzw} \\ G_{zxw} & G_{zyw} & G_{zzw} \end{bmatrix} \quad (4\text{-}56)$$

G_{abt} – corresponding response of the tooling structure in a-th direction due to the force acting in the b-th direction when the other two force components are zero;

G_{abw} – corresponding response of the workpiece structure in a-th direction due to the force acting in the b-th direction when the other two force components are zero.

(a and b stand for the X/Y/Z direction respectively).

Here the assumption of linearity is accepted, i.e. the matrix **G** is symmetric ($G_{ab} = G_{ba}$).

The transfer function can be expressed in the form of:

$$G_{ab} = \frac{y_{ab}(s)}{F_{ab}(s)} = \frac{\omega_{nab}^2}{K_{ab}(s^2 + 2\zeta_{ab}\omega_{nab}s + \omega_{nab}^2)} \quad (4\text{-}57)$$

K_{ab} – structural stiffness of the workpiece and tooling system in a-th direction due to a force acting in the b-th direction when the other two force components are zero;

ω_{nab} – structural natural frequency of the workpiece and tooling system in a-th direction due to a force acting in the b-th direction when the other two force components are zero;

ζ_{ab} – damping ratio of the workpiece and tooling system in a-th direction due to a force acting in the b-th direction when the other two force components are zero.

Structural natural frequency can be estimated by:

$$\omega_{nab} = \sqrt{\frac{K_{ab}}{m_{ab}}}\sqrt{1-\xi_{ab}{}^{2}} \tag{4-58}$$

A modelling approach has been proposed to study the precision surface generation in precision turning processes. Basically, it is based on the cutting dynamics and machine tool dynamics analyses. The dynamic cutting force model is deduced to calculate the three dimensional cutting forces. The thermal model is developed to predict cutting temperature rise at tool flank-work zone. The vibration models are classified into two categories, random or free vibration, and chatter vibration. The dynamic displacements between the cutting tool and workpiece can be calculated by the machining system response model. The model enables to predict the cutting force and surface topography, and hence to study the machining factors on surface generation. But the descriptions of tool wear and chip formation are based on some experimental results. A more fundamental theoretical study is needed to explain the tool wear mechanism predictive control of the tool wear and vibrations within the cutting process.

4.12 Conclusion

During the research, a modelling approach has been proposed to study the precision surface generation in turning process. The modelling approach is basically based on

the machining process dynamics. The inputs to the modelling will cover direct and indirect inputs. The model enables to predict the dynamic cutting force, and the tool tip cutting path and surface topography. The modelling approach will enhance the study of the machining factors and their effects on the surface generation individually in collectively.

Chapter 5 Simulations on the surface generation in turning processes

5.1 Introduction

This chapter will present the simulations developed based on the modeling approach. The simulations will focus on the direct inputs, the surface generation and integration in the machining process. The effects of direct inputs on surface generation will be discussed by analyzing the simulation results.

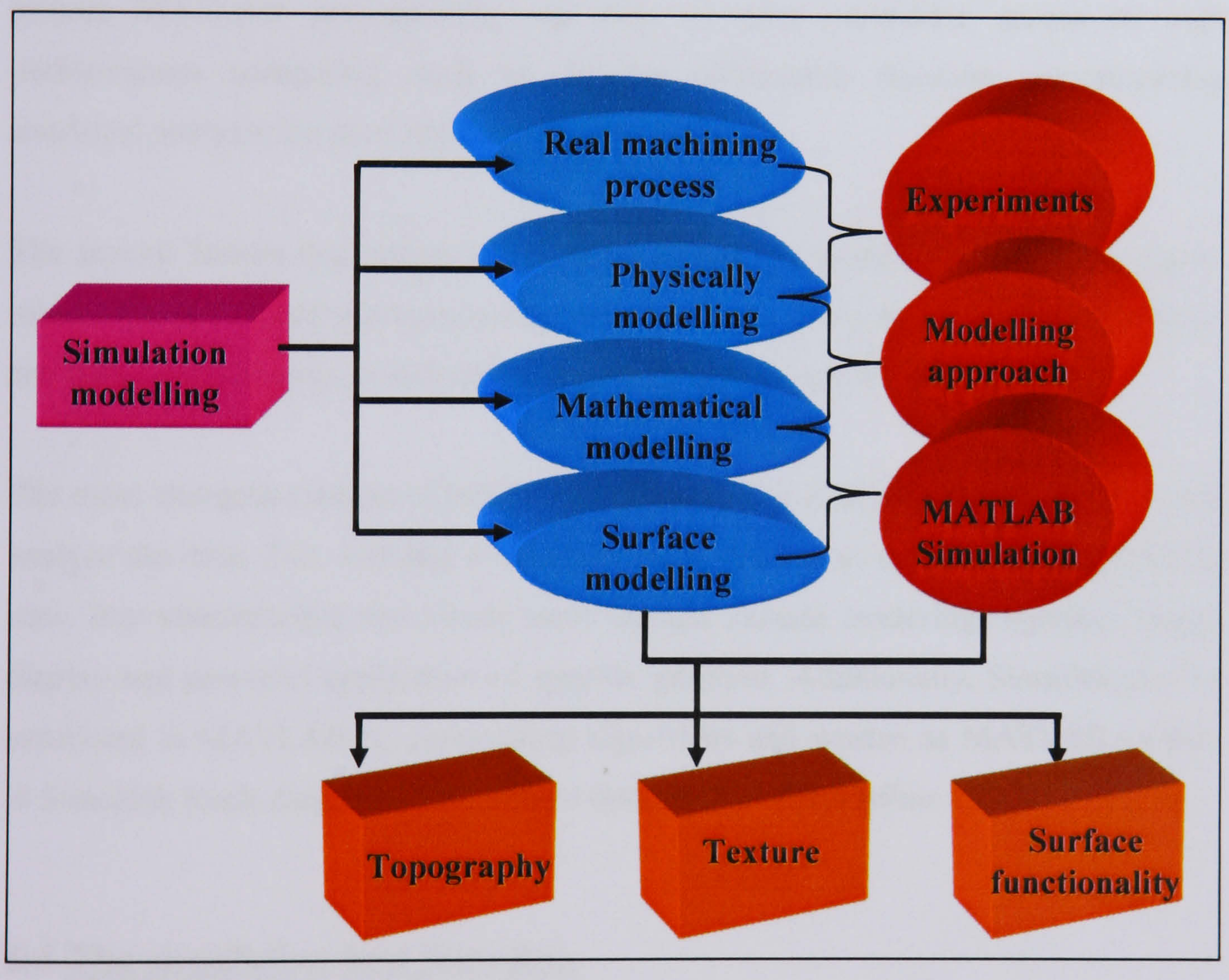

Fig. 5.1 Illustration of this proposed simulation approach

5.2 A proposed simulation approach

MATLAB is a high performance programming tool for technical computing. This program is able to simulate the complex machining process and system efficienctly.

Furthermore, MATLAB can integrate computation, visualization and programming in a user friendly environment. It also offers users the intuitive language for expressing problems and their solutions mathematically and graphically. Fig. 5.1 illustrates the proposed simulation approach which aims to bridge the gap among the real machining process, physical modeling mathematical modeling and computational output in numerical and graphical modes.

5.3 Selection of MATLAB as the simulation tool

MATLAB can produce accurate results and undertake numeric computing quickly. This feature is suitable for the cutting process modeling and simulation. During this project MATLAB programming can help to give immediate access to high performances computing such as solving differential equation, programming statistical analysis function and matrix computation.

The second feature that makes MATLAB a suitable programming tool it is a highly interactive and friendly programming tool. The programming, such as flow control and data structures, etc, is included in the MATLAB programming.

The most interactive aspect of MATLAB programming is its graphics to visualize and analyze the data. 2-D, 3-D and 4-D can be easily plotted as required for engineering data. For visualization, the visual tools include surface rendering, lighting, image display and powerful application of specific graphics. Additionally, Simulink can be combined in MATLAB by cooperating algorithms and written as MATLAB m-files in Simulink block diagrams. This will be described in detail below.

5.4 The simulation tool Simulink

There are a few features Simulink additionally suitable for simulating machining processes.

(1) Simulink has an extensive library of predefined blocks where the developers can build the models of the system easily. All the system can be built through block

diagrams and equations by "dropping" the components from the library and connecting them together.

(2) Except the high level of information makes it easy to understand although the detail information can be hidden in the sub system within the model hierarchy.

(3) Visualization of the system can be shown through the hierarchical models, blocks library, scalar and vector connections, signal and port labels, open architecture and quality graphics. The graphic also enable the visualization of the system dynamics.

For this project, MATLAB and Simulink are the best tools, particularly for simulating the linear phenomenon during the turning process. The Simulink extensive blocks give an easy way to develop the system. Furthermore, Simulink can be a better solver for the equations and high accuracy as requested by the machining system. The user friendliness is also advantage with which the developer can develop the system easily and at the same time can understand the programming language easily as well. Simulink also has lots of statistical functions which can develop to calculate the surface characterization parameters. The results of the simulation can be shown through the cutting force, machined surfaces topography and defined surface parameters.

5.5 Simulation of surfaces generation in turning processes

5.5.1 Integrated simulation model

Fig. 5.2 shows the whole simulation model of the surface generation implemented by Simulink. According to Fig. 5.2 cutting forces, turning process, wear, regenerative, vibrations and residual stress are a part of the simulation. All the system can be developed step by step. The colour codes represent the function of the system to some extent.

The light blue colour blocks represent some indirect outputs and many of the inputs for nonlinear output connected with the machining response by manual switch blocks. It is a big advantage to develop or remove/add the effect model during the simulation

easily. The black colour blocks are a part of direct inputs and they represent temperature model, vibration model and wear model. All the details of the implementation models can be found in the respective subsystem which are hidden within the hierarchy.

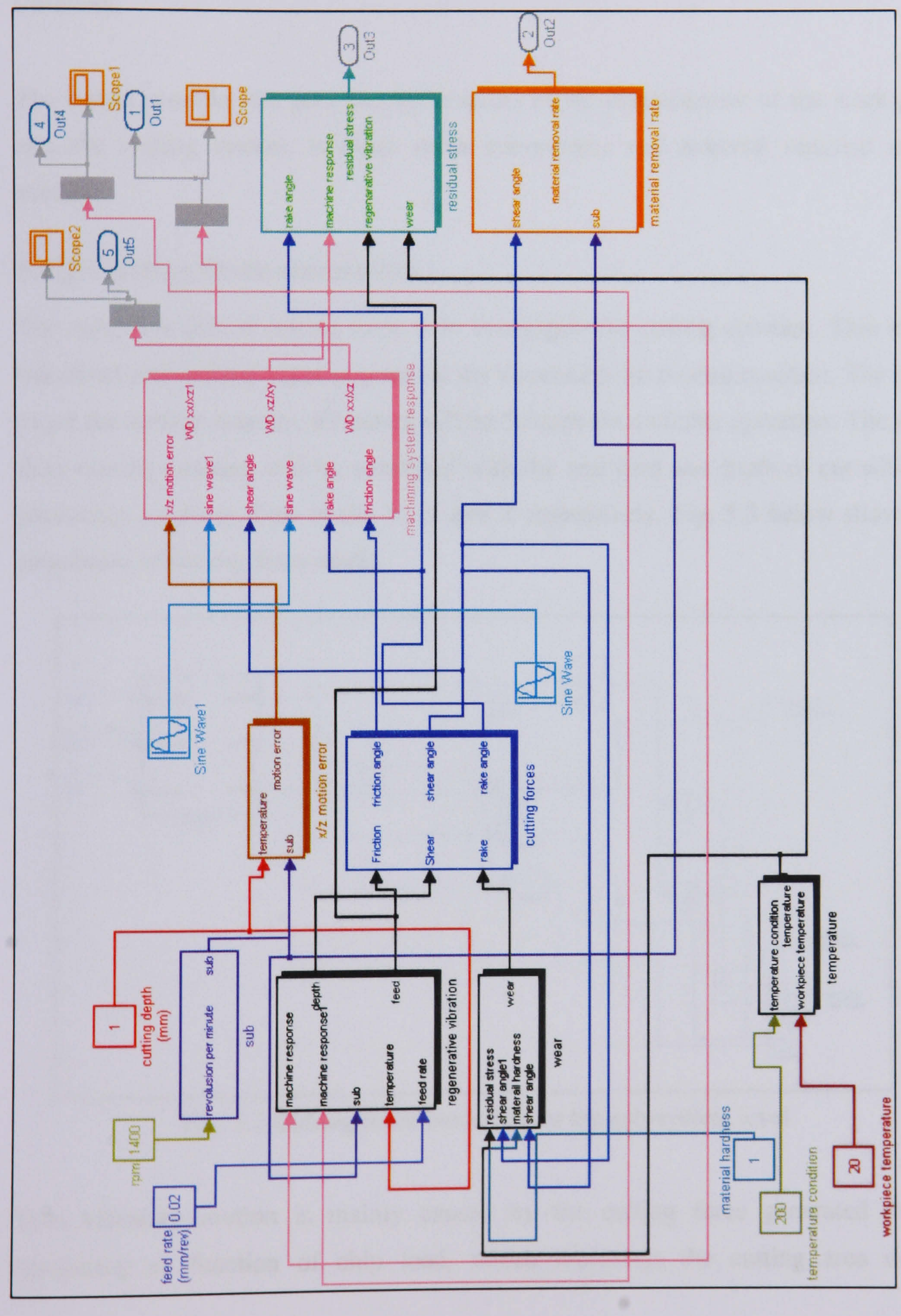

Fig. 5.2 Simulation implementation

Fig. 5.2 also shows, the turning process modeling which includes cutting forces model (the dark blue block), vibration model (the black block), temperature model or thermal model (the black block) and tool wear model (the black block). The maroon block is the machining response model developed by using transfer function blocks in Simulink.

The output module (the grey blocks) consists of the displacement of the work piece and the tooling system, residual stress sub-module and material removal sub – module.

5.5.2 Cutting force simulation

The main function of cutting force is to investigate the cutting constant. This model has direct and indirect input to generate the simulation for cutting constant. The direct to get the cutting constant, all inputs will be through the complex operation. The result from cutting constant will be combined with the real feed and depth of cut which is producing a cutting force in the X, Y and Z respectively. Fig. 5.3 below shows the simulation of cutting force model.

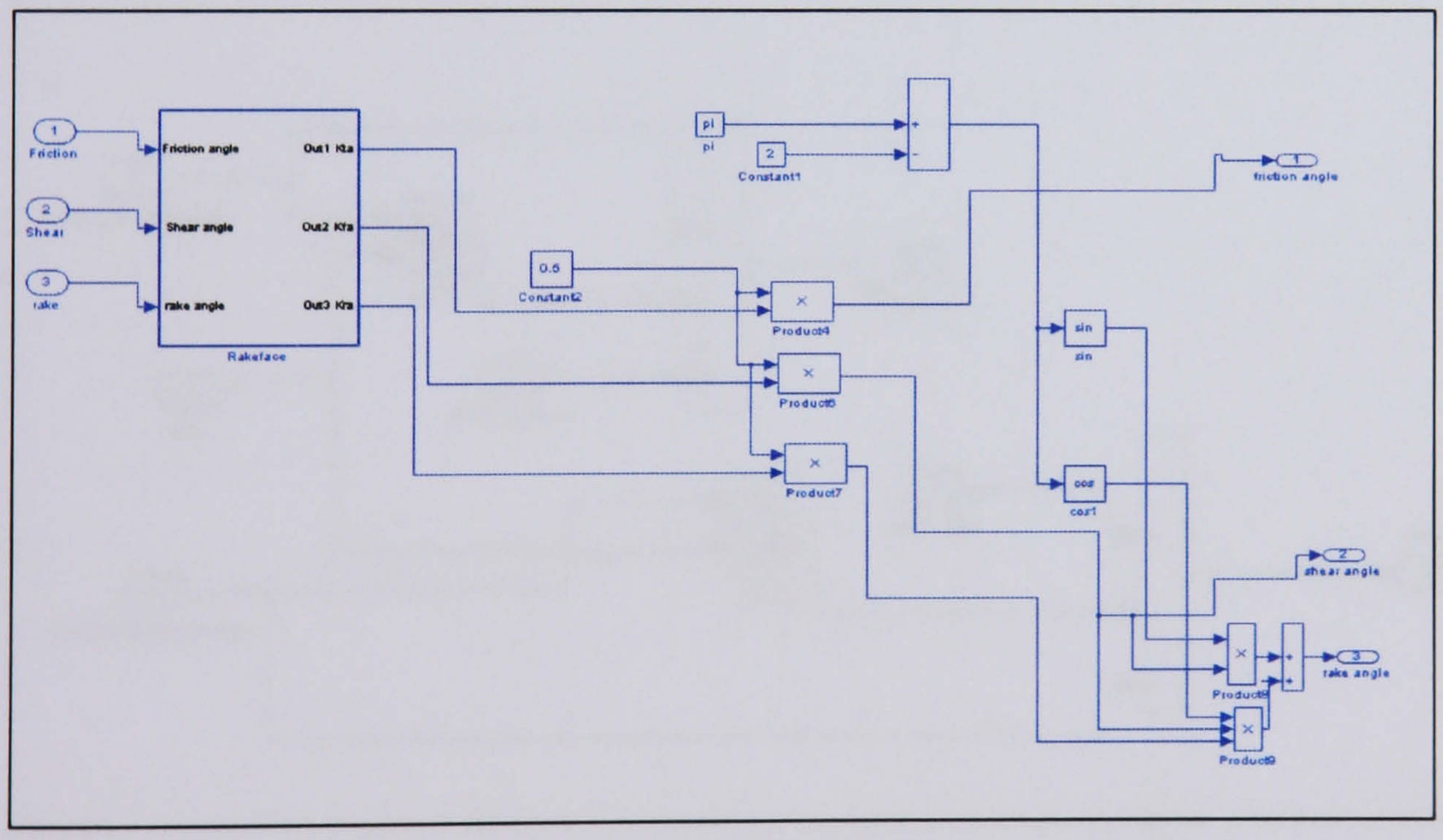

Fig. 5.3 Cutting force modelling or the sub-system level

Tool vibratory motion is mainly caused by the cutting force generated during machining as function of chip load, which represents the cutting area during

machining. The cutting area is expressed as the product of the width of cut of cut and the thickness of cut. The cutting force maybe assumed to be proportional to the chip load. Where the proportionality coefficient Equation is (4-35), (4-37) and (4-39) the detail of cutting force equation process.

5.5.3 Chatter simulation

Fig. 5.4 shows a regenerative vibration model where the vibration is simulated by Variable Transport Delay. The main reason it is simulated by Variable Transport Delay because of the varieties of feed rate and depth of cut deployed in the turning process.

The cutting force coupling will result in shear angle. Except the cutting force coupling, the variation of shear stress can be simulated also by MATLAB general functions in Simulink. The factors that cause the variation of shear stress deformation is the thermal softening and strain hardening of the workpiece chip deformation. To get this deformation the frequency of vibration is around 43 Hz at Harrison M250 turning machine.

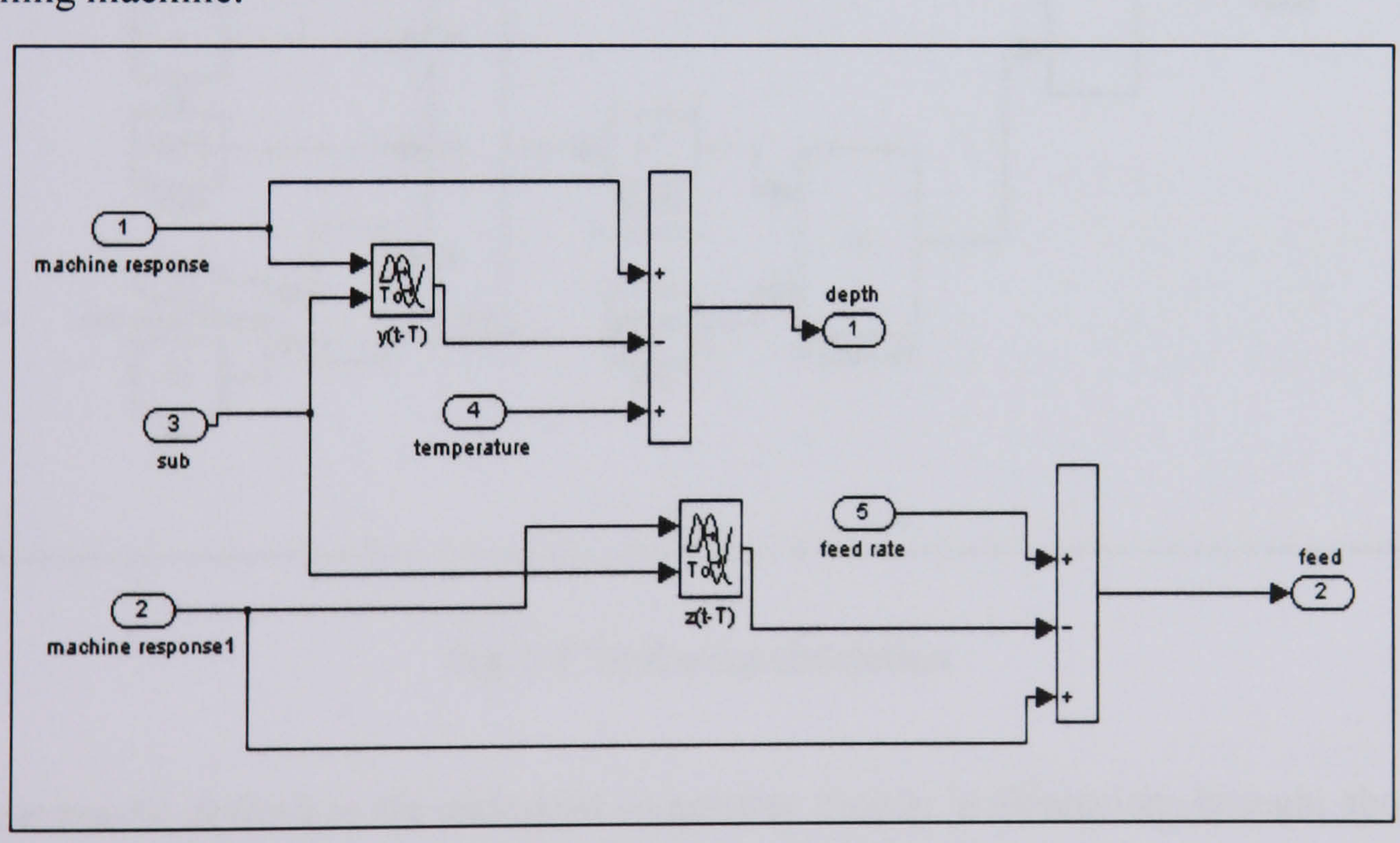

Fig. 5.4 Regenerative vibration modelling and simulation

The relative vibration between the tool and the workpiece is steady simple harmonic motion with a small amplitude and low frequency. Only the relative vibration in the in

feed cutting Z direction is considered since its effect prevails in the generation of surface roughness. When the depth of cut is small, the influence of self excited chatter and tool wear can be neglected. Although the fluctuation of cutting force due to the variation of uncut chip thickness might influence the surface roughness, the ratio of the amplitude of vibration to the depth of cut is usually very small in machining. Equation (4-46) and (4-47) show the variation of cutting thickness and width.

5.5.4 Tool wear simulation

According to Fig. 5.5, the tool flank wear is an input to the cutting force simulator. For this process an indirect factor can be integrated easy to control where the manual switch can be used to remove the indirect factors from the simulation process.

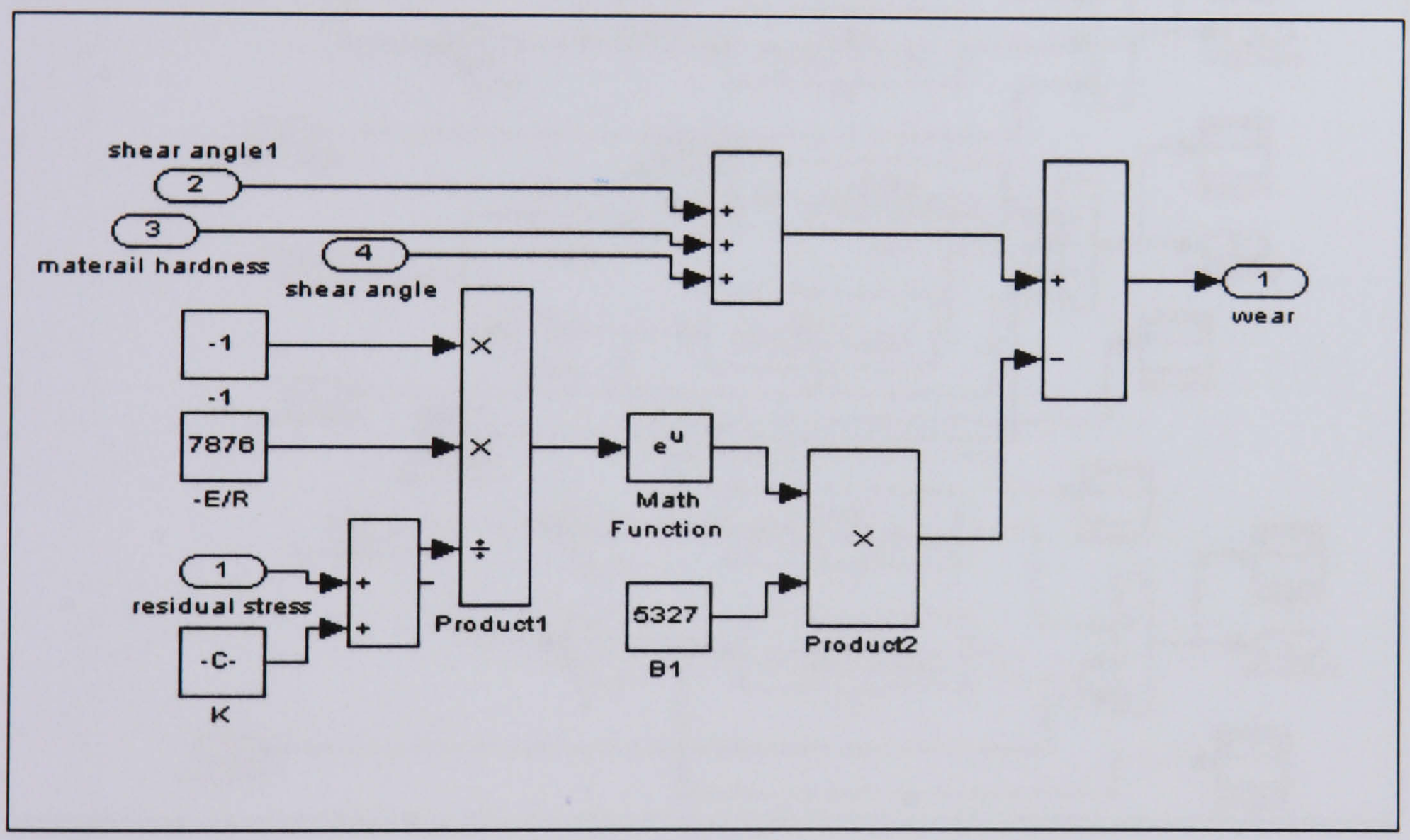

Fig. 5.5 Tool wear simulation

Wear maybe defined as the undesired cumulative change in dimensions brought about by the gradual removal of discrete particles from contacting surfaces in motion, due predominantly to mechanical action. The complexicity of the wear process may be better appreciated by recognizing that many variables including hardness, toughness,

ductility, modulus of elasticity, yield strength, fatigue properties and etc. The details of tool wear can be described in Equation (4-51).

5.5.5 Machining response simulation

Transfer blocks are used to build the machining system response simulation. The user only needs to change the parameters in the Transfer function block based on the modal parameter within the machining system response simulation as shown in Fig. 5.6.

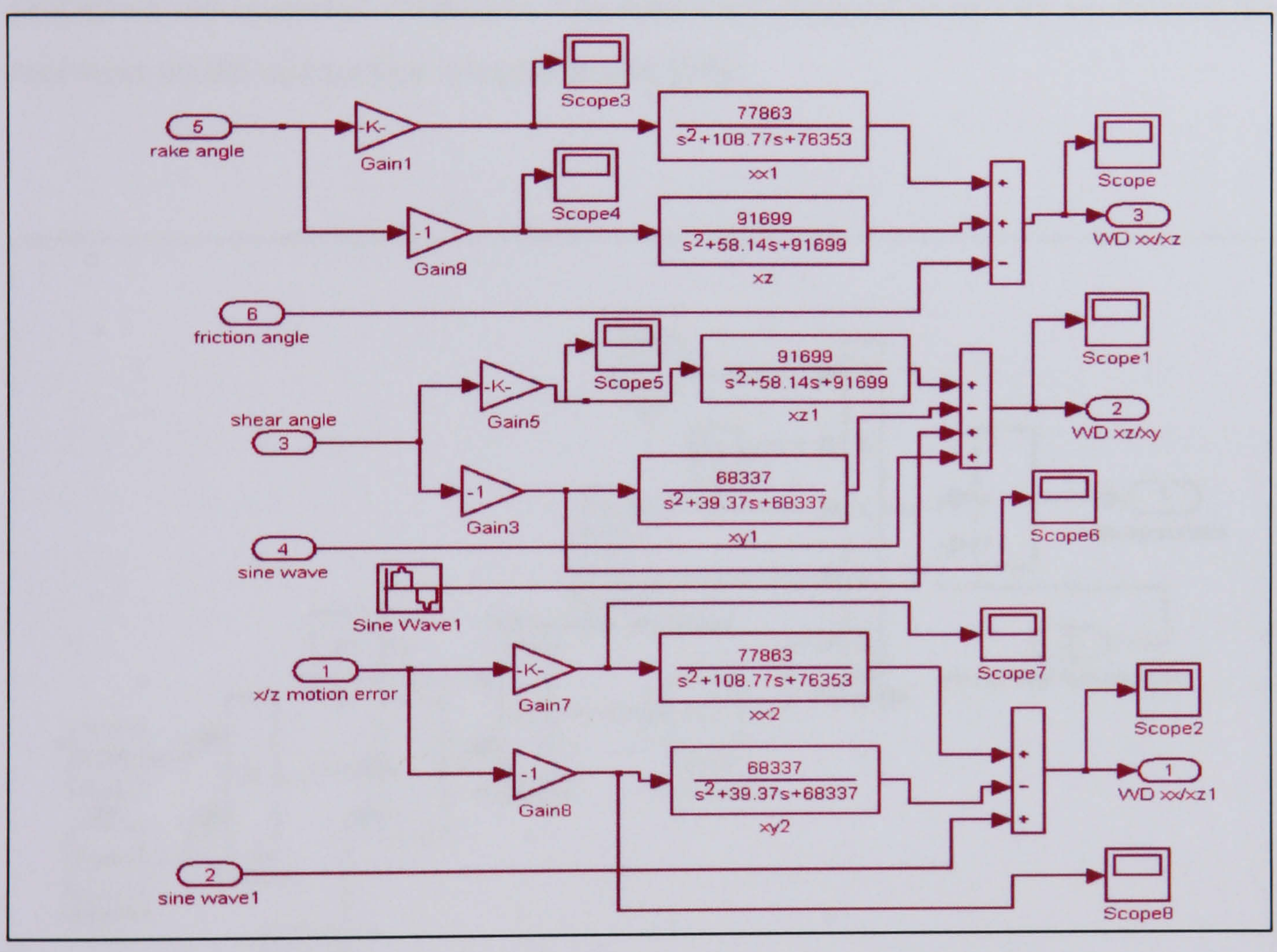

Fig. 5.6 Machining system simulation

Figure 5.6 shows machining response simulation. The machining response simulation is referring to the machining system simulation. According to X.C. Luo *et al* [161], machining response is related to the tooling structure in direction due to the force acting in the opposite direction when the other two force component are zero. X.C. Luo *et al*, also estimated the structural natural frequency according to the tooling and

workpiece system structural dimensions and components specification provided by manufacturer. For more detail of transfer function refer to equation (4-57 and 4-58).

5.5.6 Temperature simulation

The temperature will rise at the interface between the tool flank face and the machined surface. However, the increasing of temperature will occur in the simulation model shown in Fig. 5.7 when there are the inputs from material thermal properties and operation conditions. The simulated temperature will be an input to the tool wear model and surface integrity model [50].

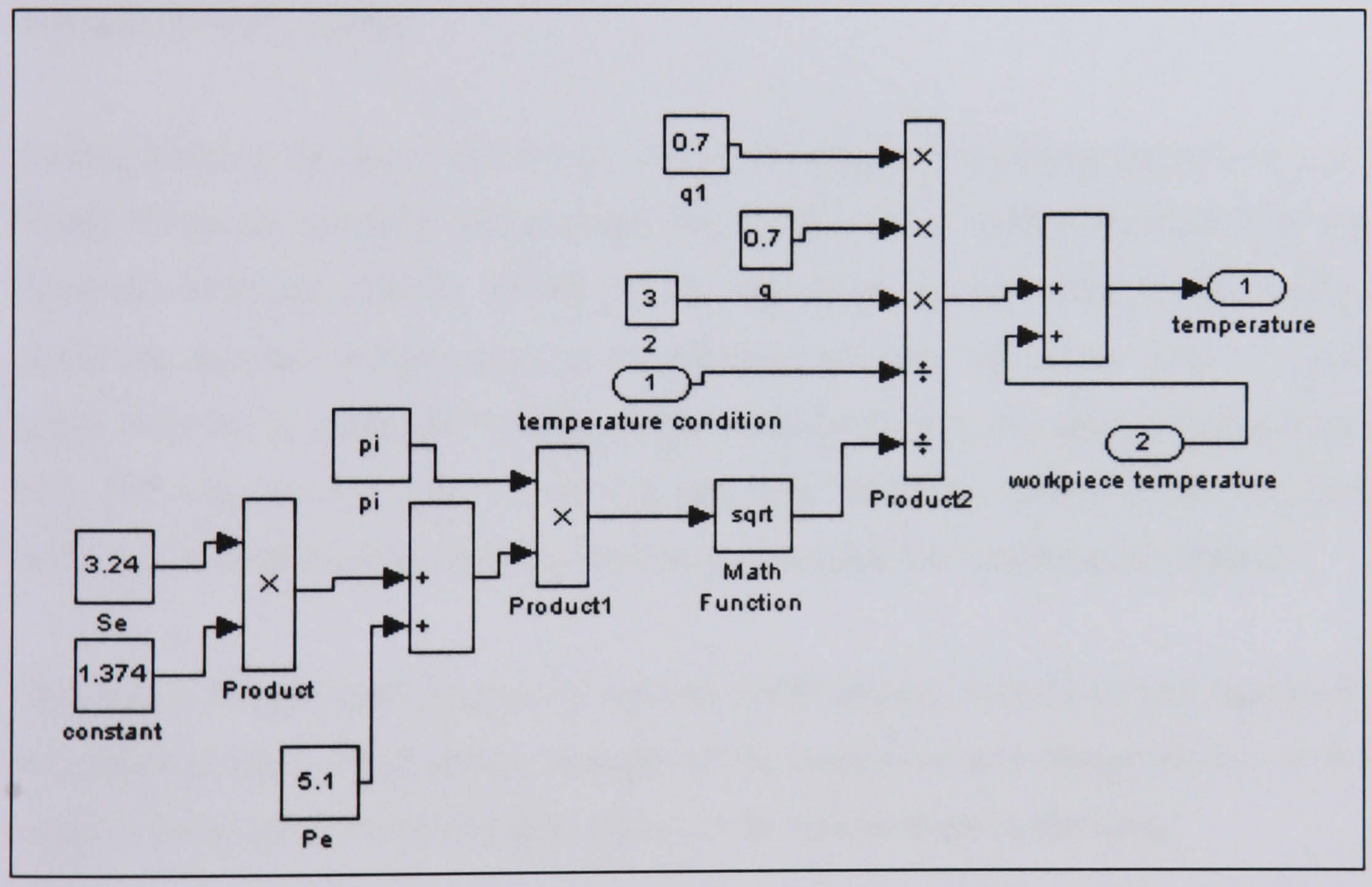

Fig. 5.7 Temperature simulation

In turning process it is significant that temperature will rise in chip. This is without considering the additional heating due to friction between the chip and tool. It is important to understand how much of the heat generated in convicted in to the chip

and what are the additional temperature rises caused by friction with the tool. This can be referred to Equation (4-50)

5.6 Discussion

From the series of simulations, the cutting force, turning process and surface generation can be fully simulated and the effects of each factors individually and collectively. The results from the simulation can be used for process optimization and feed into the production practices.

To study the turning process, the cutting forces are important, Since there are lots of information that can be found through cutting forces simulation especially in the material removal process.

Cutting speed is the rate at which the material moves past the cutting edge of the tool. There will be an optimum cutting speed for a certain set of machining conditions and from this speed the spindle (RPM) can be calculated. Factors affecting the cutting speed are material being machined, the material and tool life of the cutter. Cutting speed is set on the assumption that optimum conditions exist including metal removal rate, full and constant flow of cooling and chip flushing, rigidity of the machine reduction of vibrations or chatters, continuity of cut and the condition of materials.

Feed rate is set up depending on the surface finish desired. Spindle power, rigidity of the machine and tooling set up, strength of the workpiece and characteristics of the material being cut are also essential factors to be take account in the setup.

The depth of cut directly influences the machine performance and tool life. If the depth of cut is too large for the width and the feed is too high, the tool insert may be overloaded and cause the breakage immediately. If the depth of cut relative to the feed is too small, the resulting side of forces will not be sufficient to properly defect tool, and vibration may be occurred.

The weakest loop can be as a control objective in the system. If it can be set in a stable state it can achieve the desired surface quality where the whole system will be stable. In the cutting system, the stability is very sensitive in the radial direction, and its effect prevails upon the generation of surface texture. Based on the mechanism of regenerative vibration, the chip thickness is:

$$h(r) = h_0 - y(r) + e^{-sT} y(r) \tag{5-1}$$

According to the transfer function between the radial cutting force and the workpiece displacement between cutting tool and workpiece, equation (5-1) can be rewritten as:

$$h(r) = h_0 + (e^{-sT} - 1) K_r b h(r) G_{yy} \tag{5-2}$$

The resulted transfer function between the dynamic and the reference chip loads becomes:

$$\frac{h(r)}{h_0(r)} = \frac{1}{1 + (1 - e^{-sT}) K_r a \varphi(r)} \tag{5-3}$$

The stability of this transfer function is determined by the roots of its characteristic equation, that is:

$$1 + (1 - e^{-sT}) K_r a \varphi(r) = 0 \tag{5-4}$$

Indirect factors have significant effects on the surface topography and texture produced. When indirect factors are not part of the system, the feed rate becomes the important factor affecting the machined surface finish. The significance of indirect effects on surface quality and accuracy can be assessed by:

$$Nig_x = \frac{|N_x - N_0|}{N_x} \times 100\% \tag{5-5}$$

Nig_x - significance of indirect factors;

N - value of characterization parameters of simulated surface;

N_x - indirect factors are turn on;

N_0 - indirect factors turn off.

The significance of each nonlinear factor can be assessed by running simulations again with only the studied nonlinear factors turned on.

$$Nig_{xi} = \frac{N_{xi}}{N_x} \times 100\% \tag{5-6}$$

Nig_{xi} - significance of i-th nonlinear factor;

N_{xi} - value of characterization parameters simulated surface when i-th indirect factor is turned on.

Spindle error motion has significant effect on surface finish. The contributions of indirect chip formation and tool wear to surface finish are also remarkable, where tool wear makes a significant contribution to tensile residual stress.

A series of simulations have been performed to study the cutting forces, machining operation and indirect factors on high precision surface generation and the stability analysis of the machining system in order to find out the operational condition for zero or minimum chatter.

Simulink is able to develop a modelling and simulation of the complex machining process and visualization of the machined surfaces. The high frequency vibrations dominate the fluctuation of cutting forces. The first vibration mode is associated with the spindle rotation synchronous with the error motion and regenerative vibration frequency. It may also cause the vibrations between the cutting tool and the workpiece. The vibrations have lower amplitudes than the machined surface roughness, and low frequency as well.

In surface generation feed rate plays an important role in precision which influences the relative vibration between the cutting tool and the workpiece on surface roughness

where it may diminish by the small feed rate. In precision turning the machining errors are mainly caused by spindle error motion and regenerative vibrations. Environmental vibration makes less contribution than spindle error motion and regenerative vibration. Spindle synchronous error motion has significant effect on surface finish. The contributions of nonlinear chip formation and tool wear to surface finish are also remarkable. Tool wear has significant contribution to tensile residual stress.

5.7 Conclusion

The simulation of surface generation in precision turning process is implemented by MATLAB & Simulink. A series of simulations have been performed to study the effects of cutting forces, machining process and direct factors on high precision surface generation. Stability analysis is also carried out through this research. The findings of this investigation are:

(1) MATLAB & Simulink is a powerful development tool for modelling and simulation of the complex machining process and visualization of the machined surfaces. The extensive block library of Simulink eases the simulation of direct factors.
(2) The fluctuation of cutting forces is dominated by high frequency vibrations.
(3) The relative vibration between the cutting tool and the workpiece is mainly caused by spindle synchronous error motions, regenerative vibration and environmental vibrations.
(4) The Feed rate influences relative vibrations between the cutting tool and the workpiece on the surface roughness.
(5) The machining errors are mainly caused by spindle error motion and regenerative vibrations. The BUE and environmental vibrations make less contribution than spindle error motion and regenerative vibrations. Spindle synchronous error motion has significant effect on the surface roughness.

Chapter 6 Validation of the modelling and simulations through machining trials

6.1 Introduction

This chapter is concerned with the experimental studies on the surface generation in the turning process. There are 27 machining trials being carried out and the purposes of the experiment are:

(1) To evaluate and make a validation of the modeling approach by measuring cutting forces and machined surfaces.
(2) To investigate on the effects of direct and indirect factors on the surface generation.
(3) To analyze the results of the experiment.
(4) To investigate in-depth on the machining stability and effects on the surface topography.

6.2 Facilities and workpiece materials for cutting experiments

6.2.1 Facilities for turning experiments

The facilities for this experimental study include a Lathe (Harrison M250) and a Zygo 3D surface profiler.

The lathe is shown in Fig. 6.1 has the cross slides in the X and Y directions. The lead screws will drive into those three directions. The spindle of the lathe machine has a variety of speed beginning with 250 rpm to 1500 rpm and spinning continuously. During the trials, the carbide and high speed steel cutting tools are used. The Carbide and high speed steel tools are purchased from Widia Valenite and West Yorkshire Steel Co.

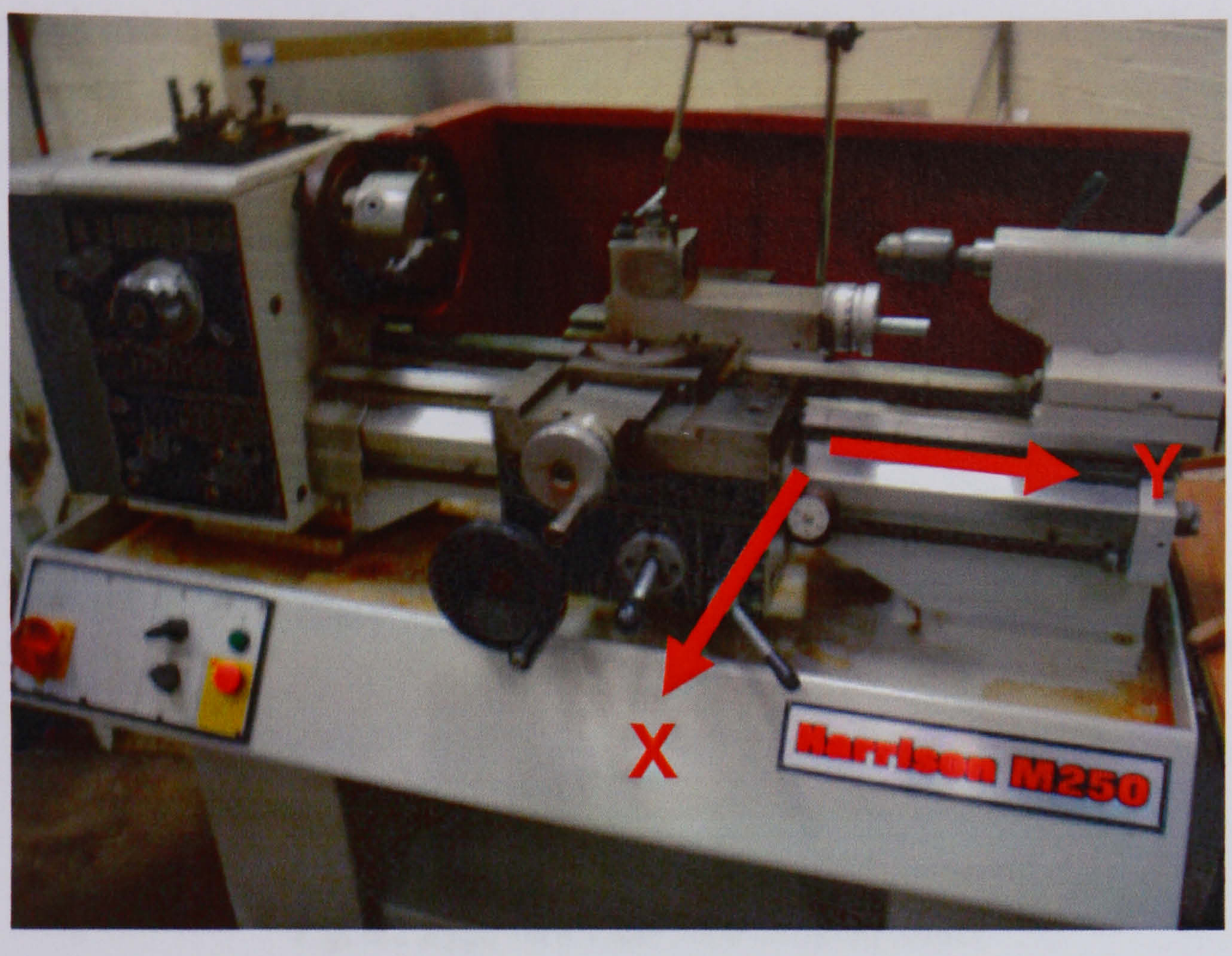

Fig. 6.1 Harrison M250 turning machine

The machined surfaces from the trials will be measured and assessed by a 3D surface profiler - Zygo New View 5000 optical microscope.

This 3D surface profiler can provide non – contact and high precision numerical measurement. The detailed specifications of the 3D surface profiler are presented in Appendix 1.

The NewView 5000 System shown in Fig. 6.2 has two basic subsystems which are the optical microscope and computer analysis system. The raw data needed for the analysis can be acquired from the sample surface through the microscope.

The computer analysis system can also play as the surface measurement controller during the measurement process. It performs the visualization, calculations and analysis visualizes the measurement results. The Zygo MetroPro software is installed in the systems, which has the full set of 3D surface parameters covering amplitude,

spatial, hybrid , set of functional parameters and their functions in both graphical and numerical modes. Appendix 2 lists all the Zygo Metropro surface texture parameters and their detailed formulations and descriptions

Fig. 6.2 Zygo NewView 5000 surface profiler

6.2.2 Workpiece materials for turning experiments

As listed in the Table 6.1, two types of workpiece materials are used for the turning experiments. They are Aluminum alloy and low carbon steel. The materials used in in turning trials are 50mm in diameter. The main reason for choosing those two materials because they have all the properties necessary for the process and they are the most commonly used material in the manufacturing industry.

Table 6.1 Material properties for Aluminum alloy and low carbon steel

Material	Modulus of elasticity (GPa)	Yield Stress (MPa)	Vickers Hardners (GPa)	Thermal conductivity (W/mK)	Heat Capacity (MJ/m³)	Diffusivity (mm²/s)
Aluminium alloy	69	270	1	200	2.5	13
Low carbon steel	200	400	21	35	3.5	65

6.2.3 Cutting tools for turning experiments

For cutting tools, only material coated carbide cutting inserts and high speed steel cutting tools are used. However, these tools have different rake angle, clearance angle and nose radius.

Table 6.2 Tool nose radius

Carbide tool inserts	Tool nose radius (mm)
VBMT	0.4,0.8,1.2
SCMT	0.8,1.2,1.6
CNMA	0.4,0.8,1.2
High speed steel	1.2

Table 6.3 Rake angle

Carbide tool inserts	Rake angle (°)	
	back	side
VBMT	10	10
SCMT	10	10
CNMA	10	10
High speed steel	0, ± 10, ± 25	10

Table 6.4 Clearance angle

Carbide tool inserts	Clearance angle (°)	
	back	side
VBMT	6	0
SCMT	6	7
CNMA	6	5
High speed steel	10	0, 4, 6, 10

6.3 The experiment plans

6.3.1 Machine tool measurement

To get a good result especially an accurate result, the rotational run-out must be measured by using dial gauge. The best average of radial run-out is 0.8 μm be

measured. The average amplitude is then used as a parameter for the rotational run–out error function. The straightness of the slideway can be measured roughly by the spirit level method and to find the slideway straightness error.

6.3.2 The machining trials plan

As shown at the flow chart in Fig. 6.4 the experiments are carried out in two sections and particularly investigate the influences the speed level of the spindle and tool geometry during the turning process. Fig. 6.3 shows the machining trials process.

During the turning process, the speed level will be varied at three levels which are low, medium and high. For the influences of tool geometry, trials will be undertaken in two groups which are known as trial test A and trial B.

The cylindrical turning process is carried out to evaluate the modelling approach and investigate the influences of direct and indirect factors under different stages of operational conditions. In this trial the spindle speed is fixed between 350 - 550 rpm. Table 6.5 lists the operational variables in the cylindrical trials. The trials plan can be found in appendix 3.

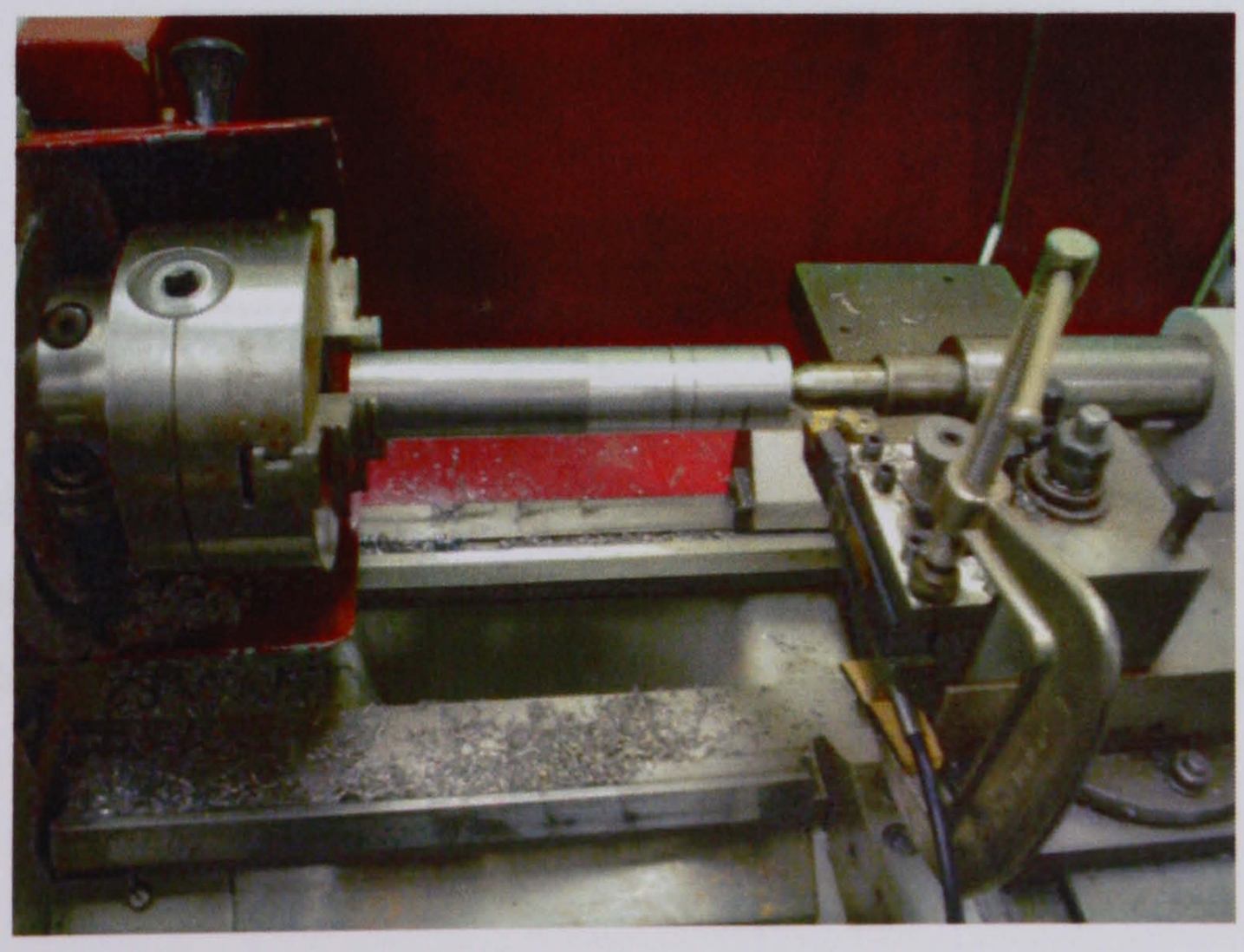

Fig. 6.3 Machining trials process

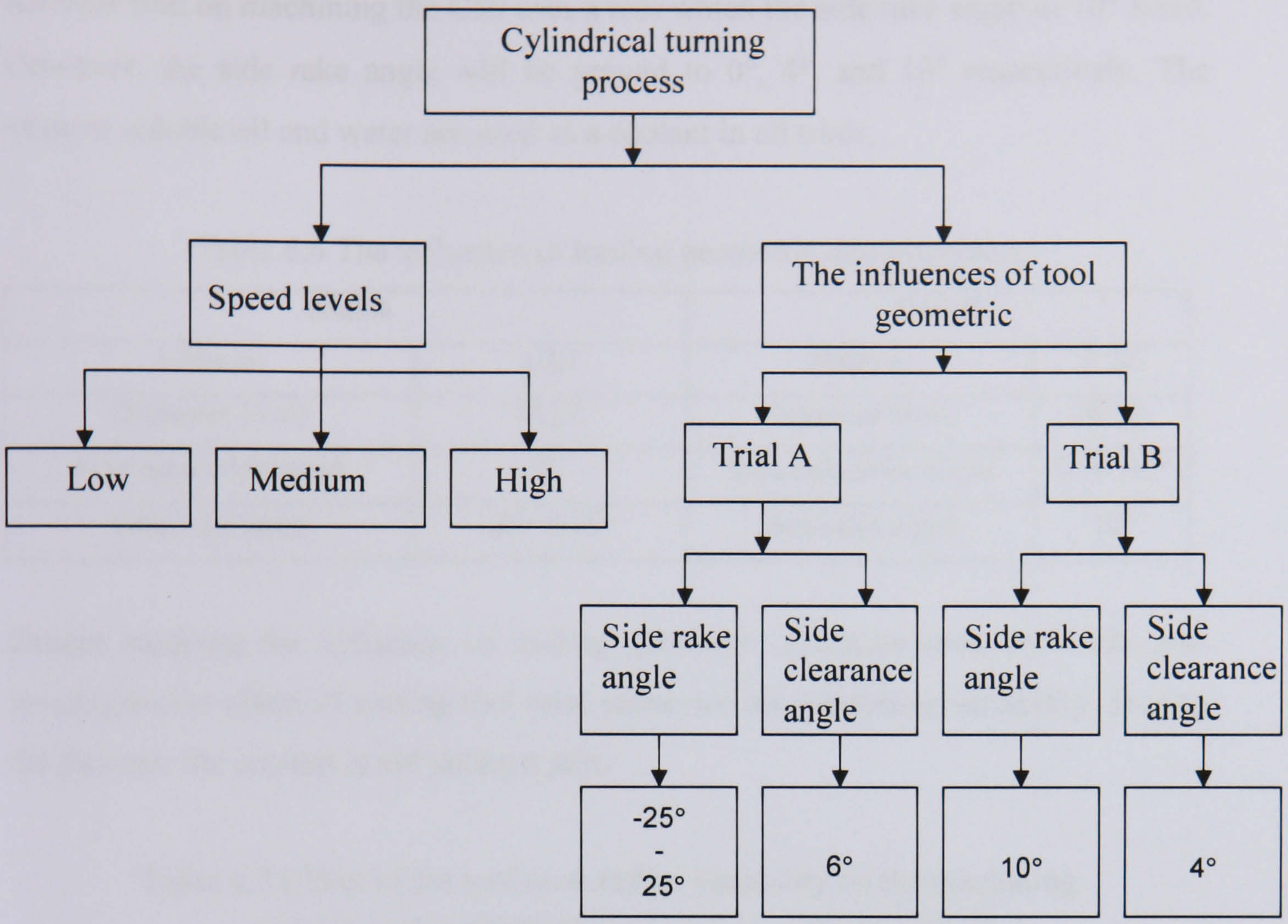

Fig. 6.4 Experiment flow chart

Table 6.5 Variables in cylindrical turning trials

Variables (1)	Conditions
Spindle speed (rpm)	320-550
Feed rate (mm/rev)	0.1
Depth of cut (mm)	0.2, 0.3, 0.4, 1.0
Tool nose radius (mm)	0.8

The trials also plan a study on the influence of tooling geometric characteristics, including that of the side rake angle and side clearance angle. In trial (Trial A) the tool with side clearance angle of 6° is used with side rake angle varying from -25° to 25° as listed in Table 6.6.

Another trial on machining the C50 uses a tool which the side rake angle of 10° fixed. However, the side rake angle will be ground to 0°, 4°, and 10° respectively. The mineral soluble oil and water are used as a coolant in all trials.

Table 6.6 The influence of tooling geometric characteristics

Trial A		**Trial B**	
Material	C50	Material	C 50
Diameter (mm)	Ø 32	Diameter (mm)	Ø 32
Side clearance angle	6°	Side clearance angle	0°,4°,10°
Side rake angle	-25° to 25°	Side rake angle	10°

Except studying the influence of tooling geometric characteristics, the trials also investigate the effect of cutting tool nose radius on the machining instability. During the process, the coolant is not taking a part.

Table 6.7 Effect of the tool nose radius instability on the machining

Variables (2)	**Conditions**
Spindle speed (rpm)	550
Feed rate (mm/rev)	0.1
Depth of cut (mm)	0.2, 0.3, 0.4, 1.0
Tool nose radius (mm)	0.8

Table 6.7 shows the details of tool nose radius and their effect on machining instability. As listed in the Table, the tool nose radius used in the trial 0.8 mm, spindle speed 550 rpm, the feed rate 0.1 mm/rev and depth of cut are 0.2, 0.3, 0.4, 1.0 mm respectively. Once again, there is no coolant applied in the trial.

6.4 Results and discussions

All the results are listed in Appendix 3, but with detailed descriptions in the following subsections. Those results are used to evaluate the modelling approach and further study on the effects of direct and indirect factors on surface generation in the turning process.

6.4.1 Cutting force validation

Fig. 6.5 shows the comparison of the measured cutting forces in the depth of cut direction in the turning trials with their corresponding simulation ones under the same operational conditions. In turning the cutting force in the direction of depth of cut plays an important role in the generation of surface finish. The differences between measured cutting force and simulated cutting force are around 40.85% and 43.2%.

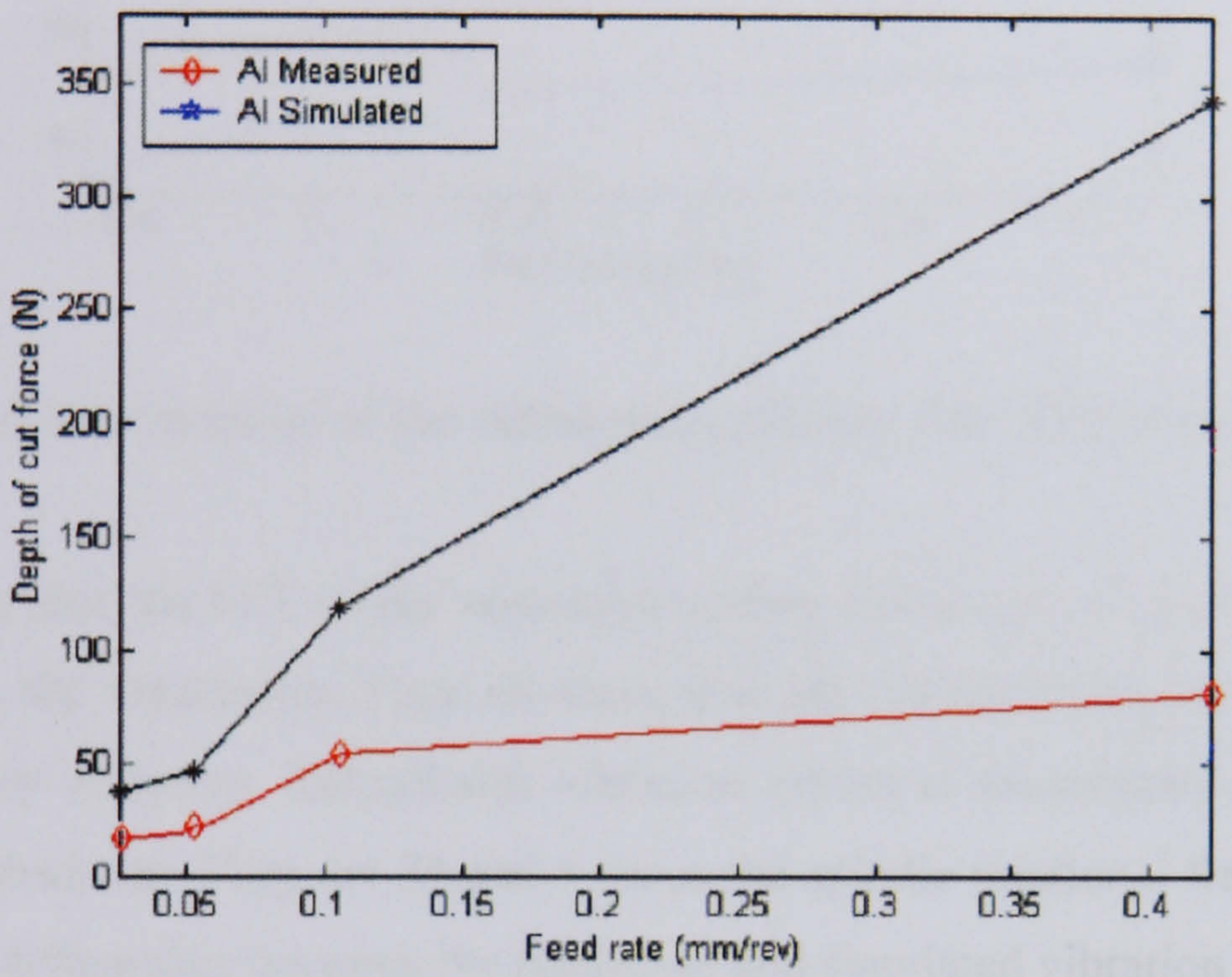

Fig. 6.5 The comparison of measured and simulated cutting forces.

Fig. 6.6 shows the results of simulated and measured cutting forces in the depth of cut direction when the cutting is undertaken at the same conditions. The cutting force in the depth cut direction is also very significant to surface finish. The differences between the measured and simulated value are 33.03% for machining alloy. Therefore the simulated cutting forces agree reasonable well with the measured results. The increase of cutting force with the increasing of feed rate can also be observed. This is because the removal volumes of workpiece material increases with increasing feed rate.

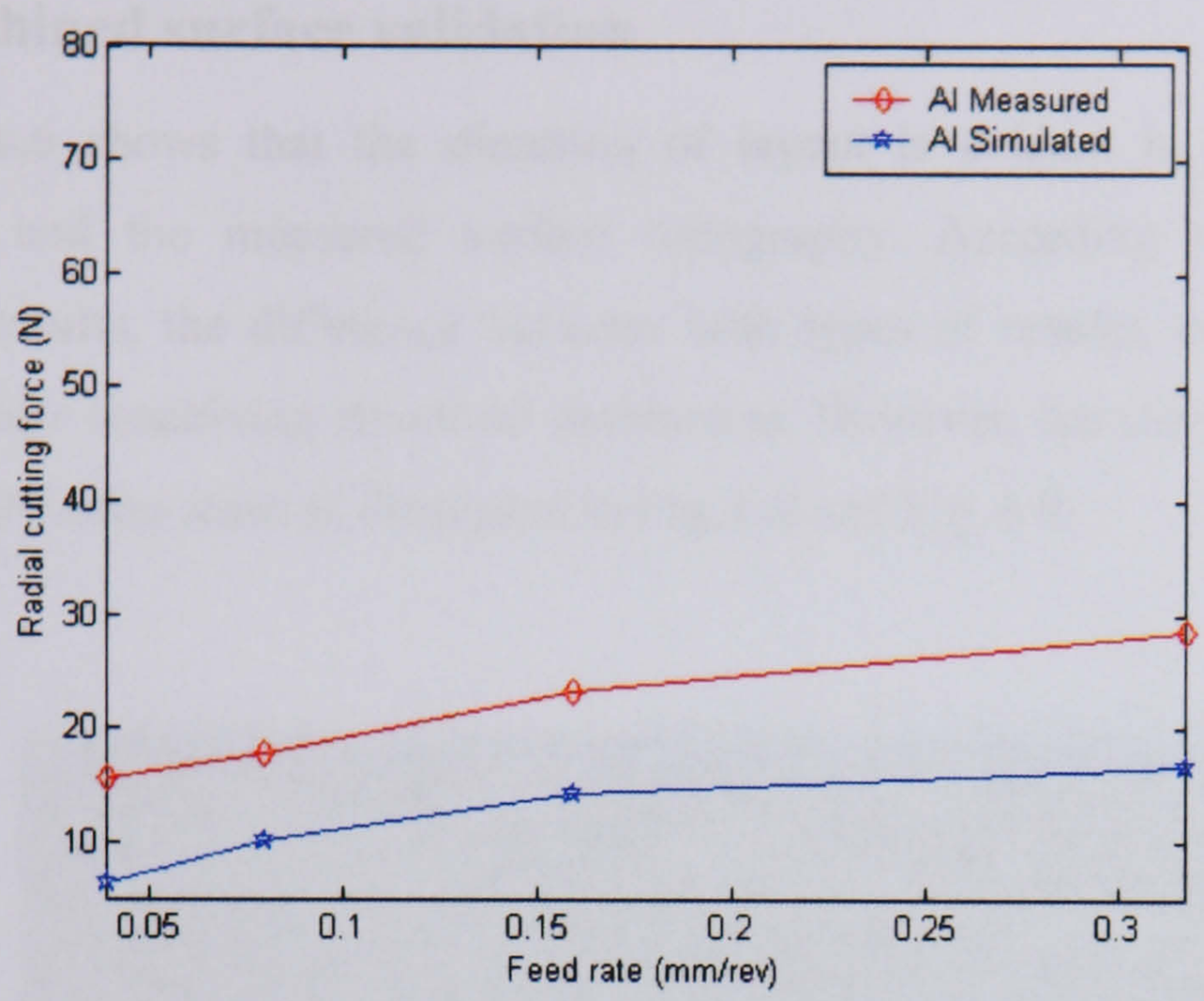

Fig. 6.6 The variation of the radial cutting forces with different feed rate.

Fig. 6.7 illustrates the FFT of the measured cutting force under the same operational conditions as the simulation. They all show that the cutting forces are dominated by high frequency vibration. Remarkable vibration modes at frequencies of 799 Hz and 187 HZ are observed. They are 34 and 8 times the spindle rotational frequency. There are no major differences between the measured and simulated vibration frequency.

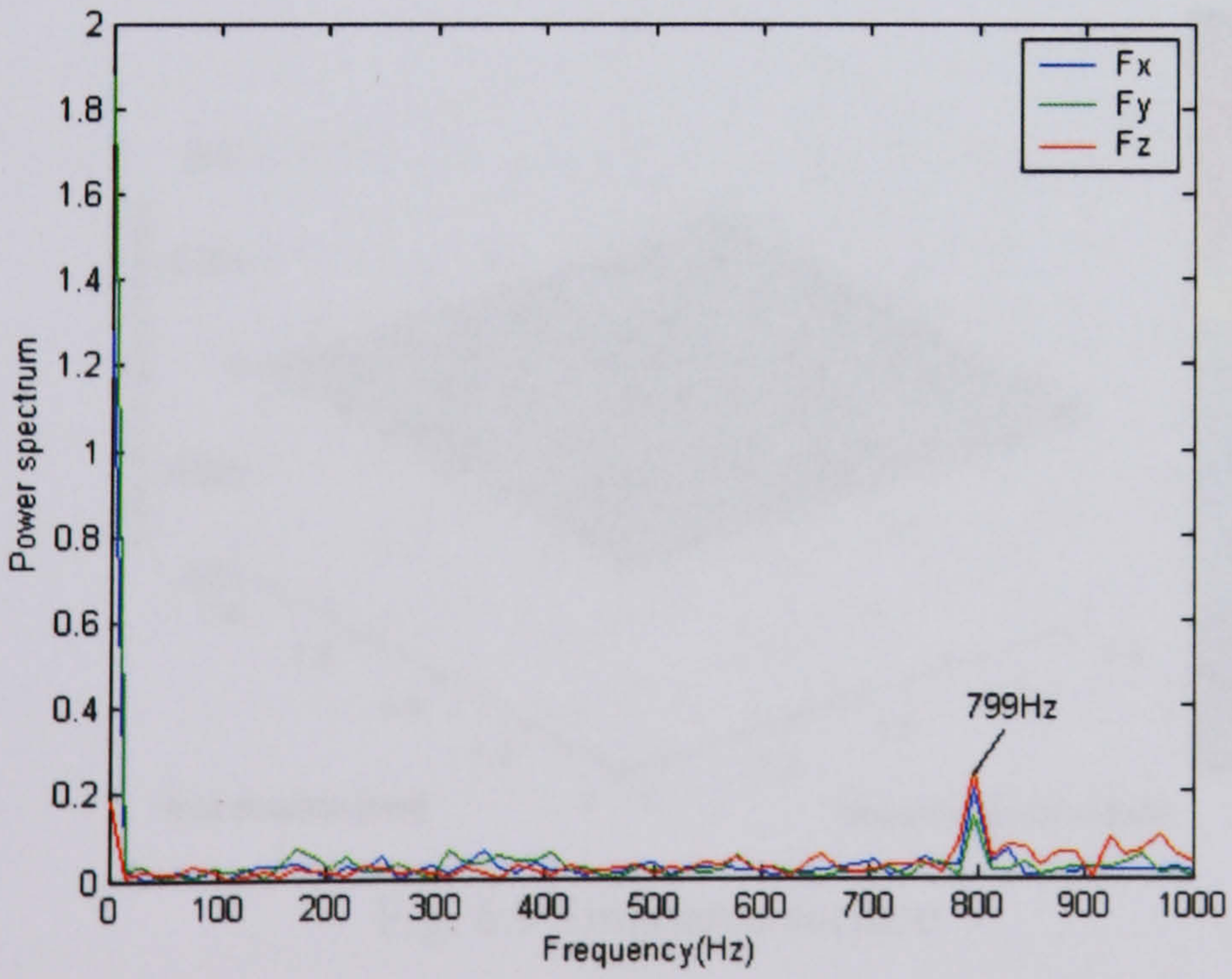

Fig. 6.7 FFT transforms of the measured dynamic cutting force.

6.4.2 Machined surface validation

The trial no.6 shows that the direction of layout is evident in both the surface topography and the measured surface topography. According to the trials and simulation results, the difference between both types of results, may be caused by estimated static machining structural parameters. However, the simulation results are still in the deviation scale as illustrated in Fig. 6.8 and Fig. 6.9.

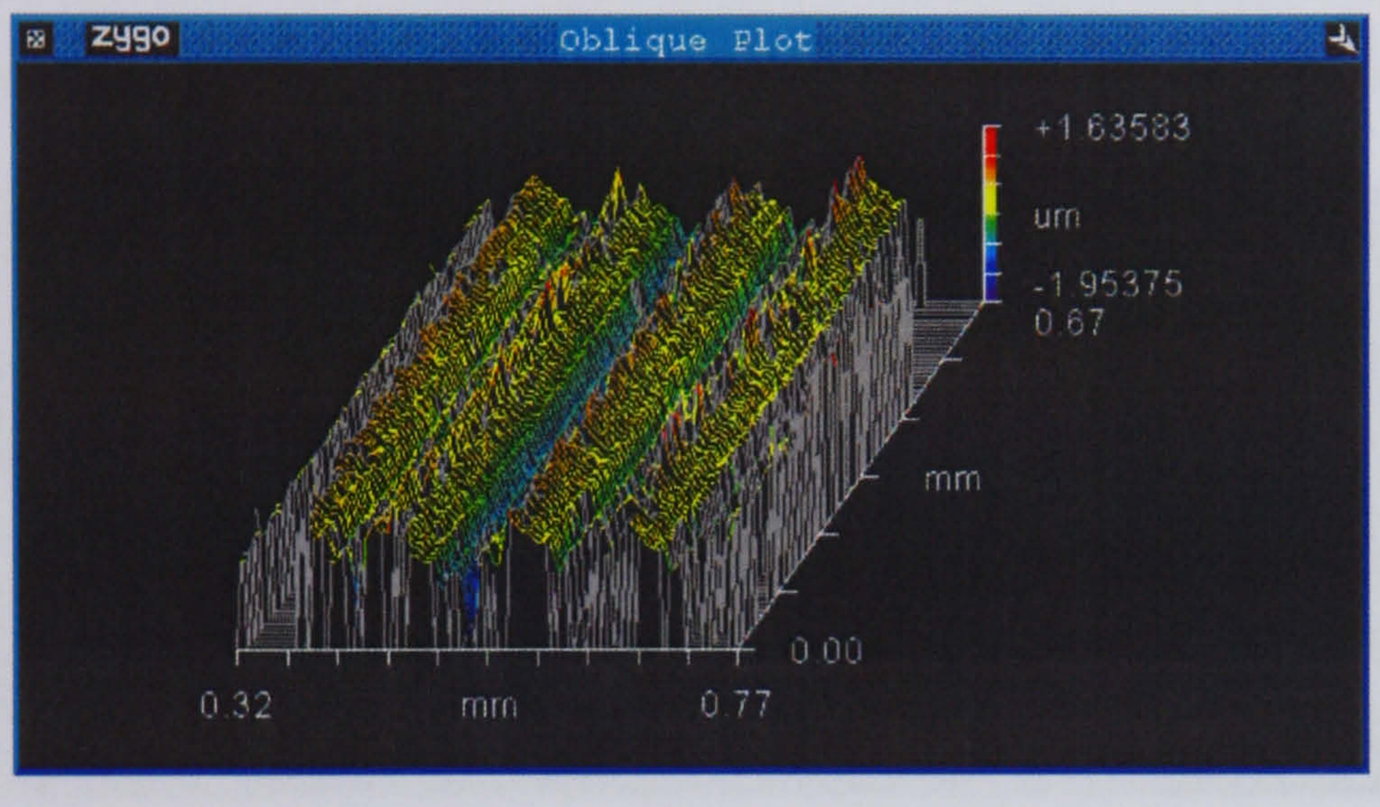

Fig. 6.8 Machined surface

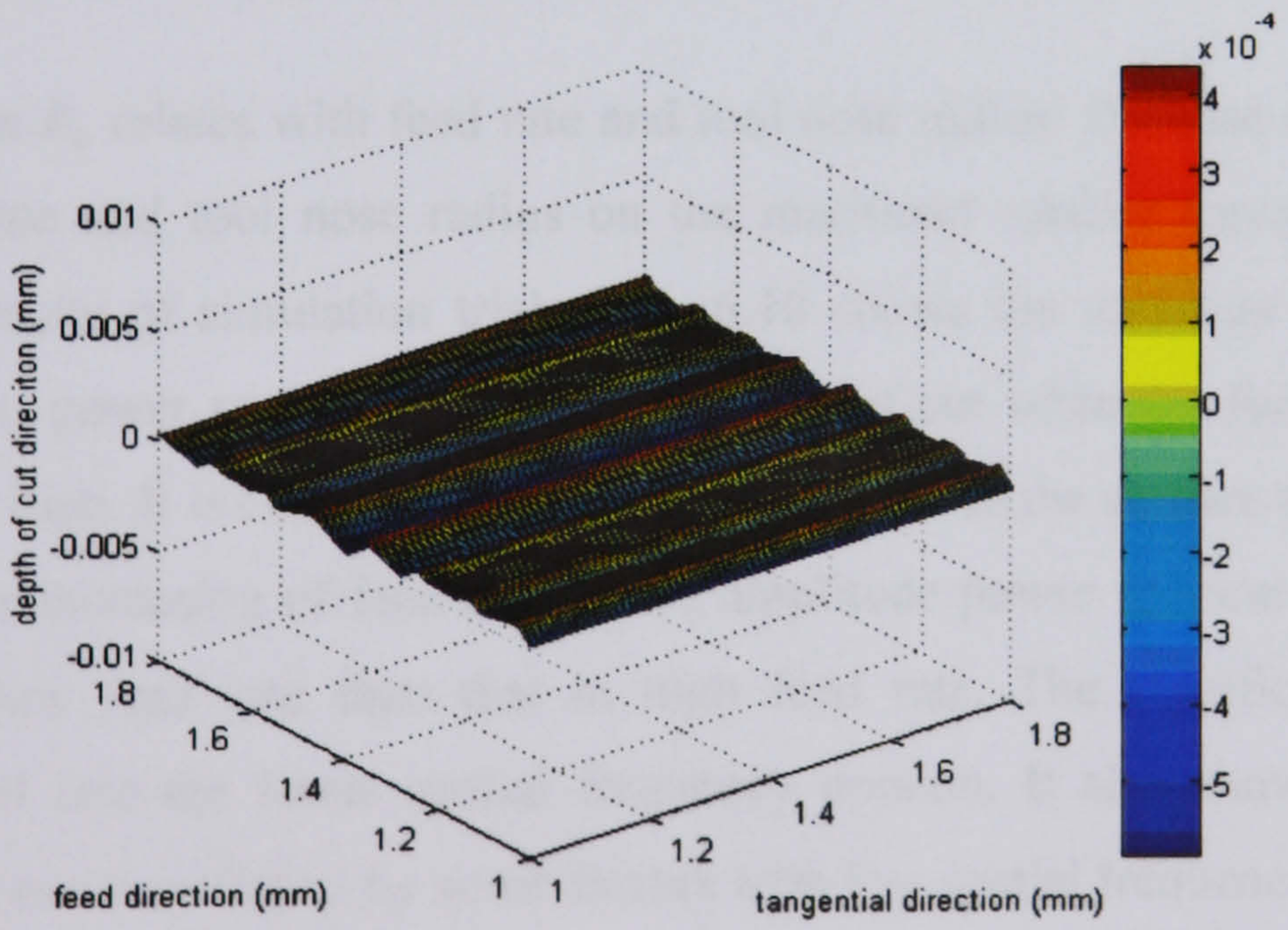

Fig. 6.9 Simulated surface

6.4.3 Effects of feed rate and tool nose radius

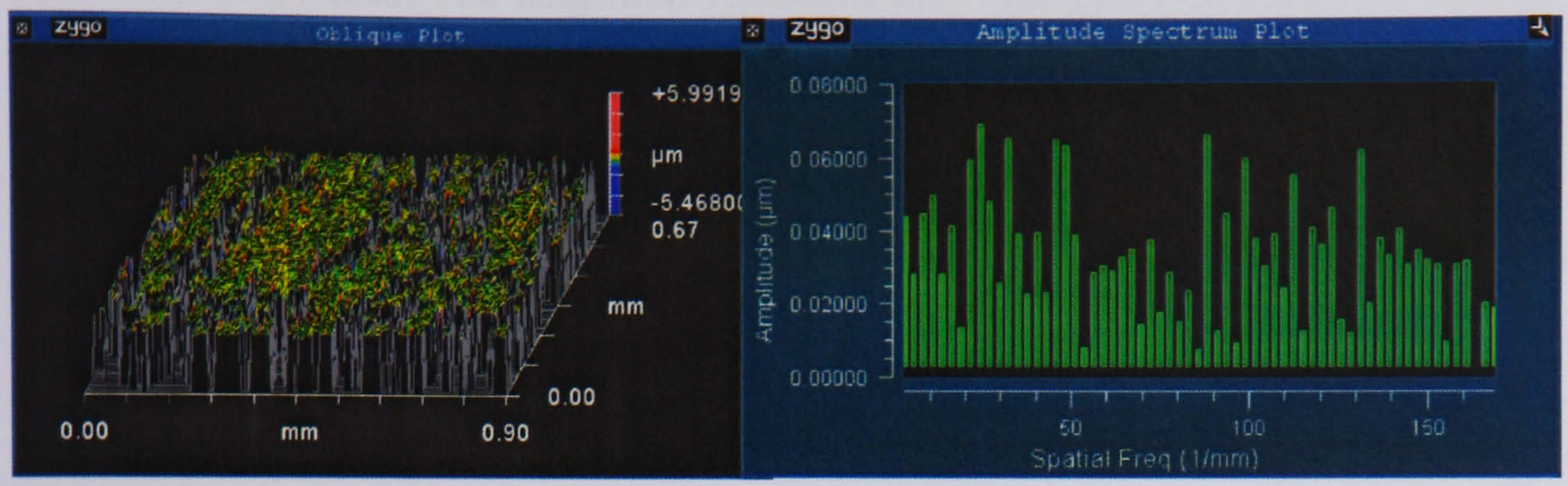

(a) Surface topography (No.5) (b) Amplitude power spectrum (No.5)

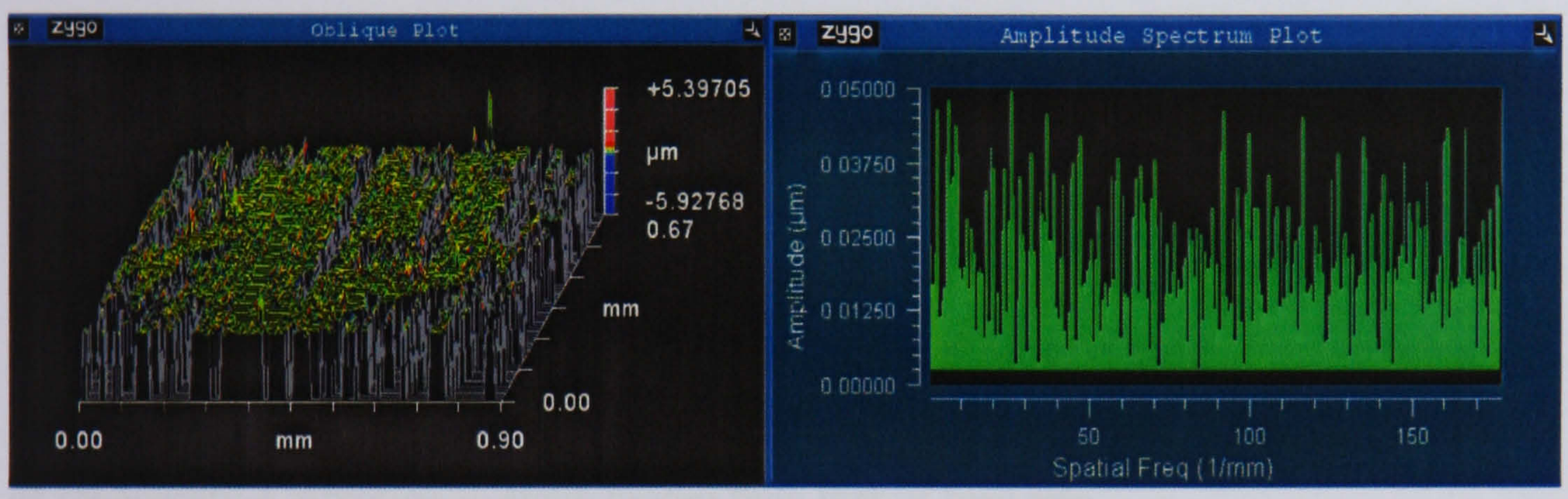

(c) Surface topography (No.6) (d) Amplitude power spectrum (No.6)

Fig. 6.10 Surface topographic characteristics under different feed rate

Surface roughness R_a relates with feed rate and tool nose radius. Because of that, the effects of feed rate and tool nose radius on the machined surface topography are studied by the results of simulation trials. Fig. 6.10 shows the variation of surface topography and its power spectrum under small depth of cut when the feed rates are low, medium and high. It is clear that the width of tool mark in the surface topography increases with the increasing of feed rate. More amplitude power spectral peaks can be observed in low feed rate than that in high feed rate. The significant power amplitude can fall into the lower spatial frequency domain. It also shows that the machined surface can be affected by some factors with low spatial frequencies.

The width and depth of tool mark and the spatial frequencies of significant amplitude power spectra of the machined surfaces are listed in Table 6.8. It shows that the width of the measured tool mark is smaller than their corresponding feed rate when the feed

rate is low. The machined surface profile is constructed by intersecting the tool tip profiles in every feed. The tangential vibrations may change the positions of cutting tool tip and the small feed rate will help to adjust the intersection points within the feed rate range to make the width of tool marks become smaller. The existence of elastic recovery of the machined surface also will decrease the width and depth of tool marks. In tests No.5 and No.6 power spectrum are significant in the power spectra of the machined surfaces. When feed rate is high, the width of tool mark is bigger than the feed rate. It is because the tangential vibrations become dominant when high feed rate is adopted, the cutting tool tip vibrates far away from the ideal feed positions, the width of tool marks become bigger than the feed rate. In the tests the depths of tool marks are very close to the maximum form heights of the machined surface. Although the power spectrum of feed rate is very significant when low feed rate is employed the effects of some nonlinear factors with low spatial frequencies, such as spindle run-out, built-up edge and environmental vibration cannot be omitted since their power spectra are also clearly observed. High feed rate is used the effect of regenerative vibration on surface roughness is more significant than that of feed rate since the power spectrum of regenerative vibration is much higher than that of feed rate.

Table 6.8 Surface profiles characteristics and spatial frequencies

Test No	No.5	No.6
Ra (μm)	0.338	0.481
Tool mark width (mm)	0.0473	0.11
Tool mark depth (μm)	1.3	3.03
Max form height (μm)	1.738	2.869
Significant spatial frequencies (cycle/mm)	19.6, 37.3, 17.8, 10.7, 7.1 12.4, 8.9, 5.3, 30.2	8.9, 10.7, 17.8, 5.3, 373.3, 19.6

For measured surface roughness, the width and depth of tool mark, maximum form heights and significant spatial frequencies are listed in Table 6.9. The measured value of tool profile proves that tool mark will be wide when cutting tool nose radius is big. The depth of tool mark decreases with the increasing of tool nose radius. It can be noticed that the spatial power spectrum of spindle rotational run-out. Fig. 6.10 (b)

shows the spatial power spectrum of regenerative vibration is not very significant, which the tool nose radius may have some influences on machining stability.

Table 6.9 Surface roughness characteristics under different tool nose radius

Tool nose radius (mm)	0.8	1.2
Ra (μm)	1.8	1.942
Tool mark width (mm)	0.174	0.185
Tool mark depth (μm)	5.53	6.0
Max form height (μm)	6.956	7.997
Significant spatial frequencies (cycle/mm)	6.3, 5.6, 3.5, 2.8, 0.7	1.4, 5.6, 6.3, 2.1

In Fig. 6.11 it can be seen that the power spectrum of environmental vibration appears in the spatial power spectrum when tool nose radius of 1.2 mm is used. It may explain why the machined surface roughness is a little bit higher than that using tool nose radius of 0.8 mm. The influences of tool nose radius are studied by machining. Fig. 6.11 shows the surface roughness profiles and power spectra when the cutting tool, with nose radius of 0.8 and 1.2 mm respectively, is used, which stands for the medium and big tool nose radius. The surface roughness profiles clearly show the width of tool mark increase with the increasing of tool nose radius. More high frequency components can be observed in the surface roughness profiles when cutting tools with medium and big size tool nose radius are used.

The measured surface roughness, the width and depth of tool mark, maximum form heights and significant spatial frequencies are listed in Table 6.9. The measured value of tool profile proves that tool mark will be wide when cutting tool nose radius is big. The depth of tool mark decreases with the increasing of tool nose radius.

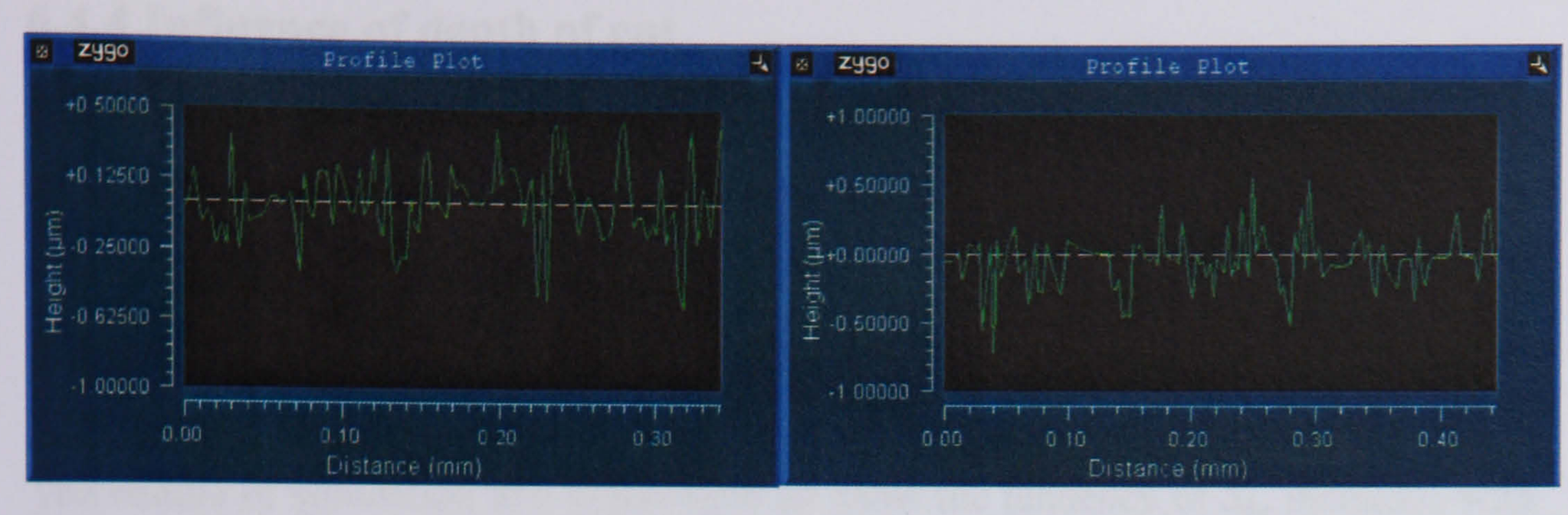

(a) Surface profile (R = 0.8 mm) (b) Surface profile (R = 1.2 mm)

Fig.6.11 Surface roughness characteristics under different tool nose radius

Fig. 6.12 shows the influences of tool nose radius and feed rate. Both simulation and experimental results show the value of surface root-mean-square deviation S_q decreases as the decreasing of feed rate. The tendency is consistent with the conventional cutting theory. The decrement of feed rate will decrease the cutting force and then decrease the cutting system vibrations excited by the cutting force, so the

surface finish is improved when the low feed rate is adopted. The feed rate has significant effects on the machined surface roughness. But the effect of the tool nose radius depends on the feed rate. The simulation results show that the root-mean-square deviation S_q decreases with the increase of the tool nose radius in all level of feed rates. The experimental results show that the surface root-mean-square deviation S_q decreases with the increasing of the tool nose radius at low feed rate.

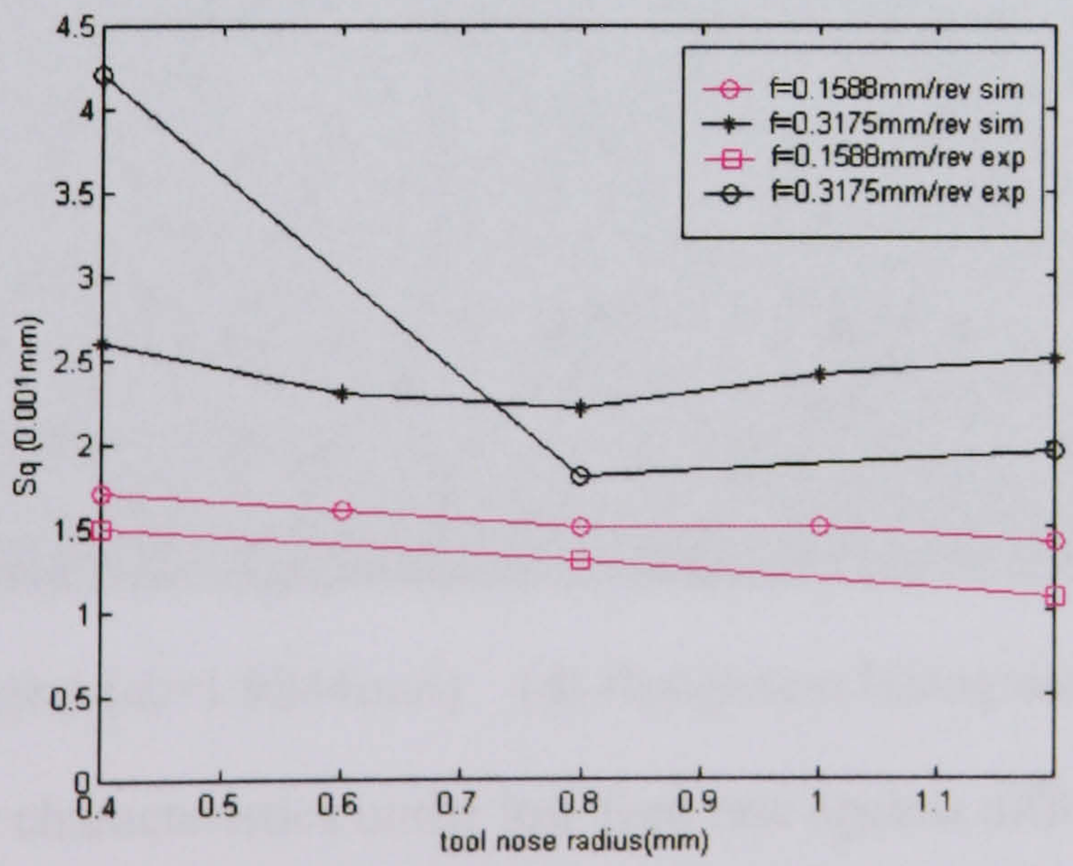

Fig.6.12 The effects of feed rate and tool nose radius on the surface roughness

6.4.4 Influence of depth of cut

Fig. 6.13 shows surface topography and histogram of the machined surface when the depth of cut varies under the same feed rate. Illustration of the normal distribution of surface heights can be achieved when small depth of cut is applied. A distribution with the shape of sharp peaks has a kurtosis value larger than 3.

The results of simulation and experiment all show the tendency of S_{ku} increases with the increasing of depth of cut. It means a small depth of cut should be used if one intends to achieve product/component with wide distributed surface height on its surface. The results also show that medium feed rate with small depth of cut will benefit obtaining this kind of surface. Therefore depth of cut can be an important parameter for controlling some surface functionality.

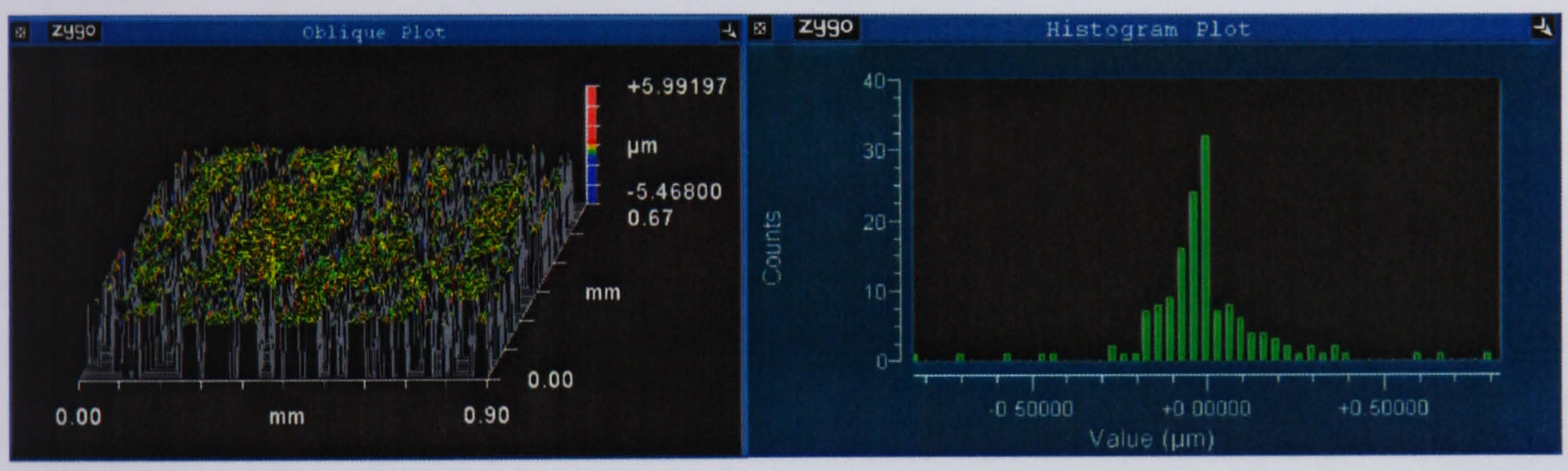

(a) Surface topography (d_c=1.5875mm) (b) Roughness histogram (d_c=1.5875mm)

(d) Surface topography (d_c=1.9844mm) (d) Roughness histogram (d_c=1.9844mm)

Fig.6.13 Surface characteristics under low feed rate against different depth of cut

6.5 Conclusions

This chapter aims to validate the modelling approach and simulation of surface generation. Precision turning trials have been undertaken to achieve this aim. Based on the comparison of results from machining trials and simulations, the following conclusions can be drawn:

(1) The simulation results agree quite well with the machining trials results. The modelling and simulation proposed in the previous chapters can accurately predict the precision surfaces generation to some extent.

(2) The feed rate and insert nose radius were remain influencing factors on the surface functionality.

(3) Surface roughness increased with increasing feed rate but decreased with increasing insert tool nose radius.

(4) Depth of cut was not informative than feed rate and insert tool nose radius.

(5) Decreases in feed rate and increase of nose radius provided better surface functionality.

(6) The negative rake angle (about -5°) will be significant for the achievement of good surface finish in finish machining. A proper clearance angle (about 5°~7°) may introduce process damping in the machining process and can improve the surface finish and surface bearing ability of the machined surfaces.

(7) Tool nose radius has effects on machining instability. Its influences should be included in developing the criterion for maintaining machining stability.

Chapter 7 Optimization and control of the surface functionality in precision machining

7.1 Introduction

Predicting the machinability and the process models and determining the optimal values of process parameters in machining system have been the areas of interest for researchers and manufacturing engineers alike. Machinability database system is essential for the selection of optimal process parameters during the process planning stage, which represents an important component in computer integrated manufacturing (CIM).

7.2 Optimization control

The surface of a machined component is defined by the surface roughness value. It is important to control the machining parameters and tooling geometry so as to achieve the required surface roughness as the component functionality and performance demand. Furthermore, it can help to increase the machining effectiveness, reduce the machining costs and to improve productivity.

7.3 Optimization parameters

Selection of process parameters has very significant impact on the product quality, production costs and production times. The quality and costs are much related to tool life, surface roughness and cutting forces which they are functions of process parameters such as cutting speed, feed rate, depth of cut and tooling geometry. In this chapter, the optimization model is developed against the requirement for tool life, surface roughness and cutting forces. Model is the basis for the optimization, although it is carried out through back-propagation in a non-continuous mode.

Response surface method (RSM) and neural networks (NN) data mining techniques are used for the optimization purpose. The data of 27 experiments have been used to generate, compare and evaluate the proposed model against the requirement on tool life, cutting force and surface roughness for a selected cutting tool.

7.4 Optimization modelling

Taylor tool life equations have been expanded to determine the proper machining conditions based on the minimum production cost, maximum production rate and maximum profit rate per item. These criteria have been considered in both constrained and unconstrained problems of machining economics.

Considerable research has been undertaken on the general effect of process parameters such as cutting speed, feed rate, depth of cut, on the process functions, including tool life, cutting force and surface roughness. Most of these models are based on Regression analysis (RA). There are only a few papers presenting using computer neural network (NN) [185-190].

Tool life, surface roughness and cutting force have been important for cost, time, design feature and quality measure in machining operations. Their modelling and modes are critical constraints for process parameter selections in process planning systems. These models can only be evaluated and validated with experimental work on specific materials under specified conditions. The ideal tool life equation used by researchers is [191-197]:

$$vt^{x} f^{y} d^{z} = C \tag{7-1}$$

v - cutting speed;

t - time;

f - feed rate;

d - depth of cut;

x, y, z - tool life exponents;

C - constant.

The following surface roughness and cutting force model are generally for surface roughness [198]:

$$R_a = \frac{f^2}{32r} \tag{7-2}$$

r - the nose radius;

f - cutting feed rate.

For cutting force, there is [198]:

$$Fc = Kf^{n1}d^{n2} \tag{7-3}$$

K –constant;

n - cutting force exponents;

f - feed rate;

d - depth of cut.

Tool life, surface roughness and cutting force are functions of the process and tooling geometrical variables using different data mining techniques and model building methods. The relationships between machining functions and variables are commonly approximated by polynomial functions. Response surface method (RSM) and computational neural network (NN) are used to represent the models and thus these process functions.

In this research the data of Box-Behnken design of three responses such as tool life, cutting force and surface roughness when Harrison M250 turning machine is used to predict the machineability models using response surface method (RSM) and neural network (NN). The obtained machineability models are compared against each other using the relative error analysis, descriptive statistics and hypothesis testing.

A non linear optimization model is used to determine the optimum values of the process parameters when minimizing the total production cost per workpiece, and the associated production time per workpiece. The suggested model considered the tool selection base on the optimum selected tool nose radius when determining the optimal values of process parameters.

7.5 Design experiments

7.5.1 Introduction

Design of experiment is a test or series of tests where purposeful changes are made to the input variables of processes so that we may observe and identify corresponding changes in the output of responses. The process variables are known as controllable and uncontrollable. However, sometimes uncontrollable variables are known as noise factors. The objectives of the experiment are to:

(1) Determine which variables are the most influential on the response y;

(2) Confirm where to set the influential x, therefore y is near nominal requirement;

(3) Decide where to set the influential x so that the variability in y is very small;

(4) Determine where to set the influential x so that the effect of the uncontrollable variable z is minimized.

Therefore, the experimental design method may be used either in process development or process troubleshooting to improve process performance or to obtain a process that is robust or insensitive to external source of variability. Experimental design method can also be very useful in establishing statistical control of a process and be used to identify these process influence variables. This is a critically important engineering tool to improve a manufacturing process. It also has extensive application in the development of these techniques early in process development, which can result in:

(a) Improved yield;

(b) Reduce variability and closer conformance to nominal;

(c) Reduce development time;

(d) Reduce overall cost.

Experimental design method can also play a major role in engineering design activities, where products are developed and existing ones improved. Some application of statistical experiment design includes:

(1) Evaluation and comparison of basic design configurations;

(2) Evaluation of material alternatives;

(3) Determination of key product design parameters of performance.

7.5.2 Design of experiments

Design of experiments is a powerful method to approach improvement of the process. It is important to have an idea for the experiments at the first stage. Therefore, the objective of the research can be identified clearly, know what are the factors, how the experiment will be conducted and understanding how the data will be analyzed. Montgomery gives an outline of the recommended procedure [148].

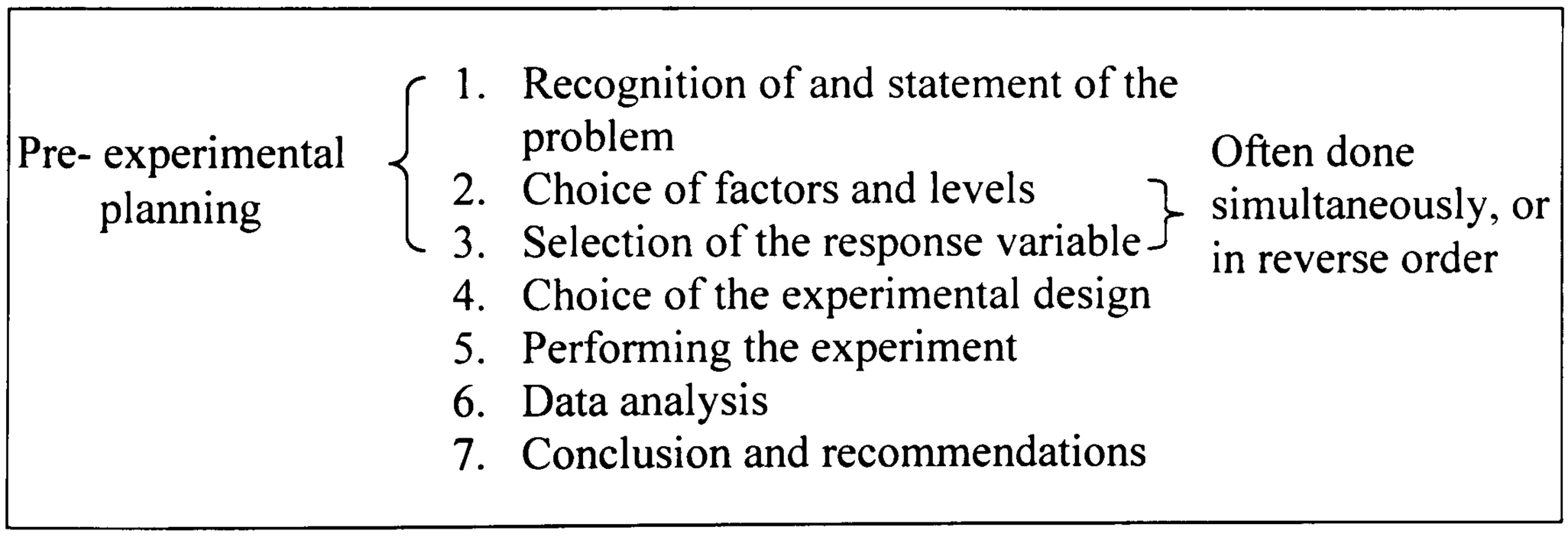

Fig. 7.1 Procedure of designing an experiment

(1) Recognition of problem

Design of experiments is needed to fully develop all ideas about the problem and the specific objectives of the experiment. However, a clear statement of the problem and objectives of the experiment often contribute substantially to better understanding and eventual solution of the problem.

(2) Factor and level

The factors must be chosen to be varied and the specific level at which these factors will be varied and the specific level at which runs will be made. Process knowledge is required to do this. The process knowledge is usually a combination of practical experience and theoretical understanding. All factors must be investigated that may be of importance and to avoid being overly influenced by past experience, particularly in the early stages of experimentation or when the process is not very mature.

27 experiments have been conducted on Harrison M250 with Ø50 mm diameter and 500 mm length. We considered four machining parameters including cutting speed (v m/s), feed rate (f mm/rev), depth of cut (d mm) and tool nose radius (r mm). The considered outputs are tool life (T min), cutting force (Fc N) and surface finish (Ra μm). The parameters were considered at three levels (-1, 0 and1) as shown in Table 7.1. Table 7.1 shows factors and levels for experiments. There are four factors for the experiment and three levels for factors. These are medium low, low and high. (-1) indicates low level, (0) for medium and (1) for high. The experiments are conducted based on Box Behnken design as illustrated in Table 7.2. This design is rotational and consists of blocks in an orthogonal arrangement.

Table 7.1 Factors and level of the experiments for the model constructions

Factors	Level		
	low -1	medium 0	high 1
Cutting speed v (m/s)	25	60	144
Feed f (mm/rev)	0.1	0.25	0.75
Depth of cut d (mm)	0.3	0.4	0.5
Nose radius r (mm)	0.4	0.8	1.6

(3) Response factors and variables

It is important to ensure that the variables really provide useful information about the process under investigation. For this research, the average of the measured

characteristics will be the response variable. However, multiple responses are not unusual. Gauge capability is also an important factor. If gauge capability is poor, then only relatively large factors will be detected by the experiment or additional replication will be required.

Table 7.2 Box-Behken design for experiment construction

v (m/min)	*d* (mm)	*f* (mm/r)	*r* (mm)	*T* (min)	*Ra* (μm)	*Fc* (N)
-1	-1	0	0	18.729	1.25	872
-1	1	0	0	5.71	11.25	157
1	-1	0	0	17.56	6.25	1785
1	1	0	0	12.11	2.25	1201
0	0	-1	-1	18.85	2.25	188
0	0	-1	1	12.73	6.25	1327
0	0	1	-1	6.547	21.25	654
0	0	1	1	11.42	11.25	1314
-1	0	0	-1	1.190	11.25	419
-1	0	0	1	1.42	2.25	314
1	0	0	-1	5.25	11.25	452
1	0	0	1	1.42	11.25	1314
0	-1	-1	0	8.380	2.25	838
0	-1	1	0	10.05	11.25	100
0	1	-1	0	15.71	11.25	157
0	1	1	0	3.928	11.25	392
-1	0	-1	0	3.491	0.45	1349
-1	0	1	0	11.1	11.25	113
1	0	-1	0	4.190	16.25	419
1	0	1	0	15.71	11.25	157
0	-1	0	-1	10.28	06.25	502
0	-1	0	1	2.73	11.25	327
0	1	0	-1	18.85	11.25	1188
0	1	0	1	20.95	06.25	1209
0	0	0	0	8.729	11.25	872
0	0	0	0	3.491	11.25	340
0	0	0	0	25.25	0.45	452

(4) Performing the experiment

It is important to monitor the process to ensure that everything is carried out according to the plan. The error in the experimental procedure at this stage will usually destroy experiment validity.

(5) Data analysis

Statistical methods should be used to analyze the data so that the result and conclusion are objective rather then judgmental. If the experiment has been designed correctly and if it has been performed according to the design, the type of statistical methods required is not elaborate. Many experiment software packages are available to assist the data analysis and simple graphical methods play an important role in data interpretation. Residual analysis and model validity checking are also important.

(6) Conclusion and recommendations

Once the data have been analyzed, the experiment must draw practical conclusions about result and recommend a course of actions. Graphical methods are often used in these stages, particularly in presenting the results. Follow up runs and confirmation testing should be performed to validate the conclusion from the experiment

7.6 Response surface methodology (RSM)

Response Surface Methodology (RSM) is used to examine the relationship between one or more response variable and a set of quantitative experimental variables. The method is often employed after identifying the controllable factors and the objective is to find factors settings that optimize the response. Designs of this type are usually chosen when there is suspecting curvature in the response surface. In this research, RSM is use to examine the relationship between the surface machined, process parameters and tooling geometry as variables. The relationship is then used for the process optimization and surface functionality control.

7.6.1 MINITAB 15 software

7.6.1.1 Software features

Minitab 15 is simple to use and also contains the depth and breadth of tools and guidance to satisfy the rigorous quality improvement in a project. Minitab is one of the most popular choices on solving problems. In summary, the software tool has the following features:

(1) Minitab makes it easy to use data from outside sources and manages work automatically.

(2) It is easy to import (or copy and paste) data from any number of sources such as Excel, HTML spreadsheet, or even Notepad for quick analysis.

(3) Minitab's Project Manager will automatically organize the worksheet into a single, convenient project file. The password protection can be used to keep sensitive projects under wraps.

(4) The Minitab data window offers many advanced features like associating formulae with columns. Sophisticated yet simple data manipulation allows organizing the data in any manner possible.

(5) Regression analysis allows investigating and modelling the relationship between a response variable and one or more predictors. Minitab offers a broad range of regression commands including least squares, partial least squares, and logistic regression procedures.

(6) Minitab's DOE gives the tools to create experimental designs and analyze and plot the results to improve the processes quickly and efficiently.

(7) Minitab offers a full suite of Measurement Systems Analysis commands to help determine if the measurement system makes the grade, as well as how to go about correcting it if it doesn't.

(8) Minitab's collection of ANOVA (Analysis of Variance) capabilities include procedures for choosing ANOVA models, for fitting MANOVA models (multiple response), and ANOM models (analysis of means). It also includes graphs for

testing equal variances, confidence interval plots, and graphs of main effects and interactions.

(10) Minitab gives the tools to:

(a) Identify the factors most responsible for the data's underlying structure

(b) Group observations in "clusters" to discover the simple structures in complex data, or to investigate how the predictors contribute to the groupings

(c) Examine how the categories of different variables are related to one another

7.6.2 Regression equation

The regression equation is an algebraic representation of the regression line and is used to describe the relationship between the response and predictor variables. The regression equation takes the form of:

Response = constant + coefficient (predictor) + ... + coefficient (predictor)

$$y = b_o + b_1X_1 + b_2X_2 + \ldots + b_kX_k \qquad (7\text{-}4)$$

y - value of the response

b_o - value of the response variable when predictor is zero,

X - value of the predictor variable,

$b_1, b_2 \ldots\ldots, b_k$ - estimated change in mean response for each unit change in predictor value

Using the Equation 7-4, the regression analysis is carried out on the tool life, cutting force in the process, and the process roughness generated. . It is clear from the literature that the tool life, cutting force and surface finish equations are not linear and they could

be predicted using the response surface method. The initial analysis of the developed models based on RSM is shown Table 7.3- 7.5. The models are reduced by neglecting the elements which have no significant effect on responses. The revised RSM analysis is illustrated in Table 7.6- 7.8.

Table 7.3 Initial response surface regression analysis: T versus *v*; *f; d*; *r*

Response Surface Regression Analysis: T versus v; f; d; r.

The analysis was undertaken using uncoded units.

Estimated regression coefficients for T

Predictor	Coef	SE Coef	T	P
Constant	59.001	3.784	12.380	0.000
v	-0.19723	0.04295	-14.590	0.000
f	-18.535	9.823	-1.317	0.000
d	-17.00	9.110	-1.19	0.852
r	-0.850	4.588	0.19	0.853
v*v	0.0016	0.0002227	7.27	0.000
f*f	35.042	9.822	3.706	1.000
d*d	22.748	8.505	4.597	1.000
r*r	0.248	2.027	0.129	1.000
v*d	0.08587	0.02674	6.95	0.043
v*r	-0.09293	0.01205	-7.71	0.874
f*d	9.719	5.238	7.58	0.119
f*r	-10.859	2.361	-8.41	0.830
d*r	10.022	2.677	-0.636	0.986

S = 1.68087 R-Sq = 92.8% R-Sq(adj) =94.8%

Table 7.4 Initial response analysis: Ra versus *v*; *f; d*; *r*

Response Surface Regression Analysis: Ra versus v; f; d; r.

The analysis was done undertaken uncoded units.

Estimated regression coefficients for Ra

Predictor	Coef	SE Coef	T	P
Constant	1.3467	5.662	0.148	0.018
v	0.029512	0.06426	0.322	0.000
f	27.73	14.70	1.587	0.160
d	1.254	13.63	0.096	0.852
r	-0.1272	6.865	-0.863	0.453
v*v	-0.00024222	0.0003332	-0.491	0.620
f*f	28.748	14.70	1.926	0.076
d*d	-1.476	1.273	-0.189	0.853
r*r	4.2019	3.033	1.377	0.112
v*d	0.007811	0.04002	-0.391	0.702
v*r	0.003905	0.01804	0.023	0.982
f*d	-5.9430	7.838	0.172	0.886
f*r	29.715	3.532	-0.305	0.003
d*r	0.5470	4.005	0.121	0.905

S = 2.325 R-Sq = 94.0% R-Sq(adj) = 87.5%

Table 7.5 Initial response analysis: Fc versus *v*; *f; d*; *r*

Response Surface Regression Analysis: Fc versus v; f; d; r.

The analysis was undertaken using uncoded units.

Estimated regression coefficients for Fc

Predictor	Coef	SE Coef	T	P
Constant	588.22	637.09	2.38	0.323
v	-1.9332	4.210	-4.59	0.786
f	-181.67	1296.28	-1.89	0.895
d	-166.6	890.30	-0.19	0.125
r	283.30	440.97	-0.19	0.668
v*v	0.015867	0.02183	7.27	0.819
f*f	2147.60	1196.27	0.00	0.093
d*d	1576.83	830.36	0.00	0.024
r*r	-81.43	190.87	0.00	0.742
v*d	-1.8217	2.621	-6.95	0.715
v*r	-0.9109	11.81	-7.71	0.990
f*d	1389.30	513.4	7.58	0.979
f*r	-194.65	231.4	8.41	0.724
d*r	66.84	262.4	6.36	0.820

S = 184.3 R-Sq = 94.6% R-Sq(adj) = 87.5%

Table 7.6 Updated response analysis: T versus *v*; *f; d*; *r*

Response Surface Regression Analysis: T versus v, f, d, r.

The analysis was undertaken using uncoded units.

Estimated regression coefficients for T

Predictor	Coef	SE Coef	T	P
Constant	30.602	6.693	14.57	0.000
v	-0.64233	0.08791	-7.31	0.000
f	-51.9747	0.76	-6.00	0.000
d	-40.9756	6.26	-6.00	0.000
v*v	0.0028049	0.0004685	5.99	0.000
f*f	34.2576	10.50	4.00	0.001
d*d	22.3558	4.86	-5.00	0.000
v*f	0.1263	0.03229	3.912	0.001
v*d	0.0680	0.02693	2.525	0.021
f*d	4.540	50.418	2.61	0.030

S = 4.23 R-Sq = 93.6% R-Sq(adj) = 92.2%

Analysis of Variance

Source	DF	SS	MS	F	P
Regression	7	17090	195.84	73.06	0.000
Residual Error	15	421.832	17.95		
Lack of Fit	9	15.07	6.32	3.86	0.045
Pure Error	6	8.25	4.58		

Table 7.7 Updated response analysis: Fc versus *v*; *f*; *d*; *r*

Response Surface Regression Analysis: Fc versus v, f, d, r.

The analysis was undertaken using uncoded units.

Estimated regression coefficients for Fc

Predictor	Coef	SE Coef	T	P
Constant	100.64	142.60	2.75	0.456
f	158.8	565.30	-0.280	0.779
d	-1644.0	691.3	-2.241	0.048
f*f	2185.6	936.6	2.268	0.033
d*d	1615.8	502.4	3.216	0.004
f*d	1379.3	625.0	2.207	0.038

S = 2.172 R-Sq = 93.0% R-Sq(adj) = 98.5%

Analysis of Variance

Source	DF	SS	MS	F	P
Regression	4	693907	123477	65.90	0.000
Residual Error	20	47392	553560		
Lack of Fit	4	233213	371803	13.59	0.000
Pure Error	14	144179	173608		

Table 7.8 Updated response analysis: Ra versus *v*; *f; d*; *r*

Response Surface Regression Analysis: Ra versus v, f, d, r.

The analysis undertaken using uncoded units.

Estimated regression coefficients for Ra

Predictor	Coef	SE Coef	T	P
Constant	-5.459	1.041	-2.978	0.007
f	45.590	1.696	8.990	0.000
r	2.780	1.911	1.455	0.159
f*r	-25.228	1.313	3.98	0.001

S = 2.53 R-Sq = 95.4% R-Sq(adj) = 94.7%

Analysis of Variance

Source	DF	SS	MS	F	P
Regression	3	1276.38	425.46	66.27	0.000
Residual Error	23	534.33	6.42		
Lack of Fit	5	104.19	120.838	44.05	0.000
Pure Error	14	8.33	0.56		
Total	27	1168.85			

P value- Determines the appropriateness of rejecting the null hypothesis in a hypothesis test. P-values range from 0 to 1. The smaller the p-value, the smaller the probability that rejecting the null hypothesis is a mistake. The p-value is calculated from the observed sample and represents the probability of incorrectly rejecting the null hypothesis when it is actually true. In other words, it is the probability of obtaining a difference at least as large as the one between the observed value and the hypothesized value through random error alone.

SE coeff- The standard deviation of the estimate of a regression coefficient. It measures how precisely the data can estimate the coefficient's unknown value. Its value is always positive, and smaller values indicate a more precise estimate.
The standard error of a coefficient helps determine whether the value of the coefficient is significantly different than zero – in other words, whether the predictor has a significant effect on the response

Coeff- The numbers by which the variables in an equation are multiplied. When calculating a regression equation to model data, Minitab estimates the coefficients for each predictor variable based on the sample.

T- Test statistic for the t-test family, it measures the difference between an observed statistic and its hypothesized population parameter in units of standard error. A t-test compares this observed t-value to a critical value on the t-distribution with (n-1) degrees of freedom to determine whether the difference between the estimated and hypothesized values of the population parameter is statistically significant.

R- Sq- Coefficient of determination; indicates how much variation in the response is explained by the model. The higher the R2 , the better the model fits the data.

MS- Represents an estimate of population variance. It is calculated by dividing the corresponding sum of squares by the degrees of freedom.
In regression, mean squares are used to determine whether terms in the model are significant. The term mean square is obtained by dividing the term sum of squares by the degrees of freedom. The error mean square is obtained by dividing the error sum of squares by the degrees of freedom. The error mean square is the variance (s2) around the fitted regression line.

S- The most common measure of dispersion, or how spread out the data are from the mean. While the range estimates the spread of the data by subtracting the minimum value

from the maximum value, the standard deviation roughly estimates the "average" distance of the individual observations from the mean. The greater the standard deviation, the greater the spread in the data.

F- If the calculated F -value is greater than the F-critical value from the F-distribution, then at least one of the coefficients is not equal to zero. The F-value is used to determine the p-value.

SS- Represents a measure of variation or deviation from the mean. It is calculated as a summation of the squares of the differences from the mean. The calculation of the total sum of squares considers both the sum of squares from the factors and from random chance or error.

adj- Adjusted

From the above analysis and results at tables 7.6-7.8, the empirical models of the tool life, cutting force and surface roughness are formulated as follows:

$$T = 30.602 - 0.64233v - 51.97475f - 40.9756d + 0.0028049v^2 + 34.2576f^2 + 22.3558d^2 + 0.1263vf + 0.0680vd + 4.540fd \quad (7\text{-}5)$$

$$Fc = 100.64 + 158.8f - 1644.0d + 2185.6f^2 + 1615.8d^2 + 1379.3fd \quad (7\text{-}6)$$

$$Ra = -5.459 + 45.590f + 2.780r - 25.228fr \quad (7\text{-}7)$$

7.7 MATLAB neural network

Computational neural networks posses a number of attractive features, for modelling complex machining operations, such as universal function approximation capability,

resistance to noise of missing data, accommodation of multiple non-linear variables, unknown interaction for good generalization capability. The data mining used by CNN is a feed forward back propagation (BP) multilayer network.

7.7.1 Design of experiments

Fig. 7.2 Shows the design of experiments using Box-Behnken design. From the table it is found, there are four factors such as cutting speeds (v), depth of cut (d), feed rate (f) and tool nose radius (r). All variables have been written as three level of (-1), (0) and (1), where (-1) indicates low, (0) medium and (1) high.

Design Tree

- Designs
  - Actual Design
  - Generic Design

Properties - Generic Design

Design Style	Box-Behnken
Number of Points	27
Number of Constraints	0
Last Changed	06-Feb-2008, 12:59:31
Model	nnet_[20,15]

Design Table

	v	d	f	r
1	-1	-1	0	0
2	-1	1	0	0
3	1	-1	0	0
4	1	1	0	0
5	0	0	-1	-1
6	0	0	-1	1
7	0	0	1	-1
8	0	0	1	1
9	-1	0	0	-1
10	-1	0	0	1
11	1	0	0	-1
12	1	0	0	1
13	0	-1	-1	0
14	0	-1	1	0
15	0	1	-1	0
16	0	1	1	0
17	-1	0	-1	0
18	-1	0	1	0
19	1	0	-1	0
20	1	0	1	0
21	0	-1	0	-1
22	0	-1	0	1
23	0	1	0	-1
24	0	1	0	1
25	0	0	0	0
26	0	0	0	0
27	0	0	0	0

Fig. 7.2 Design of experiments using Box- Behnken design

7.7.2 Modelling data plot

Fig. 7.3 shows views of data modelling for feed rate, cutting speed, cutting force and depth of cut. The data have been viewed as 3D data plots. There are colours indicating three different types of factors in green, blue and red. All factors will be allocated at x, y and z axes.

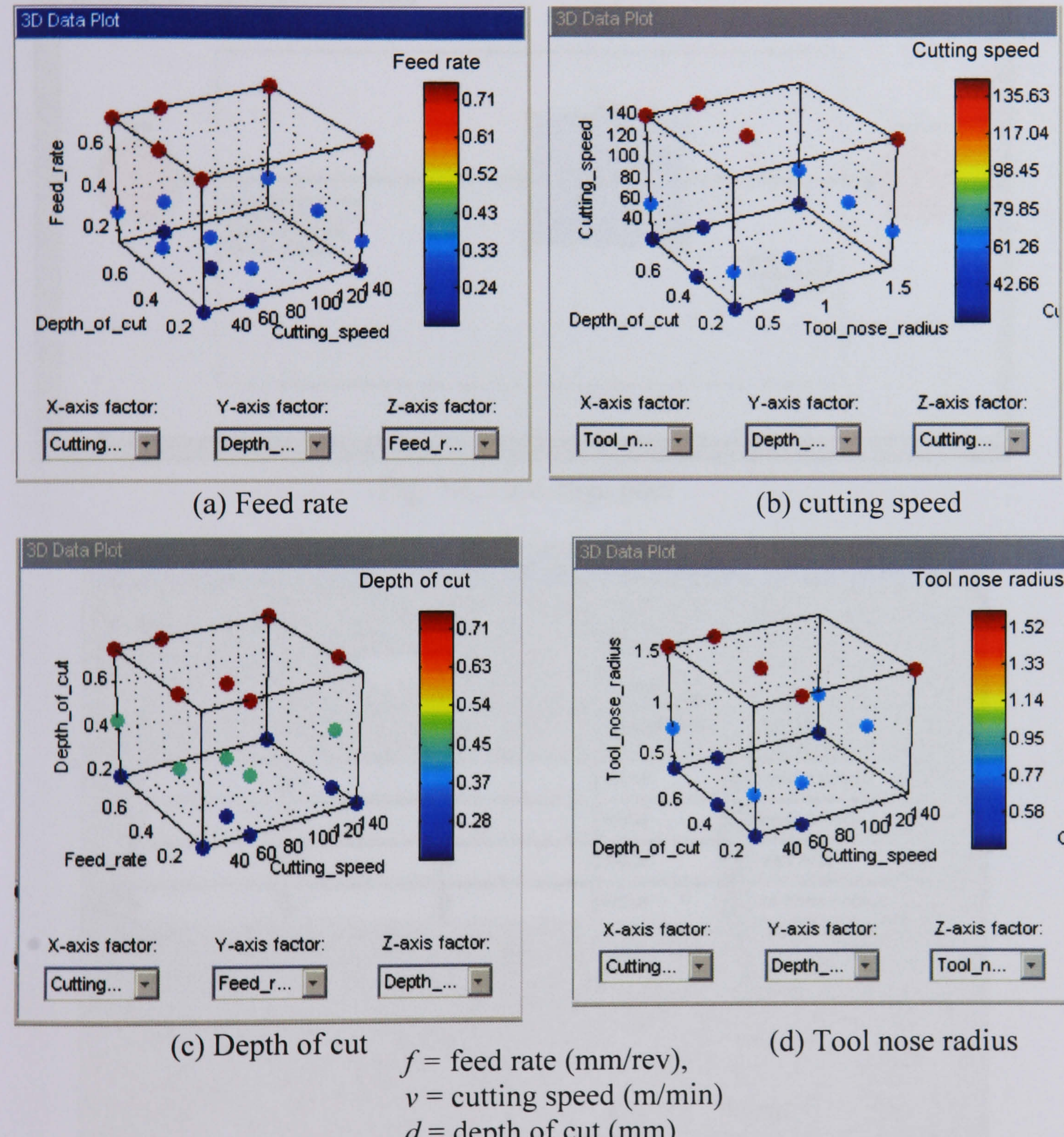

(a) Feed rate (b) cutting speed

(c) Depth of cut (d) Tool nose radius

f = feed rate (mm/rev),
v = cutting speed (m/min)
d = depth of cut (mm)
r = tool nose radius (mm)

Fig. 7.3 3D views of data modelling for feed rate, cutting speed, depth of cut and tool nose radius

7.7.2.1 Level of the input set up

Test plan is the main function in developing MATLAB Neural Network test. Fig. 7.4 shows one stage plan where one input, one model and response will be produced.

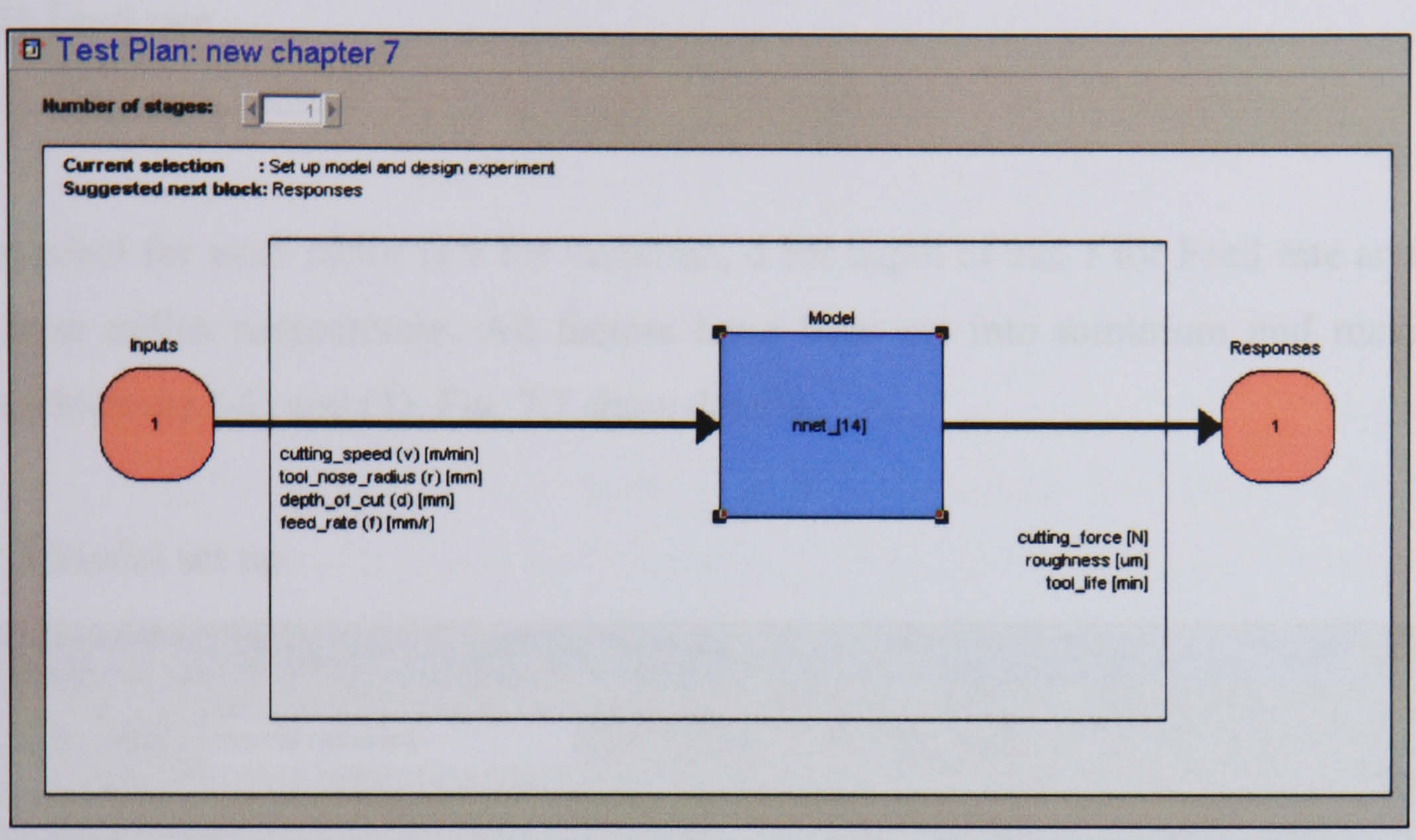

Fig. 7.4. One stage plan

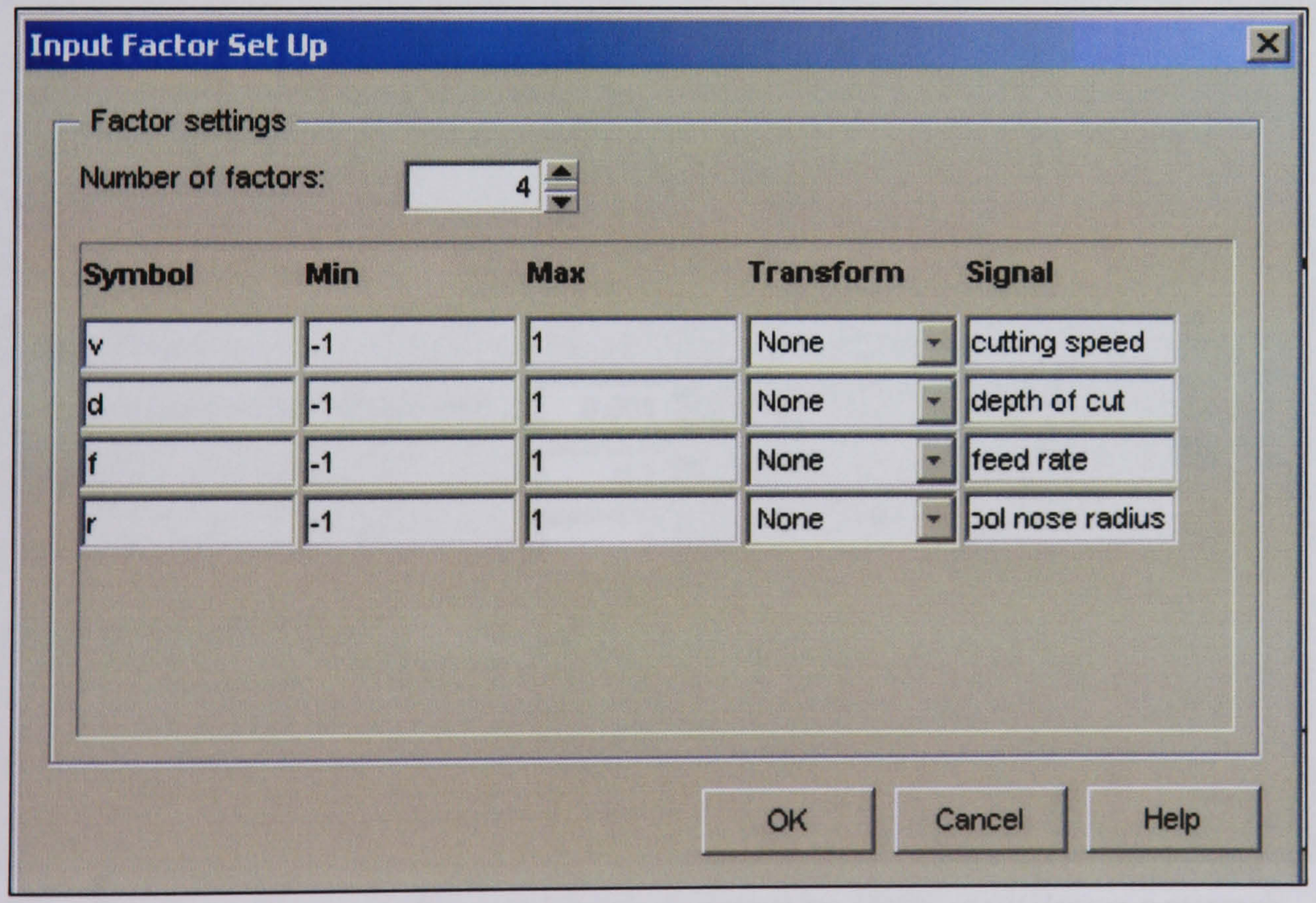

Fig. 7.5 Factors and level of the experiment for the model construction using MATLAB Neural Network

There are four members of factors:

(1) Cutting speed

(2) Depth of cut

(3) Feed rate

(4) Tool nose radius

The symbol for each factor is v for vibration, d for depth of cut, f for Feed rate and r for tool nose radius respectively. All factors have been set into minimum and maximum value which are (-1) and (1). Fig. 7.7 show details.

7.7.2.2 Model set up

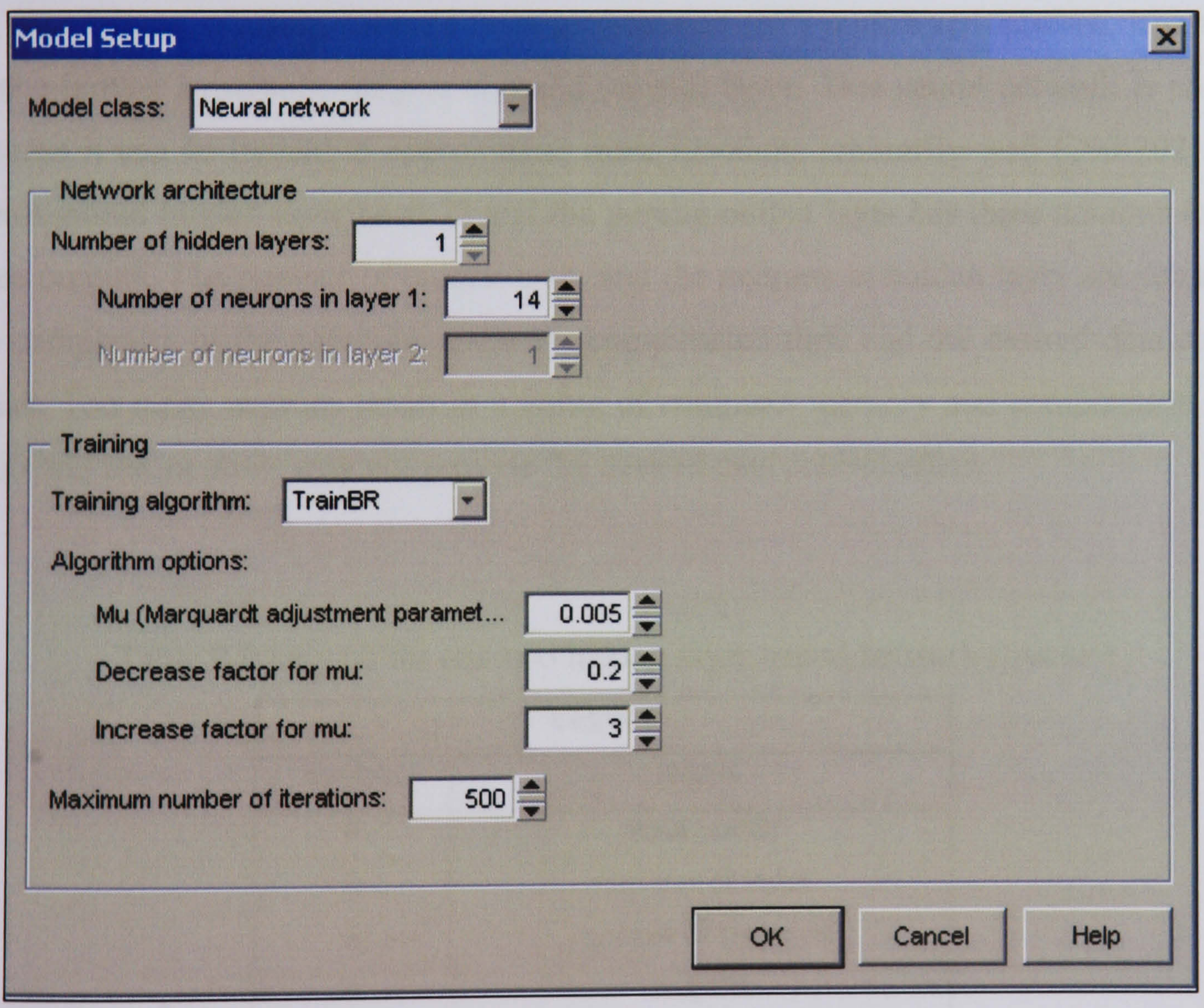

Fig. 7.6 Free forward–forward back regression (BR) multilayer network

Fig. 7.6 shows the free forward-forward back regression (BR) multi layer network, which has been created in the model setup. Model class for this experiment is Neural Network architecture, which as one hidden layers. The training algorithms has been chosen with 0.005 Mu-Marquard adjustment parameters, 0.2 for decrease factor Mu and 3 increases for Mu. The maximum number of iteration for this test is 500. It consists of one hidden hyperbolic tangent sigmoid and normalized to a range of -1.0 until 1.0.

Computational neural networks possess a number of attractive features for modelling complex manufacturing operations: universal function approximation capability, resistance to noise of missing data, accommodation of multiple non-linear variables for unknown interactions and good generalisation capability [199]. The neural network used for data mining is a feed-forward back-propagation (BP) multilayer network. It consists of one-hidden hyperbolic tangent sigmoid (tansig) layer. This neural network is chosen, because it can be trained to approximate most functions arbitrarily well [200-202]. The Tan-Sigmoid hidden layer have 73 and the purelin output layer has three neurons for the three outputs. The number of hidden layer and the neurons in hidden layer are subject to the complexity of the computer memory, computation time and the desired data control effect. Too many neurons result in a waste of computer memory and computation time, while too few neurons may not provide the desired data control effect.

Table 7.9 Legend for one two hidden layer neural network structure

Legend	
symbol	signal
P	input vector
R	number of input
S	number of neurons
a	outputs
F1	hyperbolic tangent sigmoid

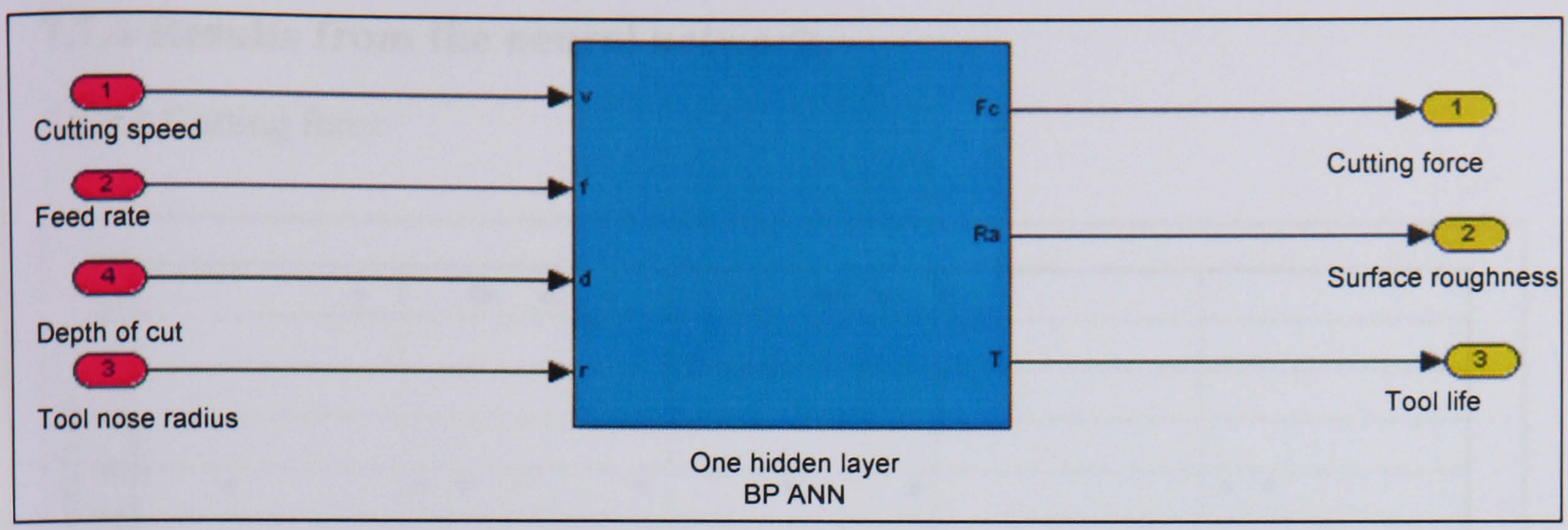

Fig. 7.7 One hidden layer BP neural network

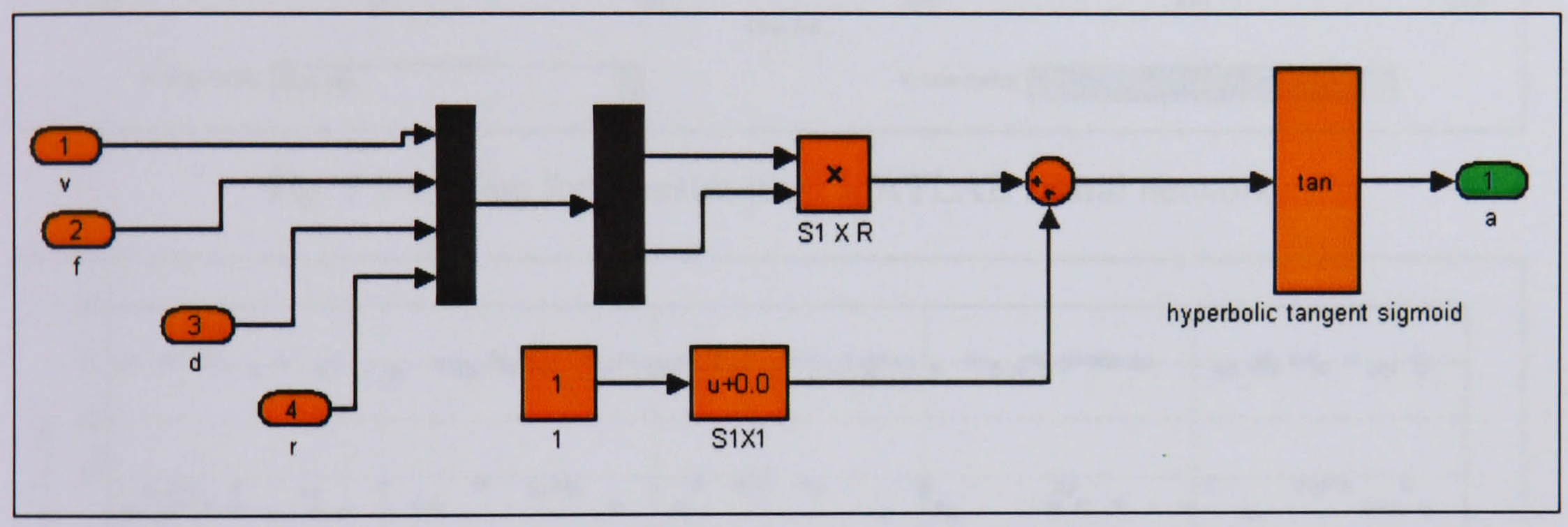

Fig. 7.8 One hidden layer neural network structure

Table 7.9 shows the legend for one hidden layer of neural network structure as created by using MATLAB simulink as shown in Fig. 7.8. Fig. 7.7 shows four factors such as the cutting speed, feed rate, depth of cut and tool nose radius and all considered as an input s. There are three outputs that will be produced such as cutting force (Fc), surface roughness (Ra) and tool life (T). Figure 7.8 shows the subsystem of tone hidden layer BP of Neural network structure. Fig. 7.8 shows the stage of one layer.

7.7.4 Results from the neural network

7.7.4.1 Cutting force

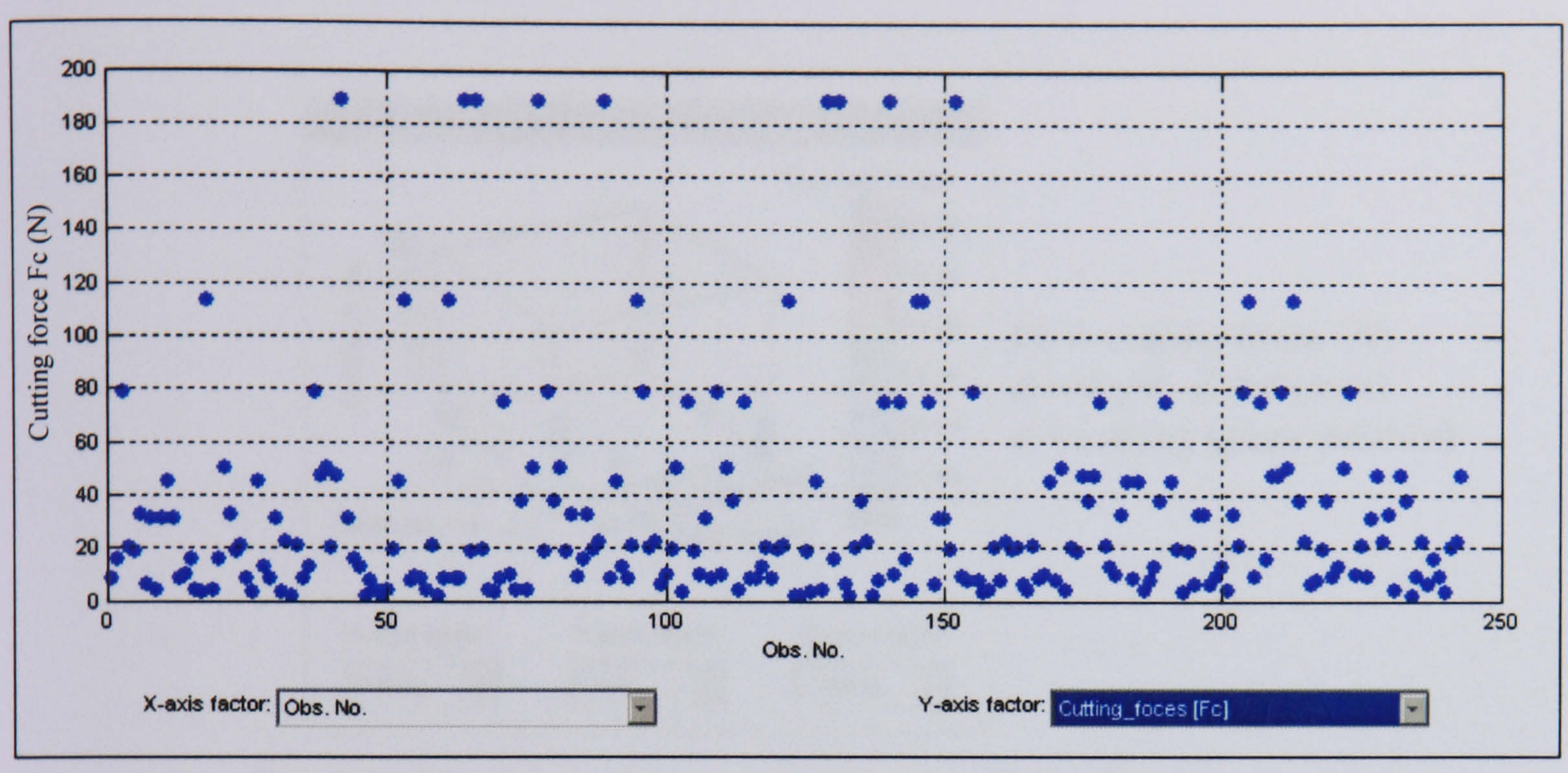

Fig. 7.9 Cutting force result from MATLAB neural network

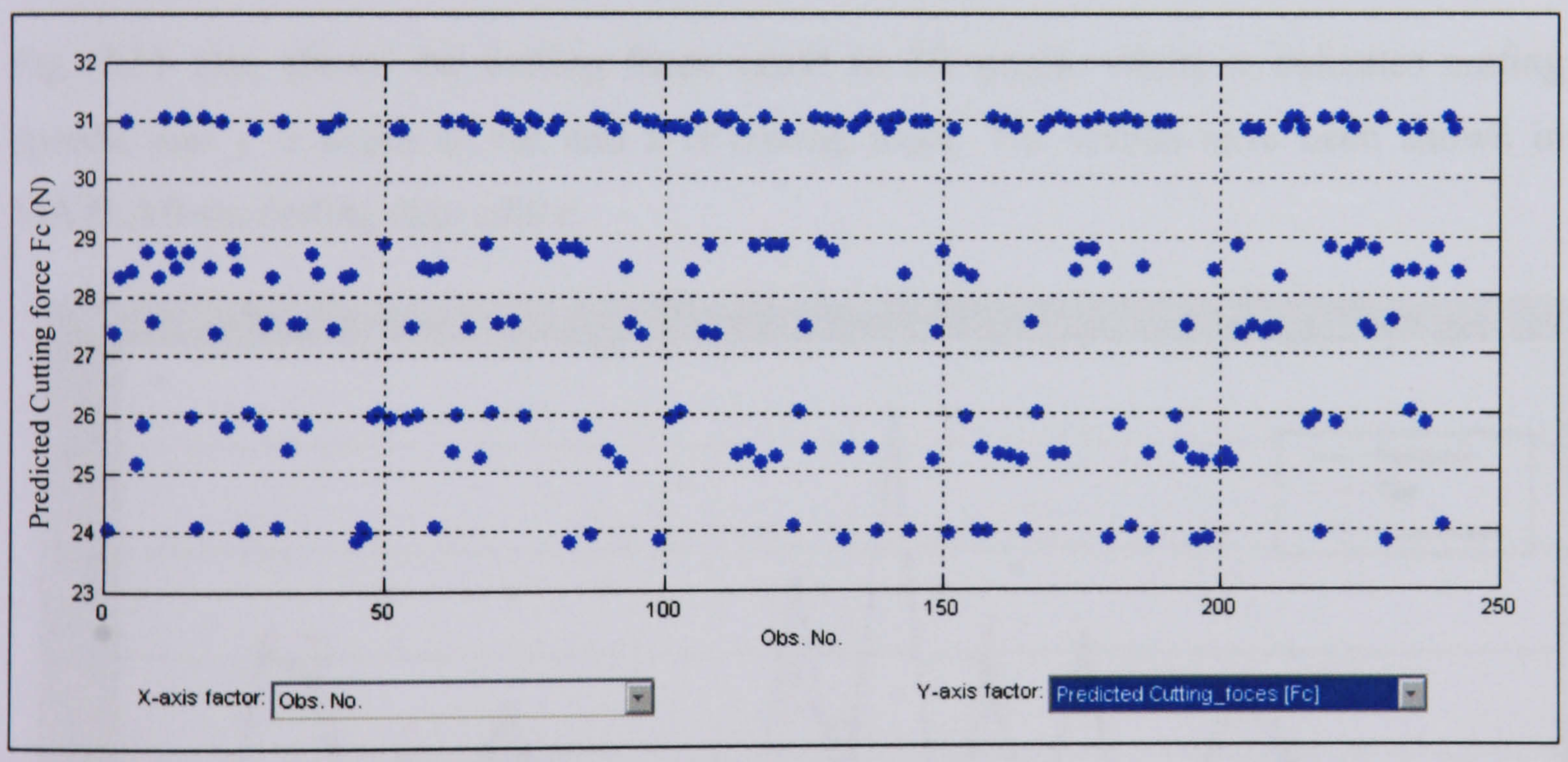

Fig. 7.10 Predicted cutting force result from MATLAB neural network

Fig. 7.9 shows cutting force result from MATLAB neural network. The result has been taken from 250 experiments, but only 27 experiments have been selected for observation. The result has been shown in 2D graph where x indicates the number of observations and

y is the cutting force. Meanwhile Fig. 7.10 shows the predicted cutting force result from the neural network. From the figure, it is found that the predicted cutting force results are more organized as compared with the results shown in Fig. 7.10.

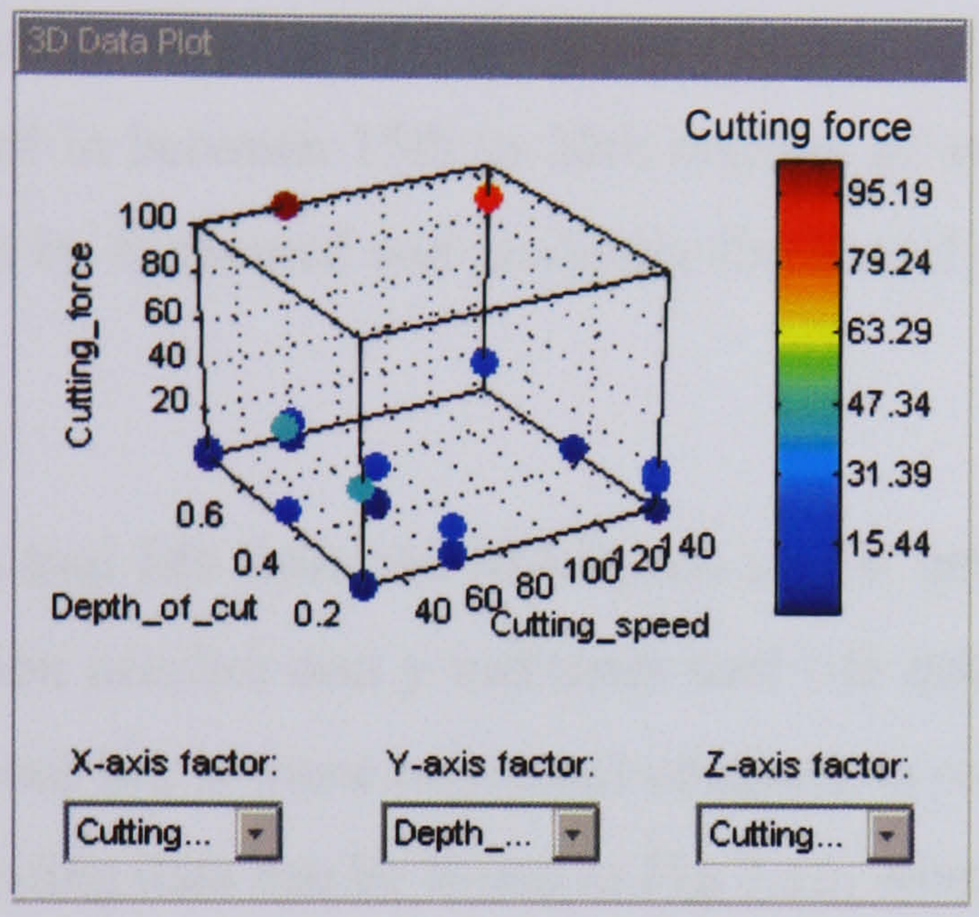

Fc = cutting force (N)
d = depth of cut (mm)
v = cutting speed (m/min)

Fig. 7.11 3D views of data modelling for cutting force

Fig. 7.11 also shows the cutting force result in 3D graph, where x indicates cutting speeds, and y is depth of cut and z is cutting force. The results have been shown in MATLAB modelling data editor.

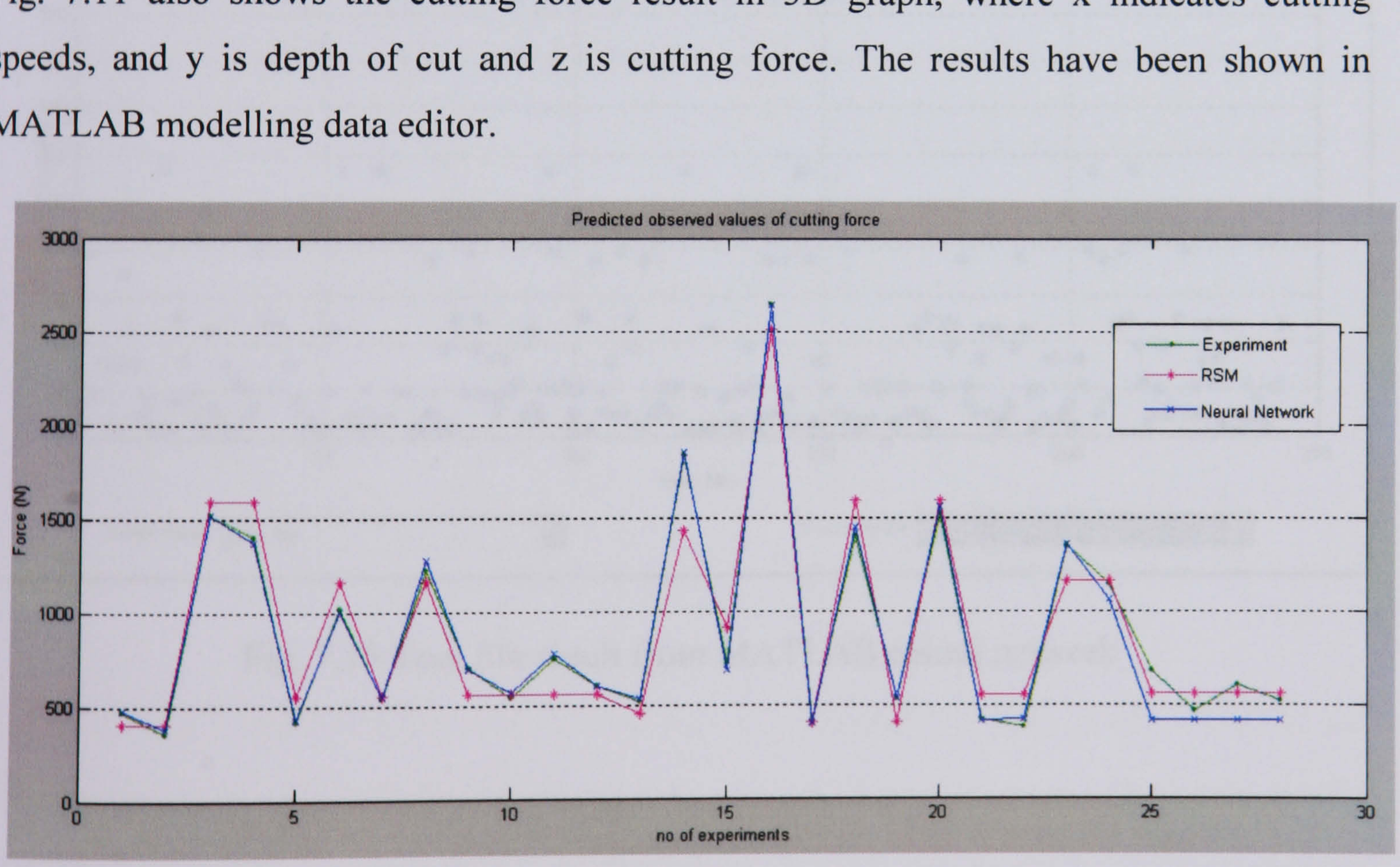

Fig. 7.12 The predicted observed value of cutting force result.

Fig.7.12 shows the predicted observed value of cutting force result. Three results out are calculated from three different method such as cutting trail experiments, RSM and Neural Network. According to the graph, light blue colour indicates cutting trial experiment results, pink colour line is RSM results and dark blue colour represents Neural Network results. The numbers of 27 experiments have been selected. The maximum cutting force has been detected in between 15th to 20th number of experiments, and then it's become decreased follow by fluctuated and gradually flat at end of experiment session.

7.7.4.2 Tool life

Fig. 7.13 shows tool life from the MATLAB neural network. The result shows tool life versus observation number and y indicates tool life data. Fig 7.14 shows that the result from predicted tool life is more organized compare to experiment results. The position of tool life in modelling data can be found in Fig 7.15, which shows the results data in 3D.

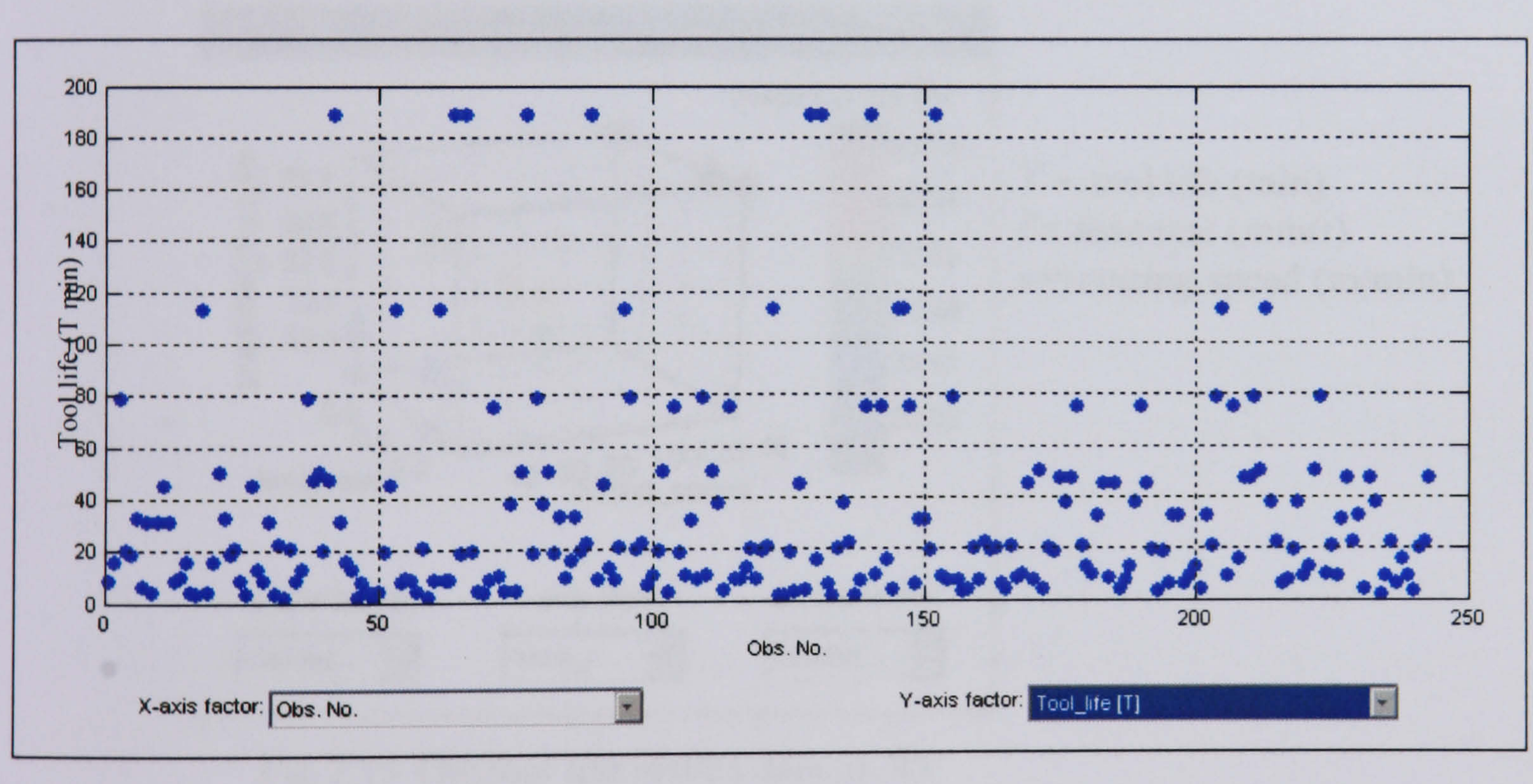

Fig. 7.13 Tool life result from MATLAB neural network

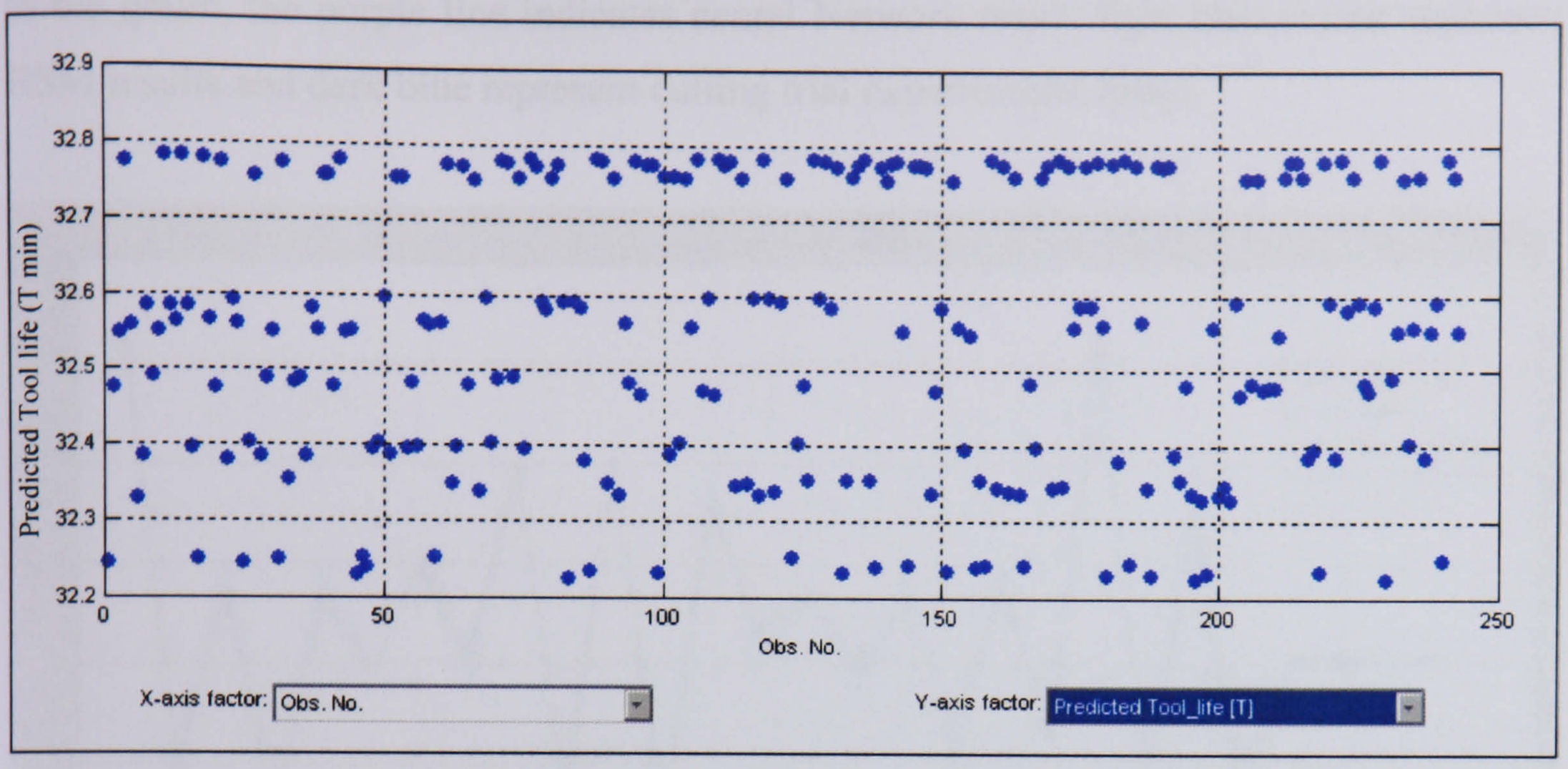

Fig. 7.14 Predicted tool life result from MATLAB neural network

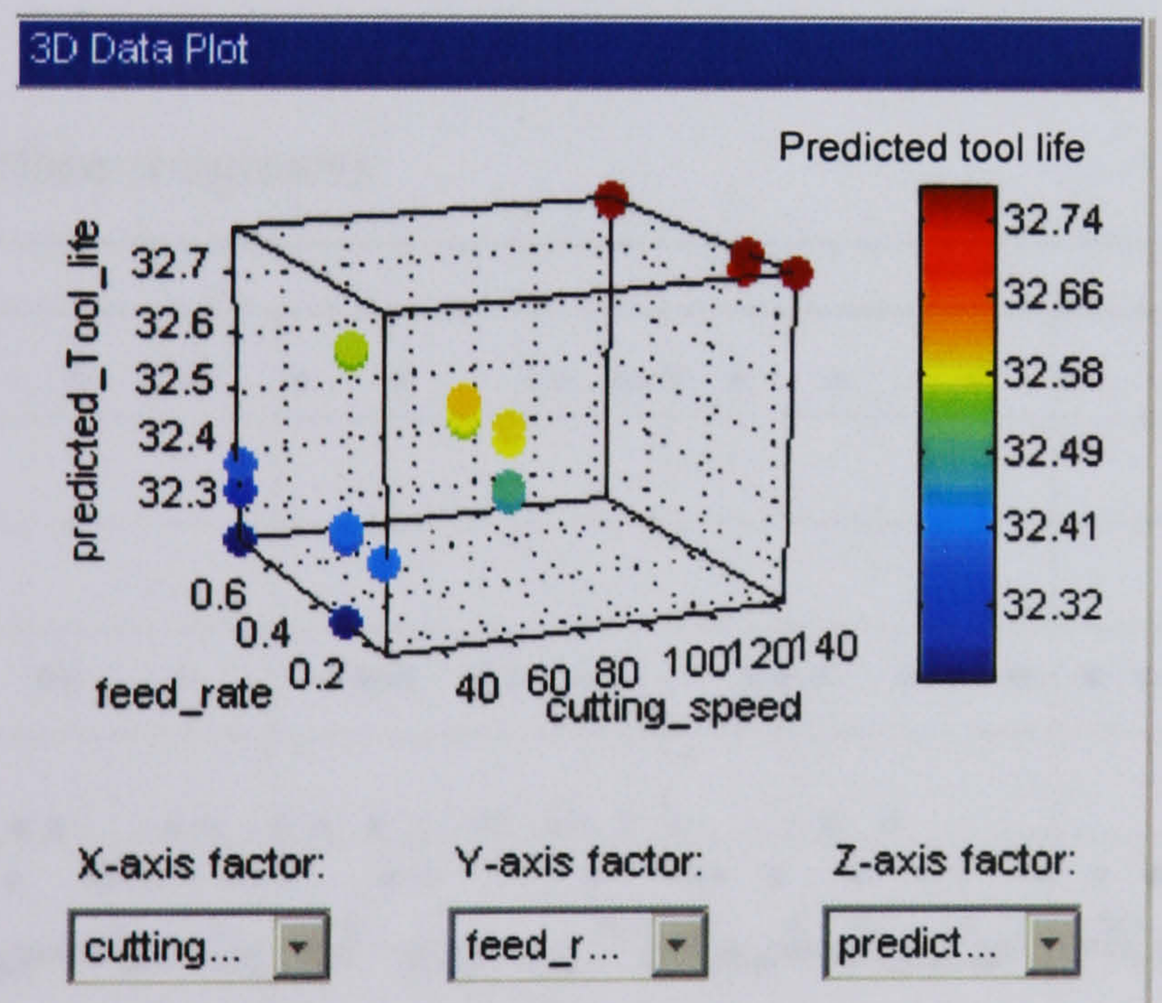

T = tool life (min)
f = feed rate (mm/r)
v = cutting speed (m/min)

Fig 7.15 The tool life results data in 3D

Fig. 7.16 shows the predicted observed value result of tool life. The graph combines the result from three type's experiments such as cutting trail experiment, RSM and Neural Network. There are three different colour represent each type of experiment. According

to the graph, the purple line indicates neural Network result, light blue colour represent RSM results and dark blue represent cutting trial experimental result.

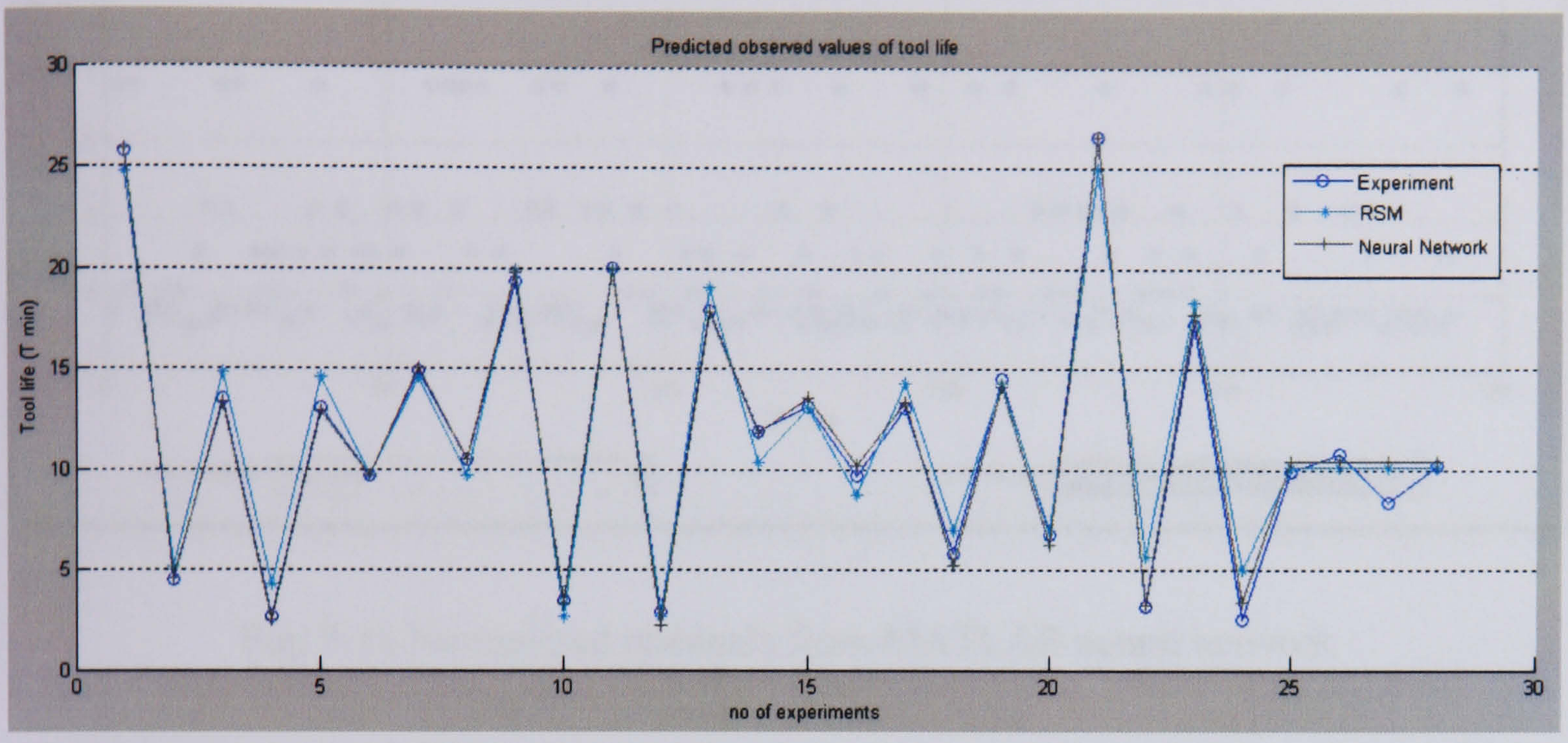

Fig. 7.16 Predicted observed value results of tool life

7.7.4.3 Surface roughness

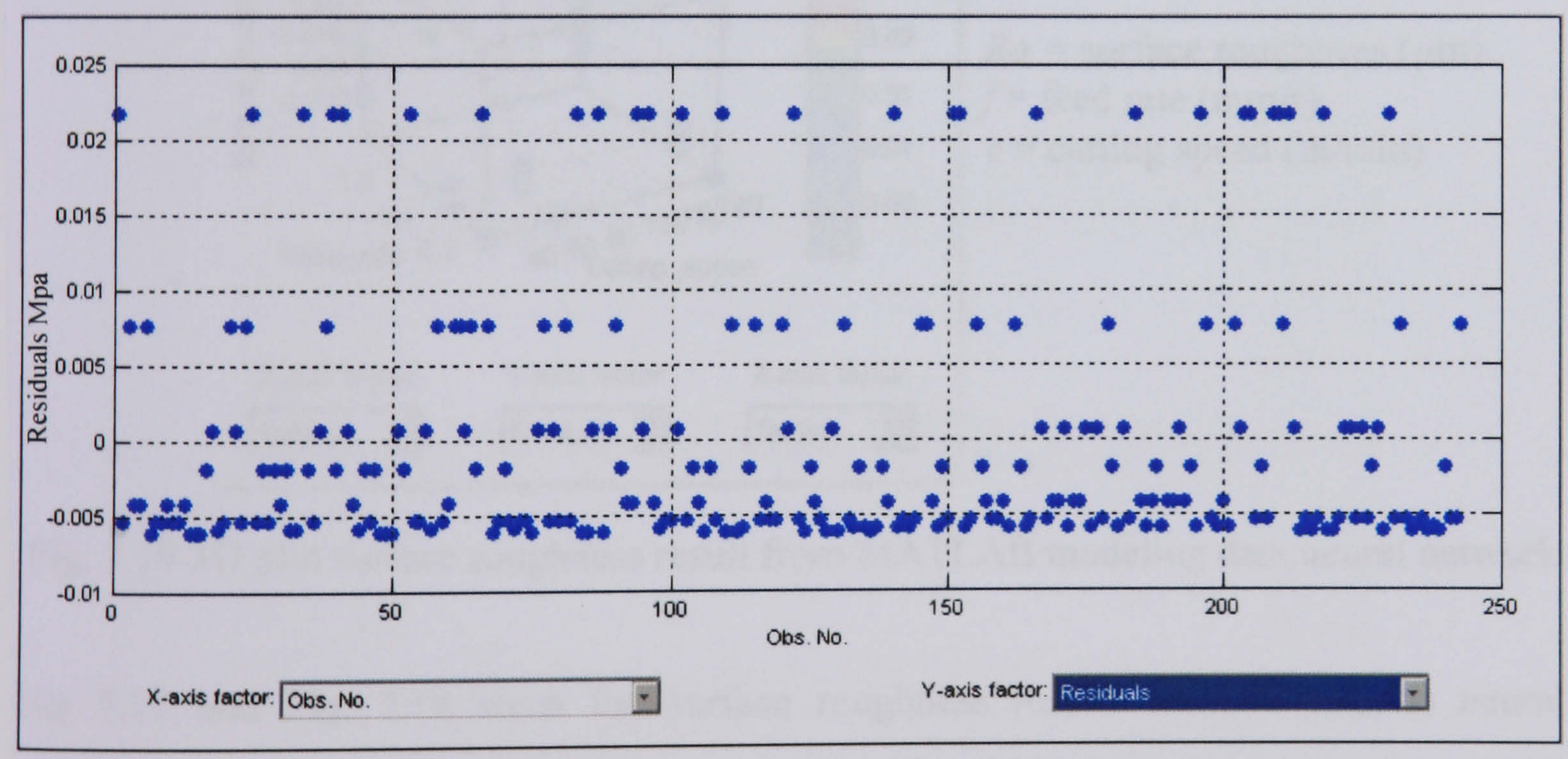

Fig. 7.17 Surface roughness result from MATLAB neural network

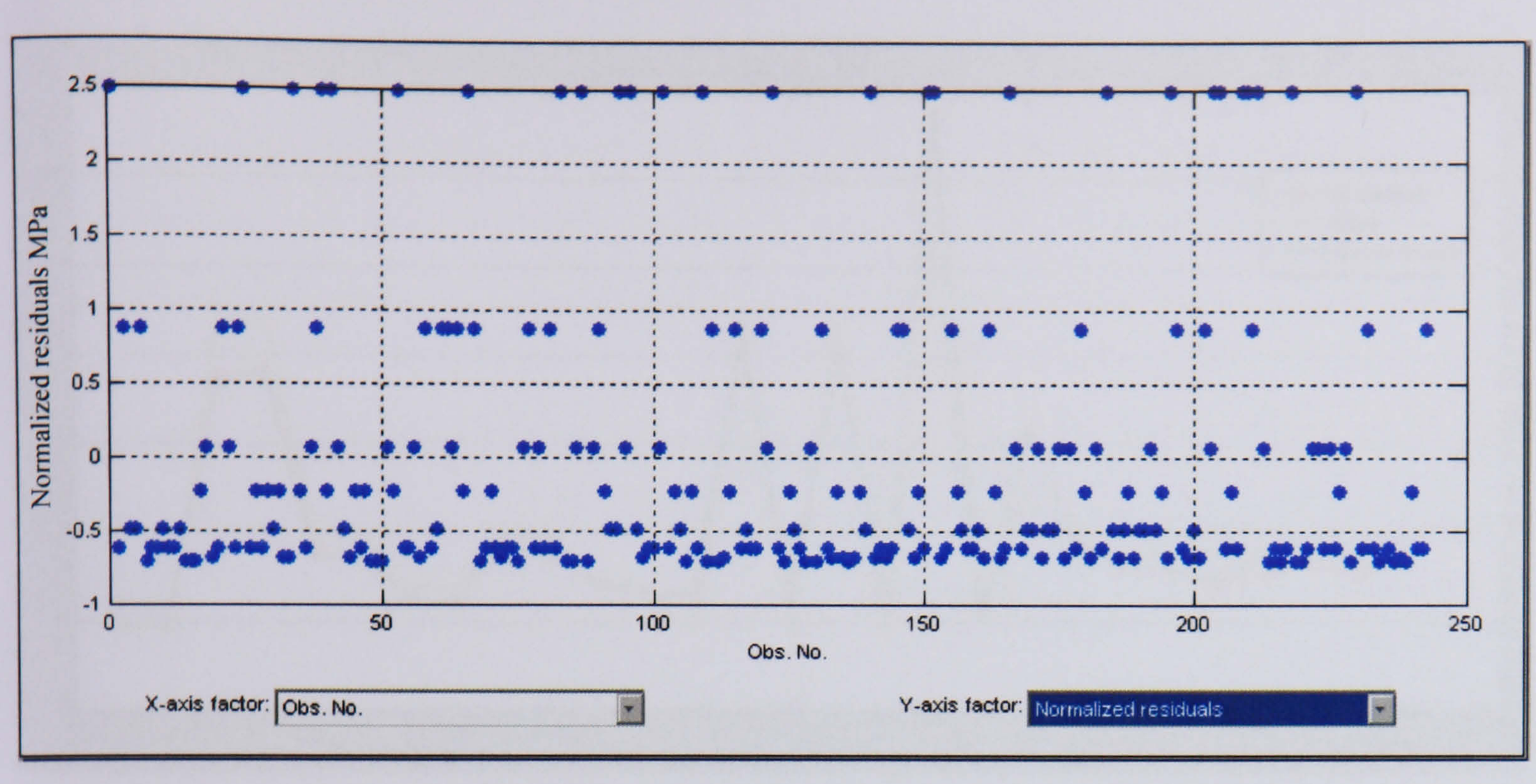

Fig. 7.18 Normalized residuals from MATLAB neural network

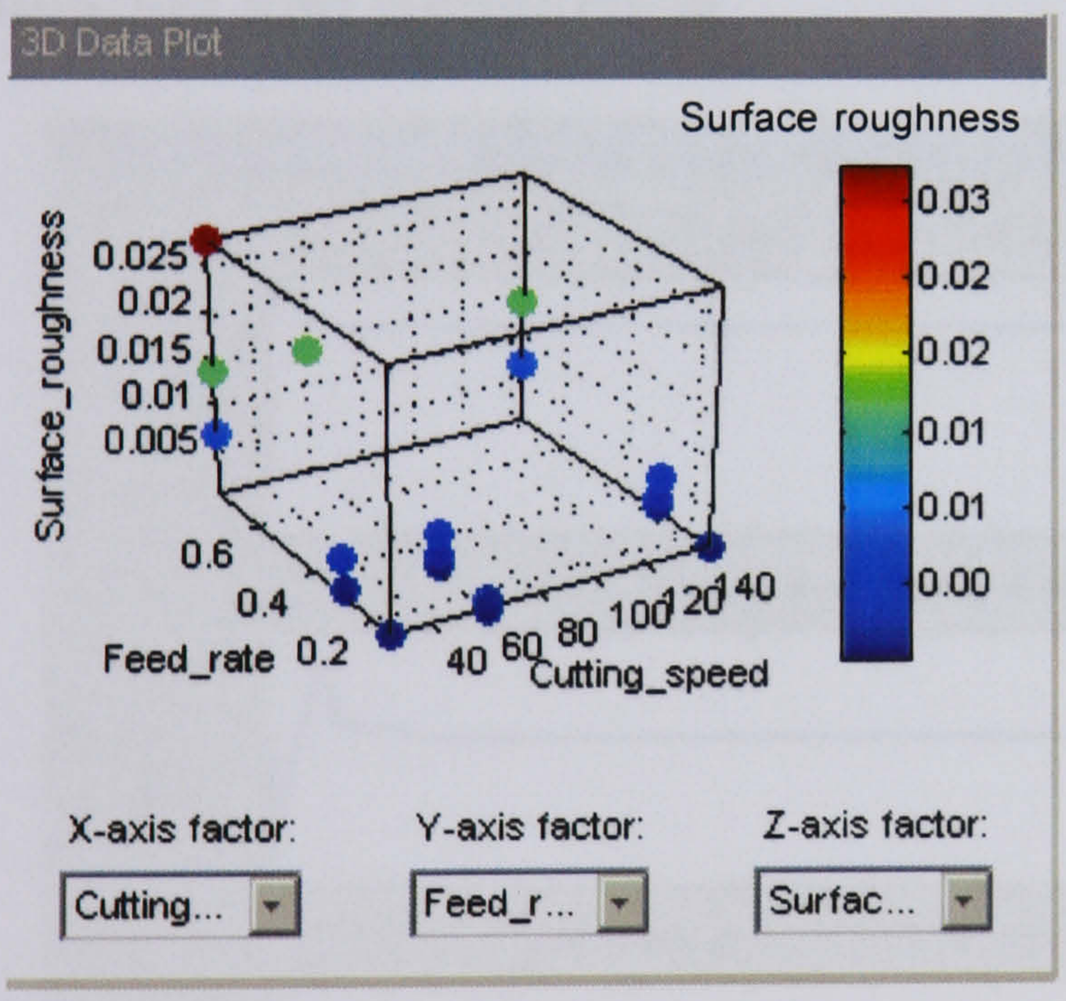

Ra = surface roughness (μm)
f = feed rate (mm/r)
v = cutting speed (m/min)

Fig. 7.19 3D plot surface roughness result from MATLAB modeling data neural network

Fig 7.17 and Fig. 7.18 show the surface roughness results from MATLAB neural network. The comparison results are shown in Fig. 7.20 show the comparison result between the cutting trial experiment, RSM and Neural Network. The graph explains the value of surface roughness can be achieved by different type of experimental method.

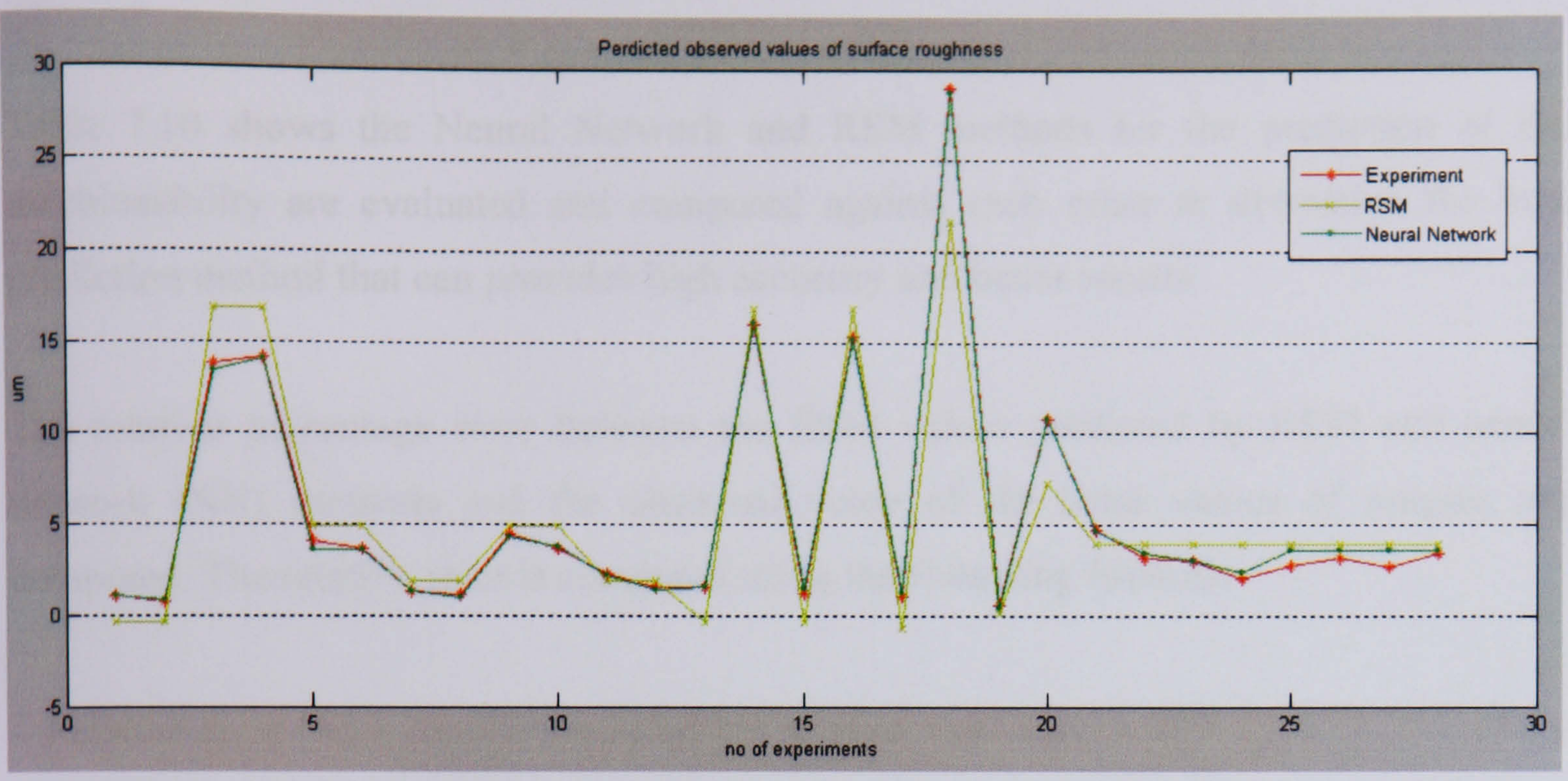

Fig. 7.20 Predicted observed values of surface roughness

7.7.5 Evaluation and comparison

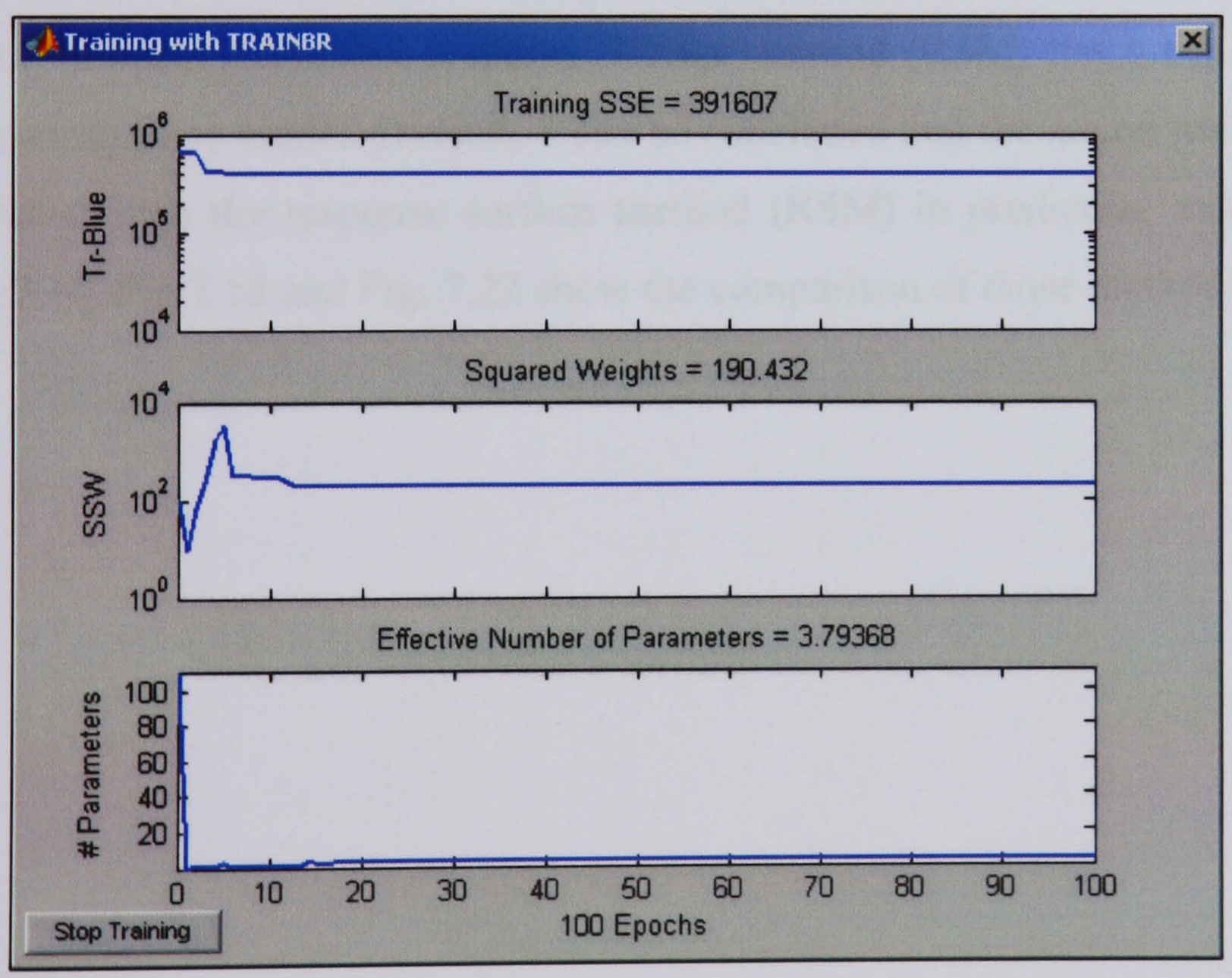

Fig. 7.21 Training Error result from MATLAB neural network

Fig. 7.21 shows training error during running the neural network (NN) data. From the figure the error can be found at the beginning of the process and flat after 10 Epochs.

Table 7.10 shows the Neural Network and RSM methods for the prediction of the machineability are evaluated and compared against each other to determine the best prediction method that can provides high accuracy and better results.

The relative percentage error between the fitted values predicted by RSM and neural network (NN) methods and the observed value of the three values of outputs are computed. The relative error is computed using the following formula:

$$\text{Relative error (\%)} = \frac{\text{(model predicted value- observed value) x 100}}{\text{Observed value}} \qquad (7\text{-}8)$$

Table 7.11 illustrated the relative errors for the two modeling techniques. It is found that the neural network (NN) is better than the response surface method (RSM) within machineability models. However, response surface method (RSM) has a better tool life but not the cutting force model. Overall, it can be concluded that the neural network (NN) method is better than the response surface method (RSM) in predicting machineabilty models. Fig 7.14, Fig 7.18 and Fig. 7.22 show the comparison of those methods.

Table 7.10 Result of two building model techniques

The results from the two building model techniques						
No. of experiment	Predicted values using Matlab NN			Predict values using RSM		
	T(*min*)	*Fc*(N)	*Ra*(μm)	*T1*(*min*)	*F1c*(N)	*R1a*(μm)
1	18.72	12.50	8.72	8.73	28.13	8.73
2	5.71	11.25	1.57	15.71	11.25	15.71
3	17.56	6.25	17.85	78.57	14.06	78.57
4	12.11	22.50	12.01	20.11	22.50	20.11
5	18.85	22.50	1.88	18.86	22.50	18.86
6	12.73	6.250	13.27	32.74	14.06	32.74
7	6.54	21.25	6.54	6.55	28.13	6.55
8	11.42	11.00	13.14	31.43	11.25	31.43
9	1.19	11.25	4.19	4.19	11.25	4.19
10	1.42	22.50	3.14	31.43	22.50	31.43
11	5.25	11.25	4.52	45.26	11.25	45.26
12	1.42	11.25	13.14	31.43	11.25	31.43
13	8.38	22.50	8.38	8.381	22.50	8.38
14	10.05	11.25	1.00	10.06	28.13	10.06
15	15.71	11.25	1.57	15.71	28.13	15.71
16	3.93	11.25	3.92	3.93	28.13	3.93
17	3.49	45.00	13.49	3.49	45.00	3.49
18	11.1	11.25	1.13	11.31	50.31	113.14
19	4.19	16.25	4.19	4.19	56.25	4.19
20	15.71	11.25	1.57	15.71	11.25	15.71
21	10.28	6.25	5.02	50.29	14.06	50.28
22	2.73	11.25	3.27	32.74	50.31	32.74
23	18.85	11.00	11.88	18.86	11.25	18.86
24	20.95	6.25	12.09	20.95	14.06	20.95
25	8.73	11.25	8.72	8.73	28.12	8.73
26	3.49	11.25	3.40	3.49	11.25	3.49
27	25.25	45.00	4.52	45.26	45.00	45.26

Table 7.11 Relative error of using RSM and the neural network (NN)

The relative errors for the two modelling technique					
Relative error (%) of the predicted values of RSM			Relative error (%) of the predicted values of NN		
T	*Fc*	*Ra*	*T*	*Fc*	*Ra*
3.59	34.00	16.14	1.14	20.11	11.42
1.85	22.14	7.02	2.49	22.50	6.86
18.46	42.00	4.04	24.06	30.73	3.27
8.23	13.78	9.77	6.54	12.70	6.30
19.45	41.80	4.36	21.25	34.56	3.14
12.84	10.39	5.00	1.25	9.41	4.19
21.46	7.30	4.60	24.82	11.59	3.45
14.54	16.09	6.50	1.43	8.13	4.53
4.51	9.30	6.14	1.58	4.13	5.43
8.13	3.68	8.67	5.98	1.52	5.07
14.22	14.00	3.29	10.23	9.90	1.01
6.90	6.04	17.29	3.13	5.30	14.31
2.50	5.90	5.69	9.40	3.67	3.93
14.84	10.39	14.54	12.93	7.31	13.14
1.75	13.14	6.12	1.40	8.77	4.82
4.58	6.50	15.74	2.49	4.00	18.93
5.82	17.39	14.64	2.50	22.90	12.64
10.84	14.19	7.51	8.70	7.82	5.28
2.51	18.20	14.00	4.00	12.40	10.06
3.75	5.14	4.32	5.34	3.96	2.97
7.73	35.77	2.31	4.22	30.64	0.95
4.90	15.84	10.09	2.97	8.13	8.73
13.25	4.97	5.41	5.40	3.37	3.77
6.30	8.63	12.21	4.70	6.80	9.00
15.42	3.78	1.31	10.62	3.27	0.99
7.43	11.87	13.23	2.87	9.82	8.83
8.23	3.78	1.77	6.22	1.98	0.67

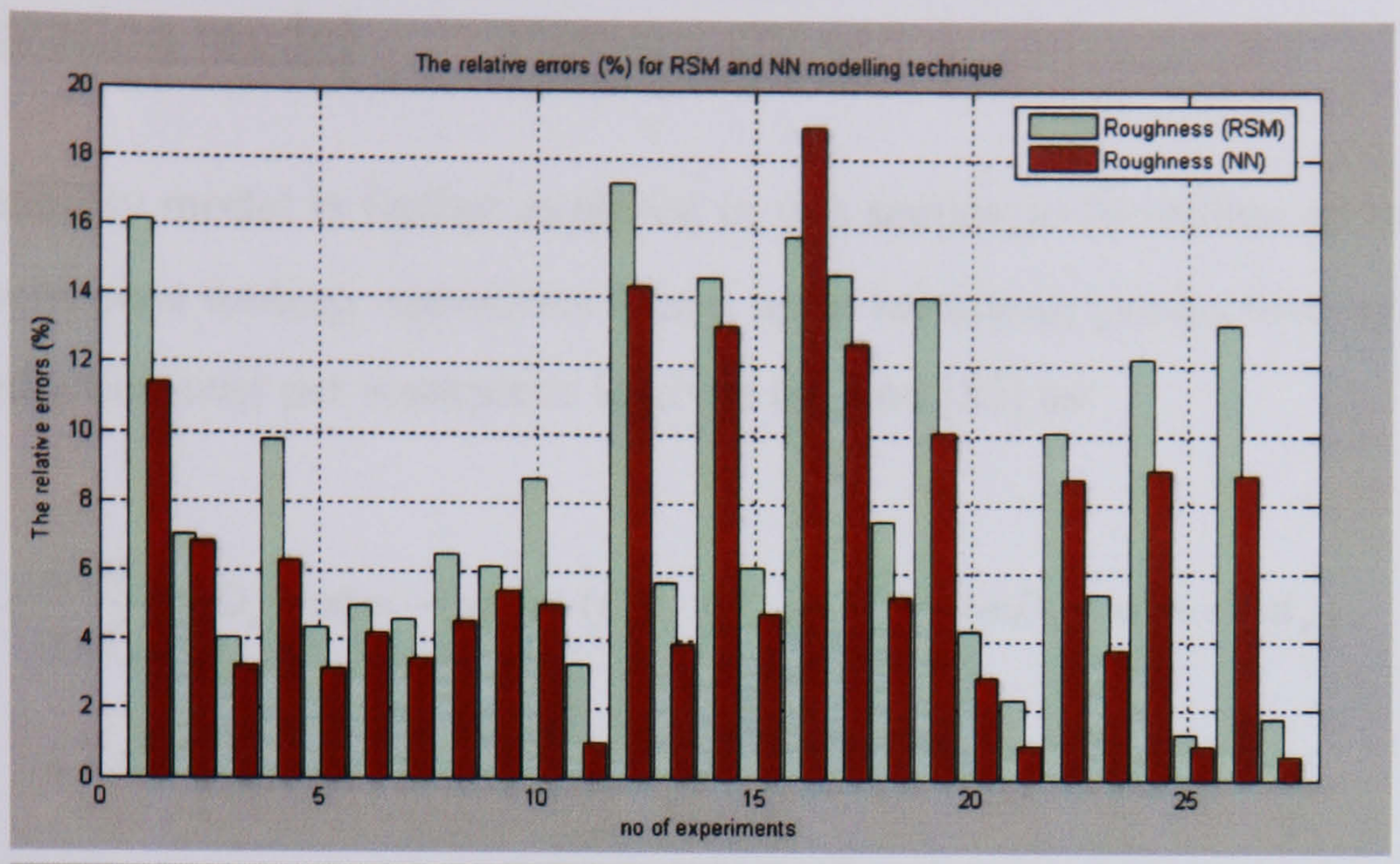

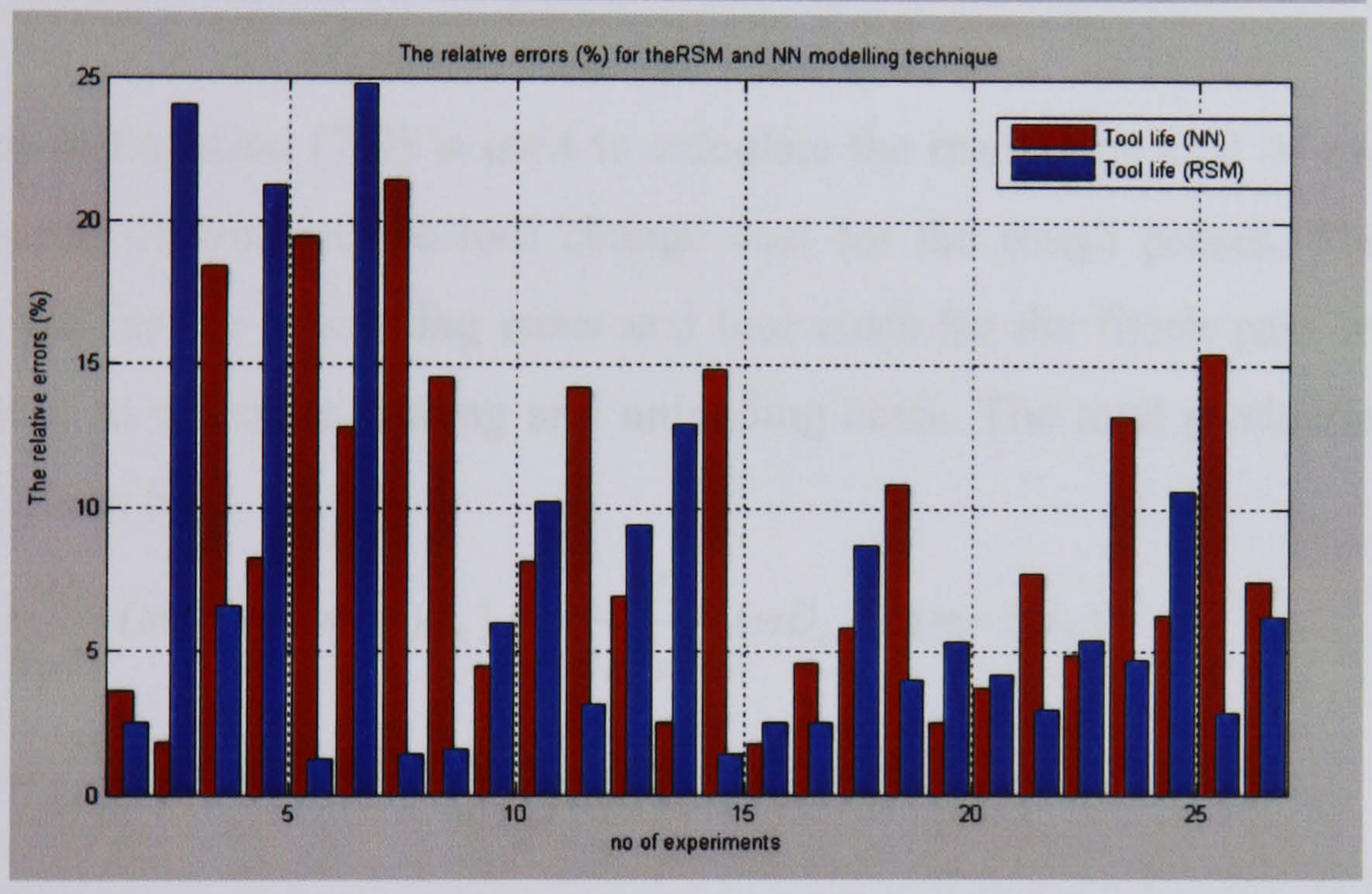

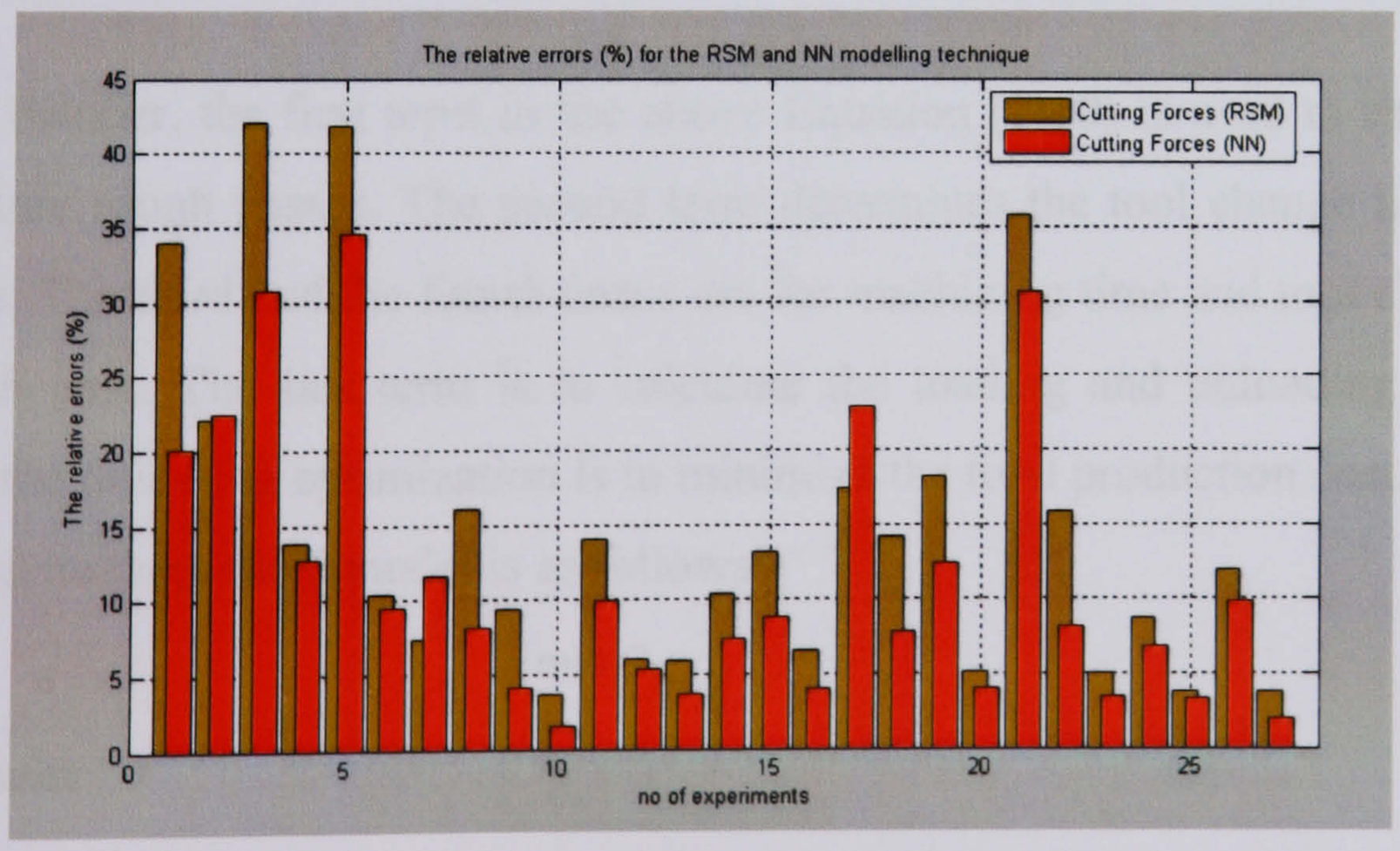

Fig. 7.22 Comparison graph of relative error using RSM and the neural network (NN)

7.8 Optimization model

The machineability model is further explored in this section to formulate an optimization model for multi pass turning operations based upon minimum production cost criterion. The total production cost per workpiece is given by Yeo [55] as:

$$C_{pr} = \frac{C_0 \pi L}{v_R f_R}(mD_o - m(m-1)d_R) + (C_o t_r + C_t)\frac{\pi L}{v_R f_R T_R}(mD_o - m(m-1)d_R)$$
$$+ \frac{C_o \pi L}{v_f f_f}(D_L + 2d_f) + (C_o t_r + C_t \frac{\pi L}{v_f f_f T_f}(D_L + 2d_f) + C_o t_h \quad (7\text{-}9)$$

The first term in Equation (7-9) is used to calculate the machining cost of rough passes. The second term determines the tool change cost for the rough passes. The third and fourth terms are for the machining costs and tool costs for the finish pass respectively. The last term is to calculate loading and unloading costs. The total production time per workpiece is given by:

$$T_{pr} = \frac{\pi L}{v_R f_R}(mD_o - m(m-1)d_R) + t_r \frac{\pi L}{v_R f_R T_R}(mD_o - m(m-1)d_R)$$
$$+ \frac{\pi L}{v_f f_f}(D_L + 2d_f) + t_r \frac{\pi L}{v_v f_f T_f}(D_L + 2d_f) + t_h \quad (7\text{-}10)$$

In the same manner, the first term in the above Equation (7-10) is used to calculate the machining time rough passes. The second term determines the tool change time for the rough passes. The third and the fourth terms are for machining time and tool change time for the finish pass. The last term is to calculate the loading and unloading time. The objective of the modeling optimization is to minimize the total production cost. Therefore the developed mathematical model is as follows:

$$\min C_{pr} \quad (7\text{-}11)$$

for rough passes

$$v_{\min} \le v_r \le v_{\max} \tag{7-12}$$

$$f_{\min} \le f_R \le f_{\max} \tag{7-13}$$

$$d_{\min} \le d_R \le d_{\max} \tag{7-14}$$

$$F_{c,R} \le F_{c,\max} \tag{7-15}$$

$$P_R \le P_{c,\max} \tag{7-16}$$

for finish pass

$$v_{\min} \le v_r \le v_{\max} \tag{7-17}$$

$$f_{\min} \le f_R \le f_{\max} \tag{7-18}$$

$$d_{\min} \le d_R \le d_{\max} \tag{7-19}$$

$$R_a \le R_{a,\max} \tag{7-20}$$

$$F_{c,f} \le F_{c,\max} \tag{7-21}$$

$$P_c \le P_{c,\max} \tag{7-22}$$

$$D_o - 2(md_R + 2d_f) = D_L \tag{7-23}$$

$$\sum_{i=1}^{n_1} x_{ip} = 1 \left[p = r, f\right] \tag{7-24}$$

The objective function (7-11) is described in equation (7-9). There are two sets of constraints which represent the boundaries and limitations of the machining process. The first set represents the rough passes constraints (7-12)–(7-16). The second set is represented by sets (7-17)–(7-22) which are related to the finish pass. The constraints sets (7-12)–(7-14) ensure that values of roughing cutting speed, feed rate, and depth of cuts are within allowable ranges. Force and power constraints of rough passes are represented by constraints (7-15) and (7-16). The constraints sets (7-17)–(7-19) ensures that values of finish cutting speed, feed rate, and depth of cuts are within allowable ranges. Constraint (7-20) ensures that the surface roughness produced is not exceeding the maximum allowable surface roughness. Force and power constraints of finish pass are represented by (-21) and (7-22). The constraint set (7-23) ensures that the total subdivisions of depths of cut in finishing and rough passes are equal to the total depth of cut. Finally, we introduce a new constraint to this optimization model as prediction and optimization models for turning operations illustrated in the constraint (7-24). This constraint ensures that only one tool is selected for every operation to select the appropriate tool for the machining operation (based on its nose radius). The above optimization model is a generic for any turning operation and can be used to find the optimal process parameters based on the data obtained from the considered machining operation.

Mozher constructed three models of tool life, cutting force and surface finish, using regression analysis (RA) technique and the logarithmic transformation of their first order models and evaluated these models using the analysis of lack of fit [81].

The three models are as follows:

$$T = \frac{406.423 r^{0.038}}{v^{0.1051} f^{0.289} d^{0.219}} \tag{7-25}$$

$$F_c = \frac{4182.220 f^{0.621} d^{0.563} r^{0.116}}{v^{0.108}} \tag{7-26}$$

$$R_a = \frac{31.254 f^{1.347}}{v^{0.159} d^{0.159} r^{0.605}} \tag{7-27}$$

In order to utilize the suggested machineability models in optimization for selected tools, Equations (7-25), (7-26) and (7-27) are modified to include the tool selection. So there are;

$$T = \frac{406.423(r_1 x_{1p} + r_2 x_{2p} + r_3 x_{3p})^{0.038}}{v^{0.1051} f^{0.289} d^{0.219}} \tag{7-28}$$

$$F_c = \frac{4182.220 f^{0.621} d^{0.563} (r_1 x_{1p} + r_2 x_{2p} + r_3 x_{3p})^{0.116}}{v^{0.108}} \tag{7-29}$$

$$R_a = \frac{31.254 f^{1.347}}{v^{0.159} d^{0.159} (r_1 x_{1p} + r_2 x_{2p} + r_3 x_{3p})^{0.605}} \tag{7-30}$$

where r_1, r_2 and r_3 are the three different tool nose radius used in the experiments, and x_1, x_2 x and x_3 are binary decision variables. In total, there are eight decision variables in the developed model. These variables are *vr, fr, dr , vf , ff , df, xir,* and *xif.*

7.9 Conclusion

In this chapter, empirical models for the prediction of machineability models such as tool life, cutting force and surface roughness have been presented based on turning experiments. The response surface methodology and neural networks are used to construct new machineabilty models. The methodologies of RSM and NN are discussed in details. The developed neural networks can predict the tool life, cutting force, and surface roughness altogether. The models based on the two methods are compared and evaluated using descriptive statistics and hypothesis testing. It is found that the neural networks models are better than RSM based models.

The developed machibeability models are utilized to formulate an optimization model for optimizing the machined surface functionality economic. The suggested optimization model is a multi pass model which minimizes the total production cost per workpiece with practical constraints. The selection of tool, when determining the optimal values of

process parameters for the minimum production cost criterion, is introduced based on the tool nose radius. The optimization is further explored against the desired surface roughness, tool life and machining stability.

PAGE NUMBERING AS ORIGINAL

References

[1] N. Ikawa, R. R. Donaldson, R. Komanduri, W. König, P. A. McKeown, T. Moriwaki and I. F. Stowers, Ultraprecision metal cutting - the past, the present, and the future, Annals of the CIRP, 1991, Vol. 40, No. 2, pp. 587-594.

[2] R. R. Donaldson and S. R. Patterson, Design and construction of a large vertical axis diamond turning machine (LODTM), Proceedings of SPIE Technical Symposium, 1983, pp. 433-438.

[3] P. A. Mc Keown, K. Carlisle, P. Shore and R. F. J. Read, Ultra-precision high stiffness CNC grinding machines for ductile mode grinding of brittle materials, SPIE, 1320, 1990, Infrared Technology and Application, pp. 301-313.

[4] T. H. C. Childs, K. Maekawa, T. Obikawa and Y. Yamane, Metal Cutting: Theory and Applications, Arnold, London, 2000.

[5] R. R. Donaldson, C. K. Syn, J. S. Taylor, N. Ikawa and S. Shimada, Minimum thickness of cut in diamond turning of electroplated copper, UCRL-97606, 1987.

[6] P. Schellekens and N. Rosielle, Design for precision: current status and trends, Annals of the CIRP, 1998, Vol. 47, No. 2, pp. 557-586.

[7] J. Z. Zhang and J. C. Chen, The development of an in-process surface roughness adaptive control system in end milling operations, International Journal of Advanced Manufacturing Technology, 2007, Vol. 31, pp. 877-887.

[8] E. J. A. Armarego and R. H. Brown, The Machining of Metals, Prentice-Hall, Inc., Englewood Cliffs, New Jersey, 1969.

[9] Y. Altintas, Manufacturing Automation: Metal Cutting Mechanics, Machine Tool Vibrations, and CNC Design, Cambridge University Press, Cambridge, 2000.

[10] K. F. Ehmann, S. G. Kapoor, R. E. Devor and I. Lazoglu, Machining process modeling: a review, Transactions of the ASME: Journal of Manufacturing Science and Engineering, 1997, Vol. 119, pp. 655–663.

[11] S. A. Tobias and W. Fishwick, The chatter of lathe tools under other cutting conditions, Transactions of the ASME, Journal of Engineering for Industry, 1958, Vol. 80, pp. 1079–1088.

[12] J. Tlusty and M. Polacek, The stability of the machine tool against self-excited vibration in machining, Int. Res. In Production Eng., ASME, 1963, pp. 465–474.

[13] Y. Altintas and P. Lee, Mechanics and dynamics of ball-end milling, Transactions of the ASME: Journal of Manufacturing Science and Engineering, 1998, Vol.120, No.4, pp. 684-692.

[14] B. W. Ikua, H. Tananka, F. Obata and S. Sakamoto, Prediction of cutting forces and machining error in ball end milling of curved surface I – theoretical analysis, Precision Engineering, 2001, Vol. 25, pp. 266–273

[15] X. Liu, K. Cheng, D. Webb and X. Luo, Improved dynamic cutting force model in peripheral milling, International Journal of Advanced Manufacturing Technology, 2002, Vol.20, No.9, pp. 631-638.

[16] P. Albrecht, Dynamics of the metal cutting process, Transactions of the ASME, Journal of Engineering for Industry, 1965, Vol. 87, pp. 429-441.

[17] N. H. Hanna and S. A. Tobias, A theory of nonlinear regenerative chatter, Transactions of the ASME: Journal of Engineering for Industry, 1974, Vol. 96, pp. 247-253.

[18] E. R. Marsh, D. S. Yantek, M. A. Davies and D. E. Gilsinn, Simulation and measurement of chatter in diamond turning, Transactions of the ASME: Journal of Manufacturing Science and Engineering, 1998, Vol. 20, pp. 230-235.

[19] J. Tlusty and F. Ismail, Basic non-linearity in machining chatter, Annals of the CIRP, 1981, Vol. 30, No. 1, pp. 299–304.

[20] Z. B. Hou and R. Komanduri, On a thermomechanical model of shear instability in machining, Annals of the CIRP, 1995, Vol. 44, No. 1, pp. 69-73.

[21] M. A. Davies, T. J. Burns and C. J. Evans, On the dynamics of chip formation in machining hard metals, Annals of the CIRP, 1997, Vol. 46, No. 1, pp. 25-30

[22] M. A. Davies and T. J. Burns, Thermo mechanical oscillations in material flow during high-speed machining, Philosophical Transactions: Mathematical, Physical and Engineering Sciences, 2001, Vol. 359 No. 1781, pp. 821-846.

[23] D. W. Wu and C. R. Liu, An analytical model of cutting dynamics, model building and verification, Transactions of the ASME: Journal of Engineering for Industry, 1985, Vol. 107, pp. 107-118.

[24] H. M. Shi, X. Wang and T. Liu, Bifurcation and catastrophes in metal-cutting processes, Transactions of the ASME: Journal of Manufacturing Science and Engineering, 1998, Vol.120, pp. 817-820.

[25] D. Lucca, R. L. Rhorer and R. Komanduri, Energy dissipation in ultra-precision machining of copper, Annals of the CIRP, 1991, Vol. 40, No. 1, pp. 69-73.

[26] D. Lucca, Energy dissipation and tool workpiece contact in ultra-precision machining, Tribology Transactions, 1994, Vol. 37, pp. 651–655.

[27] H. M. Shi and S. A. Tobias, Theory of finite amplitude machine tool instability, International Journal of Machine Tool Design and Research, 1984, Vol. 24, No.1 , pp. 45–69.

[28] K. Palanikumar, Application of Taguchi and response surface methodologies for surface roughness in machining glass fiber reinforced plastics by PCD tooling, International Journal of Advanced Manufacturing Technology, 2008, Vol. 36, pp. 19-27

[29] K. Taraman and B. Lambert, A surface roughness model for a turning operation, International Journal of Production Research, 1974. Vol. 12, No. 6, pp. 691-703.l

[30] K. C. Ching and H. Lu, Design optimization of cutting parameters for side milling operations with multiple performance characteristics, International Journal of Advanced Manufacturing Technology, 2007, Vol. 32, pp.18-26.

[31] K. Taraman, Multi machining output–multi independent variable turning research by response surface methodology, International Journal of Production Research, 1974, Vol. 12, No. 2, pp. 233-245.

[32] W. Grzesik, A revised model for predicting surface roughness in turning, Wear, 1996, Vol. 194, pp. 143–148.

[33] X. D. Fang, and H. Safi-jahanshahi, A new algorithm for developing a reference-based model for predicting surface roughness in finish machining of steels, International Journal of Production Research, 1997, Vol. 35, No. 1, pp. 179-199.

[34] B. J. Lin, C. I. Hung and E. J. Tang, An optimal design of axial-flow fan blades by the machining method and an artificial neural network, Proceedings of the Institution of Mechanical Engineers, Part C, 2002, Vol. 216, pp. 367–376.

[35] R. K, Jain and V. K. Jain, Optimum selection of machining conditions in abrasive flow machining using neural network, Journal of Materials Processing Technology, 2000, Vol. 108, pp. 62–67.

[36] J. Gradisek, E. Govekar and I. Grabec, A chaotic cutting process and determining optimal cutting parameter values using neural network, International Journal of Machine Tools & Manufacture, 1996, Vol. 36, No. 10, pp. 1161–1172.

[37] P. Palanisamy, I. Rajendran and S. Shanmugasundaram, Optimization of machining parameters using genetic algorithm and experimental validation for end-milling operations, International Journal of Advanced Manufacturing Technology, 2007, Vol. 32, pp.644-655.

[38] C. Arcona and T. A. Dow, An empirical tool force model for precision machining, Transactions of the ASME: Journal of Manufacturing Science and Engineering, 1998, Vol. 120, pp. 700–707.

[39] G. Park, M.T. Bement, D.A. Hartman, R.E. Smith, C.R. Farrar, The use of active materials for machining processes: A review, International Journal of Machine Tools and Manufacture, 2007, Vol. 47, pp. 2189-2206.

[40] I.S. Kang, J.S. Kim, M.C. Kang and K.Y. Lee, Tool condition and machined surface monitoring for micro-lens array fabrication in mechanical machining, Journal of Materials Processing Technology, 2008, Vol. 201, pp. 585-589.

[41] L. D. Chiffre, P. Lonardo, H. Trumpold, D. A. Lucca, G. Goch, C. A. Brown, J. Raja and H. N. Hansen, Quantitative characterization of surface texture, Annals of the CIRP, 2000, Vol. 49, No. 2, pp. 635-652.

[42] D. A. Lucca, E. Brinksmeier and G. Goch, Progress in assessing surface and subsurface integrity, Annals of the CIRP, 1998, Vol. 47, No. 2, pp. 669-693.

[43] K. J. Stout, Development of Methods for the Characterisation of Roughness in Three Dimensions, Penton Press, London, 2000.

[44] L. D. Chiffre, P. Lonardo, H. Trumpold, D. A. Lucca, G. Goch, C. A. Brown, J. Raja and H. N. Hansen, Quantitative characterization of surface texture, Annals of the CIRP, 2000, Vol. 49, No. 2, pp. 635-652.

[45] Y. Sahin and A.R. Motorcu, Surface roughness model in machining hardened steel with cubic boron nitride cutting tool, International Journal of Refractory Metals & Hard Materials, 2008, Vol. 26, pp. 84-90.

[46] D. Blackmore and G. Zhou, A new fractal model for anisotropic surfaces, International Journal of Machine Tools & Manufacture, 1998, Vol. 38, pp. 551-557.

[47] Y. Wang and K. S. Moon, A methodology for the multi-resolution simulation of grinding wheel surface, Wear, 1997, Vol. 211, pp. 218-225.

[48] P. Podsiadlo and G. W. Stachowiak, Multi-scale representation of tribological surfaces, Proceedings of Institution of Mechanical Engineers, Part J, 2002, Vol. 216, pp. 463-479.

[49] M. Field and J. F. Kahles, Review of surface integrity of machined components, Annals of the CIRP, 1971, Vol. 20, No. 2, pp. 153-163.

[50] H. K. Tönshoff and E. Brinksmeier, Determination of the mechanical and thermal influence on machined surface by microhardness and residual stress analysis, Annals of the CIRP, 1980, Vol. 29, No. 2, pp. 519-530.

[51] E. Brinksmeier, X-ray stress measurement - a tool for the study and layout of machining processes, Annals of the CIRP, 1985, Vol. 34, No. 1, pp. 485-490

[52] P. M. Lonardo, C. H, Trumpold and L. De Chiffre, Progress in 3D surface microtopography characterization. Annals of the CIPP, 1996, Vol. 45, No. 2, pp. 589-597.

[53] T. V. Vorburger, J. A. Dagata, G. Wilkening and K. Lizuka, Industrial uses of STM and AFM, Annals of the CIRP, 1997, Vol. 46, No. 2, pp. 597-620.

[54] D. A. Lucca, E. Brinksmeier and G. Goch, Progress in assessing surface and subsurface integrity, Annals of the CIRP, 1998, Vol. 47, No. 2, pp. 669-693.

[55] Yeo, S.H., A multipass optimisation strategy for CNC lathe operations. International Journal of Production Economic, 1995, 40, 209–218

[56] B. Bläsi, V. Boerner, A. Gombert, V. Kübler, M. Niggemann and V. Wittwer, Functional surface-relief structures manufactured by holography and subsequent microreplication, Proceedings of 2nd euspen International Conference, Turin, Italy, May 27th-31st, 2001, pp.12-15.

[57] D. J. Whitehouse, Surfaces: an essential link in nanotechnology, Nanotechnology, 1998, Vol. 9, No. 2, pp. 113-117.

[58] W. B. Lee and C. F. Cheung, A dynamic surface topography model for the prediction of nano-surface generation in ultra-precision machining, International Journal of Mechanical Sciences, 2001, Vol. 43, pp. 961-991.

[59] C. F. Cheung and W. B Lee, An investigation of cutting dynamics in single point diamond turning, International Journal of Japanese Society of Mechanical Engineering, 2000, Vol. 43, No. 1, pp. 116-126

[60] P. K. R. Rao and M. S. Shunmugam, Investigations into surface topography, microhardness and residual stress in boring trepanning association machining, Wear, 1987, Vol. 119, pp. 89 -100.

[61] B. J. Griffiths, Problems in measuring the topography of machined surfaces produced by plastic deformation mechanisms, Wear, Vol. 109, 1986, pp. 195 - 205.

[62] P. Chevrier, A. Tidu, B. Bolle, P. Cezard and J. P. Tinnes, Investigation of surface integrity in high speed end milling of a low alloyed steel, International Journal of Machine Tools & Manufacture, 2003,Vol. 43, pp.1135-1142.

[63] P. Stępień, Grinding forces in regular surface texture generation, International Journal of Machine Tools and Manufacture, 2007, Vol. 47, pp. 2098-2110.

[64] W. B. Sai, N. B. Salah and J. L. Lebrun. Influence of machining by finishing milling on surface characteristics, International Journal of Machine Tools & Manufacture, 2001, Vol. 41, pp. 443450.

[65] V. I. Syryamkin, A. V. Chesnokov, and D. V. Koval, Algorithmic and software support for computer-controlled determination of the microhardness of materials, Solid State Physics, Russian Physics Journal, Vol. 44, No. 11, 2001, pp. 1224-1229.

[66] Y. B. Guo and A. W. Warren, Microscale mechanical behavior of the subsurface by finishing processes, Transactions of the ASME, 2005, Vol. 127, pp. 333-338.

[67] L. Yurkov, N. V. Jhuravleva and E. S. Lukin, Kinetic microhardness measurements of sialon-based ceramics, Journal of Materials Science, Vol. 29, 1994, pp. 6551- 6560.

[68] B. Griffiths, Manufacturing Surface Technology (Surface Integrity and Functional Performance), Penton Press, London, 2001.

[69] M. J. Park, H. N. Yang, D. Y. Jang, J. S. Kim and T. E. Jin, Residual stress measurement on welded specimen by neutron diffraction, Journal of Materials Processing Technology, 2004, Vol. 15, pp. 171 -177.

[70] P. J. Withers and H. K. D. H Bhadeshia, Overview residual stress: part 1 - measurement techniques, Materials Science and Technology, Vol. 17, April 2001, pp. 355-365.

[71] F. V. Diaz, G. H. Kaufmann and G. E. Galizzl, Determination of residual stresses using hole drilling and digital speckle pattern interferometry with automated data analysis, Optics and Lasers in Engineering, 2000, Vol. 33, pp. 39-48.

[72] E. Brinksmeier, E. Minke and L. Nowag, Residual stresses in precision components, Fifth International Conference on Industrial Tooling, Southampton, UK, September 2003, Vol.10-11, pp. 1-21.

[73] M. R. Viotti, R. Sutbrio, A. Albertazzi Jr. and G. H. Kaufmanna, Residual stress measurement using a radial in-plane speckle interferometer and laser annealing: preliminary results, Optics and Lasers in Engineering, Vol. 42, 2004, pp. 71-84.

[74] O. Benning, Non-destructive determination of load and residual stresses by the x-ray stress method, The Rigaku Journal, Vol. 6, No. 2, 1989, pp. 15-21.

[75] B. J. Schwaru and M. H. Richardson, Experimental modal analysis, CSI Reliability Week, Orlando, Florida, October 1999, pp. 1-12.

[76] R. B. Aronson (Senior Editor), Surface finish is key to quality, Manufacturing Engineering, Vol. 127, No. 2, August 2001, pp. 1-5.

[77] M. Thomas and Y. Beauchamp, Statistical investigation of modal parameters of cutting tools in dry turning, International Journal of Machine Tools & Manufacture, Vol. 43, 2003, pp. 1093-1106.

[78] D. W. Cho and K. F. Eman, In-process identification of the milling operation, International Journal of Machine Tools & Manufacture, Vol. 30, No. 3, 1990, pp. 325-337.

[79] D. S. Kim, L C. Chang and S. W. Kim, Microscopic topographical analysis of tool vibration effects on diamond turned optical surfaces, Journal of the International Society for Precision Engineering and Nanotechnology, Vol. 26, 2002, pp. 168 -174.

[80] H. Schwenke, U. Neuschaefer-Rube, T. Pfeifer and H. Kunzmann, Optical methods for dimensional metrology in production engineering, Annals of CIRP, Vol. 51, Part 2, 2002, pp. 685-700.

[81] J. Mozher, Development of machineability models for high strength materials. Master's thesis, Industrial Engineering Department, KSU, Saudi Arabia, 1998.

[82] A. C Basheer, U. A Dabade, S. S Joshi, V.V. Bhanuprasad and V. M. Gadre, Modeling of surface roughness in precision machining of metal matrix composites using ANN. Journal of Materials Processing Technology, 2008, Vol. 197, pp. 439-444.

[83] V. G. Dhokia, S. Kumar, P. Vichare, S. T. Newman and R. D. Allen, Surface roughness prediction model for CNC machining of polypropylene, Proceedings of the Institution of Mechanical Engineers - Part B – Journal of Engineering Manufacture, 2008, Vol. 222, pp. 137-157.

[84] K. A. Desai and P. V. M. Rao, Effect of direction of parameterization on cutting forces and surface error in machining curved geometries, International Journal of Machine Tools & Manufacture, 2008, Vol. 48, pp. 249-259.

[85] Z. Brusilovski, Adjustment and readjustment of electrochemical machines and control of the process parameters in machining shaped surfaces, Journal of Materials Processing Technology, 2008, Vol. 196, pp. 311-320.

[86] W. Grzesik, A revised model for predicting surface roughness in turning, Wear, 1996, Vol. 194, pp. 143–148.

[87] S. To, Y.H. Zhu and W.B. Lee, Effects of cutting depth on the surface microstructure of a Zn–Al alloy during ultra-precision machining, Applied Surface Science, 2008, Vol. 254, pp.1559-1564.

[88] C.L.J. Lixin, An integrated surface modeling and machining approach for a marine propeller, International Journal of Advanced Manufacturing Technology, 2008, Vol. 35, pp. 1053-1064.

[89] R.S. Pawade, Joshi, S. Suhas and P. K. Brahmankar, Effect of machining parameters and cutting edge geometry on surface integrity of high-speed

turned Inconel 718, International Journal of Machine Tools & Manufacture, 2008, Vol. 48, pp. 15-28.

[90] J. Z. Yang, Q. F. Wang, D. H. Zheng and L. P. Chen, Tool path generation for machining compound surfaces with extended cut region method, International Journal of Advanced Manufacturing Technology, 2007, Vol. 35, pp. 179-185.

[91] D. R. J. Owen and M. J. Vaz, Computational techniques applied to high-speed machining under adiabatic strain location conditions, Computational Methods Application Engineering, 1999, Vol. 171, pp. 445-461.

[92] T. Inamura, N. Takezawa, Y. Kumaki and T. Sata, On a possible mechanics of shear deformation in nanometric cutting, Annals of the CIRP, 1994, Vol. 43, No. 1, pp. 47-50.

[93] R. Komanduri and Z. B. Hou, Thermal modeling of the metal cutting process - Part II: temperature rise distribution due to frictional heat source at the tool - chip interface, International Journal of Mechanical Sciences, 2001, Vol. 43, pp. 57-88.

[94] R. Komanduri and Z. B. Hou, Thermal modeling of the metal cutting process - Part III: temperature rise distribution due to the combined effects of shear plane heat source and the tool-chip interface frictional heat source, International Journal of Mechanical Sciences, 2001, Vol. 43, pp. 89-107.

[95] T. H. C. Childs, K. Maekawa and P. Maulik, Effects of coolant on temperature distribution in metal machining, Material Science Technology, 1988, Vol. 4, No. 11, pp. 1006-1019.

[96] T.I. EI-Wardany, E. Mohammed and M. A. Elbestawi, Cutting temperature of ceramic tools in high speed machining of difficult to cut materials, International Journal of Machine Tools & Manufacture, 1996, Vol. 36, No. 6, pp. 611-634.

[97] S. Fraser, M. H. Attia and M. O. M. Osman, Modelling, identification and control of thermal deformation of machine tool structures: Part I - Concept of generalized modeling, Int. Mech. Eng. Cong. Expo. PED 68, ASME, 1994, pp. 931-944.

[98] S. Fraser, M. H. Attia and M. O. M. Osman, Modelling, identification and control of thermal deformation of machine tool structures: Part II - Generalized transfer function, Int. Mech. Eng. Cong. Expo. PED 68, ASME, 1994, pp. 945-953.

[99] N. Aria, A study on the cutting of quenched steel by tool having negative rake angle, Science Engineering Revision Doshisha University, 1992, Vol. 33, No. 3, pp. 185-188.

[100] K. Maekawa and H. Ohhata, Simulation analysis of three-dimensional continuous chip formation processes (3rd Rep - Effects of tool geometry on chip flow and wear), Journal of Japanese Precision Engineering, 1996, Vol. 62, No. 4, pp. 535-539.

[101] A.J. Shih, Finite element analysis of the rake angle effects in orthogonal metal cutting, International Journal of Mechanical Sciences, 1996, Vol. 38, No. 1, pp. 1-17.

[102] G. Germain, F. Morel, J.L. Lebrun, A. Morel, Machinability and Surface Integrity for a Bearing Steel and a Titanium Alloy in Laser Assisted Machining, Lasers in Engineering (Old City Publishing), 2007, Vol. 17, pp. 329-344.

[103] M. Beghini, L. Bertini and R. Raffaelli, Numerical analysis of plasticity effects in the hole-drilling residual stress measurement, Journal of Test Evaluation, 1994, Vol. 22, No. 6, pp. 522-529.

[104] Z.C. Lin, Y.Y. Lin and C.R. Liu, Effect of thermal load and mechanical load on the residual stress of a machined workpiece, International Journal of Mechanical Sciences, 1991, Vol. 33, No. 4, pp. 263-278.

[105] P.N. Moulik, H.T.Y. Yang and S. Chandrasekar, Simulation of thermal stresses due to grinding, International Journal of Mechanical Sciences, 2001, Vol. 43, pp. 831-851.

[106] K. Honda, T. Torii and Z. Fei, Residual-stress redistribution and deformation due to material removal during the formation of a full-depth hole in a plate,

Transatons of Japanese Society of Mechanical Engineering, 1989, Vol. 55, pp. 879-887.

[107] Z.C. Lin and B. Lee, Investigation of the residual stress of a machined workpiece considering tool flank wear, Journal of Materials Processing Technology, 1995, Vol. 51, pp. 1-24.

[108] X. Yang and C.R. Liu, A new stress-based model of friction behavior in machining and its significant impact on residual stresses computed by finite element method, International Journal of Mechanical Sciences, 2002, Vol. 44, pp. 703-723.

[109] C. Schmidt, P. Frank, H. Weule, J. Schmidt, Y.C. Yen and T. Altan, Tool wear prediction and verification in orthogonal cutting, 6th CIRP International Workshop on Modeling of Machining Operations, Hamilton, Canada, May 20, 2003.

[110] Y. Altintas, D. Montgomery and E. Budak, Dynamic peripheral milling of flexible structures, Transactions of the ASME: Journal of Engineering for Industry, 1992, Vol. 114, No. 2, pp. 137-145.

[111] S. Berczynski and P. Gutowshi, Identification of parameters of machine tool dynamics models, Anal., Synth. Appl. PD 64, ASME, 1994, pp. 565-576.

[112] Z. Han, J. Li and J. Qin, Identification method of the modal parameters of lathe spindle assembly, Struct. Dyn. Vib., London, PD 64, ASME, 1994, pp. 109-113.

[113] K.Z. Yen and W.C. Hsueh, Suppression of chatter vibration in inner-diameter cutting, International Journal of Japanese Society of Mechanical Engineering, 1996, Vol. 39, Series C, pp. 25-33.

[114] S. Shimada, Chapter 3: Molecular Dynamics simulation of the atomic processes in microcutting, Micromachining of Engineering Materials (Editor: J. McGeough), Marcel Dekker, Inc., New York, 2002.

[115] W.G. Hoover, C.G. Hoover, I.F. Stowers amd W.J. Slekhaus, Interface tribology via nonequilibium Molecular Dynamics simulation. Material Research Symposium, 1989. Vol. 140, 119~124.

[116] J. Belak, W. G. Hoover, C.G. Hoover, A.J.D. Groot and I.F. Stowers. Molecular Dynamics modeling applied to indentation and metal cutting problems, J. Thrust Area Reps. 1990, Vol. 89, pp. 4-8.

[117] W.G. Hoover, A.J.D. Groot, C.G. Hoover and I.F. Stowers. Large-scale elastic-plastic indentation simulation via nonequilibrium Molecular Dynamics, Phys. Rev, 1990, A42, No. 10, pp. 5844-5853.

[118] J.F. Belak and I.F. Stowers, A molecular dynamics model of the orthogonal cutting process, Proceedings of ASPE 1990 Annual Conference, Rochester, USA, 1990, pp. 259-263.

[119] J. Belak, D.B. Boercker and I.F. Stowers, Simulation of nanomerter-scale deformation of metallic and ceramic surface, MRS Bulletin. 1993, Vol. 18, No. 5, pp. 55-60.

[120] J. Belak, J.N. Glosli, D.B. Boercker and I.F. Stowers, Molecular Dynamics simulation of mechanical deformation of ultra-thin metal and ceramic films, Material Research. Society, Symposium, Proceeding, 1995, Vol. 389, pp. 181-190.

[121] R. Komanduri, N. Chandrasekaran and L.M. Raff, Effect of geometry in nanometric cutting: a Molecular Dynamics simulation approach, Wear, 1998, Vol. 118, pp. 84-97.

[122] N. Chandrasekaran, A Noori-khajavi, L.M. Raff and R. Komanduri. A new method for Molecular Dynamics simulation of nanometric cutting, Philosophy Magazine 1998, Vol. 77B, No. 1, pp. 7-13.

[123] R. Komanduri, N. Chandrasekaran and L.M. Raff, Orientation effects in nanometric cutting of single crystal materials: an MD Simulation approach, Annals of the CIRP, 1999, Vol. 48, No. 1, pp. 296-313.

[124] R. Komanduri, N. Chandrasekaran and L.M. Raff, MD simulation of exit failure in nanometric cutting, Materials Science & Engineering, 2001, Vol. 311A, pp. 1-12.

[125]R. Komanduri, N. Chandrasekaran and L.M. Raff, Molecular Dynamics simulation of atomic-scale friction. Phys. Rev. 2000, Vol. 61B, No. 20, pp. 14007-14019.

[126]R. Komanduri, N. Chandrasekaran and L.M. Raff, MD simulation of indentation and scratching of single crystal aluminum, Wear, 2000, Vol. 240, pp. 113-143.

[127]S. Shimada, Molecular Dynamics analysis of nanometric cutting process, International Journal of Japanese Society of Precision Engineering, 1995, Vol. 29, No. 4, pp. 283-286.

[128]Shimada, N. Ikawa, Molecular Dynamics analysis of nanometric cutting mechanism, Mesoscopic Dynamics of Fracture, 1998, Vol. 264, pp. 63-77.

[129] S. Simada, N. Ikawa and H. Tanaka, Structure of micromachined surface simulated by Molecular Dynamics analysis, Annals of the CIRP, 1994, Vol. 43, No. 1, pp. 51-53.

[130]S. Shimada, R. Inoue, J. Uchikoshi and N. Ikawa. Molecular Dynamics analysis on microstructure of diamond turned surface, Proceedings of the SPIE, Tokyo, Japan, 1995, pp. 315-322.

[131]N. Ikawa, S. Shimada and H. Tanaka, Minimum thickness of cutting in micromachining, Nanotechnology, 1992, Vol. 3, No. 1, pp. 6-9.

[132]S. Shimada, N. Ikawa and H. Tanaka, Feasibility study on ultimate accuracy in microcutting using Molecular Dynamics simulation, Annals of the CIRP, 1993, Vol. 42, No. 1, pp. 91-94.

[133]S. Shimada, N. Ikawa and G. Ohmori, Molecular Dynamics analysis as compared with experimental result of micromachining, Annals of the CIRP, 1992, Vol. 41, No. 1, pp. 117-120.

[134] W. G. Hoover, Canonical dynamics: equilibrium phase-space distributions, Physical Review, 1985, Vol. 31B, No. 3, pp. 1695-1697.

[135]S. Shimada, N. Ikawa and T. Inamura, Brittle-ductile transition phenomena in microindentation and micromachining, Annals of the CIRP, 1995, Vol. 44, No. 1, pp. 523-525.

[136] S. Shimada, H. Tanaka, and N. Ikawa, Atomic mechanism of surface generation in micromachining of monocrystalline silicon, Proceedings of the 1st International Euspen Conference, Bremen, 1999, pp. 230-233.

[137] T. Inamura, S. Shimada, N. Takezawa and N. Nakahara, Brittle/Ductile transition phenomena observer in computer simulations of machining defect-free monocrystalline silicon, Annals of the CRIP, 1997, Vol. 46, No. 1, pp. 31-33.

[138] H. Tanaka, M. Sano and S. Shimada, Brittle-ductile transition in nano bending of noncrystalline silicon carbide analyzed by Molecular Dynamics simulation, Proceedings of 6th International Symposium on Advances in Abrasive Technology, Bristol, UK, 18-20 December 2003, pp.1-19.

[139] R. Rentsh and I. Inasaki. Molecular Dynamics simulation for abrasive processes, Annals of the CIRP, 1994, Vol. 43, No. 1, pp. 317-220.

[140] R. Rentsch and I. Inasaki, Investigation of surface integrity by Molecular Dynamics simulation, Annals of the CIRP, 1995, Vol. 44, No. 1, pp. 295-298.

[141] R. Rentsh, Influence of crystal orientation on the nanometric cutting process, Proceedings of the 1st International Euspen conference, Bremen, 1999, pp. 250-253.

[142] J. Kim and C. Moon, A study on microcutting for the configuration of tools using Molecular Dynamics, Journal of Materials Processing Technology, 1996, Vol. 59, pp. 301-314.

[143] X. Luo, Y. Liang, S. Dong and Q. Zhao, Atomic analysis of nanometric cutting process by a new MD simulation approach including thermal effects, Proceedings of the 2nd International Euspen Topic Conference, Copenhagen, Denmark, 2000, pp. 161-168.

[144] X. Luo, Y. Liang and S. Dong, Atomic study on some problems in nanometric cutting mechanism, High Technology Letters, 2000, Vol. 6, No. 4, pp. 50-53.

[145] Y. Liang, X. Luo and S. Dong. MDS study of the effects of micro-vibrations of the diamond tool on the nanometric machined surface roughness,

Proceedings of the 3rd Euspen International Conference, Turin, Italy, 2001, Vol.1, pp. 692-695.

[146] R.K. Kang, X.G. Guo, D.M. Guo and Z.J. Jin, A study of the Molecular Dynamics simulation in nanometric grinding, Proceedings of 6th International Symposium on Advances in Abrasive Technology, Bristol, UK, 18-20 December 2003, pp. 33-38.

[147] K.J. Stout and E.J. Davis, Surface topography of cylinder bores - the relationship between manufacture, characterization and function, Wear, 1995, pp. 111-125.

[148] D.C. Montgomery, Design and Analysis of Experiment, Wiley, New York, 2004.

[149] J. Pujana, P.J. Arrazola, R. M'Saoubi, H. Chandrasekaran, Analysis of the inverse identification of constitutive equations applied in orthogonal cutting process, International Journal of Machine Tools and Manufacture, 2007, Vol. 47, pp. 2153-2161.

[150] ISO 4287: 1997 Geometrical product specifications (GPS) – surface texture: profile method - terms, definitions and surface texture parameters.

[151] ASME B46.1 - 1995 Surface texture (surface roughness, waviness, and Lay).

[152] K. Cheng, X. Liu, D. Webb and X. Luo, Prediction of cutting force distribution and its influence on dimensional accuracy in peripheral milling, International Journal of Machine Tools and Manufacture, Vol.42, 2002, pp.791-800.

[153] Y.H. Jeong, B.K. Min, Geometry prediction of EDM-drilled holes and tool electrode shapes of micro-EDM process using simulation, International Journal of Machine Tools and Manufacture, 2007, Vol. 47, pp. 1817-1826.

[154] B. Kilic, J.A.A. Cruz, S. Raman, Inspection of the cylindrical surface feature after turning using coordinate metrology, International Journal of Machine Tools and Manufacture, 2007, Vol. 47, pp. 1893-1903.

[155] P.A.R. Rosa, O. Kolednik, P.A.F. Martins, A.G. Atkins, The transient beginning to machining and the transition to steady-state cutting, International Journal of Machine Tools and Manufacture, 2007, Vol. 47, pp. 1904-1915.

[156] P. Podsiadlo and G.W. Stachowiak, Multi-scale representation of tribological surfaces, Proceedings of Institution of Mechanical Engineers, 2002, Vol. 216, Part J, pp. 463-479.

[157] L. Wang, L.C. Chan, T.C. Lee, Process modelling of controlled forming with time variant blank holder force using RSM method, International Journal of Machine Tools and Manufacture, 2007, Vol. 47, pp. 1929-1940.

[158] M. Field, J.F. Kahles and J.T. Cammett, A review of measuring methods for surface integrity, Annals of the CIRP, 1972, Vol. 21, No. 2, pp. 219-238.

[159] T.O. Ekinci, J.R.R. Mayer, Relationships between straightness and angular kinematic errors in machines, International Journal of Machine Tools and Manufacture, 2007, Vol. 47, pp. 1997-2004.

[160] X. Liu, K. Cheng, D. Webb and X. Luo, Improved dynamic cutting force model in peripheral milling - part 2: experimental verification and prediction, International Journal of Advanced Manufacturing Technology, Vol.24 No.11-12, 2004, pp. 794-805.

[161] X.C. Luo, K. Cheng, and R. Ward, The effects of machining process variables and tooling characterisation on the surface generation: modelling, simulation and application promise, International Journal of Advanced Manufacturing Technology, Vol. 25, 2005, pp.1089-1097.

[162] X. K. Luo, K. Cheng, X.C. Luo and X. W. Liu, A simulated investigation on the machining instability and dynamic surface generation, International Journal of Advanced Manufacturing Technology, Vol. 26, 2005, pp. 457-465.

[163] M. Wan, W.H. Zhang, G. Tan, G.H. Qin, An in-depth analysis of the synchronization between the measured and predicted cutting forces for developing instantaneous milling force model, International Journal of Machine Tools and Manufacture, 2007, Vol. 47, pp. 2018-2030.

[164] O.E.E.K. Omar, T. El-Wardany, E. Ng, M.A. Elbestawi An improved cutting force and surface topography prediction model in end milling, International Journal of Machine Tools and Manufacture, 2007, Vol. 47, pp.1263-1275.

[165] V. Gagnol, B.C. Bouzgarrou, P. Ray, C. Barra, Model-based chatter stability prediction for high-speed spindles, International Journal of Machine Tools and Manufacture, 2007, Vol. 47, pp. 1176-1186.

[166] T.R. Thomas, Trends in surface roughness, International Journal of Machine Tools & Manufacture, 1998, Vol. 38, No. 5-6, pp. 405-411.

[167] I.S. Kweon and T. Kanade, Extracting topographic terrain features from elevation maps, CVGIP: Image Understanding, 1994, Vol. 59, No. 2, pp. 171-182.

[168] J.C. Russ, Fractal dimension measurement of engineering surfaces, International Journal of Machine Tools & Manufacture, 1998, Vol. 38, No. 5-6, pp. 567-571.

[169] C.A. Brown, W. A. Johnsen and K.M. Hult, Scale-sensitivity, fractal analysis and simulations, International Journal of Machine tools & Manufacture, 1998, Vol. 38, No. 5-6, pp. 633-637.

[170] X. Luo, K. Cheng, D.C. Webb and F. Wardle Design of ultraprecision machine tools with application to manufacturing of miniature and micro components, Journal of Materials Processing Technology, Vol.167, No.2-3, 2005, pp.515-528.

[171] K.M. Li, S.Y. Liang Modeling of cutting forces in near dry machining under tool wear effect, International Journal of Machine Tools and Manufacture, 2007, Vol. 47, pp. 1292-1301.

[172] M. Weck, et al., Limits of workpiece accuracy caused by geometrical and dynamic behavior of ultra precision diamond turning machines, Proceedings of UPT Conference, May 1988, pp. 153-169.

[173] H.K. Chang, J.H Kim, I.H. Kim, D.Y. Jang, D.C. Han, In-process surface roughness prediction using displacement signals from spindle motion,

International Journal of Machine Tools and Manufacture, 2007, Vol. 47, pp.1021-1026.

[174] R. Salami, M.H. Sadeghi, B. Motakef, Feed rate optimization for 3-axis ball-end milling of sculptured surfaces, International Journal of Machine Tools and Manufacture, 2007, Vol. 47, pp. 760-767.

[175] S.M. Son, H.S. Lim, J.H. Ahn, The effect of vibration cutting on minimum cutting thickness, International Journal of Machine Tools and Manufacture, 2007, Vol. 46, pp. 2066-2072.

[176] A. Simoneau, E. Ng, M.A. Elbestawi, Modeling the effects of microstructure in metal cutting, International Journal of Machine Tools and Manufacture, 2007, Vol. 47, pp. 368-375.

[177] J. Corbett, P. A. Mckeown, G. N. Peggs and R. Whatmore, Nanotechnology: international developments and emerging products, Annals of the CIRP, 2001, Vol. 49, pp. 1-23.

[178] Natural Science Foundation in the USA, 2001, Nanomanufacturing program information (http://www.eng.nsf.gov/dmii/DMIIDivdescription.doc).

[179] D. C. Papaport, The Art of Molecular Dynamics Simulation, Cambridge University Press, Cambridge, 1995.

[180] M. I. Baskes, Modified embedded-atom potentials for cubic materials and impurities, Physical Review, 1992, Vol. 46B, No. 5, pp. 2727-2741.

[181] Q. L. Zhao, D. Stephenson, J. Corbett, J. Hedge, J. H. Wang and Y. C. Liang, Single grit diamond turning of spectrosil 2000 glass on Tetraform 'C', Proceedings of 6th International Symposium on Advances in Abrasive Technology, Bristol, UK, 18-20 November 2003, pp. 107–112.

[182] L. G. D. Petrucci, Machine Tool Metrology, L&A Press, Birmingham, 1986.

[183] X. Zhao and B. Bhushan, Material removal mechanisms of single-crystal silicon on nanoscale and at ultralow loads, 1998, Wear, Vol. 223, pp. 66-78.

[184] Q. Zhao and S. Dong, Investigation of single asperity microcutting using an Atomic Force Microscope. Proceedings of the 3rd Euspen International Conference, 2001, Turin, Italy, pp. 632-635.

[185] I. Coudhury and M. El-Baradie, Machinability assessment of inconel 718 by factorial design of experiment coupled with response surface methodology. Journal Material Proceeding Technology, 1999, 95, 30–39.

[186] L. Ozler and A. Ozel, Theoretical and experimental determination of tool life in hot machining of austenitic manganese steel. International Journal Machine Tool Manufacturing, 2001, 41, 163–172.

[187] W. Chien and C. Chou, The predictive model for machinability of 304 stainless steel. Journal Material Proceeding Technology, 2001, 118, 441–447.

[188] C. Feng and X. Wang, Digitising uncertainty modeling for reverse engineering applications: regression vs. neural networks. International Journal Machine Tool Manufacturing, 2002, 13, 189–199.

[189] N. Tosum and L. Ozler, A study of tool life in hot machining using artificial neural networks and regression analysis method. Journal Material Proceeding Technology, 2002, 124, 99–104.

[190] S. Wong and A. Hamouda, Machinability data representation with artificial neural network. Material Proceeding Technology, 2003, 138, 538–544.

[191] B. Lambert and A. Walvekar, Optimisation of multipass machining operations. International Journal Production Research, 1978, 16, 259–265.

[192] D. Ermer and S. Kromodihardjo, Optimisation of multipass turning with constraints. Trans. ASME Journal Engineering Industry, 1981, 10, 462–468.

[193] I. Yellowey and E.Gunn, The optimal subdivision of cut in multipass machining operations. International Journal Production Research, 1989, 27, 1573–1579.

[194] B. Gopalakrishan and F. Al-Khayyal, Machine parameter selection for turning with constraints: an analytical approach based on geometric programming. International Journal Production Research, 1991, 29, 1897–1908.

[195] Y. Shin and Y. Joo, Optimisation of machining conditions with practical constraints. International Journal Production Research, 1992, 30, 2907–2919.

[196] R. Gupta, J. Batra and G. Lal, Determination of optimal subdivisions of depth of cut in multipass turning with constraints. International Journal Production Research, 1995, 33, 2555–2565.

[197] H. Lee, B. Yang and K. Moon, , An economic machining process model using fuzzy nonlinear programming and neural network. International Journal Production Research, 1999, 37, 835–847.

[198] A.M.A. Al-Ahmari, Mathematical model for determining machining parameters in multipass turning operations with constraints. International Journal Production Research, 2001, 39, 3367–3376.

[199] D. Coit, B. Jackson, and Smith, A., Static neural network process models: considerations and case studies. International Journal Production Research, 1998, 36, 2953–2967.

[200] D.E. Rumelhart, G.E. Hinton, and R.J. Williams, Learning internal representation by error propagation. In Parallel Data Processing, edited by D. Rumelhart and J. McClelland,1986 (MIT Press: Cambridge, MA).

[201] P.J. Werbos, Backpropagation through time: what it does and how to do it. Proceeding IEEE, 1990, 78, 1550–1560.

[202] B. Widrow, and M.A. Lehr, 30 years of adaptive neural networks: perceptron, madaline, and backpropagation. Proceeding. IEEE, 1990, 78, 1415–1444.

Appendices

Appendix 1 Specifications of Zygo NewView 5000 3D surface profiler

INDUSTRIAL

ZYGO CORPORATION'S

NewView 5000™

Precise, Rapid, Noncontact 3D Surface Profiling

At ZYGO, we continue to extend the capabilities of our products and technology to provide customer-focused solutions for many surface metrology applications and fields of interest, including:

- Precision machining and automotive engineering
- Micromachining and sensor devices
- Data storage and display technologies
- Semiconductor and microelectronics
- Biomedical engineering and surgical appliances
- Materials research and fabrication (optics, ceramics, paper, plastics, polymers, etc.)

Product highlights include:

- Noncontact technology
- Rapid measurement and data analysis
- High accuracy and repeatability
- Large dynamic vertical (Z) scan range – from nanometers to millimeters
- High resolution scanning with sub-nanometer vertical resolution
- Wide area measurement range – from microns to 100 mm
- Comprehensive and flexible software analysis package with automation modules for optimal process control

NewView 5000 is the most advanced 3D surface profiler available today. Surface metrology is critical to process control in many facets of research and manufacturing; from semiconductors and disk drives, to medical implants and fuel injector seals, surface texture controls the performance of the product. Until now, microscopes imaged surface details while surface profilers provided accurate measurements to characterize the details. By combining these two critical technologies, the NewView 5000 provides fast, quantitative, surface texture measurement and analyses on many types of surfaces, in just seconds. Simply focus and measure.

The NewView 5000 characterizes and quantifies surface roughness, step heights, critical dimensions, and other topographical features with excellent precision and accuracy. All measurements are nondestructive, fast, and require no sample preparation. Profile heights ranging from <1 nm up to 5000 µm at vertical scan speeds up to 10 µm/s with ≥0.1 nm height resolution, independent of magnification and feature height! A continuously variable image zoom, with six indexed positions, is standard on all systems, providing you with enhanced 3D profiling capabilities. Also, ZYGO's full range of imaging objectives can be mounted onto 5-position manual or motorized turrets, or used individually with quick-mount adapters.

zygo

In today's highly competitive manufacturing arena...

...monitoring critical component parameters and controlling the fabrication process are paramount. Even small percentage differences in yields can be the determining factor between success and failure. Development and manufacturing of next-generation devices depends on a series of complex processes preformed under exacting controls to create sophisticated devices. Precise 3D metrology plays a key role in characterizing and controlling critical machining and fabrication and processes.

The NewView 5000 family of 3D Optical Profilers provides noncontact, rapid, quantitative surface measurements. Integral to each system is powerful data analysis software and automation modules, satisfying the most demanding R&D and production requirements.

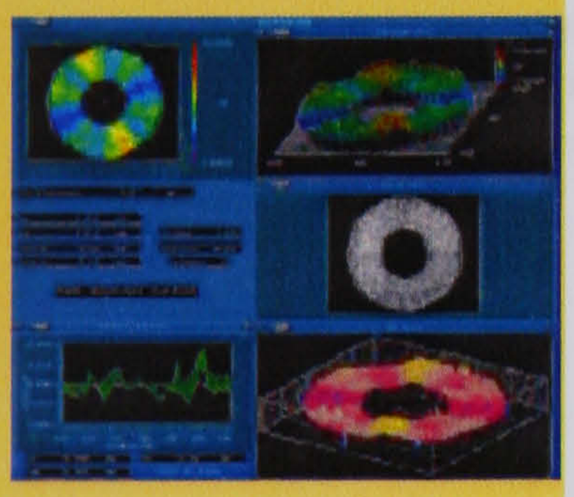

The NewView 5000 can resolve submicron x-y features, and profile areas up to 50 x 50 mm and larger using its unique image stitching capabilities. Get all the field size and resolution you need, when you need it. Now, range and resolution are no longer a trade-off.

The NewView 5000 uses noncontact scanning white light interferometry to acquire ultrahigh Z-resolution images. ZYGO's patented frequency domain analysis and proprietary scanning technique provides 0.1 nm vertical resolution – in a single measurement! A closed-loop piezo-based scanner, employing low-noise capacitive sensors, ensures accurate and repeatable linear motion over the full range.

The NewView 5000 provides highly-stable metrology; its unique platform design includes an ultra-rigid support structure, reduced-footprint dynamically stabilized vibration isolation table, and a fully integrated ergonomic workstation. The result? Precise, repeatable, measurements with unparalleled speed and accuracy – in most any environment.

As always, ZYGO certifies gage capability by extensive testing, and guarantees performance of every unit shipped, and system accuracy can be easily verified at any time using the provided NIST-traceable standards. The sum total? The confidence that your numbers mean what they say.

The diverse applications highlighted illustrate the wide performance and application spectrum of the NewView 5000 product family. By characterizing a wide range of surface parameters and identifying many aspects of the manufacturing process, the NewView gives you the insight you need to improve and control the quality of your parts and increase your production yields.

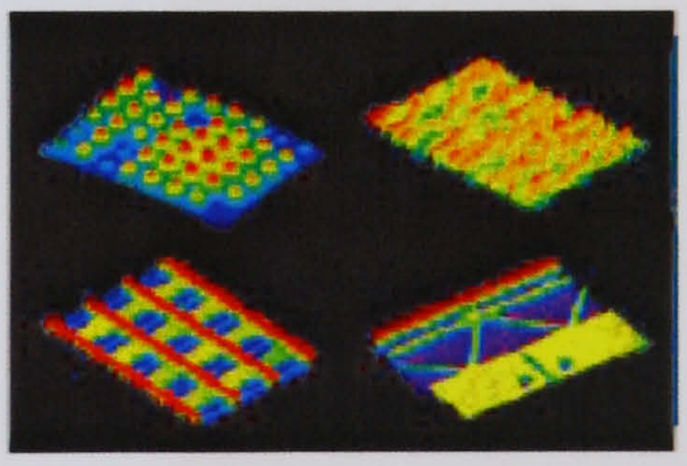

The NewView 5000 includes ZYGO's advanced and comprehensive MetroPro™ metrology software running under Windows NT® and interfaced to the latest generation Pentium® based PC. MetroPro is standard and provides full system control capabilities and quantitative surface metrology analysis on hundreds of reportable parameters such as roughness, step heights, power spectra, bearing ratio, and many more. MetroPro's intuitive and graphical user interface makes it easy to learn and use. Real time, on-screen, SPC and user-definable pass/fail flagged results are easily displayed and logged, eliminating operator subjectivity. You can use any of the standard measurement applications built into MetroPro, or easily create customized applications to handle your measurement needs with maximum efficiency. All applications can be password protected to prevent accidental changes to measurement or processing setups. This functionality, under Windows NT, allows easy handling of data files and all networking requirements.

Productivity is enhanced with a number of standard and optional automation modules. The NewView 5000 is well-suited for production environments by providing full automation, thereby eliminating operator variability and increasing throughput and yields. The motorized 5-position objective turret under programmable software control, with position sensing, eliminates operator error. Programmable stages for precise and automated sample positioning allows for repetitive control of measurements to meet high production throughput requirements. Standard and custom sample fixturing is available to provide easy and repetitive sample loading. Integrated autofocus makes sample focusing easy and automatic.

The NewView 5000 provides accurate, quantitative characterization of:

- **Surface roughness**
- **Shape**
- **Step-height**
- **Critical dimensions**
- **Angle**
- **Volume ...and more.**

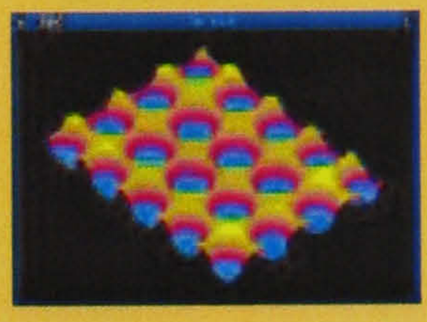

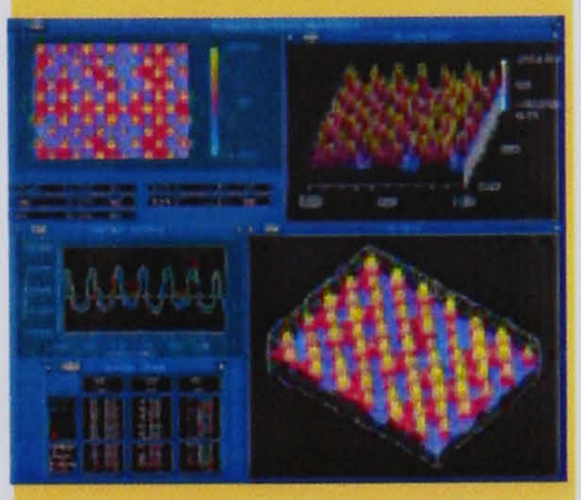

ZYGO's leading-edge metrology solutions provide you with the competitive edge you need. Contact us today to discuss your requirements and discover new solutions to your most critical metrology challenges.

NewView 5000 ™ General Specifications:

Technical Performance

Vertical (Z) Scan Range:	≤ 5 mm
Vertical (Z) Scan Rate:	≤ 10 µm/sec
Vertical (Z) Resolution:	≥ 0.1 nm
Lateral (X, Y) Resolution Range:	0.45 – 11.8 µm
Field of View Range:	0.04 – 17.5 mm; larger areas can be imaged with field stitching capability
Step Height Accuracy:	≤ 0.75% (Model 5032)
Step Height Repeatability:	≤ 0.1% (Model 5032)

System

Standard Platforms:	Models 5010, 5022, 5032; each platform is modular and upgradeable
Image Zoom:	Standard; variable with six indexed positions: 0.4X, 0.5X, 0.8X, 1.0X, 1.3X, and 2X
Imaging Objectives:	Standard: 1X, 2.5X, 5X, 10X, 20X, 50X, and 100X Super Long Working Distance: 2X, 5X, and 10X
Objective Mounting:	Single quick-mount adapter, manual, or automated 5-position indexing turret
Sample Positioning:	Manual or automated stages available
Computer:	Latest generation Dell Optiplex PC with R/W CD-ROM, floppy drive, and 19-inch color monitor; optional printers available
Software:	Zygo MetroPro™ comprehensive metrology package with advanced graphical display, data analysis, and scripting capabilities

SB-0323 4/01 2M

Zygo TeraOptix
Westborough, MA USA

Zygo TeraAutomation
Delray, FL USA

Zygo Automation
Longmont, CO USA

Zygo Western Regional
Sunnyvale CA USA

Zygo Central Region
Northbrook, IL USA

ZygoLOT
Germany

Zygo KK
Japan

Zygo Asia
Singapore

Discover the power of 3D surface metrology and get a *New View* of your parts. See for yourself why leading manufacturers worldwide have taken a *New View* of their processes and benefited from ZYGO's metrology and yield improvement solutions. Contact us today to arrange for a demonstration.

zygo

ZYGO CORPORATION
LAUREL BROOK ROAD
MIDDLEFIELD, CT 06455
VOICE: 860 347-8506
FAX: 860 346-4188

WWW.ZYGO.COM
EMAIL: inquire@zygo.com

NewView™ 5000 Specifications

Models

5010	Base model with high resolution camera and open loop transducer
5022	Model 5010 plus turret compatible and closed loop transducer
5032	Model 5022 plus high speed camera

System

Measurement Technique	Non-contact, three-dimensional, scanning white light and optical phase-shifting interferometry
Objectives	Infinite conjugate interferometric objectives; 1X, 2X, 2.5X, 5X, 10X, 20X, 50X, 100X
Image Zoom	Standard; continuous variable zoom with six indexed positions: 0.4, 0.5, 0.8, 1.0, 1.3, 2.0; repeatable to 0.2%
Field of View	From 0.04 to 17.5 millimeters; larger area imaged with field stitching; objective dependent; see Objective Specifications
Part Viewing	Standard; 9-inch b&w monitor
Focus	Standard; motorized manual and auto focus
Illuminator	Filtered white light with selectable coherence, long-life tungsten halogen lamp
Measurement Array	Standard, selectable, include: 640x480, 320x240, 160x120
Sample Stages	Manual and motorized versions available; see Options
Computer	Late-generation Dell PC configured with hard drive, 500 MB RAM, CD-R/W, floppy drive, and 17-inch flat panel monitor; printers optional
Software	Zygo MetroPro software running under Microsoft Windows 2000

Physical

Dimensions (H x W x D)	System: 62 x 52 x 35 in. (157 x 132 x 89 cm) NewView 5000: 32 x 23 x 16 in. (81 x 58 x 41 cm) Vibration Isolation Table: 30 x 24 x 24 in. (76 x 61 x 61 cm) Workstation: 33.5 x 52 x 35 in. (85 x 132 x 89 cm)
Weight	System: ≈ 950 lb (430 kg) NewView 5000: ≈ 200 lb (90 kg) Vibration Isolation Table: ≈ 600 lb (272 kg)

Performance

Scanner	Model 5010: Open-loop piezo-based transducer Models 5022 and 5032: Closed-loop piezo-based, with highly linear capacitive sensors
Vertical Scan Range	Model 5010: 100 µm (3937 µin) Models 5022 and 5032: 150 µm (5906 µin) Optional up to 5 mm (0.20 in.)
Vertical Resolution	Up to 0.1 nm (0.004 µin)
Lateral Resolution	0.45 to 11.8 µm; objective dependent
Data Scan Rate	Models 5010 and 5022: up to 4.9 µm/sec Model 5032: up to 10.5 µm/sec; rate depends upon sampling array
Maximum Data Points	307,200; dependent upon sampling array
Step Height Accuracy	Model 5010: ≤ 3.0% Models 5022 and 5032: ≤ 0.75%
Step Height Repeatability	Model 5010: ≤ 1.5% @ 1σ Model 5022: ≤ 0.5% @ 1σ Model 5032: ≤ 0.1% @ 1σ

Utility Requirements

Input Voltage	100 to 240 VAC, 50/60 Hz
Power Consumption	≤ 280 watts (manual stages), ≤ 400 watts (motorized stages)
Compressed Air	60 to 80 psi (4.1 to 5.5 bar); 1/4 in. input; dry and filtered source (1% humidity, 5 µm particulate filter)

Environmental Requirements

Temperature	15 to 30°C (59 to 86°F)
Rate of Temp. Change	<1.0°C per 15 min
Humidity	5 to 95% relative, noncondensing
Vibration Isolation	Required for vibration frequencies in the range of 1 Hz to 120 Hz

zygo®

Zygo Corporation
Laurel Brook Road
Middlefield, CT 06455

Phone: 860-347-8506
Email: inquire@zygo.com
Website: www.zygo.com

86-0001 01/03

NewView™ 5000 Specifications

Options	
Stages	Manual Tip/Tilt/X/Y with ±6° tip/tilt, ±2 in. x/y, 230° rotation Motorized Tip/Tilt/X/Y with ±4° tip/tilt, ±3 in. x/y Motorized Tip/Tilt/Y/Theta with ±4° tip/tilt , y/theta with 3 in. y travel and 360° rotation
Objectives	Standard: 1X, 2.5X, 5X, 10X, 20X, 50X, 100X; LWD versions: 2X, 5X, 10X
Turrets	Model 5010: Single objective dovetail mounting Models 5022 and 5032: Manual or Motorized 5-position turret
Vibration Isolation	Vibration Isolation System recommended
Filters Sets	Standard, Rough surface, and Combination filter sets
Standards	NIST traceable step height standards; lateral calibration standards; precision reference flat

Test Part Characteristics	
Material	Various; opaque and transparent surface; coated and uncoated; specular and nonspecular
Preparation	None (typically); measurements are noncontact and nondestructive and performed under ambient conditions
Maximum Size (H x W x D)	3.5 x 8 x 8 in. (89 x 203 x 203 mm); larger sample sizes accommodated with special configurations
Reflectivity	1 – 100%
Roughness	Model 5010: ≤ 100 µm Rp standard Model 5022 and 5032: ≤ 150 µm Rp standard; Slope dependent; see Objectives

Nominal Objective Specifications at 1X*

Power	1X	2X LWD	2.5X	5X	5X LWD	10X	10X LWD	20X	50X	100X
Sys Mag	20X	40X	50X	100X	100X	200X	200X	400X	1000X	2000X
NA	0.030	0.055	0.075	0.130	0.140	0.300	0.280	0.400	0.550	0.800
Working Dist (mm)	8.5	20.5	10.3	9.3	20.5	7.4	18.8	4.7	3.4	0.55
Focus Depth (µm)	±322.5	±95.0	±51.6	±17.2	±14.8	±3.2	±3.7	±1.8	±1.0	±0.5
Inter Depth (µm)	4.0	4.0	4.0	4.0	4.0	4.0	4.0	3.6	2.0	1.0
Lateral Res (µm)	11.8	6.43	4.72	2.72	2.53	1.18	1.26	0.88	0.64	0.45
Field of View H x V (mm)	7.00 x 5.30	3.52 x 2.64	2.82 x 2.11	1.41 x 1.06	1.41 x 1.06	0.70 x 0.53	0.70 x 0.53	0.35 x 0.26	0.14 x 0.11	0.070 x 0.053
Spatial Samp 320 x 240 (µm)	22.00	11.0	8.80	4.40	4.40	2.20	2.20	1.10	0.44	0.22
Spatial Samp 640 x 480 (µm)	11.00	5.50	4.40	2.20	2.20	1.10	1.10	0.55	0.22	0.11
Max Slope (degrees)	1.41	2.58	3.52	6.08	6.55	13.82	12.93	18.15	24.27	33.25

Nominal Objective Specifications at Other Zoom Settings

The NA, Working Distance, Focus Depth, Inter Depth, and Lateral Res specifications are the same at all zoom settings. Use the multipliers in the table below for Sys Mag, Field of View, and Spatial Samp specifications; multiply the value in the above chart times the multiplier.

Zoom Setting	*0.4*	*0.5*	*0.8*	*1.0*	*1.3*	*2.0*
Multiplier for Sys Mag	0.4	0.5	0.8	1.0	1.3	2.0
Multiplier for Field of View and Spatial Samp	2.5	2.0	1.25	1.0	0.77	0.5

***Objective Terminology**

Power	Magnifying power of the objective. LWD indicates Long Working Distance.
Sys Mag	System magnification, the enlargement of the surface as viewed on the video monitor.
NA	Numerical aperture, a number representing the resolving power of the objective.
Working Distance	The distance from the end of the objective to the test surface when focused.
Focus Depth	Vertical distance within which any specimen detail will simultaneously be in focus. The coherence bandwidth is centered within the focus depth.
Inter Depth	Interference depth, vertical distance over which interference can occur.
Lateral Res	Lateral resolution, optical resolution of the imaging system.
Field of View	The size of area imaged and measured.
Spatial Samp	Spatial sampling, the apparent pixel size at each magnification; varies based on Camera Res.
Max Slope	Maximum practical angle of surface feature from one pixel to the next that can be measured; will vary based on part and measurement attributes.

zygo®

Zygo Corporation
Laurel Brook Road
Middlefield, CT 06455

Phone: 860-347-8506
Email: inquire@zygo.com
Website: www.zygo.com

SS-0001 01/03

Appendix 2 Zygo Metropro Surface texture parameters

zygo®

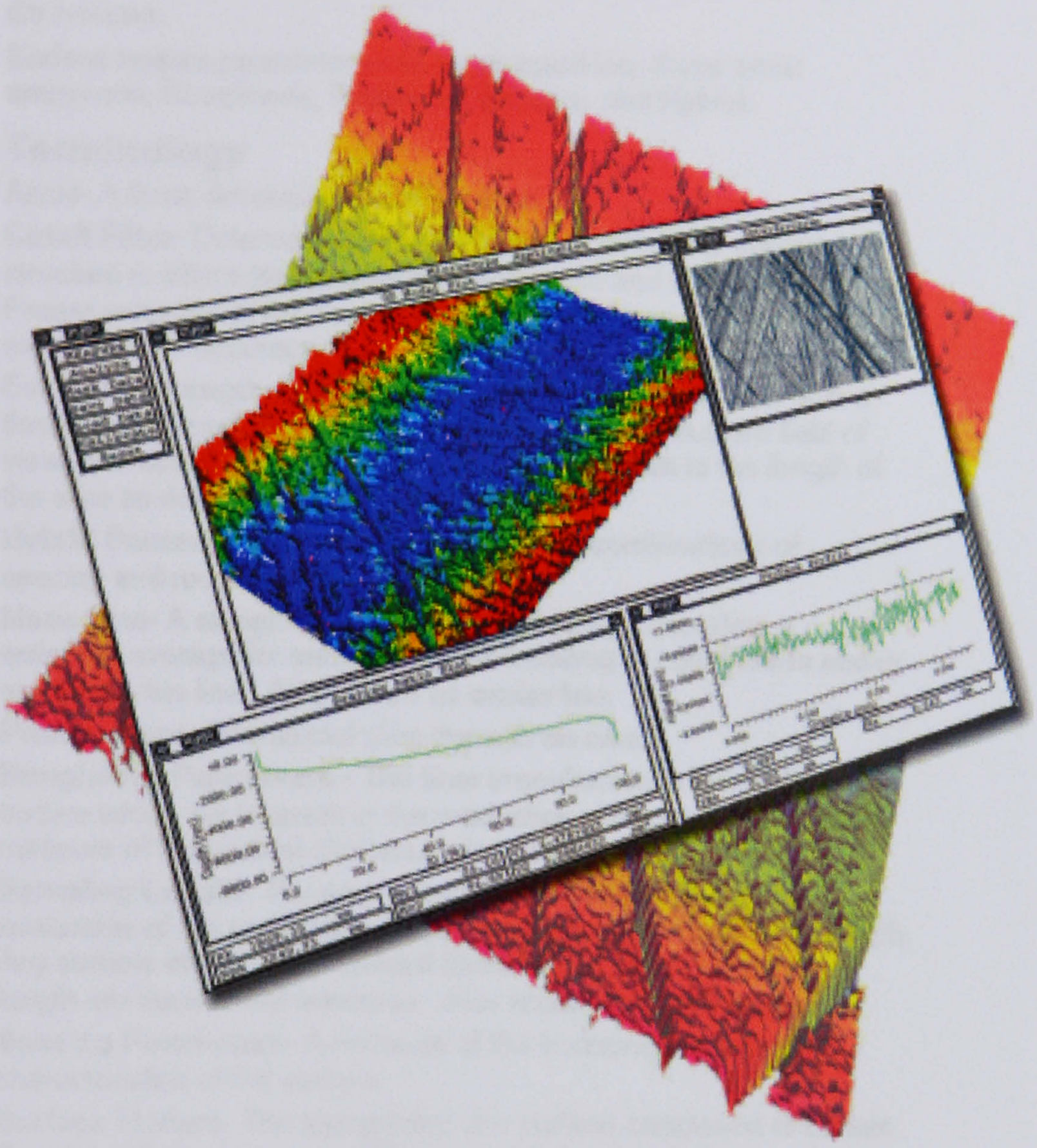

MetroPro™ Surface Texture Parameters

Understanding Surface Texture Parameters

Every part's surface is made up of texture and roughness which varies due to manufacturing techniques and the part structure itself. To understand a component's surface and to control the manufacturing process to the degree required in today's modern world, it is necessary to quantify the surface in both two and three dimensions.

Surface texture parameters can be grouped into these basic categories: Roughness, Waviness, Spacing, and Hybrid.

Terminology

Areal- A three dimensional surface area.

Cutoff Filter- Determines the wavelength at which the surface structure is differentiated between roughness and waviness data. Proper selection of the correct filter cutoff in software is critical to measurement accuracy.

Evaluation Length- The area from which data is obtained. It is a three dimensional area that corresponds to the instrument field of view, or a two dimensional profile that corresponds to the length of the slice as defined in the filled plot.

Hybrid Parameters- These parameters are combinations of spacing and roughness parameters.

Mean Line- A straight line that is generated by calculating a weighted average for each data point resulting in equal areas above and below the line. Also known as center line.

Profile- A two dimensional slice through an area.

Roughness Parameters - The finer irregularities in the surface texture which are inherent in the production process. These are a measure of the vertical characteristics of the surface.

Sampling Length- The area selected for assessment and evaluation of the roughness parameter having the cutoff wavelength. Any surface irregularities spaced farther apart than the sampling length are considered waviness. Also known as cutoff length.

Spacing Parameters- A measure of the horizontal or lateral characteristics of the surface.

Surface Texture- The topography of a surface composed of certain deviations that are typical of the real surface. It includes roughness and waviness.

Waviness Parameters - A larger component of surface texture upon which roughness is superimposed.

When two parameter names are shown, the name in parentheses is the name used in ZYGO software.

Contents

Roughness Parameters

H	Swedish height. The roughness between two predefined reference lines. The upper line exposes 5% of the data, and the lower line exposes 90%. H is less sensitive to data spikes than Rt. Available for profile and areal data.

ISO Flatness	Areal flatness deviation. The measure of surface deviation from perfectly flat. It is the distance between two parallel planes obtained by applying a Chebychev fit to the surface data. The Chebychev fit is a mathematical technique that effectively uses two parallel planes to "squeeze" the surface data points from both inside and outside, adjusting the angle to minimize the distance between the planes.

Pt ISO	Total peak-to-valley profile height. The distance between the highest peak and the deepest valley over the entire evaluation length. The profile data has form removed but is unfiltered.

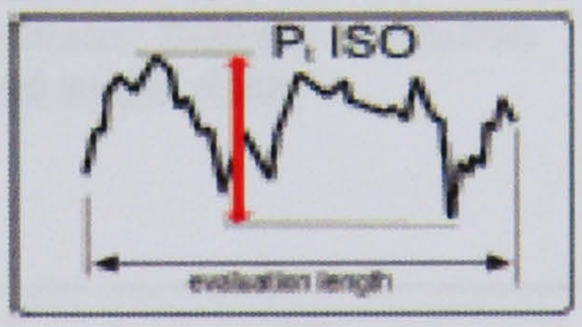

R_{3z}	Base roughness depth. The distance between the third highest peak and the third lowest valley. A peak is a portion of the surface above the mean line and between center line crossings. Available for profile and areal data.

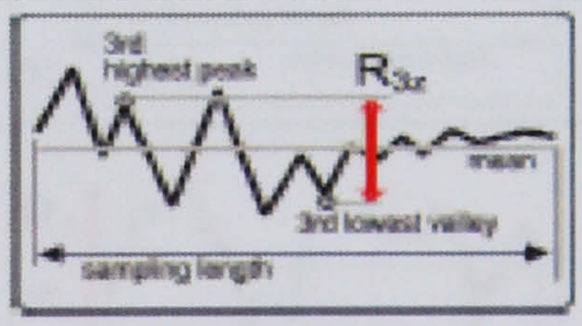

Roughness Parameters

R_{3z} ISO	Base roughness profile depth. The height of the 3rd highest peak from the 3rd lowest valley per sampling length. The base roughness depth is found in five sampling lengths and then averaged.

R_a	Arithmetical mean deviation. The average roughness or deviation of all points from a plane fit to the test part surface. Available for profile and areal data.

$$R_a = \frac{1}{L}\int_0^L |z(x)|dx$$

R_{ku}	Kurtosis is a measure of the randomness of heights, and of the sharpness of a surface. A perfectly random surface has a value of 3; the farther the result is from 3, the less random and more repetitive the surface is. Surfaces with spikes are higher values; bumpy surfaces are lower. Available for profile and areal data.

$$R_{ku} = \frac{1}{n(R_q)^4}\sum_{i=1}^{i=n}(Y_i)^4$$

R_{max} ISO	Maximum peak-to-valley profile height. The greatest peak-to-valley distance within any one sampling length.

R_p (Peak)	Highest peak. The maximum distance between the mean line and the highest point within the sample. It is the maximum data point height above the mean line through the entire data set. Available for profile and areal data.

Roughness Parameters

R_{pm} ISO	Mean peak profile height. The mean peak height based on one peak per sampling length. The single highest peak is found in five sampling lengths and then averaged. 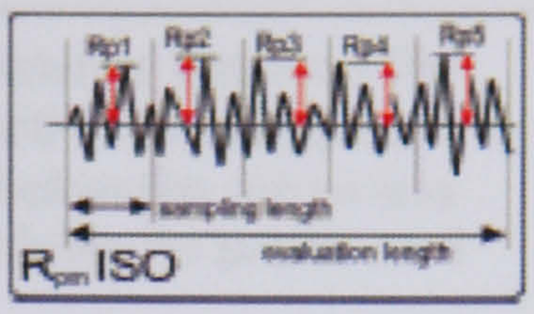
R_q (rms)	Root-mean-square (rms) roughness. The average of the measured height deviations taken within the evaluation length or area and measured from the mean linear surface. Available for profile and areal data. Rq is the rms parameter corresponding to Ra. $R_q = \sqrt{\frac{1}{L}\int_0^L z^2(x)\,dx}$
R_t (PV)	Maximum peak-to-valley height. The absolute value between the highest and lowest peaks. Available for profile and areal data. $R_t = R_p + R_v$
R_{tm}	Mean peak-to-valley roughness. It is determined by the difference between the highest peak and the lowest valley within multiple samples in the evaluation area. For profile data it is based on five sample lengths. Available for profile and areal data. $R_{tm} = \frac{Z1 + Z2 \ldots + Zn}{n}$ 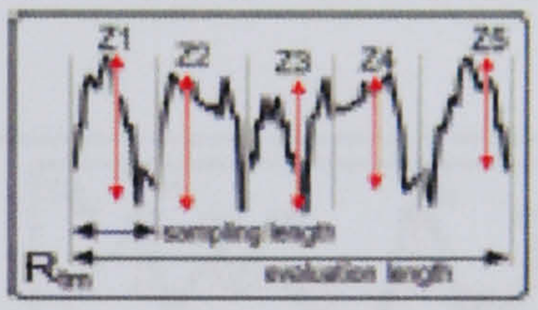
R_{tm} ISO	Mean peak-to-valley profile roughness. The mean peak-to-valley roughness based on one peak and one valley per sampling length. The single largest deviation is found in five sampling lengths and then averaged. $R_{tm}\ ISO = \frac{Rt1 + Rt2 \ldots + Rt5}{5}$ 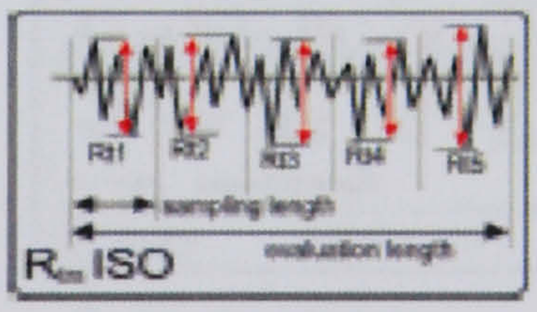

Roughness Parameters

R_v (Valley)	Lowest valley. The maximum distance between the mean line and the lowest point within the sample. It is the maximum data point height below the mean line through the entire data set. Available for profile and areal data. See Rp.
R_{vm} ISO	Mean valley profile depth. The mean valley depth based on one peak per sampling length. The single deepest valley is found in five sampling lengths and then averaged. 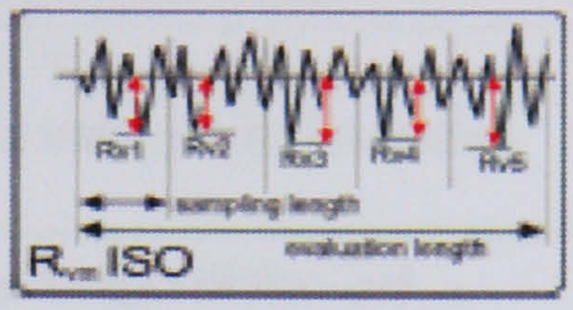
R_y (R_{max})	Maximum peak-to-valley roughness. The vertical distance between the top of the highest peak and the bottom of the deepest valley within the sampling length. It is the maximum of all the peak-to-valley values. 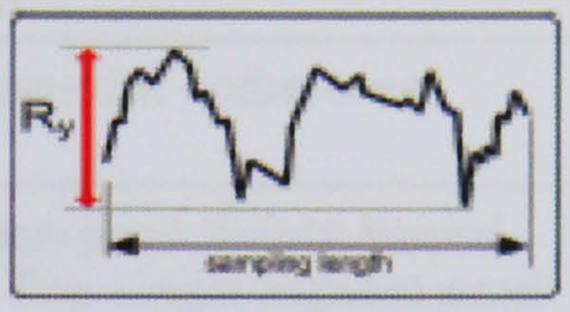
R_z	Ten-point height. The average absolute value of the five highest peaks and the five lowest valleys over the evaluation length. Available for profile and areal data. $R_z = \frac{(P1 + P2 \ldots P5) - (V1 + V2 \ldots V5)}{5}$ 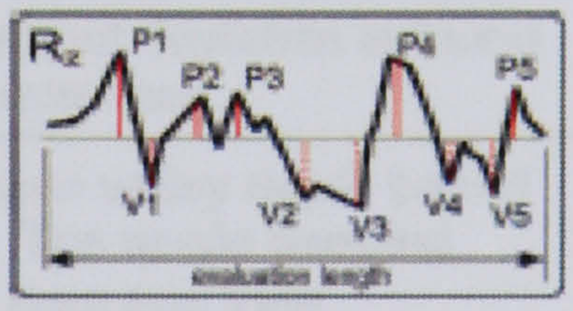
R_z ISO	Average peak-to-valley profile roughness. The average peak-to-valley roughness based on one peak and one valley per sampling length. The single largest deviation is found in five sampling lengths and then averaged. Identical to Rtm ISO. 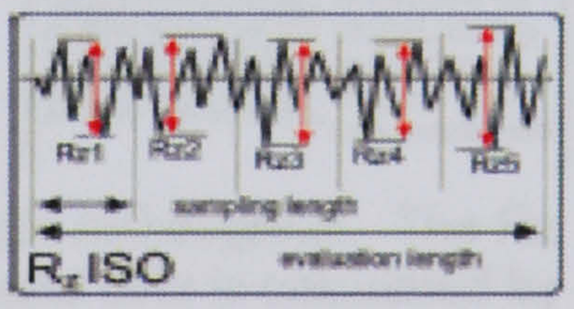

Roughness Parameters

For S_ ISO parameters, a surface area is analyzed by fitting a minimum enclosing rectangle and applying a 5 x 5 sampling grid, for a total of 25 sampling areas. All sampling areas together make up the evaluation area.

SP_t ISO	Total peak-to-valley areal height. The distance between the highest peak and the deepest valley over the entire evaluation area.
SR_{3z} ISO	Base roughness areal depth. The height of the 3rd highest peak from the 3rd lowest valley per sampling area. The base roughness depth is found in each sampling area and then averaged.
SR_{max} ISO	Maximum peak-to-valley height over the entire areal evaluation area.
SR_{pm} ISO	Mean peak areal height. The mean peak height based on one peak per sampling area. The single highest peak is found in each sampling area and then averaged.
SR_{tm} ISO	Mean peak-to-valley areal roughness. The mean peak-to-valley roughness based on one peak and one valley per sampling area. The single largest deviation is found in each sampling area and then averaged.
SR_{vm} ISO	Mean valley areal depth. The mean valley depth based on one peak per sampling area. The single deepest valley is found in each sampling area and then averaged.
SR_z	Average radial peak-to-valley areal roughness. The average of the largest half of many individual Rz results determined by slicing the areal data array about its center through 360 degrees. The Rz results are sorted by magnitude and SRz is calculated by averaging the largest 50% of the Rz values. A line-generation algorithm is used to determine the actual pixel-to-pixel path of each slice; there is no interpolation between pixels. SRz covers the entire array, and due to its radial generation it is lay independent. 

Roughness Parameters

SR_z ISO	Average peak-to-valley areal roughness. The average peak to valley roughness based on one peak and one valley per sampling area. The single largest deviation is found in each sampling area and then averaged.
SR_zX	The average of many individual Rz results, determined by slicing the data array in the x-axis. The individual Rz results are each based on a profile slice one pixel wide. SRzX is based on the entire array. See SRz.
SR_zY	The average of many individual Rz results, determined by slicing the data array in the y-axis. The individual Rz results are each based on a profile slice one pixel wide. SRzY is based on the entire array. See SRz.

Waviness Parameters

W_a	The arithmetic average roughness, or average deviation, of all points from a plane fit to the waviness data. $W_a = \frac{1}{L}\int_0^L \lvert z(x)\rvert dx$ 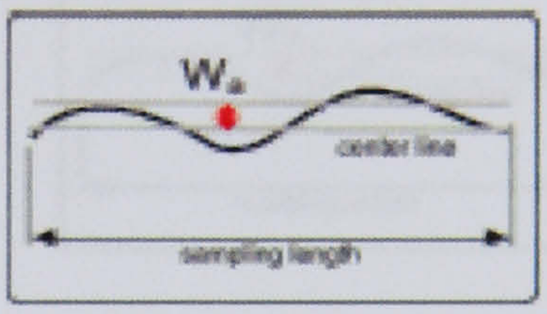
W_q	The root-mean-square (rms) roughness of all points from a plane fit to the waviness data. $W_q = \sqrt{\frac{1}{L}\int_0^L z^2(x)\,dx}$
W_y (W_{max})	The maximum height of the waviness data. 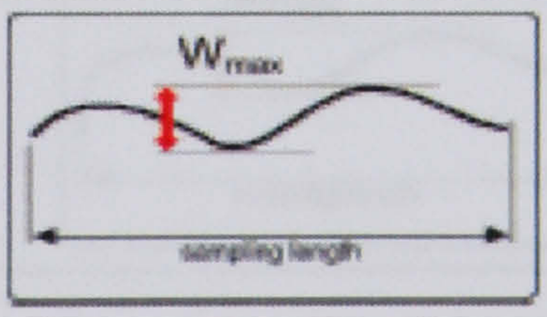

Roughness Parameters

SR_z ISO	Average peak-to-valley areal roughness. The average peak to valley roughness based on one peak and one valley per sampling area. The single largest deviation is found in each sampling area and then averaged.
SR_zX	The average of many individual Rz results, determined by slicing the data array in the x-axis. The individual Rz results are each based on a profile slice one pixel wide. SRzX is based on the entire array. See SRz.
SR_zY	The average of many individual Rz results, determined by slicing the data array in the y-axis. The individual Rz results are each based on a profile slice one pixel wide. SRzY is based on the entire array. See SRz.

Waviness Parameters

W_a	The arithmetic average roughness, or average deviation, of all points from a plane fit to the waviness data. $W_a = \frac{1}{L}\int_0^L \lvert z(x)\rvert dx$ 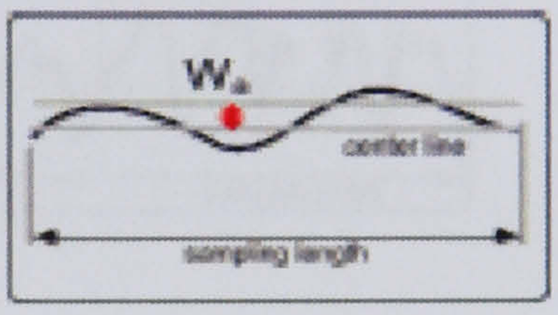
W_q	The root-mean-square (rms) roughness of all points from a plane fit to the waviness data. $W_q = \sqrt{\frac{1}{L}\int_0^L z^2(x)\,dx}$
W_y (W_{max})	The maximum height of the waviness data. 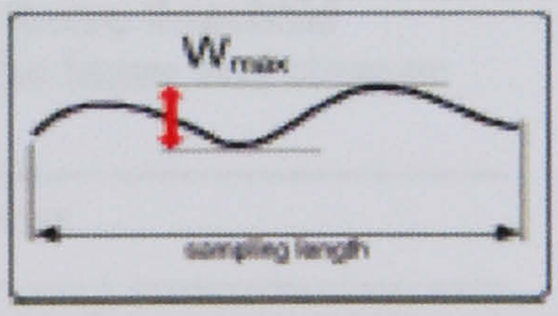

Spacing Parameters

P_c (Peaks)	Peak count or the number of peaks included in the analysis. A peak is defined as a data point whose height is above a software selected bandwidth. 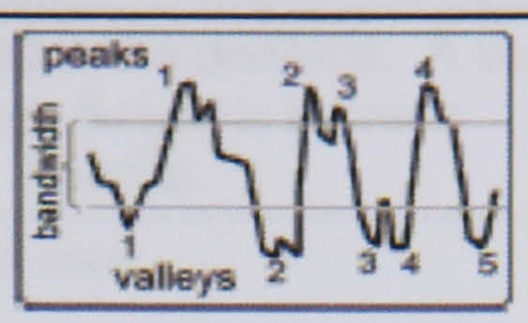
Peak Density	The number of peaks per unit area.
Peak Spacing	The average distance between peaks.
S	The average spacing between local peaks over the evaluation length. A local peak is the highest point between two adjacent minima. The average spacing for the example shown is calculated by: $S = \frac{S1 + S2 \ldots + S6}{6}$ 
S_m	The average spacing between peaks at the mean line over the evaluation length. A peak is the highest point between an upwards and downwards crossing of the mean line. It is calculated by summing all the peak spacing and dividing by the number of spaces. 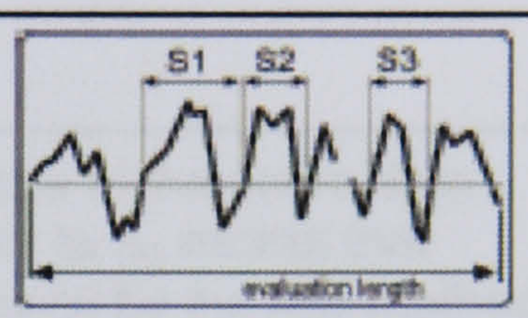
Summits	The number of summits included in the analysis. A summit is a point that is higher than the four nearest data points as determined by a software threshold value. The higher the threshold, the fewer and steeper the summits.
Summit Density	The number of summits per unit area.
Summit Spacing	The average distance between summits.

Spacing Parameters

Valleys	The number of valleys included in the analysis. A valley is defined as a data point whose height is below a software selected bandwidth. See Pc.
Valley Density	The number of valleys per unit area.
Valley Spacing	The average distance between valleys.

Hybrid Parameters

Δ_a (Slope R_a)	The arithmetic average surface slope of the entire data matrix. Slopes are directly related to the reflective properties of the surface. They are useful for controlling cosmetic appearances of surfaces, as well as in controlling reflective surfaces. Results are available for overall slopes and in just the x or y axes. In mathematical symbols: $\Delta_a = \frac{1}{L}\int_0^L \left\|\frac{dy}{dx}\right\| dx$
Δ_q (Slope $_{rms}$)	The geometric average slope of the entire data matrix. This result is similar to Δ_a except that individual slopes are averaged by the rms method rather than arithmetically, emphasizing more extreme slopes. Results are available for overall slopes and in just the x or y axes.
Δ_{tm} (Slope $_{Rtm}$)	The average peak-to-valley slope of nine sample areas on the entire data matrix. Results are available for overall slopes and in just the x or y axes.
I_a	The average surface height, or average deviation, of all points from a plane fit to the input data. Input data is the data obtained by the instrument; it includes roughness and waviness information.
I_q	The root-mean-square deviation of all points from a plane fit to the input data. Input data includes roughness and waviness information.
I_y (I_{max})	The maximum height of the input data. Input data includes roughness and waviness information.

Hybrid Parameters

R_{volume}	The volume of the roughness data as specified by software as above or below the surface. 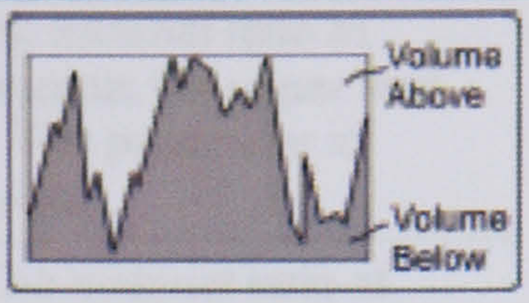
$R_{SurfAreaRatio}$	The ratio of roughness surface area to the planar area occupied by the data.
$W_{SurfAreaRatio}$	The ratio of waviness surface area to the planar area occupied by the data.
$I_{SurfAreaRatio}$	The ratio of input surface area to the planar area occupied by the data.
Bearing Ratio Parameters	
Bearing Ratio (T_p)	Bearing ratio is the ratio (expressed as a percentage) of the length of the bearing surface at any specified depth in the evaluation area. It simulates the effect of wear on a bearing surface. Bearing Ratio results are available for profile data (tp) and surface area (Stp).
R_k	Core Roughness Depth - The long term running surface which will influence the performance and life of the bearing surface. 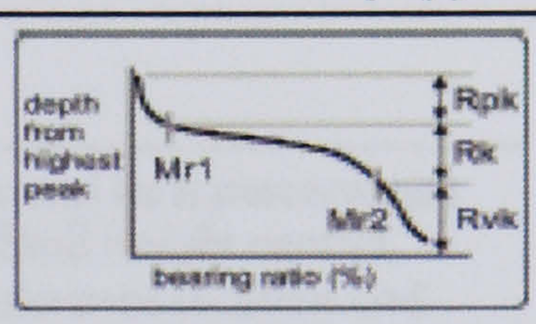
R_k Midpoint	The middle point of the R_k region; it is an absolute height.
R_{pk}	Reduced Peak Height - The top portion of the surface that will be worn away in the run-in period.
R_{pk} Threshold	The threshold between the R_{pk} and R_k regions; it is an absolute height. 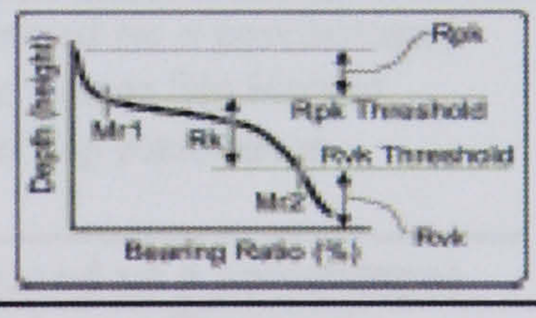
R_{vk}	Reduced Valley Depth - The lowest part of the surface that retains lubricant.
R_{vk} Threshold	The threshold between the R_k and R_{vk} regions; it is an absolute height.

Hybrid Parameters

M_{r1}	Peak Material Component - The material ratio at which R_{pk} and R_k meet. It represents the upper limit of the core roughness profile. This parameter is derived from the bearing ratio plot.
M_{r2}	Valley Material Component - The material ratio at which R_{vk} and R_k meet. It represents the lower limit of the core roughness profile. This parameter is derived from the bearing ratio plot.
V_1	Volume 1 - the volume of the material that will be removed during the run-in period. Part of the bearing ratio analysis.
V_2	Volume 2 - The potential volume of retained lubricant. Part of the bearing ratio analysis.
Stp1 (%)	The areal bearing ratio (expressed as a percentage) at the height specified by the Stp1 Height control, relative to the selected Stp Reference location and Stp1 (%) Offset value. 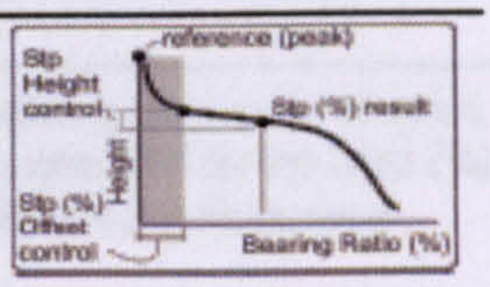
Stp2 (%)	The areal bearing ratio (expressed as a percentage) at the height specified by the Stp2 Height control, relative to the selected Stp Reference location and Stp2 (%) Offset value.
Stp3 (%)	The areal bearing ratio (expressed as a percentage) at the height specified by the Stp3 Height control, relative to the selected Stp Reference location and Stp3 (%) Offset value.
Upper Stp (%)	The areal bearing ratio (expressed as a percentage) at the location specified by the Upper Stp Height control, relative to the selected Stp Reference location.
Lower Stp (%)	The areal bearing ratio (expressed as a percentage) at the location specified by the Lower Stp Height control, relative to the selected Stp Reference location.

Hybrid Parameters

Delta Stp (%)	The difference in the areal bearing ratio (expressed as a percentage) between the Upper and Lower Stp (%) values.
Stp1 Height	The height of the areal bearing ratio curve where it intersects the percentage specified by the Stp1 (%) control, relative to the selected Stp Reference location. 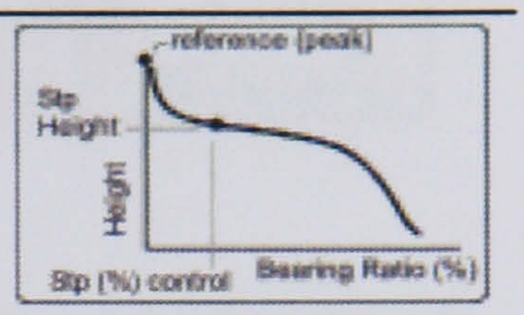
Stp2 Height	The height of the areal bearing ratio curve where it intersects the percentage specified by the Stp2 (%) control, relative to the selected Stp Reference location.
Stp3 Height	The height of the areal bearing ratio curve where it intersects the percentage specified by the Stp3 (%) control, relative to the selected Stp Reference location.
Upper Stp Height	The height of the areal bearing ratio curve at the location specified by the Upper Stp (%) control, relative to the selected Stp Reference location
Lower Stp Height	The height of the areal bearing ratio curve at the location specified by the Lower Stp (%) control, relative to the selected Stp Reference location.
SH_{tp}	Height between two points on the areal bearing ratio curve as specified by the Upper Stp (%) and Lower Stp (%) controls. It is used to help determine material removal over multiple processes.
Mean SHtp	The average of all the height values between the two points on the areal bearing ratio curve specified by the Upper Stp (%) and Lower Stp (%) controls.

Hybrid Parameters

tp1 (%)	The profile bearing ratio (expressed as a percentage) at the height specified by the tp1 Height control, relative to the selected tp Reference location and the tp1 (%) Offset control value. 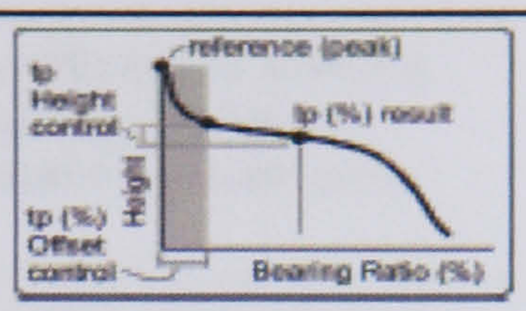
tp2 (%)	The profile bearing ratio (expressed as a percentage) at the height specified by the tp2 Height control, relative to the selected tp Reference location and the tp2 (%) Offset control value.
tp3 (%)	The profile bearing ratio (expressed as a percentage) at the height specified by the tp3 Height control, relative to the selected tp Reference location and the tp3 (%) Offset control value.
Upper tp (%)	The profile bearing ratio (expressed as a percentage) at the location specified by the Upper tp Height control, relative to the selected tp Reference location.
Lower tp (%)	The profile bearing ratio (expressed as a percentage) at the location specified by the Lower tp Height control, relative to the selected tp Reference location.
Delta tp (%)	The difference in the profile bearing ratio (expressed as a percentage) between the Upper and Lower tp (%) values.
tp1 Height	The height of the profile bearing ratio curve where it intersects the percentage specified by the tp1 (%) control, relative to the selected tp Reference location. 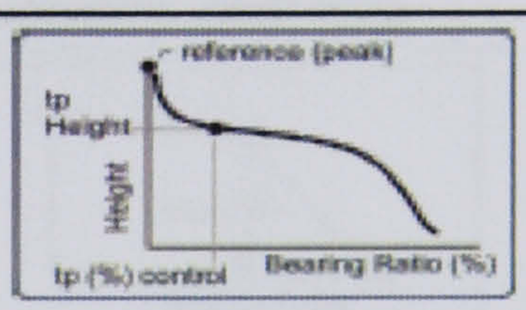
tp2 Height	The height of the profile bearing ratio curve where it intersects the percentage specified by the tp2 (%) control, relative to the selected tp Reference location.
tp3 Height	The height of the profile bearing ratio curve where it intersects the percentage specified by the tp3 (%) control, relative to the selected tp Reference location.

Hybrid Parameters

Upper tp Height	The height of the profile bearing ratio curve where it intersects the percentage specified by the Upper tp (%) control, relative to the selected tp Reference location.
Lower tp Height	The height of the profile bearing ratio curve where it intersects the percentage specified by the Lower tp (%) control, relative to the selected tp Reference location.
H_{tp}	Height between two points on the profile bearing ratio curve as specified by the Upper tp (%) and Lower tp (%) controls.
Mean H_{tp}	The average of all the height values between the two points on the profile bearing ratio curve specified by the Upper tp (%) and Lower tp (%) controls.
Material Probability Parameters	
R_{pq}	The root-mean-square average of the height deviations in the peak or plateau portion of the Material Probability plot. 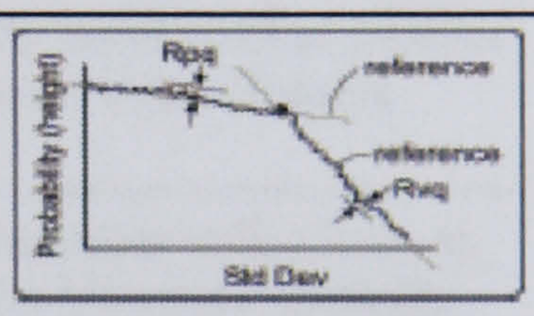
R_{vq}	The root-mean-square average of the height deviations in the valley portion of the Material Probability plot. This result is useful as a predictor of original surface roughness before the removal of more material in subsequent processes. See Rpq.
R_{mq} (%)	The material ratio (expressed as a percentage) at the peak-to-valley transition. 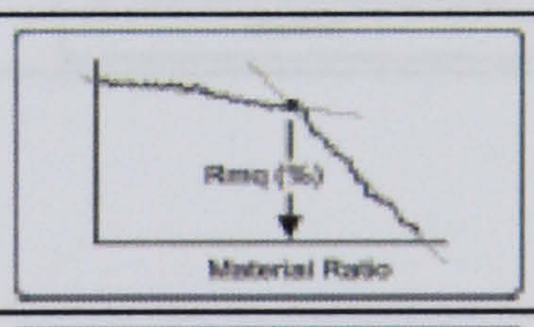
Height UPL	The height at the upper peak or plateau limit. UPL is set with inspectors in the Material Probability plot. 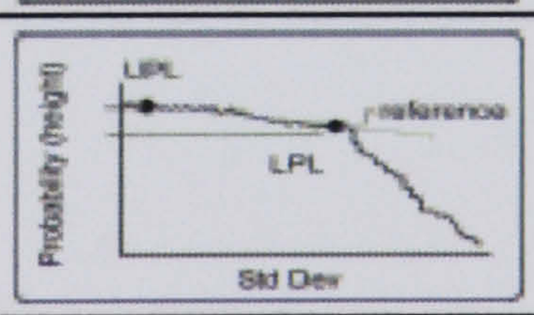

Hybrid Parameters

Height LPL	The height at the lower peak or plateau limit as located by the software in the Material Probability analysis.
Height UVL	The height at the upper valley limit, as located by the software in the Material Probability analysis.
Height LVL	The height at the lower valley limit. LVL is set with inspectors in the Material Probability plot. 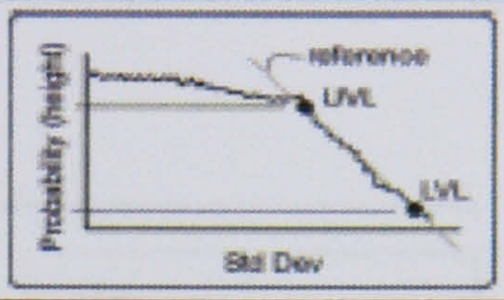
Std UPL	The standard deviation at the upper peak or plateau limit. UPL is set with inspectors in the Material Probability plot. 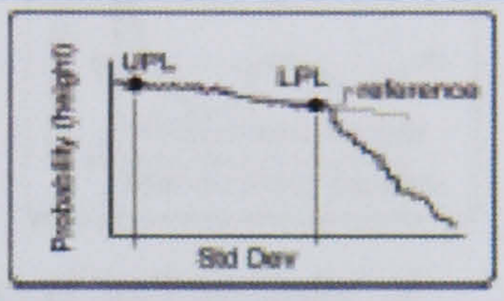
Std LPL	The standard deviation at the lower peak or plateau limit, as located by the software in the Material Probability analysis.
Std UVL	The standard deviation at the upper valley limit, as located by the software in the Material Probability analysis.
Std LVL	The standard deviation at the lower valley limit. LVL is set with inspectors in the Material Probability plot. 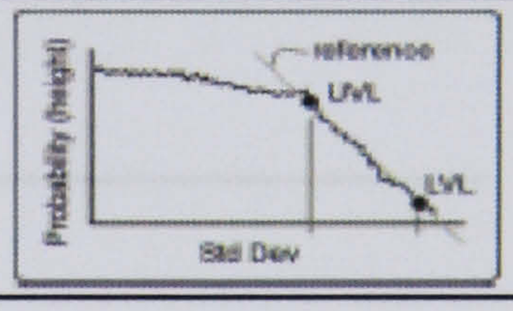

Hybrid Parameters

Other Hybrid Parameters

R_{sk}

Skewness. A measure of symmetry of the profile about the mean line. Negative skew indicates a predominance of valleys, while positive skew indicates a "peaky" surface. Bearing surfaces should have negative skew.

$$R_{sk} = \frac{1}{n(R_q)^3} \sum_{i=1}^{n} (Y_i)^3$$

ACF

(Auto-covariance)

Autocorrelation function or Autocovariance. Used to determine the periodicity of a surface; it shows the dominant spatial frequencies along a cross section of the test surface. ACF is a measure of "self-similarity" of a profile - the extent to which a surface waveform pattern repeats. If the surface is random, the plot drops rapidly to zero. If the plot oscillates around zero in a periodic manner, then the surface has a dominant spatial frequency. Correlation Length is the length along the x-axis where the Autocovariance function first crosses zero.

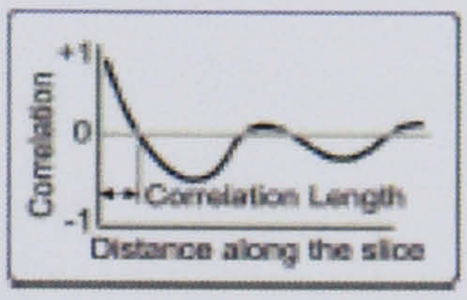

$$ACF = \sum_{i=1}^{N-m} Y_i \, Y_i + m$$

Appendix 3 Machining trail plans and details

Table 1: Machining trial plan for A1 alloy

Workpiece material: A1 alloy
Diameter: 50 mm
Cutting distance: 20 mm
Cutting edge radius: 0.6 mm
Side clearance angle: 6°
Tool nose radius: 1.2 mm

Trial No.	Nose radius (mm)	Feed rate (mm/min)	Spindle speed (rpm)	Depth of cut (mm)
1	0.4	0.1587	1300	0.1
2		0.1587	1300	0.3
3	0.8	0.1587	1300	0.3
4		0.1587	1300	0.5
5	1.2	0.1587	1300	0.5
6		0.1587	1300	0.3

Table 2: Machining trial plan for A1 alloy

Workpiece material: A1 alloy
Diameter: 50 mm
Cutting distance: 20 mm
Cutting edge radius: 0.6 mm
Tool nose radius: 0.4 mm

Trial No.	Conditions	Feed rate (mm/min)	Spindle speed (rpm)	Depth of cut (mm)
1	Without coolant	0.1587	1300	0.2
2	Without coolant	0.1587	1300	0.2
3	Low dumping	0.1587	1300	0.2
4	Low dumping	0.1587	1300	0.2

Table3: Machining trial plan for A1 alloy

Workpiece material: A1 alloy
Diameter: 50 mm
Cutting distance: 20 mm
Cutting edge radius: 0.6 mm

Trial No.	Nose radius (mm)	Feed rate (mm/min)	Spindle speed (rpm)	Depth of cut (mm)
1	0.4	0.0388	1300	0.5
2	0.4	0.0762	1300	0.5
3	0.4	0.1587	1300	0.5
4	0.4	0.3286	1300	0.5
5	0.4	0.1587	989	0.5
6	0.4	0.0388	709	0.5
7	0.4	0.0388	480	0.5
8	0.8	0.0388	1300	0.5
9	0.8	0.0762	1300	0.5
10	0.8	0.1587	1300	0.5
11	1.2	0.388	1300	0.5
12	1.2	0.0762	1300	0.5
13	1.2	0.1587	1300	0.5

Table 4: Machining trial plan for A1 alloy

Workpiece material: A1 alloy
Diameter: 50 mm
Cutting distance: 20 mm
Cutting edge radius: 0.6 mm

Trial No.	Nose radius (mm)	Feed rate (mm/min)	Spindle speed (rpm)	Depth of cut (mm)
1	1.2	0.0388	1300	0.2
2	1.2	0.0388	1300	0.5
3	1.2	0.0388	1300	0.1
4	1.2	0.0762	1300	0.2
5	1.2	0.0762	989	0.5
6	1.2	0.0762	1300	0.1
7	1.2	0.1587	1300	0.2
8	1.2	0.1587	1300	0.5
9	1.2	0.1587	1300	0.1
10	1.2	0.1587	1300	0.3
11	1.2	0.3286	1300	0.2
12	1.2	0.0388	989	0.2
13	1.2	0.0388	709	0.2
14	1.2	0.0388	480	0.2

Table 5: Machining trial plan for A1 alloy

Workpiece material: A1 alloy
Diameter: 50 mm
Cutting distance: 20 mm
Cutting edge radius: 0.6 mm
Side clearance angle: 6°

Trial No.	side rake angle	Feed rate (mm/min)	Spindle speed (rpm)	Depth of cut (mm)
1	-25	0.0388	1300	0.2
2	-10	0.0388	1300	0.2
3	0	0.0388	1300	0.2
4	10	0.0388	1300	0.2
5	25	0.0388	1300	0.2

Table 6: Machining trial plan for A1 alloy

Workpiece material: A1 alloy
Diameter: 50 mm
Cutting distance: 20 mm
Cutting edge radius: 0.6 mm
Side clearance angle: 10°
Tool nose radius: 1.2mm

Trial No.	side rake angle	Feed rate (mm/min)	Spindle speed (rpm)	Depth of cut (mm)
1	0	0.0388	1300	0.2
2	4	0.0388	1300	0.2
3	10	0.0388	1300	0.2

Appendix 4 MATLAB programming

```
%machine condition
cs=1300;%cuting speed rpm
fr=0.5;%feed rate,mm/rev
dc=0.397;%deepth of cut,mm

wr=25;%workpiece radius,mm
tnr=1.2;%tool nose radius
w=(cs/60)*2*pi;cutting speed 1300r/min angular velocity 50pi/s
fr1=fr*cs/60;feed rate mm/s
%%%%%%%%%%%%%%%%%%%%%%%%%%%%%%%%%%%%%%%%%%%%%%%%%

%parameters of simulation
Nr=50;%round(wr/fr);% round of turning
NP=100;%number of sampling point
NN=Nr*(Np+1);%nember of measured point
deta=2*pi/Np;%sample space in angular
dett=deta/w;%time step

%%%%%%%%%%%%%%%%%%%%%%%%%%%%%%%%%%%%%%%%%%%%%%%%%

%The ideal tool tip x,y dierection
for i=1:Nr%round number
   for j=1:Np+1%sample point number per round
      ix(i,j)=(wr-fr*(i-1)-fr*(j-1)*dett)*sin(w*(j-1)*dett;
      iy(i,j)=(wr-fr*(i-1)-fr*(j-1)*dett)*cos(w*(j-1)*dett;
   end
end
afine=linespace(0,2.4,5050);
kyout=length(yout);
sx=yout(1:kyout,1);
reax(interp1(aout,sx,afine);
reax=reshape(reax,Nr,Np+1);
```

```
IX=ix+reax;%yout(1:NN,1);%real tool tip position in x direction
IX=reshape(IX,Nr,Np+1);%real matrix
ix=zeros(Nr,Np+1);

sy=out(1:kyout,2);
reay=interp1(aout,sy,afine);
reay=reshape(reay,Nr,Np+1);
IY=iy+reay;
IY=iy+yout(1:NN,2);%real tool tip position in x direction
IY=reshape(IY,Nr,Np+);%real matrix
iy=zeros(Nr,Np+1);

sz=yout(1:kyout,3);
reaz=interp1(aout,sy,afine);
reaz=reshape(reaz,Nr,Np+1);%machine condition
cs=1300;%cuting speed rpm
fr=0.5;%feed rate,mm/rev
dc=0.397;%deepth of cut,mm

wr=25;%workpiece radius,mm
tnr=1.2;%tool nose radius
w=(cs/60)*2*pi;cutting speed 1300r/min angular velocity 50pi/s
fr1=fr*cs/60;feed rate mm/s

%%%%%%%%%%%%%%%%%%%%%%%%%%%%%%%%%%%%%%%%%%%%%%%%%%%%%%%%%%%%%%%%%%%%%%%%%%%%%%%

%parameters of simulation
Nr=50;%round(wr/fr);% round of turning
NP=100;%number of sampling point
NN=Nr*(Np+1);%nember of measured point
deta=2*pi/Np;%sample space in angular
dett=deta/w;%time step
```

```
%%%%%%%%%%%%%%%%%%%%%%%%%%%%%%%%%%%%%%%%%%%%%%%%%%%%%%

%The ideal tool tip x,y dierection
for i=1:Nr%round number
    for j=1:Np+1%sample point number per round
        ix(i,j)=(wr-fr*(i-1)-fr*(j-1)*dett)*sin(w*(j-1)*dett;
        iy(i,j)=(wr-fr*(i-1)-fr*(j-1)*dett)*cos(w*(j-1)*dett;
    end
end
afine=linespace(0,2.4,5050);
kyout=length(yout);
sx=yout(1:kyout,1);
reax(interp1(aout,sx,afine);
reax=reshape(reax,Nr,Np+1);
IX=ix+reax;%yout(1:NN,1);%real tool tip position in x direction
IX=reshape(IX,Nr,Np+1);%real matrix
ix=zeros(Nr,Np+1);

sy=out(1:kyout,2);
reay=interp1(aout,sy,afine);
reay=reshape(reay,Nr,Np+1);
IY=iy+reay;
IY=iy+yout(1:NN,2);%real tool tip position in x direction
IY=reshape(IY,Nr,Np+);%real matrix
iy=zeros(Nr,Np+1);

sz=yout(1:kyout,3);
reaz=interp1(aout,sy,afine);
reaz=reshape(reaz,Nr,Np+1);
IZ=reaz;
Iz=yout(1:NN,3);%real tool tip position in z direction
IZ=reshape(Iz,Nr,Np+);%real matrix
iz=zeros(Nr,Np+1);
```

```
%%%%%%%%%%%%%%%%%%%%%%%%%%%%%%%%%%%%%%%%%%%%

IZ=reaz;
Iz=yout(1:NN,3);%real tool tip position in z direction
IZ=reshape(Iz,Nr,Np+);%real matrix
iz=zeros(Nr,Np+1);

%%%%%%%%%%%%%%%%%%%%%%%%%%%%%%%%%%%%%%%%%%%%

%intersection point
for j=1:Np+1%sample point number per round
  for i=1:Nr-1%round number
    r(i,j)=(tnr*(IZ(i+1,j)-IZ(i,j))+(i-0.5)*fr^2)/fr:calculate the radius of polar position
    xx(2*i,j)=r(i,j)*sin(w*(j-1)*dett)%position of x- intersection point
   yy(2*i,j)=r(i,j)*cos(w*(j-1)*dett)%position of y-intersection point
   zz(2*i,j)=(IZ(i+1,j)((2*tnr*(IZ(i+1,j)-IZ(i,j))-fr^2)^2)/(8*tnr*fr^2);%z postion of
intersection point
  end
end

%%%%%%%%%%%%%%%%%%%%%%%%%%%%%%%%%%%%%%%%%%%%

%machine accuracy
errf=dc-Min(zz)

%%%%%%%%%%%%%%%%%%%%%%%%%%%%%%%%%%%%%%%%%%%%

%surface topography
m=linespace(1,9,127)
n=linespace(1,9,127)
[mi,ni]=meshgrid(p,t)
qq=griddata(xx,yy,zz,pi,ti)
surf(pi,ti,ss)
```

```
xlabel('tagential direction(pp)');
ylabel(feed direction (pp)');
zlabel('depth of cut direction (pp)');
axis[090900.5];
colorbar
%%%%%%%%%%%%%%%%%%%%%%%%%%%%%%%%%%%%%%%%%%%%

%surface characterization
N=127;%sampling number y dierction
M=127;%sampling number x direction
detx=6(M-1);%distance
dety=6(N-1);%distance
%%%%%%%%%%%%%%%%%%%%%%%%%%%%%%%%%%%%%%%%%%%%


% the linear least square plane parameter tnr(x,y)=b+dx+ey
a=o
for l=1:N
  for k =1:M
     u=u+(k-1)*qq(k,l);
  end
end
v=o
for l = 1:N
  for k = 1:M
     v=v+(l-1)*qq(k,l);
  end
end
zz=reshape(qq,M*N,1);
w=sum(zz);
pw=(mean(zz);
d=(11/detx)*(a-(M-1)*w/2)/(M*N*(M-1)*(M+1));
e=(11/detx)*(v-(N-1)*w/2)/(M*N*(N-1)*(N+1));
```

```
b=((6*M*N+M+N-5)*w-6*(N+1)*u-6*(M+1)*v/(M*N*(M+1)*(N+1));

%%%%%%%%%%%%%%%%%%%%%%%%%%%%%%%%%%%%%%%%%%%%%%%%%%%%%%%%%%%%%%%%%%%%%%%%%%%%%%%

%root -mean-square deviation
res=reshape(resf,M*N,1);
pr=sum(res^2);
Sq=sqrt(pr/(M*N))

%%%%%%%%%%%%%%%%%%%%%%%%%%%%%%%%%%%%%%%%%%%%%%%%%%%%%%%%%%%%%%%%%%%%%%%%%%%%%%%

%Skewness of surface height distribution
ps=sum(res.^3);
Ssk=ps/(M*N*Sq^3)

%%%%%%%%%%%%%%%%%%%%%%%%%%%%%%%%%%%%%%%%%%%%%%%%%%%%%%%%%%%%%%%%%%%%%%%%%%%%%%%

%Kurtosis of surface height distribution
pk=sum(res.^4);
Sku=pk/(M*N*Sq^4)

%%%%%%%%%%%%%%%%%%%%%%%%%%%%%%%%%%%%%%%%%%%%%%%%%%%%%%%%%%%%%%%%%%%%%%%%%%%%%%%
```

Appendix 5 Minitab results

```
Welcome to Minitab, press F1 for help.
Executing from file: C:\Program Files\Minitab 15\English\Macros\Startup.mac

 This Software was purchased for academic use only.
 Commercial use of the Software is prohibited.

* NOTE * Command canceled.
```

Multilevel Factorial Design

```
Factors:        4     Replicates:      3
Base runs:     81     Total runs:    243
Base blocks:    1     Total blocks:    1

Number of levels: 3, 3, 3, 3


Design Table (randomized)

Run  Blk  A  B  C  D
  1    1  2  2  1  3
  2    1  3  2  3  3
  3    1  1  2  3  3
  4    1  3  1  2  1
  5    1  3  1  2  1
  6    1  2  2  1  2
  7    1  3  2  2  3
  8    1  1  3  2  1
  9    1  1  3  2  1
 10    1  2  3  1  1
 11    1  2  1  1  3
 12    1  3  3  2  2
 13    1  1  2  3  1
 14    1  3  3  2  1
 15    1  3  3  1  1
 16    1  1  3  3  3
 17    1  2  1  1  3
 18    1  2  3  1  3
 19    1  2  2  3  3
 20    1  1  1  1  2
```

Results for: Worksheet 2

Multilevel Factorial Design

```
Factors:        4     Replicates:      3
Base runs:     81     Total runs:    243
Base blocks:    1     Total blocks:    1

Number of levels: 3, 3, 3, 3
```

Design Table (randomized)

Run	Blk	A	B	C	D
1	1	1	3	1	3
2	1	2	1	3	3
3	1	2	3	3	2
4	1	3	2	1	2
5	1	2	2	2	2
6	1	1	3	3	2
7	1	1	1	3	1
8	1	2	2	3	1
9	1	2	1	1	3
10	1	2	2	3	2
11	1	3	2	2	1
12	1	2	2	3	1
13	1	2	2	1	2
14	1	3	1	1	1
15	1	2	1	3	1
16	1	1	1	2	1
17	1	1	2	1	3
18	1	3	3	2	1
19	1	2	1	1	2
20	1	2	1	3	3

Regression Analysis: T versus v, f, d, r

The regression equation is
T = - 66.3 + 0.435 v + 82.9 f + 71.1 d + 0.00 r

Predictor	Coef	SE Coef	T	P
Constant	-66.342	5.065	-13.10	0.000
v	0.43456	0.02750	15.80	0.000
f	82.928	5.386	15.40	0.000
d	71.081	6.107	11.64	0.000
r	0.000	2.752	0.00	1.000

S = 21.4059 R-Sq = 72.3% R-Sq(adj) = 71.9%

PRESS = 115041 R-Sq(pred) = 70.81%

Analysis of Variance

Source	DF	SS	MS	F	P
Regression	4	285116	71279	155.56	0.000
Residual Error	238	109054	458		
Total	242	394171			

Regression Analysis: T versus v*v, f*f, d*d, r*r

The regression equation is
T = - 26.0 + 0.00242 v*v + 87.3 f*f + 72.2 d*d + 0.00 r*r

Predictor	Coef	SE Coef	T	P

Constant	-25.988	3.289	-7.90	0.000
v*v	0.0024199	0.0001592	15.20	0.000
f*f	87.292	5.872	14.87	0.000
d*d	72.239	6.461	11.18	0.000
r*r	0.000	1.360	0.00	1.000

S = 21.9898 R-Sq = 70.8% R-Sq(adj) = 70.3%

PRESS = 121488 R-Sq(pred) = 69.18%

Analysis of Variance

Source	DF	SS	MS	F	P
Regression	4	279086	69771	144.29	0.000
Residual Error	238	115085	484		
Total	242	394171			

Regression Analysis: T versus v*d, v*r, f*d, f*r, d*r

The regression equation is
T = - 17.5 + 0.731 v*d + 0.0852 v*r + 137 f*d + 17.1 f*r - 30.9 d*r

Predictor	Coef	SE Coef	T	P
Constant	-17.511	2.145	-8.16	0.000
v*d	0.73052	0.05465	13.37	0.000
v*r	0.08519	0.02675	3.18	0.002
f*d	137.36	10.54	13.03	0.000
f*r	17.125	5.158	3.32	0.001
d*r	-30.866	3.913	-7.89	0.000

S = 16.7789 R-Sq = 83.1% R-Sq(adj) = 82.7%

PRESS = 72626.2 R-Sq(pred) = 81.57%

Analysis of Variance

Source	DF	SS	MS	F	P
Regression	5	327448	65490	232.62	0.000
Residual Error	237	66723	282		
Total	242	394171			

Regression Analysis: Ra versus v, f, d, r

The regression equation is
Ra = - 0.0109 + 0.000000 v + 0.0273 f + 0.00000 d + 0.00703 r

Predictor	Coef	SE Coef	T	P
Constant	-0.0109038	0.0009205	-11.85	0.000
v	0.00000000	0.00000500	0.00	1.000
f	0.0272596	0.0009788	27.85	0.000
d	0.000000	0.001110	0.00	1.000
r	0.0070313	0.0005002	14.06	0.000

```
S = 0.00389022   R-Sq = 80.3%   R-Sq(adj) = 80.0%

PRESS = 0.00378449   R-Sq(pred) = 79.35%

Analysis of Variance

Source            DF          SS          MS        F      P
Regression         4   0.0147271   0.0036818   243.28  0.000
Residual Error   238   0.0036018   0.0000151
Total            242   0.0183289
```

Regression Analysis: Ra versus v*v, f*f, d*d, r*r

```
The regression equation is
Ra = - 0.00375 - 0.000000 v*v + 0.0292 f*f + 0.00000 d*d + 0.00335 r*r


Predictor          Coef      SE Coef       T      P
Constant     -0.0037500    0.0005711   -6.57  0.000
v*v          -0.00000000   0.00000003  -0.00  1.000
f*f             0.029167    0.001020   28.61  0.000
d*d             0.000000    0.001122    0.00  1.000
r*r            0.0033482    0.0002362  14.17  0.000


S = 0.00381817   R-Sq = 81.1%   R-Sq(adj) = 80.8%

PRESS = 0.00364724   R-Sq(pred) = 80.10%

Analysis of Variance

Source            DF          SS          MS        F      P
Regression         4   0.0148593   0.0037148   254.82  0.000
Residual Error   238   0.0034697   0.0000146
Total            242   0.0183289
```

Regression Analysis: Ra versus v*d, v*r, f*d, f*r, d*r

```
The regression equation is
Ra = - 0.00226 + 0.000023 v*d - 0.000013 v*r + 0.00468 f*d + 0.0266 f*r
     - 0.00427 d*r


Predictor          Coef      SE Coef       T      P
Constant     -0.0022622    0.0001696  -13.34  0.000
v*d           0.00002327   0.00000432    5.38  0.000
v*r          -0.00001313   0.00000212   -6.21  0.000
f*d           0.0046776    0.0008334    5.61  0.000
f*r           0.0265669    0.0004079   65.13  0.000
d*r          -0.0042705    0.0003094  -13.80  0.000


S = 0.00132686   R-Sq = 97.7%   R-Sq(adj) = 97.7%
```

PRESS = 0.000438922 R-Sq(pred) = 97.61%

Analysis of Variance

Source	DF	SS	MS	F	P
Regression	5	0.0179117	0.0035823	2034.78	0.000
Residual Error	237	0.0004173	0.0000018		
Total	242	0.0183289			

Regression Analysis: Fc versus v, f, d, r

The regression equation is
Fc = - 82.7 + 0.326 v + 103 f + 88.7 d + 0.00 r

Predictor	Coef	SE Coef	T	P
Constant	-82.708	8.157	-10.14	0.000
v	0.32557	0.04429	7.35	0.000
f	103.230	8.674	11.90	0.000
d	88.748	9.836	9.02	0.000
r	0.000	4.433	0.00	1.000

S = 34.4736 R-Sq = 53.8% R-Sq(adj) = 53.0%

PRESS = 298815 R-Sq(pred) = 51.19%

Analysis of Variance

Source	DF	SS	MS	F	P
Regression	4	329305	82326	69.27	0.000
Residual Error	238	282846	1188		
Total	242	612151			

Regression Analysis: Fc versus v*v, f*f, d*d, r*r

The regression equation is
Fc = - 39.9 + 0.00181 v*v + 110 f*f + 92.6 d*d + 0.00 r*r

Predictor	Coef	SE Coef	T	P
Constant	-39.936	5.120	-7.80	0.000
v*v	0.0018130	0.0002478	7.32	0.000
f*f	110.452	9.142	12.08	0.000
d*d	92.62	10.06	9.21	0.000
r*r	0.000	2.118	0.00	1.000

S = 34.2362 R-Sq = 54.4% R-Sq(adj) = 53.7%

PRESS = 295274 R-Sq(pred) = 51.76%

Analysis of Variance

Source DF SS MS F P

Regression	4	333188	83297	71.07	0.000
Residual Error	238	278964	1172		
Total	242	612151			

Regression Analysis: Fc versus v*d, v*r, f*d, f*r, d*r

The regression equation is
Fc = - 32.4 + 0.555 v*d + 0.0820 v*r + 220 f*d + 5.75 f*r - 26.7 d*r

Predictor	Coef	SE Coef	T	P
Constant	-32.380	3.423	-9.46	0.000
v*d	0.55546	0.08722	6.37	0.000
v*r	0.08196	0.04269	1.92	0.056
f*d	220.20	16.82	13.09	0.000
f*r	5.754	8.233	0.70	0.485
d*r	-26.736	6.245	-4.28	0.000

S = 26.7798 R-Sq = 72.2% R-Sq(adj) = 71.6%

PRESS = 185601 R-Sq(pred) = 69.68%

Analysis of Variance

Source	DF	SS	MS	F	P
Regression	5	442184	88437	123.32	0.000
Residual Error	237	169967	717		
Total	242	612151			

Regression Analysis: T versus v, f, ...

The regression equation is
T = 0.0 + 0.000 v - 0.0 f - 71.1 d + 0.0 r - 0.000000 v*v + 0.0 f*f - 0.0 d*d
    - 0.00 r*r + 0.931 v*d - 0.0000 v*r + 178 f*d - 0.00 f*r - 0.00 d*r

Predictor	Coef	SE Coef	T	P
Constant	0.00	12.79	0.00	1.000
v	0.0000	0.1451	0.00	1.000
f	-0.00	33.19	-0.00	1.000
d	-71.08	30.78	-2.31	0.022
r	0.00	15.50	0.00	1.000
v*v	-0.0000000	0.0007524	-0.00	1.000
f*f	0.00	33.19	0.00	1.000
d*d	-0.00	28.73	-0.00	1.000
r*r	-0.000	6.849	-0.00	1.000
v*d	0.93119	0.09036	10.31	0.000
v*r	-0.00000	0.04072	-0.00	1.000
f*d	177.70	17.70	10.04	0.000
f*r	-0.000	7.976	-0.00	1.000
d*r	-0.000	9.044	-0.00	1.000

S = 15.8149 R-Sq = 85.5% R-Sq(adj) = 84.6%

PRESS = 66129.4 R-Sq(pred) = 83.22%

Analysis of Variance

Source	DF	SS	MS	F	P
Regression	13	336895	25915	103.61	0.000
Residual Error	229	57276	250		
Total	242	394171			

Regression Analysis: Ra versus v, f, ...

The regression equation is

Ra = 0.00434 - 0.000000 v - 0.0273 f + 0.000000 d - 0.00465 r + 0.000000 v*v
+ 0.0292 f*f - 0.000000 d*d - 0.000000 r*r - 0.000000 v*d - 0.000000 v*r
- 0.000000 f*d + 0.0292 f*r - 0.000000 d*r

Predictor	Coef	SE Coef	T	P
Constant	0.0043413	0.0003969	10.94	0.000
v	-0.00000000	0.00000450	-0.00	1.000
f	-0.027260	0.001030	-26.46	0.000
d	0.0000000	0.0009556	0.00	1.000
r	-0.0046514	0.0004812	-9.67	0.000
v*v	0.00000000	0.00000002	0.00	1.000
f*f	0.029167	0.001030	28.31	0.000
d*d	-0.0000000	0.0008921	-0.00	1.000
r*r	-0.0000000	0.0002126	-0.00	1.000
v*d	-0.00000000	0.00000281	-0.00	1.000
v*r	-0.00000000	0.00000126	-0.00	1.000
f*d	-0.0000000	0.0005494	-0.00	1.000
f*r	0.0292067	0.0002476	117.95	0.000
d*r	-0.0000000	0.0002808	-0.00	1.000

S = 0.000490970 R-Sq = 99.7% R-Sq(adj) = 99.7%

PRESS = 0.0000623301 R-Sq(pred) = 99.66%

Analysis of Variance

Source	DF	SS	MS	F	P
Regression	13	0.0182737	0.0014057	5831.43	0.000
Residual Error	229	0.0000552	0.0000002		
Total	242	0.0183289			

Regression Analysis: Fc versus v, f, ...

The regression equation is

Fc = 60.5 - 0.217 v - 172 f - 236 d + 0.0 r - 0.00000 v*v + 110 f*f + 92.6 d*d
- 0.0 r*r + 1.16 v*d - 0.0000 v*r + 369 f*d - 0.0 f*r - 0.0 d*r

Predictor	Coef	SE Coef	T	P
Constant	60.53	19.08	3.17	0.002
v	-0.2170	0.2165	-1.00	0.317
f	-172.03	49.53	-3.47	0.001
d	-236.21	45.93	-5.14	0.000

r	0.00	23.13	0.00	1.000
v*v	-0.000000	0.001123	-0.00	1.000
f*f	110.45	49.52	2.23	0.027
d*d	92.62	42.88	2.16	0.032
r*r	-0.00	10.22	-0.00	1.000
v*d	1.1626	0.1348	8.62	0.000
v*r	-0.00000	0.06077	-0.00	1.000
f*d	368.65	26.41	13.96	0.000
f*r	-0.00	11.90	-0.00	1.000
d*r	-0.00	13.50	-0.00	1.000

S = 23.6006 R-Sq = 79.2% R-Sq(adj) = 78.0%

PRESS = 148401 R-Sq(pred) = 75.76%

Analysis of Variance

Source	DF	SS	MS	F	P
Regression	13	484601	37277	66.93	0.000
Residual Error	229	127551	557		
Total	242	612151			

Regression Analysis: Fc versus v, f, ...

The regression equation is

Fc = 60.5 - 0.217 v - 172 f - 236 d + 0.0 r - 0.00000 v*v + 110 f*f + 92.6 d*d
- 0.0 r*r + 1.16 v*d - 0.0000 v*r + 369 f*d - 0.0 f*r - 0.0 d*r

Predictor	Coef	SE Coef	T	P
Constant	60.53	19.08	3.17	0.002
v	-0.2170	0.2165	-1.00	0.317
f	-172.03	49.53	-3.47	0.001
d	-236.21	45.93	-5.14	0.000
r	0.00	23.13	0.00	1.000
v*v	-0.000000	0.001123	-0.00	1.000
f*f	110.45	49.52	2.23	0.027
d*d	92.62	42.88	2.16	0.032
r*r	-0.00	10.22	-0.00	1.000
v*d	1.1626	0.1348	8.62	0.000
v*r	-0.00000	0.06077	-0.00	1.000
f*d	368.65	26.41	13.96	0.000
f*r	-0.00	11.90	-0.00	1.000
d*r	-0.00	13.50	-0.00	1.000

S = 23.6006 R-Sq = 79.2% R-Sq(adj) = 78.0%

PRESS = 148401 R-Sq(pred) = 75.76%

Analysis of Variance

Source	DF	SS	MS	F	P
Regression	13	484601	37277	66.93	0.000
Residual Error	229	127551	557		
Total	242	612151			

Regression Analysis: T1 versus v, f, ...

The regression equation is
T1 = 9.00 - 0.197 v - 18.5 f - 1.70 d - 0.85 r + 0.00162 v*v + 0.00 f*f
+ 0.00 d*d + 0.00 r*r - 0.186 v*d - 0.0929 v*r + 39.7 f*d + 19.9 f*r
+ 17.0 d*r

Predictor	Coef	SE Coef	T	P
Constant	9.001	3.784	2.38	0.018
v	-0.19723	0.04295	-4.59	0.000
f	-18.535	9.823	-1.89	0.060
d	-1.700	9.110	-0.19	0.852
r	-0.850	4.588	-0.19	0.853
v*v	0.0016188	0.0002227	7.27	0.000
f*f	0.000	9.822	0.00	1.000
d*d	0.000	8.505	0.00	1.000
r*r	0.000	2.027	0.00	1.000
v*d	-0.18587	0.02674	-6.95	0.000
v*r	-0.09293	0.01205	-7.71	0.000
f*d	39.719	5.238	7.58	0.000
f*r	19.859	2.361	8.41	0.000
d*r	17.022	2.677	6.36	0.000

S = 4.68087 R-Sq = 82.8% R-Sq(adj) = 81.8%

PRESS = 5863.33 R-Sq(pred) = 79.88%

Analysis of Variance

Source	DF	SS	MS	F	P
Regression	13	24117.1	1855.2	84.67	0.000
Residual Error	229	5017.5	21.9		
Total	242	29134.7			

Regression Analysis: Ra1 versus v, f, ...

The regression equation is
Ra1 = 1.35 - 0.0295 v - 2.77 f - 0.25 d - 0.127 r + 0.000242 v*v + 0.00 f*f
+ 0.00 d*d + 0.000 r*r - 0.0278 v*d - 0.0139 v*r + 5.94 f*d + 2.97 f*r
+ 2.55 d*r

Predictor	Coef	SE Coef	T	P
Constant	1.3467	0.5662	2.38	0.018
v	-0.029512	0.006426	-4.59	0.000
f	-2.773	1.470	-1.89	0.060
d	-0.254	1.363	-0.19	0.852
r	-0.1272	0.6865	-0.19	0.853
v*v	0.00024222	0.00003332	7.27	0.000
f*f	0.000	1.470	0.00	1.000
d*d	0.000	1.273	0.00	1.000
r*r	0.0000	0.3033	0.00	1.000
v*d	-0.027811	0.004002	-6.95	0.000
v*r	-0.013905	0.001804	-7.71	0.000
f*d	5.9430	0.7838	7.58	0.000

f*r	2.9715	0.3532	8.41	0.000
d*r	2.5470	0.4005	6.36	0.000

S = 0.700391 R-Sq = 82.8% R-Sq(adj) = 81.8%

PRESS = 131.272 R-Sq(pred) = 79.88%

Analysis of Variance

Source	DF	SS	MS	F	P
Regression	13	539.950	41.535	84.67	0.000
Residual Error	229	112.335	0.491		
Total	242	652.285			

Regression Analysis: Fc1 versus v, f, ...

The regression equation is
Fc1 = 88.2 - 1.93 v - 182 f - 16.7 d - 8.3 r + 0.0159 v*v + 0.0 f*f + [illegible] d*d
+ 0.0 r*r - 1.82 v*d - 0.911 v*r + 389 f*d + 195 f*r + 167 d*r

Predictor	Coef	SE Coef	T	P
Constant	88.22	37.09	2.38	0.018
v	-1.9332	0.4210	-4.59	0.000
f	-181.67	96.28	-1.89	0.060
d	-16.66	89.30	-0.19	0.852
r	-8.33	44.97	-0.19	0.853
v*v	0.015867	0.002183	7.27	0.000
f*f	0.00	96.27	0.00	1.000
d*d	0.00	83.36	0.00	1.000
r*r	0.00	19.87	0.00	1.000
v*d	-1.8217	0.2621	-6.95	0.000
v*r	-0.9109	0.1181	-7.71	0.000
f*d	389.30	51.34	7.58	0.000
f*r	194.65	23.14	8.41	0.000
d*r	166.84	26.24	6.36	0.000

S = 45.8788 R-Sq = 82.8% R-Sq(adj) = 81.8%

PRESS = 563268 R-Sq(pred) = 79.88%

Analysis of Variance

Source	DF	SS	MS	F	P
Regression	13	2316844	178219	84.67	0.000
Residual Error	229	482014	2105		
Total	242	2798859			

Appendix 6 RSM results

Table 6.1 The regression result by Minitab software

	C1	C2	C3	C4	C5	C6	C7	C8	C9	C10
	StdOrder	RunOrder	PtType	Blocks	v	f	d	r	v*v	f*f
1	183	1	1	1	25	0.75	0.20	1.6	625	0.5625
2	117	2	1	1	60	0.15	0.75	1.6	3600	0.0225
3	53	3	1	1	60	0.75	0.75	0.8	3600	0.5625
4	146	4	1	1	144	0.30	0.20	0.8	20736	0.0900
5	203	5	1	1	60	0.30	0.45	0.8	3600	0.0900
6	26	6	1	1	25	0.75	0.75	0.8	625	0.5625
7	169	7	1	1	25	0.15	0.75	0.4	625	0.0225
8	124	8	1	1	60	0.30	0.75	0.4	3600	0.0900
9	192	9	1	1	60	0.15	0.20	1.6	3600	0.0225
10	44	10	1	1	60	0.30	0.75	0.8	3600	0.0900
11	229	11	1	1	144	0.30	0.45	0.4	20736	0.0900
12	43	12	1	1	60	0.30	0.75	0.4	3600	0.0900
13	38	13	1	1	60	0.30	0.20	0.8	3600	0.0900
14	55	14	1	1	144	0.15	0.20	0.4	20736	0.0225
15	196	15	1	1	60	0.15	0.75	0.4	3600	0.0225
16	166	16	1	1	25	0.15	0.45	0.4	625	0.0225
17	93	17	1	1	25	0.30	0.20	1.6	625	0.0900
18	76	18	1	1	144	0.75	0.45	0.4	20736	0.5625
19	110	19	1	1	60	0.15	0.20	0.8	3600	0.0225
20	198	20	1	1	60	0.15	0.75	1.6	3600	0.0225
21	74	21	1	1	144	0.75	0.20	0.8	20736	0.5625
22	187	22	1	1	25	0.75	0.75	0.4	625	0.5625
23	202	23	1	1	60	0.30	0.45	0.4	3600	0.0900
24	209	24	1	1	60	0.75	0.20	0.8	3600	0.5625
25	21	25	1	1	25	0.75	0.20	1.6	625	0.5625
26	172	26	1	1	25	0.30	0.20	0.4	625	0.0900
27	150	27	1	1	144	0.30	0.45	1.6	20736	0.0900
28	97	28	1	1	25	0.30	0.75	0.4	625	0.0900
29	120	29	1	1	60	0.30	0.20	1.6	3600	0.0900
30	206	30	1	1	60	0.30	0.75	0.8	3600	0.0900
31	174	31	1	1	25	0.30	0.20	1.6	625	0.0900
32	221	32	1	1	144	0.15	0.45	0.8	20736	0.0225
33	2	33	1	1	25	0.15	0.20	0.8	625	0.0225
34	48	34	1	1	60	0.75	0.20	1.6	3600	0.5625
35	39	35	1	1	60	0.30	0.20	1.6	3600	0.0900
36	178	36	1	1	25	0.30	0.75	0.4	625	0.0900
37	214	37	1	1	60	0.75	0.75	0.4	3600	0.5625
38	212	38	1	1	60	0.75	0.45	0.8	3600	0.5625
39	75	39	1	1	144	0.75	0.20	1.6	20736	0.5625
40	147	40	1	1	144	0.30	0.20	1.6	20736	0.0900
41	132	41	1	1	60	0.75	0.45	1.6	3600	0.5625
42	160	42	1	1	144	0.75	0.75	0.4	20736	0.5625
43	125	43	1	1	60	0.30	0.75	0.8	3600	0.0900
44	116	44	1	1	60	0.15	0.75	0.8	3600	0.0225
45	180	45	1	1	25	0.30	0.75	1.6	625	0.0900
46	165	46	1	1	25	0.15	0.20	1.6	625	0.0225
47	177	47	1	1	25	0.30	0.45	1.6	625	0.0900
48	85	48	1	1	25	0.15	0.45	0.4	625	0.0225
49	82	49	1	1	25	0.15	0.20	0.4	625	0.0225

Table 6.2 The regression result by Minitab software

	C1	C2	C3	C4	C5	C6	C7	C8	C9	C10
	StdOrder	RunOrder	PtType	Blocks	v	f	d	r	v*v	f*f
50	190	50	1	1	60	0.15	0.20	0.4	3600	0.0225
51	22	51	1	1	25	0.75	0.45	0.4	625	0.5625
52	69	52	1	1	144	0.30	0.45	1.6	20736	0.0900
53	159	53	1	1	144	0.75	0.45	1.6	20736	0.5625
54	13	54	1	1	25	0.30	0.45	0.4	625	0.0900
55	114	55	1	1	60	0.15	0.45	1.6	3600	0.0225
56	100	56	1	1	25	0.75	0.20	0.4	625	0.5625
57	29	57	1	1	60	0.15	0.20	0.8	3600	0.0225
58	128	58	1	1	60	0.75	0.20	0.8	3600	0.5625
59	84	59	1	1	25	0.15	0.20	1.6	625	0.0225
60	200	60	1	1	60	0.30	0.20	0.8	3600	0.0900
61	239	61	1	1	144	0.75	0.45	0.8	20736	0.5625
62	20	62	1	1	25	0.75	0.20	0.8	625	0.5625
63	19	63	1	1	25	0.75	0.20	0.4	625	0.5625
64	161	64	1	1	144	0.75	0.75	0.8	20736	0.5625
65	204	65	1	1	60	0.30	0.45	1.6	3600	0.0900
66	81	66	1	1	144	0.75	0.75	1.6	20736	0.5625
67	185	67	1	1	25	0.75	0.45	0.8	625	0.5625
68	109	68	1	1	60	0.15	0.20	0.4	3600	0.0225
69	10	69	1	1	25	0.30	0.20	0.4	625	0.0900
70	201	70	1	1	60	0.30	0.20	1.6	3600	0.0900
71	151	71	1	1	144	0.30	0.75	0.4	20736	0.0900
72	137	72	1	1	144	0.15	0.20	0.8	20736	0.0225
73	30	73	1	1	60	0.15	0.20	1.6	3600	0.0225
74	63	74	1	1	144	0.15	0.75	1.6	20736	0.0225
75	4	75	1	1	25	0.15	0.45	0.4	625	0.0225
76	154	76	1	1	144	0.75	0.20	0.4	20736	0.5625
77	80	77	1	1	144	0.75	0.75	0.8	20736	0.5625
78	121	78	1	1	60	0.30	0.45	0.4	3600	0.0900
79	133	79	1	1	60	0.75	0.75	0.4	3600	0.5625
80	144	80	1	1	144	0.15	0.75	1.6	20736	0.0225
81	155	81	1	1	144	0.75	0.20	0.8	20736	0.5625
82	40	82	1	1	60	0.30	0.45	0.4	3600	0.0900
83	189	83	1	1	25	0.75	0.75	1.6	625	0.5625
84	112	84	1	1	60	0.15	0.45	0.4	3600	0.0225
85	115	85	1	1	60	0.15	0.75	0.4	3600	0.0225
86	25	86	1	1	25	0.75	0.75	0.4	625	0.5625
87	186	87	1	1	25	0.75	0.45	1.6	625	0.5625
88	58	88	1	1	144	0.15	0.45	0.4	20736	0.0225
89	79	89	1	1	144	0.75	0.75	0.4	20736	0.5625
90	101	90	1	1	25	0.75	0.20	0.8	625	0.5625
91	231	91	1	1	144	0.30	0.45	1.6	20736	0.0900
92	98	92	1	1	25	0.30	0.75	0.8	625	0.0900
93	119	93	1	1	60	0.30	0.20	0.8	3600	0.0900
94	210	94	1	1	60	0.75	0.20	1.6	3600	0.5625
95	157	95	1	1	144	0.75	0.45	0.4	20736	0.5625
96	216	96	1	1	60	0.75	0.75	1.6	3600	0.5625
97	227	97	1	1	144	0.30	0.20	0.8	20736	0.0900
98	140	98	1	1	144	0.15	0.45	0.8	20736	0.0225

Table 6.3 The regression result by Minitab software

	C1	C2	C3	C4	C5	C6	C7	C8	C9	C10
	StdOrder	RunOrder	PtType	Blocks	v	f	d	r	v*v	f*f
99	9	99	1	1	25	0.15	0.75	1.6	625	0.0225
100	138	100	1	1	144	0.15	0.20	1.6	20736	0.0225
101	103	101	1	1	25	0.75	0.45	0.4	625	0.5625
102	237	102	1	1	144	0.75	0.20	1.6	20736	0.5625
103	91	103	1	1	25	0.30	0.20	0.4	625	0.0900
104	72	104	1	1	144	0.30	0.75	1.6	20736	0.0900
105	122	105	1	1	60	0.30	0.45	0.8	3600	0.0900
106	136	106	1	1	144	0.15	0.20	0.4	20736	0.0225
107	45	107	1	1	60	0.30	0.75	1.6	3600	0.0900
108	118	108	1	1	60	0.30	0.20	0.4	3600	0.0900
109	54	109	1	1	60	0.75	0.75	1.6	3600	0.5625
110	217	110	1	1	144	0.15	0.20	0.4	20736	0.0225
111	236	111	1	1	144	0.75	0.20	0.8	20736	0.5625
112	223	112	1	1	144	0.15	0.75	0.4	20736	0.0225
113	5	113	1	1	25	0.15	0.45	0.8	625	0.0225
114	234	114	1	1	144	0.30	0.75	1.6	20736	0.0900
115	182	115	1	1	25	0.75	0.20	0.8	625	0.5625
116	199	116	1	1	60	0.30	0.20	0.4	3600	0.0900
117	179	117	1	1	25	0.30	0.75	0.8	625	0.0900
118	64	118	1	1	144	0.30	0.20	0.4	20736	0.0900
119	37	119	1	1	60	0.30	0.20	0.4	3600	0.0900
120	104	120	1	1	25	0.75	0.45	0.8	625	0.5625
121	46	121	1	1	60	0.75	0.20	0.4	3600	0.5625
122	78	122	1	1	144	0.75	0.45	1.6	20736	0.5625
123	3	123	1	1	25	0.15	0.20	1.6	625	0.0225
124	1	124	1	1	25	0.15	0.20	0.4	625	0.0225
125	123	125	1	1	60	0.30	0.45	1.6	3600	0.0900
126	92	126	1	1	25	0.30	0.20	0.8	625	0.0900
127	148	127	1	1	144	0.30	0.45	0.4	20736	0.0900
128	28	128	1	1	60	0.15	0.20	0.4	3600	0.0225
129	241	129	1	1	144	0.75	0.75	0.4	20736	0.5625
130	34	130	1	1	60	0.15	0.75	0.4	3600	0.0225
131	242	131	1	1	144	0.75	0.75	0.8	20736	0.5625
132	171	132	1	1	25	0.15	0.75	1.6	625	0.0225
133	83	133	1	1	25	0.15	0.20	0.8	625	0.0225
134	228	134	1	1	144	0.30	0.20	1.6	20736	0.0900
135	143	135	1	1	144	0.15	0.75	0.8	20736	0.0225
136	139	136	1	1	144	0.15	0.45	0.4	20736	0.0225
137	164	137	1	1	25	0.15	0.20	0.8	625	0.0225
138	15	138	1	1	25	0.30	0.45	1.6	625	0.0900
139	71	139	1	1	144	0.30	0.75	0.8	20736	0.0900
140	162	140	1	1	144	0.75	0.75	1.6	20736	0.5625
141	218	141	1	1	144	0.15	0.20	0.8	20736	0.0225
142	232	142	1	1	144	0.30	0.75	0.4	20736	0.0900
143	197	143	1	1	60	0.15	0.75	0.8	3600	0.0225
144	168	144	1	1	25	0.15	0.45	1.6	625	0.0225
145	77	145	1	1	144	0.75	0.45	0.8	20736	0.5625
146	158	146	1	1	144	0.75	0.45	0.8	20736	0.5625
147	152	147	1	1	144	0.30	0.75	0.8	20736	0.0900

Table 6.4 The regression result by Minitab software

	C1	C2	C3	C4	C5	C6	C7	C8	C9	C10
	StdOrder	RunOrder	PtType	Blocks	v	f	d	r	v*v	f*f
148	8	148	1	1	25	0.15	0.75	0.8	625	0.0225
149	207	149	1	1	60	0.30	0.75	1.6	3600	0.0900
150	205	150	1	1	60	0.30	0.75	0.4	3600	0.0900
151	24	151	1	1	25	0.75	0.45	1.6	625	0.5625
152	243	152	1	1	144	0.75	0.75	1.6	20736	0.5625
153	32	153	1	1	60	0.15	0.45	0.8	3600	0.0225
154	94	154	1	1	25	0.30	0.45	0.4	625	0.0900
155	134	155	1	1	60	0.75	0.75	0.8	3600	0.5625
156	96	156	1	1	25	0.30	0.45	1.6	625	0.0900
157	173	157	1	1	25	0.30	0.20	0.8	625	0.0900
158	87	158	1	1	25	0.15	0.45	1.6	625	0.0225
159	145	159	1	1	144	0.30	0.20	0.4	20736	0.0900
160	14	160	1	1	25	0.30	0.45	0.8	625	0.0900
161	59	161	1	1	144	0.15	0.45	0.8	20736	0.0225
162	23	162	1	1	25	0.75	0.45	0.8	625	0.5625
163	66	163	1	1	144	0.30	0.20	1.6	20736	0.0900
164	170	164	1	1	25	0.15	0.75	0.8	625	0.0225
165	6	165	1	1	25	0.15	0.45	1.6	625	0.0225
166	129	166	1	1	60	0.75	0.20	1.6	3600	0.5625
167	181	167	1	1	25	0.75	0.20	0.4	625	0.5625
168	219	168	1	1	144	0.15	0.20	1.6	20736	0.0225
169	230	169	1	1	144	0.30	0.45	0.8	20736	0.0900
170	176	170	1	1	25	0.30	0.45	0.8	625	0.0900
171	73	171	1	1	144	0.75	0.20	0.4	20736	0.5625
172	167	172	1	1	25	0.15	0.45	0.8	625	0.0225
173	65	173	1	1	144	0.30	0.20	0.8	20736	0.0900
174	41	174	1	1	60	0.30	0.45	0.8	3600	0.0900
175	49	175	1	1	60	0.75	0.45	0.4	3600	0.5625
176	224	176	1	1	144	0.15	0.75	0.8	20736	0.0225
177	130	177	1	1	60	0.75	0.45	0.4	3600	0.5625
178	70	178	1	1	144	0.30	0.75	0.4	20736	0.0900
179	47	179	1	1	60	0.75	0.20	0.8	3600	0.5625
180	99	180	1	1	25	0.30	0.75	1.6	625	0.0900
181	56	181	1	1	144	0.15	0.20	0.8	20736	0.0225
182	106	182	1	1	25	0.75	0.75	0.4	625	0.5625
183	67	183	1	1	144	0.30	0.45	0.4	20736	0.0900
184	102	184	1	1	25	0.75	0.20	1.6	625	0.5625
185	68	185	1	1	144	0.30	0.45	0.8	20736	0.0900
186	191	186	1	1	60	0.15	0.20	0.8	3600	0.0225
187	95	187	1	1	25	0.30	0.45	0.8	625	0.0900
188	18	188	1	1	25	0.30	0.75	1.6	625	0.0900
189	62	189	1	1	144	0.15	0.75	0.8	20736	0.0225
190	233	190	1	1	144	0.30	0.75	0.8	20736	0.0900
191	149	191	1	1	144	0.30	0.45	0.8	20736	0.0900
192	184	192	1	1	25	0.75	0.45	0.4	625	0.5625
193	11	193	1	1	25	0.30	0.20	0.8	625	0.0900
194	42	194	1	1	60	0.30	0.45	1.6	3600	0.0900
195	89	195	1	1	25	0.15	0.75	0.8	625	0.0225
196	27	196	1	1	25	0.75	0.75	1.6	625	0.5625

Table 6.5 The regression result by Minitab software

	C1	C2	C3	C4	C5	C6	C7	C8	C9	C10
	StdOrder	RunOrder	PtType	Blocks	v	f	d	r	v*v	f*f
197	107	197	1	1	25	0.75	0.75	0.8	625	0.5625
198	90	198	1	1	25	0.15	0.75	1.6	625	0.0225
199	113	199	1	1	60	0.15	0.45	0.8	3600	0.0225
200	17	200	1	1	25	0.30	0.75	0.8	625	0.0900
201	86	201	1	1	25	0.15	0.45	0.8	625	0.0225
202	188	202	1	1	25	0.75	0.75	0.8	625	0.5625
203	127	203	1	1	60	0.75	0.20	0.4	3600	0.5625
204	135	204	1	1	60	0.75	0.75	1.6	3600	0.5625
205	240	205	1	1	144	0.75	0.45	1.6	20736	0.5625
206	33	206	1	1	60	0.15	0.45	1.6	3600	0.0225
207	153	207	1	1	144	0.30	0.75	1.6	20736	0.0900
208	36	208	1	1	60	0.15	0.75	1.6	3600	0.0225
209	51	209	1	1	60	0.75	0.45	1.6	3600	0.5625
210	213	210	1	1	60	0.75	0.45	1.6	3600	0.5625
211	215	211	1	1	60	0.75	0.75	0.8	3600	0.5625
212	156	212	1	1	144	0.75	0.20	1.6	20736	0.5625
213	238	213	1	1	144	0.75	0.45	0.4	20736	0.5625
214	142	214	1	1	144	0.15	0.75	0.4	20736	0.0225
215	60	215	1	1	144	0.15	0.45	1.6	20736	0.0225
216	7	216	1	1	25	0.15	0.75	0.4	625	0.0225
217	175	217	1	1	25	0.30	0.45	0.4	625	0.0900
218	105	218	1	1	25	0.75	0.45	1.6	625	0.5625
219	61	219	1	1	144	0.15	0.75	0.4	20736	0.0225
220	31	220	1	1	60	0.15	0.45	0.4	3600	0.0225
221	16	221	1	1	25	0.30	0.75	0.4	625	0.0900
222	235	222	1	1	144	0.75	0.20	0.4	20736	0.5625
223	52	223	1	1	60	0.75	0.75	0.4	3600	0.5625
224	57	224	1	1	144	0.15	0.20	1.6	20736	0.0225
225	208	225	1	1	60	0.75	0.20	0.4	3600	0.5625
226	195	226	1	1	60	0.15	0.45	1.6	3600	0.0225
227	126	227	1	1	60	0.30	0.75	1.6	3600	0.0900
228	211	228	1	1	60	0.75	0.45	0.4	3600	0.5625
229	220	229	1	1	144	0.15	0.45	0.4	20736	0.0225
230	108	230	1	1	25	0.75	0.75	1.6	625	0.5625
231	111	231	1	1	60	0.15	0.20	1.6	3600	0.0225
232	131	232	1	1	60	0.75	0.45	0.8	3600	0.5625
233	225	233	1	1	144	0.15	0.75	1.6	20736	0.0225
234	163	234	1	1	25	0.15	0.20	0.4	625	0.0225
235	194	235	1	1	60	0.15	0.45	0.8	3600	0.0225
236	222	236	1	1	144	0.15	0.45	1.6	20736	0.0225
237	88	237	1	1	25	0.15	0.75	0.4	625	0.0225
238	35	238	1	1	60	0.15	0.75	0.8	3600	0.0225
239	193	239	1	1	60	0.15	0.45	0.4	3600	0.0225
240	12	240	1	1	25	0.30	0.20	1.6	625	0.0900
241	226	241	1	1	144	0.30	0.20	0.4	20736	0.0900
242	141	242	1	1	144	0.15	0.45	1.6	20736	0.0225
243	60	243	1	1	60	0.75	0.45	0.8	3600	0.5625

Table 6.6 The regression result by Minitab software

	C11	C12	C13	C14	C15	C16	C17	C18	C19	C20
	d*d	r*r	v*d	v*r	f*d	f*r	d*r	Ra	T	Fc
1	0.0400	2.56	5.00	40.0	0.1500	1.20	0.32	0.0281250	8.730	3.033
2	0.5625	2.56	45.00	96.0	0.1125	0.24	1.20	0.0011250	15.714	4.095
3	0.5625	0.64	45.00	48.0	0.5625	0.60	0.60	0.0140625	78.569	102.372
4	0.0400	0.64	28.80	115.2	0.0600	0.24	0.16	0.0022500	20.114	2.795
5	0.2025	0.64	27.00	48.0	0.1350	0.24	0.36	0.0022500	18.857	5.897
6	0.5625	0.64	18.75	20.0	0.5625	0.60	0.60	0.0140625	32.737	42.655
7	0.5625	0.16	18.75	10.0	0.1125	0.06	0.30	0.0002812	6.547	1.706
8	0.5625	0.16	45.00	24.0	0.2250	0.12	0.30	0.0011250	31.428	16.380
9	0.0400	2.56	12.00	96.0	0.0300	0.24	0.32	0.0011250	4.190	0.291
10	0.5625	0.64	45.00	48.0	0.2250	0.24	0.60	0.0022500	31.428	16.380
11	0.2025	0.16	64.80	57.6	0.1350	0.12	0.18	0.0011250	45.256	14.152
12	0.5625	0.16	45.00	24.0	0.2250	0.12	0.30	0.0011250	31.428	16.380
13	0.0400	0.64	12.00	48.0	0.0600	0.24	0.16	0.0022500	8.381	1.165
14	0.0400	0.16	28.80	57.6	0.0300	0.06	0.08	0.0002812	10.057	0.699
15	0.5625	0.16	45.00	24.0	0.1125	0.06	0.30	0.0002812	15.714	4.095
16	0.2025	0.16	11.25	10.0	0.0675	0.06	0.18	0.0002812	3.928	0.614
17	0.0400	2.56	5.00	40.0	0.0600	0.48	0.32	0.0045000	3.492	0.485
18	0.2025	0.16	64.80	57.6	0.3375	0.30	0.18	0.0070313	113.140	88.450
19	0.0400	0.64	12.00	48.0	0.0300	0.12	0.16	0.0005625	4.190	0.291
20	0.5625	2.56	45.00	96.0	0.1125	0.24	1.20	0.0011250	15.714	4.095
21	0.0400	0.64	28.80	115.2	0.1500	0.60	0.16	0.0140625	50.284	17.472
22	0.5625	0.16	18.75	10.0	0.5625	0.30	0.30	0.0070313	32.737	42.655
23	0.2025	0.16	27.00	24.0	0.1350	0.12	0.18	0.0011250	18.857	5.897
24	0.0400	0.64	12.00	48.0	0.1500	0.60	0.16	0.0140625	20.952	7.280
25	0.0400	2.56	5.00	40.0	0.1500	1.20	0.32	0.0281250	8.730	3.033
26	0.0400	0.16	5.00	10.0	0.0600	0.12	0.08	0.0011250	3.492	0.485
27	0.2025	2.56	64.80	230.4	0.1350	0.48	0.72	0.0045000	45.256	14.152
28	0.5625	0.16	18.75	10.0	0.2250	0.12	0.30	0.0011250	13.095	6.825
29	0.0400	2.56	12.00	96.0	0.0600	0.48	0.32	0.0045000	8.381	1.165
30	0.5625	0.64	45.00	48.0	0.2250	0.24	0.60	0.0022500	31.428	16.380
31	0.0400	2.56	5.00	40.0	0.0600	0.48	0.32	0.0045000	3.492	0.485
32	0.2025	0.64	64.80	115.2	0.0675	0.12	0.36	0.0005625	22.628	3.538
33	0.0400	0.64	5.00	20.0	0.0300	0.12	0.16	0.0005625	1.746	0.121
34	0.0400	2.56	12.00	96.0	0.1500	1.20	0.32	0.0281250	20.952	7.280
35	0.0400	2.56	12.00	96.0	0.0600	0.48	0.32	0.0045000	8.381	1.165
36	0.5625	0.16	18.75	10.0	0.2250	0.12	0.30	0.0011250	13.095	6.825
37	0.5625	0.16	45.00	24.0	0.5625	0.30	0.30	0.0070313	78.569	102.372
38	0.2025	0.64	27.00	48.0	0.3375	0.60	0.36	0.0140625	47.142	36.854
39	0.0400	2.56	28.80	230.4	0.1500	1.20	0.32	0.0281250	50.284	17.472
40	0.0400	2.56	28.80	230.4	0.0600	0.48	0.32	0.0045000	20.114	2.795
41	0.2025	2.56	27.00	96.0	0.3375	1.20	0.72	0.0281250	47.142	36.854
42	0.5625	0.16	108.00	57.6	0.5625	0.30	0.30	0.0070313	188.566	245.694
43	0.5625	0.64	45.00	48.0	0.2250	0.24	0.60	0.0022500	31.428	16.380
44	0.5625	0.64	45.00	48.0	0.1125	0.12	0.60	0.0005625	15.714	4.095
45	0.5625	2.56	18.75	40.0	0.2250	0.48	1.20	0.0045000	13.095	6.825
46	0.0400	2.56	5.00	40.0	0.0300	0.24	0.32	0.0011250	1.746	0.121
47	0.2025	2.56	11.25	40.0	0.1350	0.48	0.72	0.0045000	7.857	2.457
48	0.2025	0.16	11.25	10.0	0.0675	0.06	0.18	0.0002812	3.928	0.614
49	0.0400	0.16	5.00	10.0	0.0300	0.06	0.08	0.0002812	1.746	0.121

Table 6.7 The regression result by Minitab software

	C11	C12	C13	C14	C15	C16	C17	C18	C19	C20
	d*d	r*r	v*d	v*r	f*d	f*r	d*r	Ra	T	Fc
50	0.0400	0.16	12.00	24.0	0.0300	0.06	0.08	0.0002812	4.190	0.291
51	0.2025	0.16	11.25	10.0	0.3375	0.30	0.18	0.0070313	19.642	15.356
52	0.2025	2.56	64.80	230.4	0.1350	0.48	0.72	0.0045000	45.256	14.152
53	0.2025	2.56	64.80	230.4	0.3375	1.20	0.72	0.0281250	113.140	88.450
54	0.2025	0.16	11.25	10.0	0.1350	0.12	0.18	0.0011250	7.867	2.457
55	0.2025	2.56	27.00	96.0	0.0675	0.24	0.72	0.0011250	9.428	1.474
56	0.0400	0.16	5.00	10.0	0.1500	0.30	0.08	0.0070313	8.730	3.033
57	0.0400	0.64	12.00	48.0	0.0300	0.12	0.16	0.0005625	4.190	0.291
58	0.0400	0.64	12.00	48.0	0.1500	0.60	0.16	0.0140625	20.952	7.280
59	0.0400	2.56	5.00	40.0	0.0300	0.24	0.32	0.0011250	1.746	0.121
60	0.0400	0.64	12.00	48.0	0.0600	0.24	0.16	0.0022500	8.381	1.165
61	0.2025	0.64	64.80	115.2	0.3375	0.60	0.36	0.0140625	113.140	88.450
62	0.0400	0.64	5.00	20.0	0.1500	0.60	0.16	0.0140625	8.730	3.033
63	0.0400	0.16	5.00	10.0	0.1500	0.30	0.08	0.0070313	8.730	3.033
64	0.5625	0.64	108.00	115.2	0.5625	0.60	0.60	0.0140625	188.566	245.694
65	0.2025	2.56	27.00	96.0	0.1350	0.48	0.72	0.0045000	18.857	5.897
66	0.5625	2.56	108.00	230.4	0.5625	1.20	1.20	0.0281250	188.566	245.694
67	0.2025	0.64	11.25	20.0	0.3375	0.60	0.36	0.0140625	19.642	15.356
68	0.0400	0.16	12.00	24.0	0.0300	0.06	0.08	0.0002812	4.190	0.291
69	0.0400	0.16	5.00	10.0	0.0600	0.12	0.08	0.0011250	3.492	0.485
70	0.0400	2.56	12.00	96.0	0.0600	0.48	0.32	0.0045000	8.381	1.165
71	0.5625	0.16	108.00	57.6	0.2250	0.12	0.30	0.0011250	75.426	39.311
72	0.0400	0.64	28.80	115.2	0.0300	0.12	0.16	0.0005625	10.057	0.699
73	0.0400	2.56	12.00	96.0	0.0300	0.24	0.32	0.0011250	4.190	0.291
74	0.5625	2.56	108.00	230.4	0.1125	0.24	1.20	0.0011250	37.713	9.828
75	0.2025	0.16	11.25	10.0	0.0675	0.06	0.18	0.0002812	3.928	0.614
76	0.0400	0.16	28.80	57.6	0.1500	0.30	0.08	0.0070313	50.284	17.472
77	0.5625	0.64	108.00	115.2	0.5625	0.60	0.60	0.0140625	188.566	245.694
78	0.2025	0.16	27.00	24.0	0.1350	0.12	0.18	0.0011250	18.857	5.897
79	0.5625	0.16	45.00	24.0	0.5625	0.30	0.30	0.0070313	78.569	102.372
80	0.5625	2.56	108.00	230.4	0.1125	0.24	1.20	0.0011250	37.713	9.828
81	0.0400	0.64	28.80	115.2	0.1500	0.60	0.16	0.0140625	50.284	17.472
82	0.2025	0.16	27.00	24.0	0.1350	0.12	0.18	0.0011250	18.857	5.897
83	0.5625	2.56	18.75	40.0	0.5625	1.20	1.20	0.0281250	32.737	42.655
84	0.2025	0.16	27.00	24.0	0.0675	0.06	0.18	0.0002812	9.428	1.474
85	0.5625	0.16	45.00	24.0	0.1125	0.06	0.30	0.0002812	15.714	4.095
86	0.5625	0.16	18.75	10.0	0.5625	0.30	0.30	0.0070313	32.737	42.655
87	0.2025	2.56	11.25	40.0	0.3375	1.20	0.72	0.0281250	19.642	15.356
88	0.2025	0.16	64.80	57.6	0.0675	0.06	0.18	0.0002812	22.628	3.538
89	0.5625	0.16	108.00	57.6	0.5625	0.30	0.30	0.0070313	188.566	245.694
90	0.0400	0.64	5.00	20.0	0.1500	0.60	0.16	0.0140625	8.730	3.033
91	0.2025	2.56	64.80	230.4	0.1350	0.48	0.72	0.0045000	45.256	14.152
92	0.5625	0.64	18.75	20.0	0.2250	0.24	0.60	0.0022500	13.095	6.825
93	0.0400	0.64	12.00	48.0	0.0600	0.24	0.16	0.0022500	8.381	1.165
94	0.0400	2.56	12.00	96.0	0.1500	1.20	0.32	0.0281250	20.952	7.280
95	0.2025	0.16	64.80	57.6	0.3375	0.30	0.18	0.0070313	113.140	88.450
96	0.5625	2.56	45.00	96.0	0.5625	1.20	1.20	0.0281250	78.569	102.372
97	0.0400	0.64	28.80	115.2	0.0600	0.24	0.16	0.0022500	20.114	2.795
98	0.2025	0.64	64.80	115.2	0.0675	0.12	0.36	0.0005625	22.628	3.538

Table 6.8 The regression result by Minitab software

	C11	C12	C13	C14	C15	C16	C17	C18	C19	C20
	d*d	r*r	v*d	v*r	f*d	f*r	d*r	Ra	T	Fc
99	0.5625	2.56	18.75	40.0	0.1125	0.24	1.20	0.0011250	6.547	1.706
100	0.0400	2.56	28.80	230.4	0.0300	0.24	0.32	0.0011250	10.057	0.699
101	0.2025	0.16	11.25	10.0	0.3375	0.30	0.18	0.0070313	19.642	15.356
102	0.0400	2.56	28.80	230.4	0.1500	1.20	0.32	0.0281250	50.284	17.472
103	0.0400	0.16	5.00	10.0	0.0600	0.12	0.08	0.0011250	3.492	0.485
104	0.5625	2.56	108.00	230.4	0.2250	0.48	1.20	0.0045000	75.426	39.311
105	0.2025	0.64	27.00	48.0	0.1350	0.24	0.36	0.0022500	18.857	5.897
106	0.0400	0.16	28.80	57.6	0.0300	0.06	0.08	0.0002812	10.057	0.699
107	0.5625	2.56	45.00	96.0	0.2250	0.48	1.20	0.0045000	31.428	16.380
108	0.0400	0.16	12.00	24.0	0.0600	0.12	0.08	0.0011250	8.381	1.165
109	0.5625	2.56	45.00	96.0	0.5625	1.20	1.20	0.0281250	78.569	102.372
110	0.0400	0.16	28.80	57.6	0.0300	0.06	0.08	0.0002812	10.057	0.699
111	0.0400	0.64	28.80	115.2	0.1500	0.60	0.16	0.0140625	50.284	17.472
112	0.5625	0.16	108.00	57.6	0.1125	0.06	0.30	0.0002812	37.713	9.828
113	0.2025	0.64	11.25	20.0	0.0675	0.12	0.36	0.0005625	3.928	0.614
114	0.5625	2.56	108.00	230.4	0.2250	0.48	1.20	0.0045000	75.426	39.311
115	0.0400	0.64	5.00	20.0	0.1500	0.60	0.16	0.0140625	8.730	3.033
116	0.0400	0.16	12.00	24.0	0.0600	0.12	0.08	0.0011250	8.381	1.165
117	0.5625	0.64	18.75	20.0	0.2250	0.24	0.60	0.0022500	13.095	6.825
118	0.0400	0.16	28.80	57.6	0.0600	0.12	0.08	0.0011250	20.114	2.795
119	0.0400	0.16	12.00	24.0	0.0600	0.12	0.08	0.0011250	8.381	1.165
120	0.2025	0.64	11.25	20.0	0.3375	0.60	0.36	0.0140625	19.642	15.356
121	0.0400	0.16	12.00	24.0	0.1500	0.30	0.08	0.0070313	20.952	7.280
122	0.2025	2.56	64.80	230.4	0.3375	1.20	0.72	0.0281250	113.140	88.450
123	0.0400	2.56	5.00	40.0	0.0300	0.24	0.32	0.0011250	1.746	0.121
124	0.0400	0.16	5.00	10.0	0.0300	0.06	0.08	0.0002812	1.746	0.121
125	0.2025	2.56	27.00	96.0	0.1350	0.48	0.72	0.0045000	18.857	5.897
126	0.0400	0.64	5.00	20.0	0.0600	0.24	0.16	0.0022500	3.492	0.485
127	0.2025	0.16	64.80	57.6	0.1350	0.12	0.18	0.0011250	45.256	14.152
128	0.0400	0.16	12.00	24.0	0.0300	0.06	0.08	0.0002812	4.190	0.291
129	0.5625	0.16	108.00	57.6	0.5625	0.30	0.30	0.0070313	188.566	245.694
130	0.5625	0.16	45.00	24.0	0.1125	0.06	0.30	0.0002812	15.714	4.095
131	0.5625	0.64	108.00	115.2	0.5625	0.60	0.60	0.0140625	188.566	245.694
132	0.5625	2.56	18.75	40.0	0.1125	0.24	1.20	0.0011250	6.547	1.706
133	0.0400	0.64	5.00	20.0	0.0300	0.12	0.16	0.0005625	1.746	0.121
134	0.0400	2.56	28.80	230.4	0.0600	0.48	0.32	0.0045000	20.114	2.795
135	0.5625	0.64	108.00	115.2	0.1125	0.12	0.60	0.0005625	37.713	9.828
136	0.2025	0.16	64.80	57.6	0.0675	0.06	0.18	0.0002812	22.628	3.538
137	0.0400	0.64	5.00	20.0	0.0300	0.12	0.16	0.0005625	1.746	0.121
138	0.2025	2.56	11.25	40.0	0.1350	0.48	0.72	0.0045000	7.857	2.457
139	0.5625	0.64	108.00	115.2	0.2250	0.24	0.60	0.0022500	75.426	39.311
140	0.5625	2.56	108.00	230.4	0.5625	1.20	1.20	0.0281250	188.566	245.694
141	0.0400	0.64	28.80	115.2	0.0300	0.12	0.16	0.0005625	10.057	0.699
142	0.5625	0.16	108.00	57.6	0.2250	0.12	0.30	0.0011250	75.426	39.311
143	0.5625	0.64	45.00	48.0	0.1125	0.12	0.60	0.0005625	15.714	4.095
144	0.2025	2.56	11.25	40.0	0.0675	0.24	0.72	0.0011250	3.928	0.614
145	0.2025	0.64	64.80	115.2	0.3375	0.60	0.36	0.0140625	113.140	88.450
146	0.2025	0.64	64.80	115.2	0.3375	0.60	0.36	0.0140625	113.140	88.450
147	0.5625	0.64	108.00	115.2	0.2250	0.24	0.60	0.0022500	75.426	39.311

Table 6.9 The regression result by Minitab software

	C11	C12	C13	C14	C15	C16	C17	C18	C19	C20
	d*d	r*r	v*d	v*r	f*d	f*r	d*r	Ra	T	Fc
148	0.5625	0.64	18.75	20.0	0.1125	0.12	0.60	0.0005625	6.547	1.706
149	0.5625	2.56	45.00	96.0	0.2250	0.48	1.20	0.0045000	31.428	16.380
150	0.5625	0.16	45.00	24.0	0.2250	0.12	0.30	0.0011250	31.428	16.380
151	0.2025	2.56	11.25	40.0	0.3375	1.20	0.72	0.0281250	19.642	15.356
152	0.5625	2.56	108.00	230.4	0.5625	1.20	1.20	0.0281250	188.566	245.694
153	0.2025	0.64	27.00	48.0	0.0675	0.12	0.36	0.0005625	9.428	1.474
154	0.2025	0.16	11.25	10.0	0.1350	0.12	0.18	0.0011250	7.857	2.457
155	0.5625	0.64	45.00	48.0	0.5625	0.60	0.60	0.0140625	78.569	102.372
156	0.2025	2.56	11.25	40.0	0.1350	0.48	0.72	0.0045000	7.857	2.457
157	0.0400	0.64	5.00	20.0	0.0600	0.24	0.16	0.0022500	3.492	0.485
158	0.2025	2.56	11.25	40.0	0.0675	0.24	0.72	0.0011250	3.928	0.614
159	0.0400	0.16	28.80	57.6	0.0600	0.12	0.08	0.0011250	20.114	2.795
160	0.2025	0.64	11.25	20.0	0.1350	0.24	0.36	0.0022500	7.857	2.457
161	0.2025	0.64	64.80	115.2	0.0675	0.12	0.36	0.0005625	22.628	3.538
162	0.2025	0.64	11.25	20.0	0.3375	0.60	0.36	0.0140625	19.642	15.356
163	0.0400	2.56	28.80	230.4	0.0600	0.48	0.32	0.0045000	20.114	2.795
164	0.5625	0.64	18.75	20.0	0.1125	0.12	0.60	0.0005625	6.547	1.706
165	0.2025	2.56	11.25	40.0	0.0675	0.24	0.72	0.0011250	3.928	0.614
166	0.0400	2.56	12.00	96.0	0.1500	1.20	0.32	0.0281250	20.952	7.280
167	0.0400	0.16	5.00	10.0	0.1500	0.30	0.08	0.0070313	8.730	3.033
168	0.0400	2.56	28.80	230.4	0.0300	0.24	0.32	0.0011250	10.057	0.699
169	0.2025	0.64	64.80	115.2	0.1350	0.24	0.36	0.0022500	45.256	14.152
170	0.2025	0.64	11.25	20.0	0.1350	0.24	0.36	0.0022500	7.857	2.457
171	0.0400	0.16	28.80	57.6	0.1500	0.30	0.08	0.0070313	50.284	17.472
172	0.2025	0.64	11.25	20.0	0.0675	0.12	0.36	0.0005625	3.928	0.614
173	0.0400	0.64	28.80	115.2	0.0600	0.24	0.16	0.0022500	20.114	2.795
174	0.2025	0.64	27.00	48.0	0.1350	0.24	0.36	0.0022500	18.857	5.897
175	0.2025	0.16	27.00	24.0	0.3375	0.30	0.18	0.0070313	47.142	36.854
176	0.5625	0.64	108.00	115.2	0.1125	0.12	0.60	0.0005625	37.713	9.828
177	0.2025	0.16	27.00	24.0	0.3375	0.30	0.18	0.0070313	47.142	36.854
178	0.5625	0.16	108.00	57.6	0.2250	0.12	0.30	0.0011250	75.426	39.311
179	0.0400	0.64	12.00	48.0	0.1500	0.60	0.16	0.0140625	20.952	7.280
180	0.5625	2.56	18.75	40.0	0.2250	0.48	1.20	0.0045000	13.095	6.825
181	0.0400	0.64	28.80	115.2	0.0300	0.12	0.16	0.0005625	10.057	0.699
182	0.5625	0.16	18.75	10.0	0.5625	0.30	0.30	0.0070313	32.737	42.655
183	0.2025	0.16	64.80	57.6	0.1350	0.12	0.18	0.0011250	45.256	14.152
184	0.0400	2.56	5.00	40.0	0.1500	1.20	0.32	0.0281250	8.730	3.033
185	0.2025	0.64	64.80	115.2	0.1350	0.24	0.36	0.0022500	45.256	14.152
186	0.0400	0.64	12.00	48.0	0.0300	0.12	0.16	0.0005625	4.190	0.291
187	0.2025	0.64	11.25	20.0	0.1350	0.24	0.36	0.0022500	7.857	2.457
188	0.5625	2.56	18.75	40.0	0.2250	0.48	1.20	0.0045000	13.095	6.825
189	0.5625	0.64	108.00	115.2	0.1125	0.12	0.60	0.0005625	37.713	9.828
190	0.5625	0.64	108.00	115.2	0.2250	0.24	0.60	0.0022500	75.426	39.311
191	0.2025	0.64	64.80	115.2	0.1350	0.24	0.36	0.0022500	45.256	14.152
192	0.2025	0.16	11.25	10.0	0.3375	0.30	0.18	0.0070313	19.642	15.356
193	0.0400	0.64	5.00	20.0	0.0600	0.24	0.16	0.0022500	3.492	0.485
194	0.2025	2.56	27.00	96.0	0.1350	0.48	0.72	0.0045000	18.857	5.897
195	0.5625	0.64	18.75	20.0	0.1125	0.12	0.60	0.0005625	6.547	1.706
196	0.5625	2.56	18.75	40.0	0.5625	1.20	1.20	0.0281250	32.737	42.655

Table 6.10 The regression result by Minitab software

	C11	C12	C13	C14	C15	C16	C17	C18	C19	C20
	d*d	r*r	v*d	v*r	f*d	f*r	d*r	Ra	T	Fc
197	0.5625	0.64	18.75	20.0	0.5625	0.60	0.60	0.0140625	32.737	42.655
198	0.5625	2.56	18.75	40.0	0.1125	0.24	1.20	0.0011250	6.547	1.706
199	0.2025	0.64	27.00	48.0	0.0675	0.12	0.36	0.0005625	9.428	1.474
200	0.5625	0.64	18.75	20.0	0.2250	0.24	0.60	0.0022500	13.095	6.825
201	0.2025	0.64	11.25	20.0	0.0675	0.12	0.36	0.0005625	3.928	0.614
202	0.5625	0.64	18.75	20.0	0.5625	0.60	0.60	0.0140625	32.737	42.655
203	0.0400	0.16	12.00	24.0	0.1500	0.30	0.08	0.0070313	20.952	7.280
204	0.5625	2.56	45.00	96.0	0.5625	1.20	1.20	0.0281250	78.569	102.372
205	0.2025	2.56	64.80	230.4	0.3375	1.20	0.72	0.0281250	113.140	88.450
206	0.2025	2.56	27.00	96.0	0.0675	0.24	0.72	0.0011250	9.428	1.474
207	0.5625	2.56	108.00	230.4	0.2250	0.48	1.20	0.0045000	75.426	39.311
208	0.5625	2.56	45.00	96.0	0.1125	0.24	1.20	0.0011250	15.714	4.095
209	0.2025	2.56	27.00	96.0	0.3375	1.20	0.72	0.0281250	47.142	36.854
210	0.2025	2.56	27.00	96.0	0.3375	1.20	0.72	0.0281250	47.142	36.854
211	0.5625	0.64	45.00	48.0	0.5625	0.60	0.60	0.0140625	78.569	102.372
212	0.0400	2.56	28.80	230.4	0.1500	1.20	0.32	0.0281250	50.284	17.472
213	0.2025	0.16	64.80	57.6	0.3375	0.30	0.18	0.0070313	113.140	88.450
214	0.5625	0.16	108.00	57.6	0.1125	0.06	0.30	0.0002812	37.713	9.828
215	0.2025	2.56	64.80	230.4	0.0675	0.24	0.72	0.0011250	22.628	3.538
216	0.5625	0.16	18.75	10.0	0.1125	0.06	0.30	0.0002812	6.547	1.706
217	0.2025	0.16	11.25	10.0	0.1350	0.12	0.18	0.0011250	7.857	2.457
218	0.2025	2.56	11.25	40.0	0.3375	1.20	0.72	0.0281250	19.642	15.356
219	*0.5625*	*0.16*	*108.00*	57.6	0.1125	0.06	0.30	0.0002812	37.713	9.828
220	0.2025	0.16	27.00	*24.0*	*0.0675*	*0.06*	*0.18*	*0.0002812*	9.428	1.474
221	0.5625	0.16	18.75	10.0	0.2250	0.12	0.30	*0.0011250*	*13.095*	*6.825*
222	0.0400	0.16	28.80	57.6	0.1500	0.30	0.08	0.0070313	50.284	17.472
223	0.5625	0.16	45.00	24.0	0.5625	0.30	0.30	0.0070313	78.569	102.372
224	0.0400	2.56	28.80	230.4	0.0300	0.24	0.32	0.0011250	10.057	0.699
225	0.0400	0.16	12.00	24.0	0.1500	0.30	0.08	0.0070313	20.952	7.280
226	0.2025	2.56	27.00	96.0	0.0675	0.24	0.72	0.0011250	9.428	1.474
227	0.5625	2.56	45.00	96.0	0.2250	0.48	1.20	0.0045000	31.428	16.380
228	0.2025	0.16	27.00	24.0	0.3375	0.30	0.18	0.0070313	47.142	36.854
229	0.2025	0.16	64.80	57.6	0.0675	0.06	0.18	0.0002812	22.628	3.538
230	0.5625	2.56	18.75	40.0	0.5625	1.20	1.20	0.0281250	32.737	42.655
231	0.0400	2.56	12.00	96.0	0.0300	0.24	0.32	0.0011250	4.190	0.291
232	0.2025	0.64	27.00	48.0	0.3375	0.60	0.36	0.0140625	47.142	36.854
233	0.5625	2.56	108.00	230.4	0.1125	0.24	1.20	0.0011250	37.713	9.828
234	0.0400	0.16	5.00	10.0	0.0300	0.06	0.08	0.0002812	1.746	0.121
235	0.2025	0.64	27.00	48.0	0.0675	0.12	0.36	0.0005625	9.428	1.474
236	0.2025	2.56	64.80	230.4	0.0675	0.24	0.72	0.0011250	22.628	3.538
237	0.5625	0.16	18.75	10.0	0.1125	0.06	0.30	0.0002812	6.547	1.706
238	0.5625	0.64	45.00	48.0	0.1125	0.12	0.60	0.0005625	15.714	4.095
239	0.2025	0.16	27.00	24.0	0.0675	0.06	0.18	0.0002812	9.428	1.474
240	0.0400	2.56	5.00	40.0	0.0600	0.48	0.32	0.0045000	3.492	0.485
241	0.0400	0.16	28.80	57.6	0.0600	0.12	0.08	0.0011250	20.114	2.795
242	0.2025	2.56	64.80	230.4	0.0675	0.24	0.72	0.0011250	22.628	3.538
243	0.2025	0.64	27.00	48.0	0.3375	0.60	0.36	0.0140625	47.142	36.854

Table 6.11 The tool life, surface finish and cutting force result by *Minitab software*

	C21	C22	C23
	T1	Ra1	Fc1
1	19.2672	2.8829	188.844
2	6.0210	0.9009	59.014
3	15.0525	2.2523	147.534
4	0.6690	0.1001	6.557
5	3.6126	0.5405	35.408
6	36.1259	5.4055	354.083
7	3.6126	0.5405	35.408
8	3.0105	0.4505	29.507
9	1.6056	0.2402	15.737
10	6.0210	0.9009	59.014
11	0.7526	0.1126	7.377
12	3.0105	0.4505	29.507
13	1.6056	0.2402	15.737
14	0.1672	0.0250	1.639
15	1.5052	0.2252	14.753
16	2.1676	0.3243	21.245
17	7.7069	1.1532	75.538
18	1.8816	0.2815	18.442
19	0.8028	0.1201	7.869
20	6.0210	0.9009	59.014
21	1.6725	0.2503	16.393
22	18.0630	2.7027	177.041
23	1.8063	0.2703	17.704
24	4.0140	0.6006	39.343
25	19.2672	2.8829	188.844
26	1.9267	0.2883	18.884
27	3.0105	0.4505	29.507
28	7.2252	1.0811	70.817
29	3.2112	0.4805	31.474
30	6.0210	0.9009	59.014
31	7.7069	1.1532	75.538
32	0.7526	0.1126	7.377
33	1.9267	0.2883	18.884
34	8.0280	1.2012	78.685
35	3.2112	0.4805	31.474
36	7.2252	1.0811	70.817
37	7.5262	1.1261	73.767
38	9.0315	1.3514	88.521
39	3.3450	0.5005	32.785
40	1.3380	0.2002	13.114
41	18.0630	2.7027	177.041
42	3.1359	0.4692	30.736
43	6.0210	0.9009	59.014
44	3.0105	0.4505	29.507
45	28.9007	4.3244	283.266
46	3.8534	0.5766	37.769
47	17.3404	2.5946	169.960
48	2.1676	0.3243	21.245
49	0.9634	0.1441	9.442

Table 6.12 The tool life, surface finish and cutting force result by Minitab software

	C21	C22	C23
	T1	Ra1	Fc1
50	0.4014	0.0601	3.934
51	10.8378	1.6216	106.225
52	3.0105	0.4505	29.507
53	7.5262	1.1261	73.767
54	4.3351	0.6487	42.490
55	3.6126	0.5405	35.408
56	4.8168	0.7207	47.211
57	0.8028	0.1201	7.869
58	4.0140	0.6006	39.343
59	3.8534	0.5766	37.769
60	1.6056	0.2402	15.737
61	3.7631	0.5631	36.884
62	9.6336	1.4415	94.422
63	4.8168	0.7207	47.211
64	6.2719	0.9384	61.473
65	7.2252	1.0811	70.817
66	12.5437	1.8769	122.945
67	21.6756	3.2433	212.450
68	0.4014	0.0601	3.934
69	1.9267	0.2883	18.884
70	3.2112	0.4805	31.474
71	1.2544	0.1877	12.295
72	0.3345	0.0501	3.279
73	1.6056	0.2402	15.737
74	2.5087	0.3754	24.589
75	2.1676	0.3243	21.245
76	0.8362	0.1251	8.196
77	6.2719	0.9384	61.473
78	1.8063	0.2703	17.704
79	7.5262	1.1261	73.767
80	2.5087	0.3754	24.589
81	1.6725	0.2503	16.393
82	1.8063	0.2703	17.704
83	72.2519	10.8109	708.165
84	0.9031	0.1351	8.852
85	1.5052	0.2252	14.753
86	18.0630	2.7027	177.041
87	43.3511	6.4866	424.899
88	0.3763	0.0563	3.688
89	3.1359	0.4692	30.736
90	9.6336	1.4415	94.422
91	3.0105	0.4505	29.507
92	14.4504	2.1622	141.633
93	1.6056	0.2402	15.737
94	8.0280	1.2012	78.685
95	1.8816	0.2815	18.442
96	30.1049	4.5046	295.069
97	0.6690	0.1001	6.557
98	0.7526	0.1126	7.377

Table 6.13 The tool life, surface finish and cutting force result by Minitab software

	C21	C22	C23
	T1	Ra1	Fc1
99	14.4504	2.1622	141.633
100	0.6690	0.1001	6.557
101	10.8378	1.6216	106.225
102	3.3450	0.5005	32.785
103	1.9267	0.2883	18.884
104	5.0175	0.7508	49.178
105	3.6126	0.5405	35.408
106	0.1672	0.0250	1.639
107	12.0420	1.8018	118.028
108	0.8028	0.1201	7.869
109	30.1049	4.5046	295.069
110	0.1672	0.0250	1.639
111	1.6725	0.2503	16.393
112	0.6272	0.0938	6.147
113	4.3351	0.6487	42.490
114	5.0175	0.7508	49.178
115	9.6336	1.4415	94.422
116	0.8028	0.1201	7.869
117	14.4504	2.1622	141.633
118	0.3345	0.0501	3.279
119	0.8028	0.1201	7.869
120	21.6756	3.2433	212.450
121	2.0070	0.3003	19.671
122	7.5262	1.1261	73.767
123	3.8534	0.5766	37.769
124	0.9634	0.1441	9.442
125	7.2252	1.0811	70.817
126	3.8534	0.5766	37.769
127	0.7526	0.1126	7.377
128	0.4014	0.0601	3.934
129	3.1359	0.4692	30.736
130	1.5052	0.2252	14.753
131	6.2719	0.9384	61.473
132	14.4504	2.1622	141.633
133	1.9267	0.2883	18.884
134	1.3380	0.2002	13.114
135	1.2544	0.1877	12.295
136	0.3763	0.0563	3.688
137	1.9267	0.2883	18.884
138	17.3404	2.5946	169.960
139	2.5087	0.3754	24.589
140	12.5437	1.8769	122.945
141	0.3345	0.0501	3.279
142	1.2544	0.1877	12.295
143	3.0105	0.4505	29.507
144	8.6702	1.2973	84.980
145	3.7631	0.5631	36.864
146	3.7631	0.5631	36.864
147	2.5087	0.3754	24.589

Table 6.14 The tool life, surface finish and cutting force result by Minitab software

	C21	C22	C23
	T1	Ra1	Fc1
148	7.2252	1.0811	70.817
149	12.0420	1.8018	118.028
150	3.0105	0.4505	29.507
151	43.3511	6.4866	424.899
152	12.5437	1.8769	122.945
153	1.8063	0.2703	17.704
154	4.3351	0.6487	42.490
155	15.0525	2.2523	147.534
156	17.3404	2.5946	169.960
157	3.8534	0.5766	37.769
158	8.6702	1.2973	84.980
159	0.3345	0.0501	3.279
160	8.6702	1.2973	84.980
161	0.7526	0.1126	7.377
162	21.6756	3.2433	212.450
163	1.3380	0.2002	13.114
164	7.2252	1.0811	70.817
165	8.6702	1.2973	84.980
166	8.0280	1.2012	78.685
167	4.8168	0.7207	47.211
168	0.6690	0.1001	6.557
169	1.5052	0.2252	14.753
170	8.6702	1.2973	84.980
171	0.8362	0.1251	8.196
172	4.3351	0.6487	42.490
173	0.6690	0.1001	6.557
174	3.6126	0.5405	35.408
175	4.5157	0.6757	44.260
176	1.2544	0.1877	12.295
177	4.5157	0.6757	44.260
178	1.2544	0.1877	12.295
179	4.0140	0.6006	39.343
180	28.9007	4.3244	283.266
181	0.3345	0.0501	3.279
182	18.0630	2.7027	177.041
183	0.7526	0.1126	7.377
184	19.2672	2.8829	188.844
185	1.5052	0.2252	14.753
186	0.8028	0.1201	7.869
187	8.6702	1.2973	84.980
188	28.9007	4.3244	283.266
189	1.2544	0.1877	12.295
190	2.5087	0.3754	24.589
191	1.5052	0.2252	14.753
192	10.8378	1.6216	106.225
193	3.8534	0.5766	37.769
194	7.2252	1.0811	70.817
195	7.2252	1.0811	70.817
196	72.2519	10.8109	708.165

Table 6.15 The tool life, surface finish and cutting force result by Minitab software

	C21	C22	C23
	T1	Ra1	Fc1
197	36.1259	5.4055	354.083
198	14.4504	2.1622	141.633
199	1.8063	0.2703	17.704
200	14.4504	2.1622	141.633
201	4.3351	0.6487	42.490
202	36.1259	5.4055	354.083
203	2.0070	0.3003	19.671
204	30.1049	4.5046	295.069
205	7.5262	1.1261	73.767
206	3.6126	0.5405	35.408
207	5.0175	0.7508	49.178
208	6.0210	0.9009	59.014
209	18.0630	2.7027	177.041
210	18.0630	2.7027	177.041
211	15.0525	2.2523	147.534
212	3.3450	0.5005	32.785
213	1.8816	0.2815	18.442
214	0.6272	0.0938	6.147
215	1.5052	0.2252	14.753
216	3.6126	0.5405	35.408
217	4.3351	0.6487	42.490
218	43.3511	6.4866	424.899
219	0.6272	0.0938	6.147
220	0.9031	0.1351	8.852
221	7.2252	1.0811	70.817
222	0.8362	0.1251	8.196
223	7.5262	1.1261	73.767
224	0.6690	0.1001	6.557
225	2.0070	0.3003	19.671
226	3.6126	0.5405	35.408
227	12.0420	1.8018	118.028
228	4.5157	0.6757	44.260
229	0.3763	0.0563	3.688
230	72.2519	10.8109	708.165
231	1.6056	0.2402	15.737
232	9.0315	1.3514	88.521
233	2.5087	0.3754	24.589
234	0.9634	0.1441	9.442
235	1.8063	0.2703	17.704
236	1.5052	0.2252	14.753
237	3.6126	0.5405	35.408
238	3.0105	0.4505	29.507
239	0.9031	0.1351	8.852
240	7.7069	1.1532	75.538
241	0.3345	0.0501	3.279
242	1.5052	0.2252	14.753
243	9.0315	1.3514	88.521

Appendix 7 Simulation programming structure

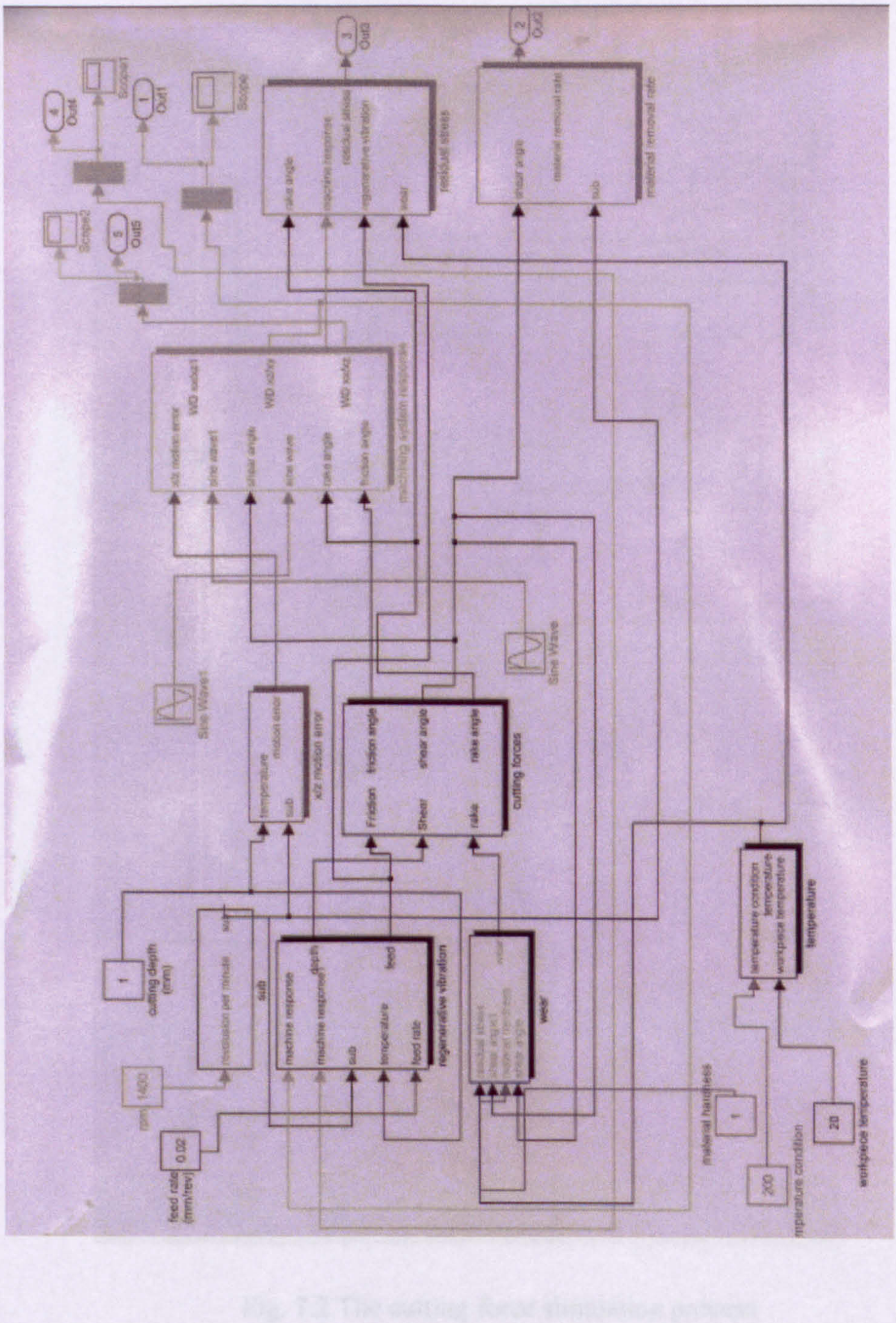

Fig. 7.1 The whole simulation process

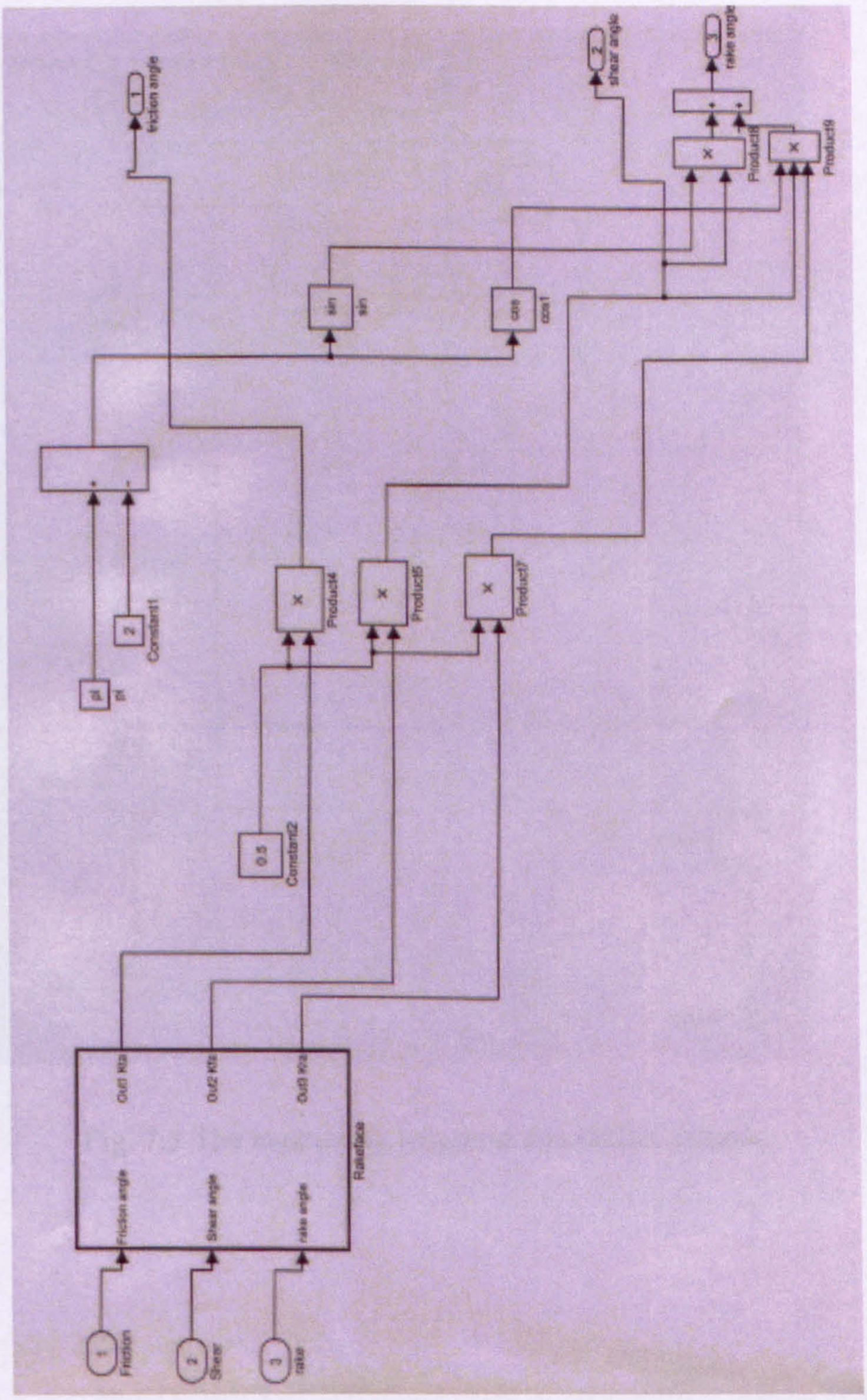

Fig. 7.2 The cutting force simulation process

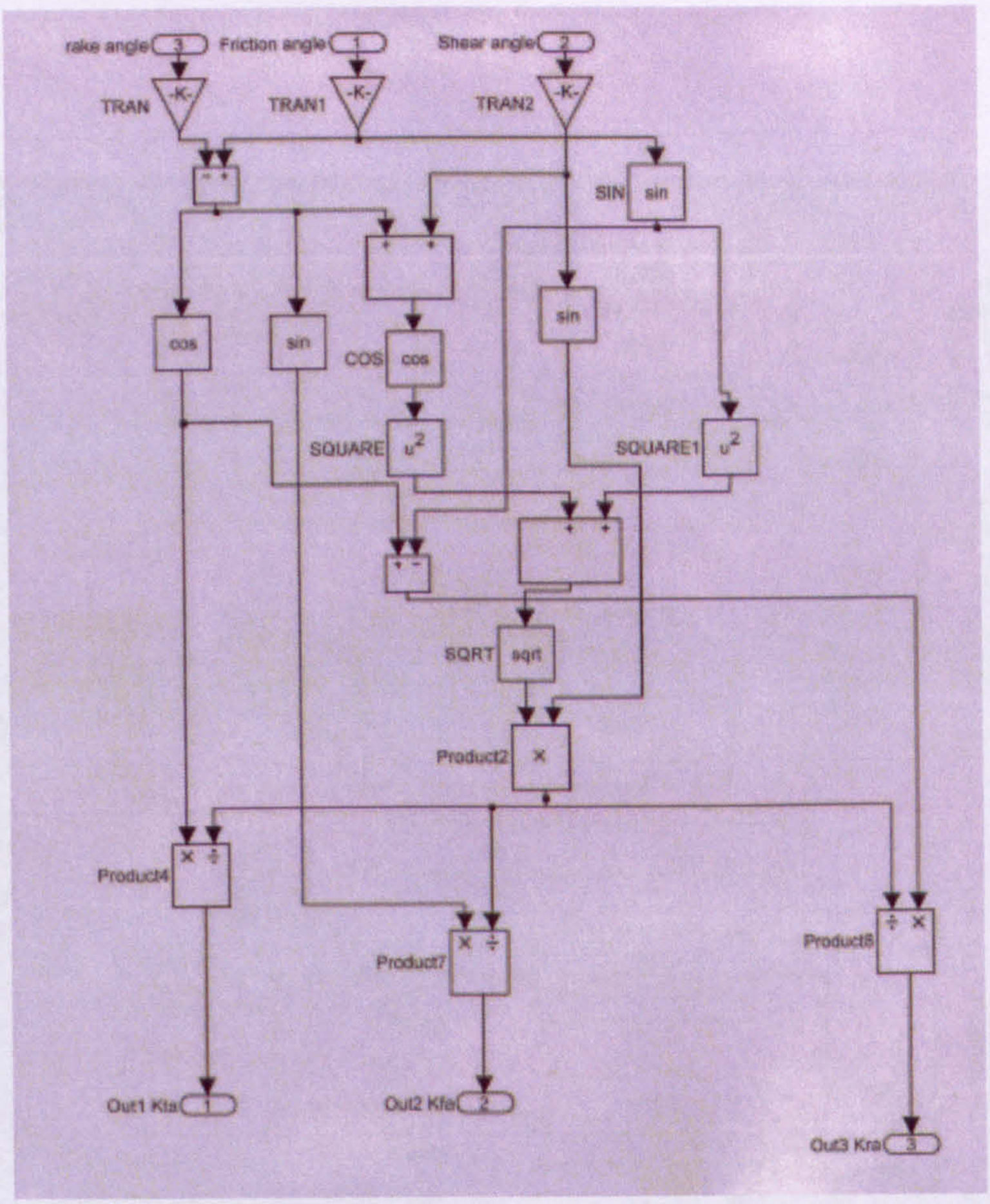

Fig. 7.3 The machining response simulation process

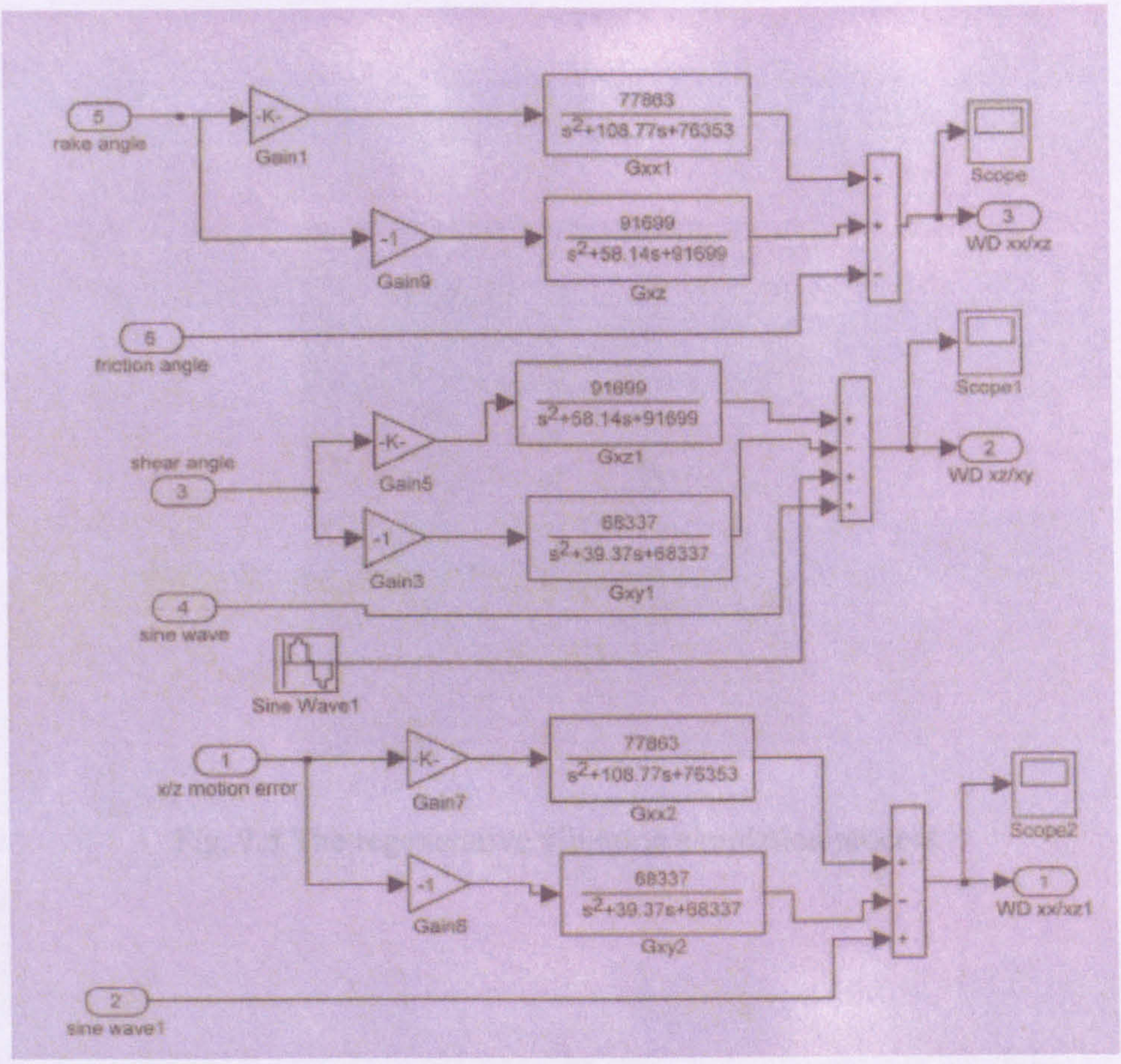

Fig. 7.4 The material removal rate simulation process

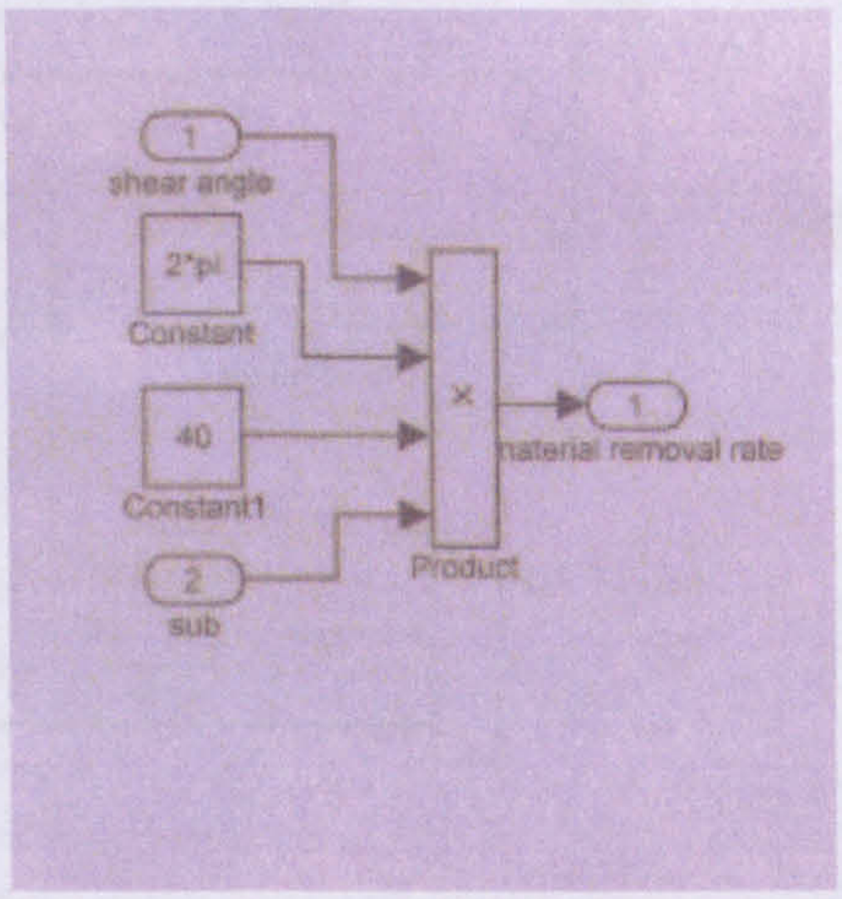

Fig. 7.5 The regenerative vibration simulation process

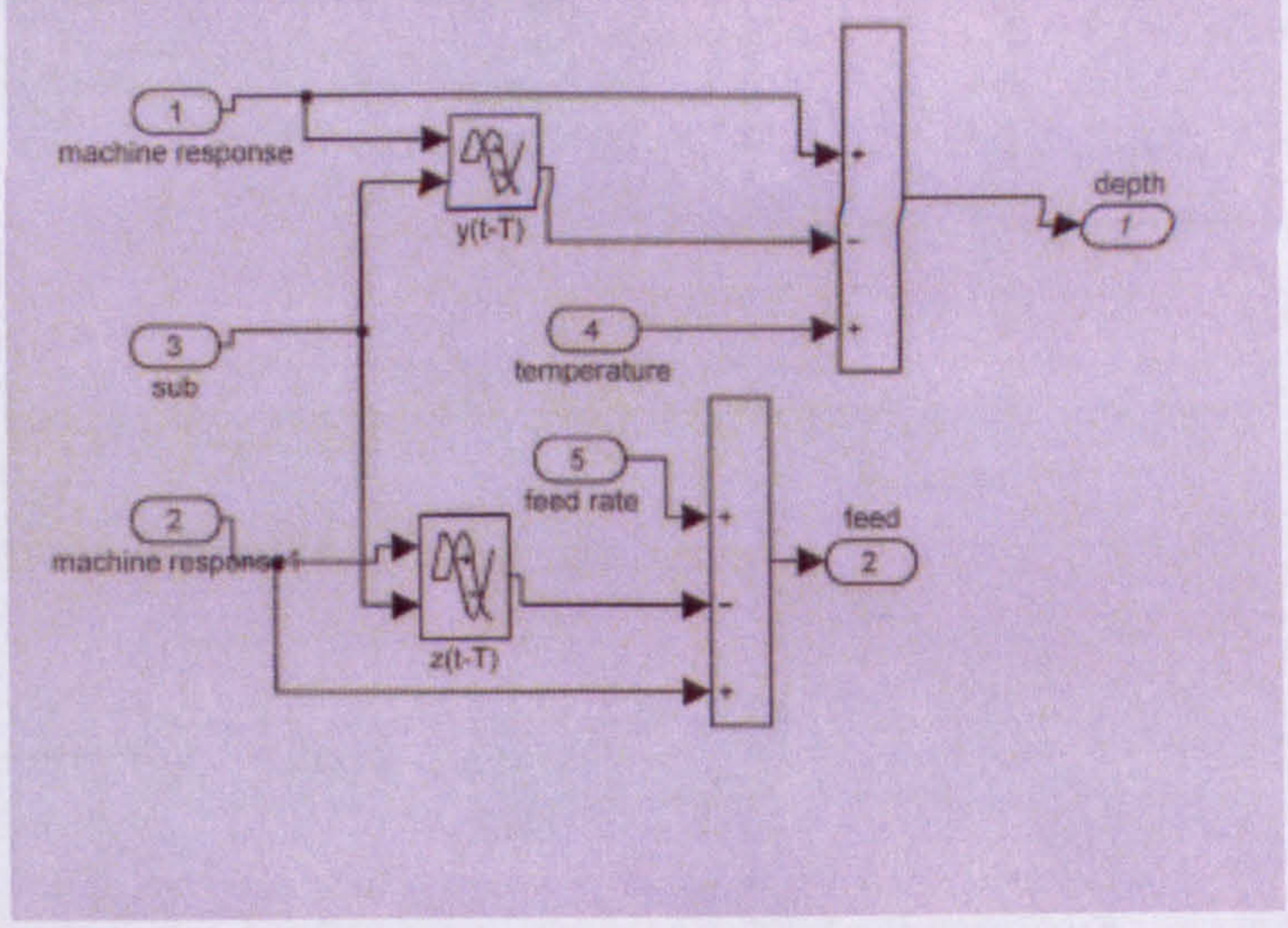

Fig. 7.6 The depth of cut and feed rate simulation process

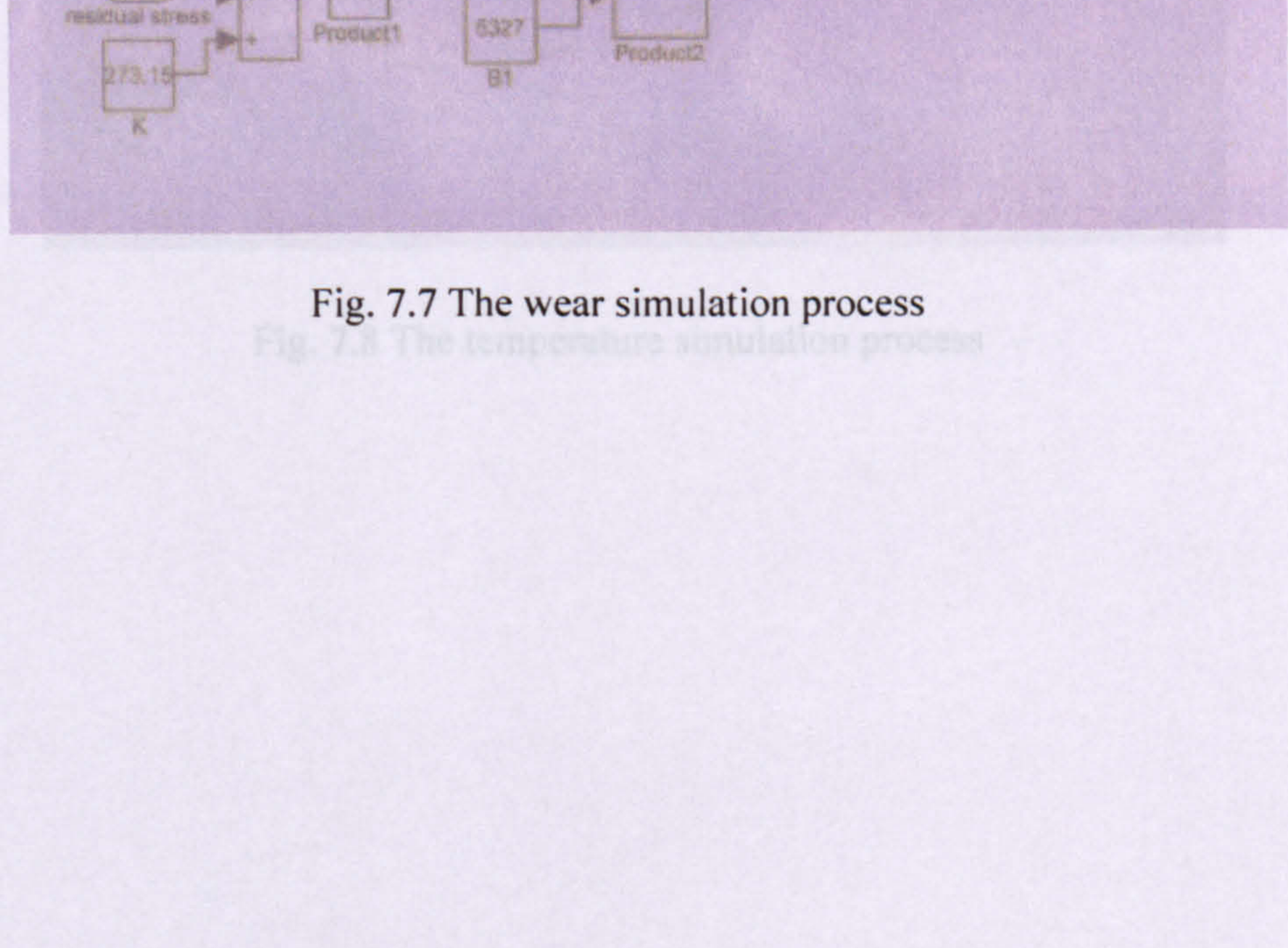

Fig. 7.7 The wear simulation process

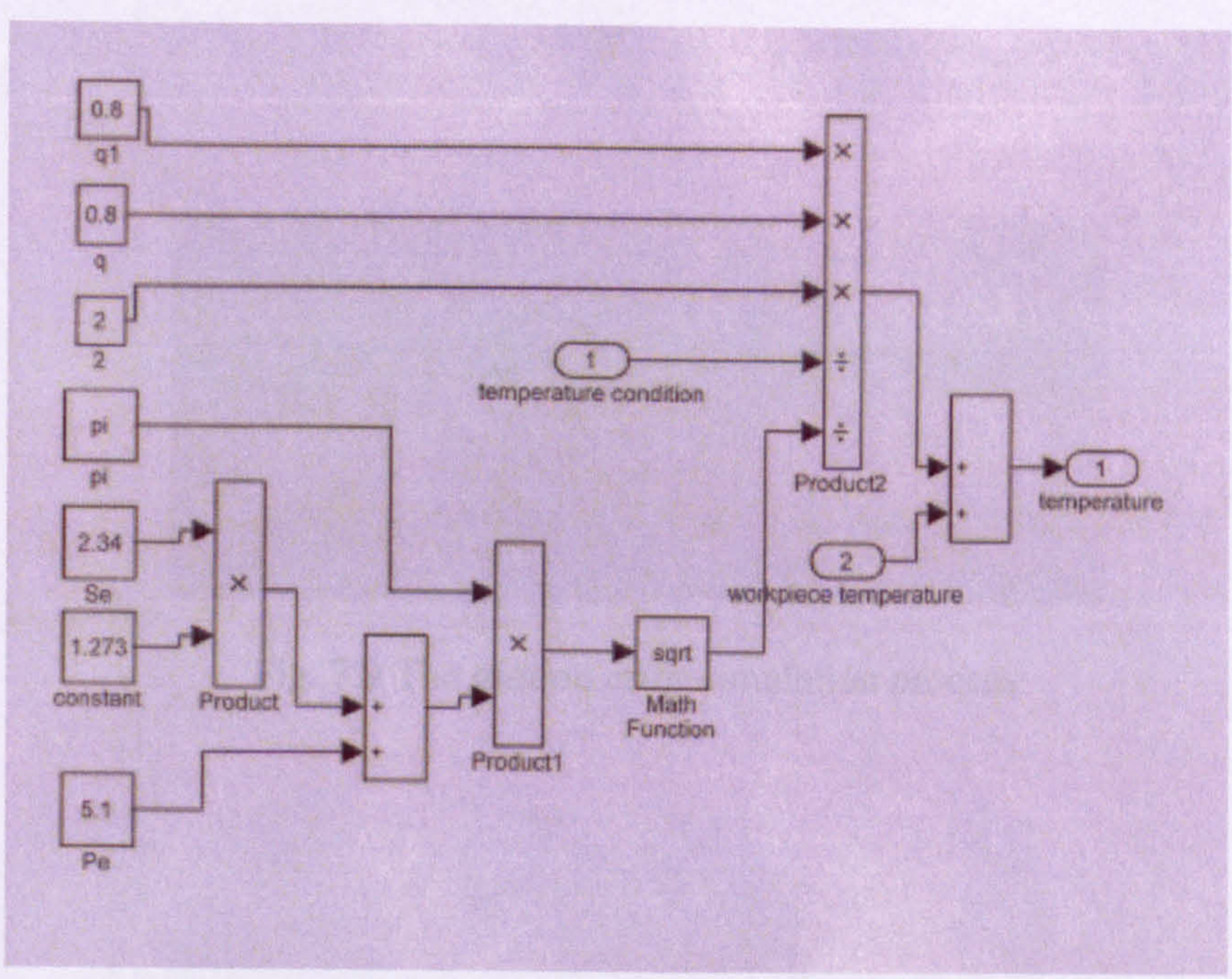

Fig. 7.8 The temperature simulation process

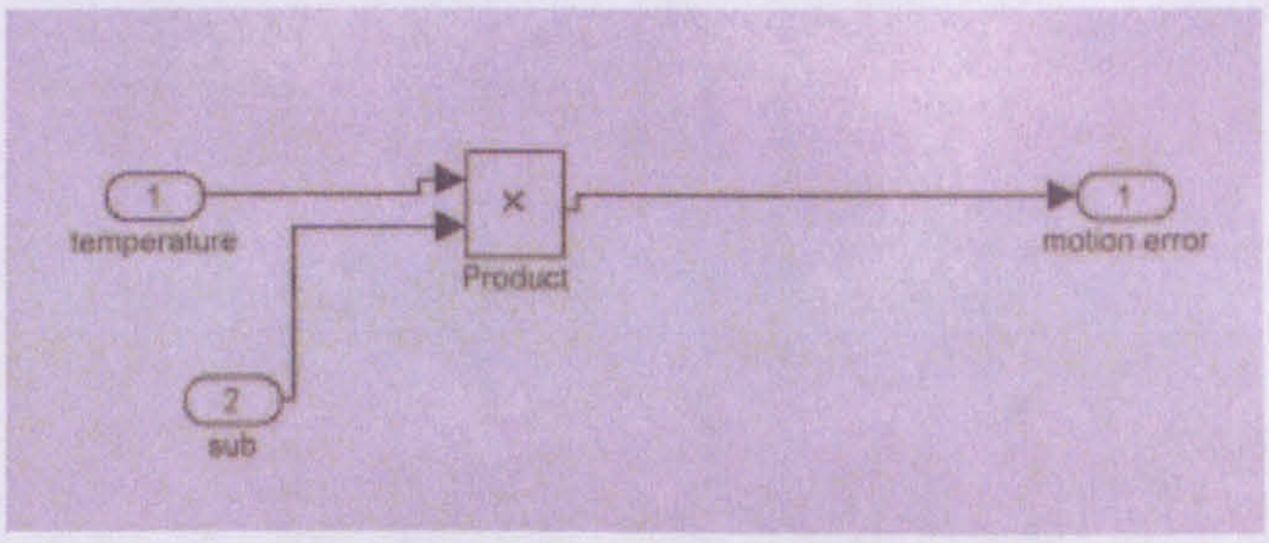

Fig. 7.9 The motion error simulation process

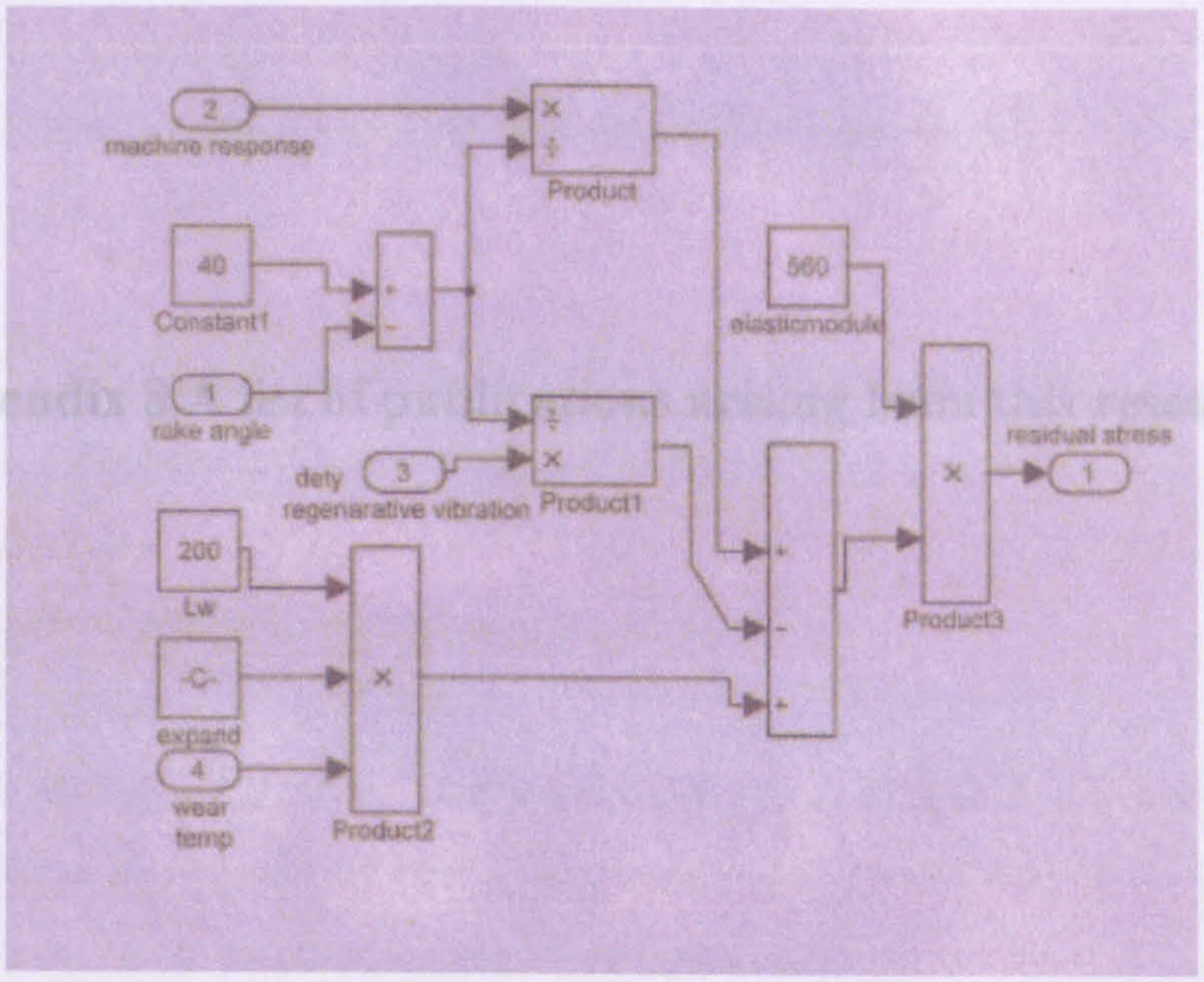

Fig. 7.10 The residual stress simulation process

Appendix 8 A list of publications arising from this research

A list of publications arising from this research

1. N. F. M. Aris, K. Cheng and R. Ward, Surface functionality of precision machined engineering surfaces: Characterisation, Simulation and Process Control, The 6th International Euspen Conference, Baden bei Wien, Austria, 28th May – 1st June 2006.

2. N. F. M. Aris, K. Cheng, Characterization of the surface functionality on precision machined engineering surfaces, Proceedings of the 4th International conference on Manufacturing Research (ICMR 2006), Liverpool, UK, 5th-7th September 2006.

3. N. F. M. Aris, K. Cheng, Investigation on GA for control and optimization of surface functionalities generation in precision turning processes, The 20th International Conference on Computer-Aided Production Engineering, Glasgow Caledonian University, 6 - 8 June 2007.

4. N. F. M. Aris, K. Cheng, Characterization of the surface functionality on precision machined engineering surfaces, International Journal of Advanced Manufacturing Technology, Accepted: March 2008.